Universidad
Carlos III de Madrid
www.uc3m.es

**Tesis Doctoral**

# EXPERIMENTAL STUDY OF *CYNARA CARDUNCULUS* L. GASIFICATION IN BUBBLING FLUIDISED BED

**Agglomeration, gas, tars and fly ash**


Autor
Daniel Serrano García

Director
Sergio Sánchez Delgado

DEPARTAMENTO DE INGENIERÍA TÉRMICA Y DE FLUIDOS


Leganés, Diciembre 2016

Universidad Carlos III de Madrid
www.uc3m.es

Tesis doctoral

# EXPERIMENTAL STUDY OF *CYNARA CARDUNCULUS* L. GASIFICATION IN BUBBLING FLUIDISED BED

Autor: Daniel Serrano García

Director de Tesis: Sergio Sánchez Delgado

Firma del Tribunal Calificador:

Firma

Presidente:
D. Alberto Gómez Barea, Universidad de Sevilla
Secretario:
D. Jose María Sánchez Hervás, Centro de Investigaciones Energéticas, Medioambientales y Tecnológicas
Vocal:
Dña. Filomena Pinto, Laboratório Nacional de Energia e Geologia
Suplente:
Dña. Mercedes de Vega Blázquez, Universidad Carlos III de Madrid

Calificación:

Leganés, 15 de Diciembre de 2016

DEPARTAMENTO DE INGENIERÍA TÉRMICA Y DE FLUIDOS
Escuela Politécnica Superior

**PhD Thesis**

# EXPERIMENTAL STUDY OF *CYNARA CARDUNCULUS* L. GASIFICATION IN BUBBLING FLUIDISED BED

**Agglomeration, gas, tars and fly ash**

Ph.D. Program in Mechanical Engineering and Industrial Organization

Author
Daniel Serrano García

PhD Advisor
Sergio Sánchez Delgado

Leganés, December 2016

*A mi familia, a los que están y a los que no*

*Play is the highest form of research*
Albert Einstein

*Ignore the obvious*
Anonimous

*16. Žmogus turi teisę būti laimingas*
*41. Nepasiduok*
Uzupio Respublikos Konstitucija

# Preface

This PhD Thesis has been performed at the Carlos III University of Madrid, School of Engineering, in the Department of Thermal and Fluid Engineering, under the supervision of Dr. Sergio Sánchez Delgado. The thesis was initiated in Autumn 2013 and lasted until Autumn 2016.

The author deeply appreciates the funding support by the Spanish Government (Project ENE2014-54942-R) and by European Union Seventh Framework Programme (FP7-INFRASTRUCTURES) under BRISK Transactional Access grant (Project 284498).

During the realisation of the PhD, two collaboration frameworks have been established with different research groups. A first research stay in the "Carbolea" research group from University of Limerick, headed by Prof. James J. Leahy and under the supervision of Dra. Marzena Kwapinska, was performed in September-December of 2014. A second research stay in the "Thermal Process Engineering" research group from the Paul Scherrer Institute (PSI), headed by Dr. Serge Biollaz, was performed during July-August of 2015.

All the results presented in this dissertation have been obtained by the author unless otherwise specified.

Daniel Serrano García
Department of Thermal and Fluid Engineering,
University Carlos III of Madrid
December 2016

# Agradecimientos

La mayoría de los agradecimientos empiezan como un punto final a una etapa que termina, sin embargo, yo quiero dar las gracias a todos aquellos que han hecho realidad esta nueva etapa que comienza.

En primer lugar, quiero agradecer a Sergio la oportunidad que me ha dado para poder realizar esta tesis, así como la dedicación y determinación ante el gran reto de abrirnos un hueco en el mundo de la transformación termoquímica. Al final parece que aquellos primeros pellets gasificados "a lo loco" en la nave, el dineral en pellets y las numerosas desavenencias experimentales han dado sus frutos.

A todos los miembros del grupo ISE y del grupo de Mecánica de Fluidos por los momentos vividos, haciendo que el trabajo fuera más llevadero. Especialmente a Celia, Carol, Domingo y Antonio Soria por sus consejos y apoyo; a Néstor por sus enseñanzas sobre la TGA y LabVIEW; al comando "¡Vaaamos chavaaales!" por su apoyo en los momentos finales de la tesis; a los miembros de Iterate por hacerme colgar las botas; y al resto de compañeros que no enumero para no dejarme ninguno y que han contribuído, en mayor o menor medida, en toda esta etapa. Mención especial requieren Alberto y, particularmente, Éduard o Edgardo (algo más que un compañero), mi quinta de tesis ("los pobres" junto con Juan), por todo este tiempo pasado juntos en el depacho en el que se respira a tesis y se regalan cacahuetes de miel y chocolatinas. También quiero agradecer a los técnicos de laboratorio por su ayuda a la hora de construir la instalación y solventar los diversos problemas experimentales, al personal de mantenimiento, por enseñarme donde armar los enchufes cada vez que saltaban, y a Cristina, por su apoyo en las gestiones administrativas, aunque alguna vez me haya llevado algún tirón de orejas. Gracias a todos.

Al servicio técnico de Agilent, por reponder amablemente a todos mis correos y llamadas y, porque sin su ayuda seguirámos teniendo unos magníficos, y siempre nuevos, $\mu$–GC y masas. A TOLSA e INCUSA, por el sumistro desinteresado de sepiolita y arena. A los revisores anónimos que han contribuído a mejorar la calidad de los trabajos publicados que forman parte de esta tesis.

A mis amigos de la banda, por los grandes momentos vividos en el pinar de Anchuelo y en las piscinas naturales de Rascafría que siempre recordaremos (cuando nos pongamos de acuerdo para ir, sino, siempre quedará el Índalo). A mis amigos de la universidad, los

cuales somos difíciles de ver aunque eso no importe. Después de esto ya no sé que excusa poner para juntarnos todos. Al grupo *Sevcenkos*, por esa amistad aunque pasen años sin vernos y, especialmente a Ángel, por hacernos ver lo dura que es su ajetreada vida, la cual hemos vivido estos últimos meses. Ahora entiendo las 3214 pestañas abiertas en el navegador. A los miembros de Athanor, por todos esos más *ff* y momentos compartidos a través de la música.

A mi familia, por estar siempre ahí y apoyarme en todo. Especialmente a mis padres, porque vendrán a la defensa de la tesis, no se enterarán de mucho y se liarán con lo de los pellets y la biomasa, pero aún así, estarán orgullosos.

Por último, a la persona más importante de todas, por estar siempre ahí, en los buenos y en los malos momentos, por explicarme una y mil veces las diferencias entre un paracetamol y un ibuprofeno a pesar de mi medio Grado en Enfermería, y lo más fundamental, por querer pasar el resto de tu vida conmigo.

# Acknowledgements

I would like to give special thanks to the personnel of the Carbolea research group from the University of Limerick during my stay in Autumn 2014. In particular to Marzena Kwapinska, who I consider a co-director in this PhD thesis, for her trust, helpful ideas, guidance, support, determination to fix all the experimental problems that we experienced during the experimental campaign and onwards, and the availability to answer any doubt I have; to Alen Horvat for his introduction and teaching in the world of tars, SPA and GC-MS instruction; to James J. Leahy for his trust, help and financial support to carry out internal and external analyses for my research; to Daya Pandey and Bashir Ghanim for helping me during the beauty of cleaning the gasifier and crushing pellets, and to Alberto Soñora who carried out numerous inorganic analyses. I hope you can use the gasifier soon again.

I am also very grateful to the personnel of the Thermal Process Engineering research group from the Paul Scherrer Institute during my stay in Summer 2015. In particular to Serge Biollaz for hosting me and his helpful advices and ideas; to Sergio Rodríguez for his help, ideas and time to carry out additional analyses, and to Martin Künstle and Jörg Scheebeli for their useful help, ideas, support and feedback.

Finally, I would like to thank Yina Guo from Materials & Surface Science Institute from the University of Limerick, who carried out SEM-EDS analyses; Kai-Jie Chen from Crystal Engineering Research Group at the University of Limerick, who carried out BET analyses; Lidia Muñoz Fernández and María Eugenia Rabanal from Grupo de Tecnología de Polvos from Carlos III University of Madrid, for their important help in the last BET analyses, and Rosa Sedano from SIDI for the analyses of adsorbed tars.

# Resumen

El uso de biomasa como recurso energético puede reducir la dependencia actual que hay de los combustibles fósiles hacia un desarrollo más concienciado con el medio ambiente. Este hecho también puede ser empleado para tratar diferentes tipos de residuos que son generados en grandes cantidades como residuos sólidos urbanos, lodos de depuradora o residuos agrícolas, obteniendo productos útiles y reduciendo su eliminación en vertederos. Una de las rutas empleadas para este fin es la transformación termoquímica y, en particular, la gasificación. La gasificación consiste en transformar la biomasa en una mezcla de diferentes productos: gases condensables y no condensables, residuo carbonoso y cenizas a través de la oxidacion parcial de la biomasa a elevadas temperaturas. El principal producto de este proceso es la fraccion de gases no condensables que pueden ser empleados en diferentes aplicaciones: combustible para calderas y motores de gas, o como producto para la generación de hidrógeno, metano o biocombustibles a través del proceso Fischer-Tropsch.

En cuanto a los reactores utilizados para llevar a cabo el proceso de gasificación, existen múltiples tecnologías: lechos fijos, lechos móviles, lechos fluidizados, etc. La alta capacidad de mezclado y de transferencia de calor y masa hacen que los lechos fluidizados sean un buena opción para la gasificación de biomasa. Sin embargo, existen tres problemas operacionales importantes que deben de ser tenidos en cuenta. El primer problema es el fenómeno de aglomeración del lecho, el cual está motivado por el alto contenido de metales alcalinos presentes en la biomasa junto con las temperaturas de reacción alcanzadas en el reactor. Estos elementos reaccionan con los compuestos de silicio de los materiales de la fase densa del lecho para formar silicatos con bajo punto de fusión que actúan como un pegamento entre las partículas o las recubren, generando aglomerados y la posible defluidización del reactor. El segundo problema es la generación de alquitranes, una fracción viscosa y pegajosa que condensa en superficies frías, pudiendo atascar y bloquear tuberías y equipos. El tercer aspecto a tener en cuenta es la generación de ceniza, lo que constituye un residuo que tiene que ser tratado o reusado adecuadamente en diferentes aplicaciones antes de su vertido final.

La presente tesis doctoral estudia los tres problemas mencionados acerca de la gasificación de biomasa en un reactor de lecho fluido burbujeante. Como biomasa se ha empleado *Cynara cardunculus* L., un cultivo energético procedente de regiones mediterráneas

y con un alto contenido en metales alcalinos, para investigar su uso potencial para la gasificación en lecho fluidizado. Este cultivo presenta alguna ventajas frente a otras plantas como la baja cantidad de agua para su cultivo o el uso de tierras no aptas para el cultivo de productos alimentarios. Otro de los aspectos importantes a tener en cuenta en la gasificación en lecho fluidizado, es la selección del material de la fase densa del lecho. En esta tesis se propone la sepiolita, un mineral arcilloso que se usa comúnmente como absorbente, como material para la fase densa del lecho, comprobando su funcionamiento en la aglomeración, la composición del gas y de los alquitranes, y la resitencia mecánica. La investigación se ha desarrollado empleando tres instalaciones experimentales: un gasificador a escala laboratorio, un gasificador en planta piloto y un lecho fluidizado frío. Se han utilizado diferentes técnicas para analizar los datos y para caracterizar los productos del proceso de gasificación.

El proceso de aglomeración se ha estudiado a través del análisis de las fluctuaciones de presión obtenidas en el interior del lecho fluidizado a escala laboratorio. Para la detección del fenómeno de la aglomeración, y en consecuencia, de la defluidización del lecho se utilizan los métodos de la energía contenida en las regiones frecuenciales, la comparación de atractores, y la desviación estándar. En función de la relaciń entre la densidad de las partículas de biomasa y del material de la fase densa del lecho, se encuentran dos comportamientos cláramente diferenciados: *jetsam* y *flotsam*. En el primero de ellos la biomasa se hunde en el lecho mientras que en el segundo la biomasa tiende a flotar sobre su superficie debido a la mayor densidad de la arena en este segundo caso. El análisis de la energía contenida en las regiones frecuenciales muestran que, para un comportamiento *jetsam* de las partículas de biomasa, se producen burbujas endógenas debido a la devolatilización de la biomasa dentro del la fase densa del lecho. Sin embargo, para partículas con un comportamiento *flotsam*, se forma un aglomerado con forma plana en toda la superficie del lecho que puede ser detectado por las altas frecuencias en el espectro de potencia. Los tiempos de defluidización son similares para cada método de análisis, obteniéndose tiempos mucho mayores en los ensayos realizados con sepiolita.

El comportamiento de la sepiolita como material de la fase densa del lecho en términos de la composición del gas y de la reducción alquitranes se ha investigado en el lecho fluidizado a escala laboratorio, comparando los resultados con ensayos similares realizados con arena. La calidad del gas resultante de la gasificación es algo menor en el caso de la sepiolita que en el de la arena. No obstante, la generación de alquitranes disminuye significativamente con sepiolita, siendo también diferente la composición de estos para los dos materiales. El área superficieal de la sepiolita así como su morfología se han analizados por medio de las técnicas BET de área superficial y microscopía electrónica de barrido (SEM-EDS) antes y después de los ensayos. El comportamiento de las partículas

de biomasa y las propiedades de la sepiolita provocan, la adsorción de los alquitranes y de las cenizas fundidas en la superficie de la sepiolita, generando un mejor comportamiento frente a los alquitranes y a la aglomeración. Admás, se ha realizado un ensayo de desgaste de larga duración en la sepiolita (100 horas), obteniendo una menor tasa de desgaste que para otros materiales usados comúnmente como la alúmina o la dolomita.

Esta biomasa, *Cynara cardunculus* L., también ha sido ensayada en la planta piloto de gasificación con magnesita y olivino como materiales de fase densa del lecho en términos de la composición del gas y de la generación de alquitranes. El gas obtenido muestra un contenido en hidrógeno relativamente alto para ambos materiales. Se observa un efecto positivo de la temperatura en los parámetros de la gasificación y de su eficiencia. Las diferencias observadas en relación a los alquitranes son poco significativas entre la magnesita y el olivino, aunque se obtienen composiciones diferentes de alquitranes en cada caso. La fracción de benceno, tolueno, etilbenceno y xilenos (BTEX) es mayor en el caso del olivino mientras que la fracción de hidrocarburos aromático policíclicos es similar en ambos casos. Se observa un comportamiento catalítico del magnesio procedente de la magnesita y el olivino en el craqueo de los alquitranes. A 700 °C, la magnesita muestra mejores resultados mientras que el olivino lo hace a 800 °C.

Finalmente, las cenizas volantes de los ensayos de gasificación en la planta piloto han sido analizadas en términos de su composición elemental y de metales, contenido en azufre y cloro, y comportamiento frente a la lixiviación. La mayoría de los finos quedan retenidos en el primer ciclón. El material de la fase densa del lecho, así como los materiales del propio reactor, también afectan a la composición de los finos. Su reutilización en la industria cementera o como fertilizante se antoja complicada como consecuencia del alto contenido en carbón, alcalinos, cloro y metales pesados, siendo su uso como combustible alternativo/secundario una buena opción por su alto contenido energético.

# Abstract

The use of biomass as an energy resource can reduce the existing dependence on fossil fuels consumption, shifting towards a more aware environmental development. It can be also an opportunity to deal with huge amounts of solid residues such as municipal solid waste, sewage sludge or agricultural residues, obtaining valuable products from them and reducing their landfill disposal. One of the routes employed for this purpose is the thermochemical conversion and, in particular, gasification. In gasification process, the biomass is transformed into a mixture of products: non condensible gases, condensible gases, solid char and ashes by means of partial oxidation at high temperature. The non condensible fraction of gas is the main product that can be use in different applications: fuel in boilers and gas engines, or raw gas to produce hydrogen, methane or biofuels through the Fischer-Tropsch process.

There are multiple gasification technologies to transform biomass by the thermochemical route: fixed beds, moving beds, fluidised beds, etc. The good mixing and high mass and heat transfer rates make fluidised beds a good option for biomass gasification. However, there are three main operational problems that need to be considered. The first problem is the bed agglomeration which is motivated by the high alkali content in biomass and the reaction temperatures reached in the reactor. These elements react with the silicon compounds from the bed material to form low melting point silicates that act as a "glue" between particles or coat them, leading to the agglomerates and to the possible defluidisation of the reactor. The second problem is the tar generation, a viscous and sticky fraction that condense on cold surfaces and may clog and block the pipes and downstream devices. The third aspect is the ash generation, which constitutes a residue that need to be treated or reused in different applications before its final disposal.

This PhD thesis studies the above three mentioned related problems of biomass gasification in a bubbling fluidised bed (BFB) reactor. *Cynara cardunculus* L., an energy crop typical from Mediterranean regions and with a high alkali content, is used as biomass feedstock in order to test its potential for gasification in a fluidised bed. This energy crop has some advantages from other plants such as the low water irrigation or the use of lands not suitable for food purposes. Another main aspect to take into account in fluidised bed gasification, is the bed material selection. In this PhD thesis, sepiolite, a clay mineral that is commonly used as adsorbent, is proposed as bed material, checking its

suitability for agglomeration, gas and tar composition, and mechanical resistance. This investigation has been performed in three experimental facilities: a lab- and a pilot-scale gasifiers, and a cold fluidised bed. Different techniques have been used to analyse the data and to characterize the products from the gasification process.

The agglomeration process has been studied by means of the analysis of the pressure fluctuation signals acquired inside a lab-scale fluidised bed. Depending on the relation between the biomass particles density and the bed material density, two clearly different behaviours are observed: jetsam and flotsam. The biomass sinks inside the bed in the first case while, in the second one, the biomass floats on the bed surface due to the higher density of the bed material. The wide band energy, the attractor comparison tool, and the standard deviation methods are used in order to detect agglomeration and, as a consequence, the defluidisation of the bed. The wide band energy analysis shows that, for jetsam fuel particles, the endogenous bubbles produced by the fuel devolatilization inside the bed change the energy distribution, while for flotsam fuel particles, the cap-clinker agglomerate formed is detected by high frequencies in the power spectrum. Similar defluidisation times are obtained for all tested methods, being the defluidisation time of sepiolite experiments considerably higher than in the silica sand tests.

The performance of sepiolite as bed material towards gas composition and tar mitigation has been investigated in a lab-scale fluidised bed gasifier, comparing the results with the same experiments operated with silica sand. The gas produced with sepiolite as bed material has a slightly lower quality than the gas generated with silica sand. However, the tar generation is rather reduced in the sepiolite bed and the tar composition is also different among the bed materials. Sepiolite properties such as surface area and morphology have been analysed by means of specific surface area (BET) and scanning electron microscopy (SEM-EDS) before and after the experiments. The fuel behaviour and the properties of sepiolite induce the adsorption of tars and molten ashes on the sepiolite surface, leading to a much better performance in terms of tars and agglomeration. In addition, a long attrition test of 100 hours has been conducted on the sepiolite, obtaining a smaller attrition rate than other common bed materials such as alumina or dolomite.

A pilot-scale gasifier has been employed to test *Cynara cardunculus* L. with magnesite and olivine as bed materials in terms of gas composition and tar generation. A relatively high hydrogen content in the product gas is obtained in both cases. A positive effect of the gasification temperature is observed in the gasification parameters and efficiency. Small differences in total tar are observed between magnesite and olivine, although tar composition is very different. The benzene, toluene, ethylbenzene and xylenes fraction (BTEX) is higher for olivine while similar polycyclic aromatic hydrocarbon fraction is obtained in both bed materials. Magnesium from magnesite and olivine shows a catalytic behaviour towards tar cracking. Better gasification performance is observed with

magnesite at 700 °C and with olivine at 800 °C.

Finally, the fly ashes from the pilot-scale gasification experiments have been analysed in terms of elemental and metal composition, sulphur and chlorine contents, and leaching behaviour. Most of the elutriated fines are retained, by far, in the first cyclone. The bed material and the reactor materials also influence the final ash composition of the fines. The reuse of these fines is quite difficult in the cement industry or as fertilizer as a consequence of the high carbon, alkali, chlorine and heavy metals contents, being the use as alternative/secondary fuel a good option due to the high energy content in the fines.

# Contents

# List of Figures

# List of Tables

CHAPTER
**ONE**

# Introduction: biomass gasification in fluidised beds

## Contents



## 1.1 Background

Nowadays, global warming is an important environmental problem due to the huge amounts of energy demand by the developed society. As a consequence, there is an urgent need to reduce the greenhouse emissions and the dependence of fossil fuels to generate energy. In this sense, biomass gasification can provide a solution to this problem as its net contribution to the $CO_2$ emissions to the atmosphere is zero. The $CO_2$ produced when burning the products from gasification has been previously absorbed by the plants in the recent past. Besides, the use of biomass has some benefits to the society such as it is a locally grown resource or that every biomass plant can prompt the development of associated industries for biomass growing, collecting, and transporting (Basu, 2010).

Biomass is a broad concept that covers from plants to wastes with a common origin, they all come from living organisms. Around a 15-20 % of the total fuel used in the world is covered by biomass for electricity generation, heating and cooking (Higman & van der Burgt, 2003). However, not every biomass can be used as a fuel in all reactors typology. A suitable selection of biomass and technology for its transformation plays an important role in the proper utilisation of biomass.

## 1.2 Thermochemical conversion processes

Biomass conversion into a useful energy resource can be done by two main different routes: biochemical/biological and thermochemical methods (Figure 1.1). In the first route, three options are available: digestion where a biogas composed mainly by $CH_4$ and $CO_2$ is produced, fermentation where ethanol is produced, and hydrolysis where ehtanol is also the main product. In the second route, three alternatives are possible: pyrolysis, gasification or combustion, depending on the oxygen provided to the processes to produce heat, electricity, chemicals or engine fuels (McKendry, 2002; Basu, 2010). This PhD thesis is focused on one of these thermochemical routes for biomass conversion, gasification, however, the other two technologies will be also briefly introduced in this section.

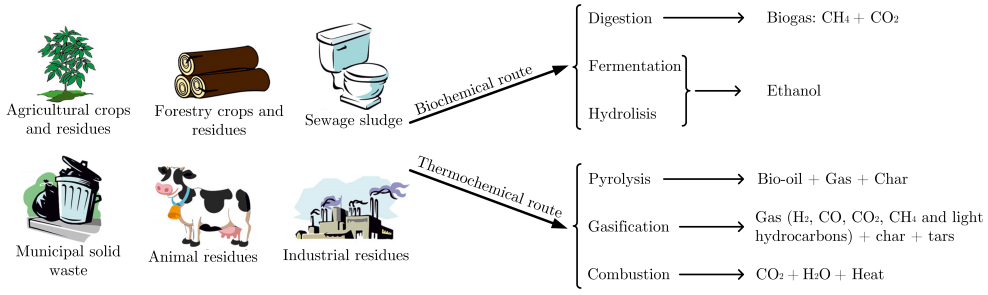


**Figure 1.1:** Biomass conversion routes into a useful energy resource.

Combustion may be the oldest energy conversion method for biomass, since fired was discovered. It consist in an exothermic reaction due to the oxidation of biomass particles to mainly produce $CO_2$, $H_2O$ and heat. This process takes place with $O_2$ enough for stoichiometric reaction as oxidizing element for the totally biomass conversion. The heat released from the combustion procedure can be used to produce steam, generate electricity or district heating, accounting for more than 90 % of the energy produced from biomass (Basu, 2010). This technology offers a wide range of scales, from domestic

heating up to industrial plants. However, the conversion efficiencies are low, between 20 and 40 % (McKendry, 2002).

The exposure of biomass to medium temperatures, between 300 and 600 °C, in the absence of $O_2$ leads to the pyrolysis process. In this second conversion route, the hydrocarbon molecules are converted into smaller ones to get liquid (bio-oil), solid (char) and gaseous fractions (McKendry, 2002). In this case, The distribution of the different fractions depends on the operating conditions such as temperature, heating rate or residence time. The proper selection of these parameters leads to the maximization of the energy products from pyrolysis, being the liquid fraction the most desired product.

A modified process from pyrolysis is torrefaction which also takes place with no $O_2$ but at lower temperatures, between 230 and 300 °C. This process generates different products, mainly $CO_2$, CO, $H_2O$, acetic acid and methanol. However, the relevance of torrefaction is the increase in the energy density of the biomass, the reduction of its weight and the increases in the hygroscopic properties (Basu, 2010).

Gasification, which is located between combustion (excess of $O_2$) and pyrolysis (absence of $O_2$), is a thermochemical process that transforms different carbonaceous materials like biomass into a useful product gas or chemical feedstock (Basu, 2010). The process needs a small amount of oxygen, less than that required for stoichiometric oxidizing conditions, to produce a solid residue or char that is further transformed into combustible gas composed of $H_2$, CO, $CH_4$, $CO_2$, $N_2$ and light hydrocarbons, with limited formation of dioxins, $SO_x$ and $NO_x$, being $NH_3$ and $H_2S$ the main nitrogen and sulphur compounds due to the gasification reduction conditions (Klein, 2002). A small fraction of condensible gases or tars, and ash is also generated. The main product of this thermochemical route is the produced gas which can be directly burned in boilers or gas engines. Besides, the gas can be further treated to generate a more specific product (syngas, $H_2$, $CH_4$ or methanol) (McKendry, 2002). In this sense, the gasification process transforms one fuel to another (gaseous product with useful heating value) with the following benefits (Basu, 2010; Higman & van der Burgt, 2003):

- Increase of the heating value of the fuel due to the rejection of non-combustible species.
- Remove of S and N that are not released to the atmosphere when the gasified fuel is burnt.
- Reduce the carbon-to-hydrogen mass ratio in the fuel, achieving a higher probability of getting a gaseous fuel.
- Increase the energy density by $O_2$ removal.

- The net contribution of $CO_2$ to the atmosphere is zero as the $CO_2$ released when burnt has been previously absorbed by the plants in the recent past.

- The dependence on fossil fuels is reduced.

All these reasons make biomass gasification a promising technology for the production of different liquid and gaseous fuels or synthetic chemicals. It can convert low-priced fuels and waste into high-value chemicals (Basu, 2010).

The gasification process involves different steps as it is shown in Figure 1.2: (1) drying, (2) pyrolysis, (3) partial combustion of gases and char, and (4) gasification of char.

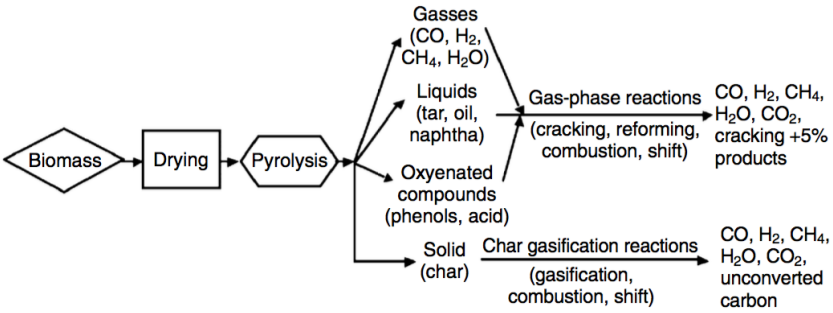


**Figure 1.2:** Gasification sequence (Basu, 2010).

Once the biomass is introduced into the reactor, its moisture content is reduced from wet (10-20 %) to dry state. In the next step, pyrolysis, the large hydrocarbon molecules are thermally split into smaller ones (Basu, 2010). The other two processes, partial combustion and char gasification, are reflected in the following most typical reactions (Higman & van der Burgt, 2003). These reactions occurs simultaneously and involve char, produced gases, steam and $O_2$.

Thermal decomposition or devolatilization:

$$C_xH_yO_zN_r + Heat \rightarrow Char + CO_2 + H_2O + CO + H_2 + CH_4 + N_2 + C_iH_jO_k \quad (1.1)$$

Oxidation reactions:

$$C + {}^1/_2O_2 \rightarrow CO - 111\ kJ/mol \quad (1.2)$$

$$CO + {}^1/_2O_2 \rightarrow CO_2 - 283\ kJ/mol \quad (1.3)$$

$$H_2 + {}^1/_2O_2 \rightarrow H_2O - 242\ kJ/mol \quad (1.4)$$

$$CH_4 + 2O_2 \rightarrow CO_2 + 2H_2O - 283\ kJ/mol \quad (1.5)$$

Char gasification reactions:

$$C + CO_2 \longleftrightarrow 2CO + 172\ kJ/mol \tag{1.6}$$

$$C + H_2O \longleftrightarrow CO + H_2 + 131\ kJ/mol \tag{1.7}$$

$$C + 2H_2 \longleftrightarrow CH_4 - 75\ kJ/mol \tag{1.8}$$

Water gas shift reaction:

$$CO + H_2O \longleftrightarrow CO_2 + H_2 - 41\ kJ/mol \tag{1.9}$$

Steam-reforming reaction:

$$CH_4 + H_2O \longleftrightarrow CO + 3H_2 + 206\ kJ/mol \tag{1.10}$$

Tars dry and steam reforming reactions:

$$C_nH_m(tar) + nCO_2 \rightarrow (m/2)H_2 + 2nCO + \Delta H > 0 \tag{1.11}$$

$$C_nH_m(tar) + nH_2O \rightarrow (n + m/2)H_2 + nCO + \Delta H > 0 \tag{1.12}$$

Cracking reactions:

$$Tar \rightarrow H_2 + CO + CO_2 + Char + C_nH_m \tag{1.13}$$

$$C_nH_m \rightarrow H_2 + Char \tag{1.14}$$

Some of the above reactions are endothermic ($\Delta$H $<$ 0) and the heat required for them is obtained from combustion reactions. From these reactions, the partial oxidation reaction Eqs. 1.2 and 1.9 (partial oxidation and water gas shift reactions, respectively) mainly govern most of the gasification processes (Higman & van der Burgt, 2003).

## 1.3 Gasification technologies

Biomass is a fuel that can come from different origins and regions and, therefore, its physical and chemical properties can differ from one biomass type to another. Additionally, not only plants are used but other residues are also employed. In this second case, sometimes it is difficult to process these residues, being fluidised beds a successful solution for this problem. These reactors can be fed with materials that have different properties and are very dirty. In this way, a useful product is obtained, the residues disappear and there is no need to storage them in a safe place until they are disintegrated. Cost savings and benefits are achieved from non valuable residues. Although this PhD thesis is focused on fluidised bed gasification there are some other technologies such as fixed beds, moving beds or entrained-flow reactors (Figure 1.3).

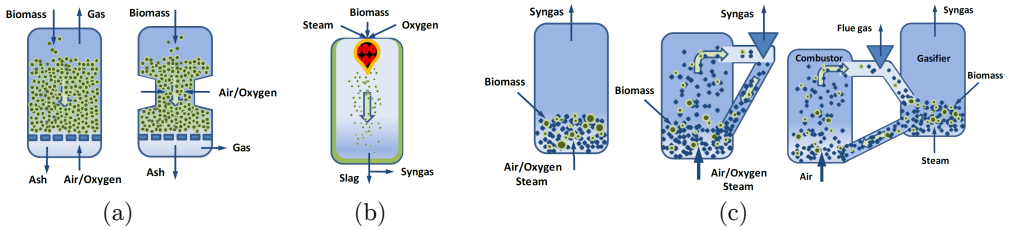


**Figure 1.3:** Gasification technologies: a) moving bed, b) entrained-flow, and c) fluidised bed (E4tech, 2009).

The main characteristic of fixed bed, is that the fuel goes downward as it is converted. A gas flow, typically the produced gas, is usually passed through the reactor in the same or opposite direction of the fuel. The entrained-flow reactor is characterized by a co-current flow of the fuel and a blast, achieving small residence times. These conditions require high temperatures to get a good conversion (Higman & van der Burgt, 2003). A fluidised bed reactor is a two phase system which is formed by particulate solid material and a fluidisation agent. The latter is passed through the former to achieve similar properties than a fluid in terms of movement, and physical properties equal to solids in terms of thermal behaviour (Kunii & Levenspiel, 1991).

The most typical reactors employed in gasification are fixed and fluidised bed reactors (Zhou *et al.*, 2009). However, the liquid-like behaviour of fluidised beds have some advantages over the fixed bed technology: uniform temperature distribution, better temperature control, good gas-solids mixing, better heat and mass transfer rates or wide variety of feedstock quality and size distribution (Kunii & Levenspiel, 1991; Warnecke, 2000).

## 1.4 Operational problems of biomass gasification in fluidised bed

Despite all mentioned benefits from biomass gasification and fluidised beds, some operational problems have to be considered at industrial scale.

### 1.4.1 Agglomeration

One of the major problems in energy conversion systems, such as fluidised bed gasifiers or combustors, is the formation of agglomerates at high temperatures where the chemical composition of the fuel and the bed particles plays an important role. Agglomerates are typically formed due to the interaction between the ash elements from the fuel, mainly

alkali compounds, and the bed material. Alkali elements from biomass tend to volatilize and condensate on the bed particle surface. Depending on the characteristics of both the fuel and the bed particles, the appearance of adhesive inter-particle forces can lead to the agglomerates formation. This phenomena can be formed by a "melt-induce" or by a "coating-induced" process (Visser, 2004). In the first case, particles from bed material and ash are "glue" by a melt phase, while in the second case, particles are coated and sintered together by necks formation between them. This process, could cause the bed defluidisation if it is not promptly detected, and, as a consequence, unscheduled shut downs of the reactor.

The knowledge of the biomass composition, the use of alternative bed materials or the variation of the operating conditions are different ways to prevent the agglomeration within fluidised beds, avoiding the fluidised bed defluidisation. Several authors have studied the influence of these parameters in the defluidisation process. Bartels *et al.* (2008) and Khan *et al.* (2009) reviewed different strategies aimed to alleviate agglomeration in fluidised beds. Some of these strategies try to define operational actions that reduce agglomeration or avoid the bed defluidisation, such as fuel pre-treatment or co-feeding an additional fuel. Abelha *et al.* (2013) used eucalyptus as a secondary fuel to reduce the agglomeration problem. Bed sintering temperature is also an indicator of the bed agglomeration. In this sense, Lin *et al.* (2003) studied the influence of different parameters such as temperature or the particle size on the agglomeration process during wheat straw combustion, finding that low temperatures can extend the fluidisation regimen. Liliedahl *et al.* (2011) investigated the effect of different parameters on the agglomeration behaviour of biomass gasifier and proposed an empirical expression to determine the maximum temperature at which the fluidisation is stable as a function of pressure, ash composition, bed material and gasifying agent. Sevonius *et al.* (2014) used three different pure potassium salts in a quartz sand fluidised bed in order to understand the role of the separate components of the biomass in the agglomeration mechanisms.

Different bed materials such as silica sand, magnesite, olivine or dolomite have been tested to elucidate their effect on the agglomeration process. Silica sand reacts with alkalis and retains them, forming alkali silicates which act as a glue between particles while materials such as dolomite promotes a higher alkali volatilization (Steenari & Lindqvist, 1998; Zevenhoven-Onderwater *et al.*, 2001). According to Bartels *et al.* (2008), bed materials low in or free of silica sand are chosen to avoid the tendency of silica to form low-melting point silicates with alkali salts which cause agglomeration. Lin *et al.* (2003) used sand as bed material during wheat straw combustion, finding $K_2O$-$SiO_2$ compounds deposited on sand particles which produced the agglomeration of the bed. Fryda *et al.* (2008) found no much difference in the defluidisation temperature using sand and olivine, concluding that these bed materials had small chemical interaction with fuel ash. Lime-

stone was used by Fernández Llorente *et al.* (2006), finding no sign of agglomeration due to the adsorption of alkali salts on the particles surface. Liliedahl *et al.* (2011) used magnesite and olivine as bed materials, obtaining a proper operation performance in both cases. defluidisation was avoided, although some clinkers from biomass ash were found inside the bed when using magnesite. The interaction between magnesite and fuel ash was negligible since this bed material has no glass-forming to react with alkali elements. Magnesite showed the best results during the experiments performed by Siedlecki & de Jong (2011) while some agglomeration was detected with sand and olivine. Xue *et al.* (2014) also used magnesite as bed material enhancing the agglomeration behaviour.

Furthermore, some materials are commonly added to the bed in order to reduce/avoid agglomeration and extent the fluidisation state (Werther *et al.*, 2000). Fernández Llorente *et al.* (2008) employed dolomite, lime and kaolin, among other materials, as additives to a silica sand fluidised bed. These materials were effective by the dilution of the biomass ash and only kaolin was capable of reacting with fuel ash, forming compounds with a higher melting point. Siedlecki & de Jong (2011) also used kaolin in their experiments, finding no agglomeration during the tests. The inorganic elements which form the fuel ash have also a significant influence in the bed agglomeration. Different authors have reported agglomeration indicators based on the fuel ash composition (Visser, 2004; Basu, 2006). The most affecting elements among these indicators are potassium, sodium, silicon, calcium and magnesium.

### 1.4.2 Tars

Another major headache in biomass gasification is the generation of a thick, black and highly viscous liquid called tar. This element condenses on those surfaces that have low temperatures leading to the clogging and a reduction in the performance of the different downstream equipments, the formation of tar aerosols or the polymerization into more complex structures (Basu, 2010). Finally, these related issues can lead to unscheduled stops of the gasification plant (Siedlecki *et al.*, 2009). As a consequence, tars are the major barrier for biomass gasification commercialization (Basu, 2010).

The definition of tar is still under discussion, being available several interpretations of this concept. Tar is a complex mixture of condensible hydrocarbons which comprises from single aromatic rings (with or without substituents such as oxygenated groups) up to 5 aromatic rings and complex polycyclic aromatic hydrocarbons (PAHs) (Devi *et al.*, 2003). Kiel *et al.* (2004) defined tar as all organic compounds with a molecular weight larger than benzene, excluding soot and char. However, the most accepted interpretation was proposed by Milne *et al.* (1998) who defined tars as the organics produced under thermal or partial-oxidation regimes of any organic material and generally assumed to

be largely aromatic.

According to Milne *et al.* (1998) tars can be classified in three different groups: primary, secondary and tertiary products. During the biomass devolatilization in the pyrolysis step of gasification, the different components of biomass (cellulose, hemicellulose and lignin) are broken down into primary tar. These type of tars released as low molecular weight oxygenated hydrocarbons start to rearrange above 500 °C to form lighter non condensible gases and heavier molecules called secondary tars. At temperature above 600 °C, primary tars are considered to be completely converted into secondary tars. Secondary tars are formed by phenols and substituted single ring aromatic species. Finally, at higher temperatures, tertiary tars are produced. Tertiary tars are further divided into alkyl tertiary tars which are characterized as aromatics with substituent alkyl chains, and PAHs tertiary tars without substituents. Figure 1.4 shows the distribution of these different groups with temperature.

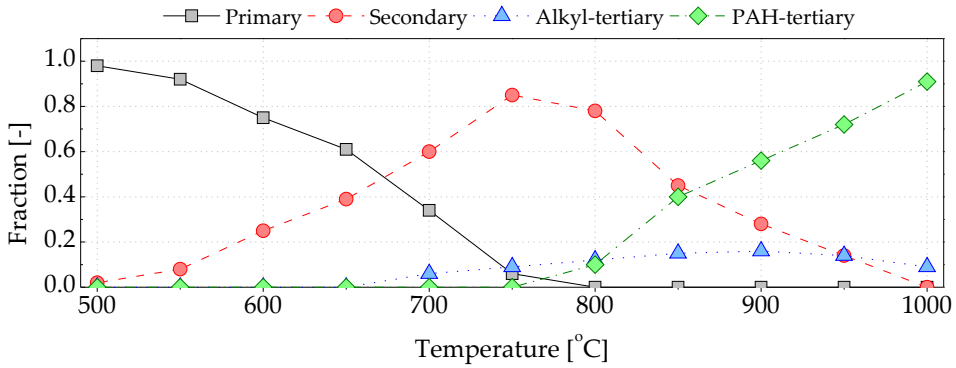


**Figure 1.4:** Distribution of the four tar groups defined by Milne *et al.* (1998). Adapted from Milne *et al.* (1998).

Tars are in a gaseous phase until the temperature of the gas is dropped, making the gas unsuitable for the final application (Basu, 2010). The end use of the product gas determines the requirements for tar concentration: compressing and piping needs less than 600 mg/Nm$^3$; the maximum tar concentration for internal combustion engines is 100 mg/Nm$^3$, being phenols and cresols corrosive for this engines; less than 0.1 mg/Nm$^3$ is required for synthesis applications; or, in the case of close-couple combustors, the gas quality is not a major issue. There are two different methods for tar reduction: primary and secondary methods. The primary methods are focused on avoiding tar generation within the gasifier while the secondary methods concentrates on the cleaning of the produced gas. These methods are available to adapt the gas characteristics to each final application of the gas (Milne *et al.*, 1998).

Different bed materials such as dolomite, magnesite, olivine or metal based catalysts are frequently used in order to reduce tar yield and to improve gas composition (Werther *et al.*, 2000; Sutton *et al.*, 2001). Corella *et al.* (2004) compared dolomite and olivine, concluding that dolomite was better for tar reduction but generated more fine particles than olivine. Many authors have studied the catalytic effect of olivine as bed material with different types of feedstock such as woody biomass or plastic waste, obtaining improvements in gas composition and tar yield compared to silica sand (Devi *et al.*, 2005; Miccio *et al.*, 2009; Mastellone & Arena, 2008). Rapagnà *et al.* (2000) used olivine particles during steam gasification of almond shells, concluding that it had good catalytic activity at temperatures around 800 °C. Siedlecki *et al.* (2009) obtained very promising results using magnesite either as a bed additive or as a bed material. The use of alkali feldspars, bauxite, limestone, activated carbon or ilmenite have also been reported as effective tar reduction materials (Berguerand *et al.*, 2016; Vilches *et al.*, 2016; Pandey *et al.*, 2016; Choi *et al.*, 2016; Larsson *et al.*, 2014; Campoy *et al.*, 2010). In addition to bed material, gasification conditions such as temperature, the biomass throughput, the type of biomass, the gasifying agent or the gasifier configuration also affect tar yield and gas composition (Corella *et al.*, 2008). Gasification temperatures between 700 and 800 °C are critically important in terms of tar mitigation as they are high enough to produce limited quantities of tar and low enough to get tars with an acceptable dew point (Zwart *et al.*, 2010).

The secondary methods include the use of cyclones, barrier filters, wet electrostatic precipitators or wet scrubbers. In this case, these processes generate wastes with high organic compounds, contaminants like acids, $NH_3$ or metals. The disposal of this waste should also be considered for a correct treatment before the final disposal (Basu, 2010).

### 1.4.3 Ash generation

Ash generation is also an important issue that is often overlooked in biomass gasification studies which usually concentrate their attention on gas yields and tar mitigation. In the case of coal/biomass combustion, there is an extensive library of literature which deals with fly ash characterization and utilization; some fly ashes can be used as a cement amendment or for soil stabilization and filler (Ahmaruzzaman, 2010; Kalembkiewicz & Chmielarz, 2012; Rajamma *et al.*, 2009; Freire *et al.*, 2015). However, the information regarding biomass gasification ash is very limited. PAHs, chlorine, heavy metals and high amount of unburned carbon are typical characteristics of gasification fly ashes which differ from those from combustion where minimal unburned carbon and PAHs are found (Ahmaruzzaman, 2010). All these features make the use of gasification fly ashes more complicated and suggest that coal combustion fly ashes utilization methods are not suit-

able for biomass gasification ash, giving rise to the requirement for some treatments (Leiva *et al.*, 2007; Gómez-Barea *et al.*, 2009). Different studies have been performed within the GASASH project (GASASH Project, 2005), trying to find sustainable and economic methods for gasification ash management. Different ash treatment techniques can be applied to the fly ashes: combustion and solidification, water wash and chemical stabilization, pelletization or sintering. Combustion of the fly ashes would reduce the un-reacted carbon and the amount of undesirable compounds such as the PAHs, chlorine and some heavy metals. As a consequence the volume of the fly ashes is reduced, additional heat can be recovered and construction applications can be considered as the new ash generated would have similar properties to combustion ashes. Similar results in terms of un-reacted carbon, PAHs, chlorine and heavy metals can be obtained from sintering processes.

The three main utilization routes for gasification fly ashes are: (1) use as a fuel, (2) use in construction and (3) use in agriculture, with the use as alternative fuel being the most promising when the carbon content is higher than 35 wt.% (GASASH Project, 2005). Construction applications from different biomass fly ashes have been investigated by many authors: concrete paving blocks (Holt & Raivio, 2006), fire-resistant boards (Leiva *et al.*, 2007), lightweight bricks (Gómez-Barea *et al.*, 2009) or clay bricks (Fernández-Pereira *et al.*, 2011). These preliminary studies conclude that fly ashes have high potential as a binding material within different construction elements.

The properties of biomass gasification fly ash collected in different locations of the cleaning section was also investigated by Liao *et al.* (2007). They observed that the more volatile compounds (CaO, $Na_2O$, MgO, Cl, $P_2O_5$, SrO, $As_2O_3$, ZnO and $Al_2O_3$) were mostly found in the ash scrubber while the higher boiling point species (NiO, $Cr_2O_3$, PbO, CuO and MnO) stayed in the cyclone. Narayan *et al.* (2016) found that cyclone ash was dominated by K and Ca silicates. They also found high fractions of K and Ca in the second cyclone. Meij (1994) investigated partitioning of elements in the combustion system and classified the trace elements into three classes according to their volatility: (1) elements that do not vaporize and are equally distributed in bottom and fly ash (class I); (2) elements that vaporize and are found in fly ashes due to condensation on ash particles (class II); and (3) elements that vaporize and condensate partially within the installation (class III). The trace element composition and distribution in the ashes arises not only from the inorganic elements in the fuel, significantly up to 20–25 wt.% can come from the gasifier system like reactor materials, lubricants, etc (Cui *et al.*, 2013).

## 1.5 *C. cardunculus* L. as biomass feedstock for fluidised bed gasification

*Cynara cardunculus* L., commonly known as cardoon or thistle, is a perennial energy crop which is native to Mediterranean regions such as Spain, Portugal or Greece. However, it also grows as weed in some parts of the world like Argentina or California (Ierna & Mauromicale, 2010). This kind of climate, characterized by hot and dry summers, makes it suitable for *C. cardunculus* adaptation (Fernández & Curt, 2005; Ierna & Mauromicale, 2010). Among the Mediterranean countries, Spain has ideal conditions for cardoon production (Zabaniotou *et al.*, 2014). This feedstock can be a good option for biomass gasification as it has some advantages from other plants as stated by Grammelis *et al.* (2008) and Fernández & Curt (2005): low water irrigation, enhancement of soil characteristics, low nitrogen oxides pollution derived from its chemical conversion, low cost, reduction of agro-chemicals and the possibility to grow in lands that are not suitable for food purposes. In addition, cardoon has high volatile matter content (more than 75 wt.% db), an important benefit for biomass gasification (Encinar *et al.*, 2000). All these properties make *C. cardunculus* an interesting option for biomass gasification.

Different studies based on the cultivation of this specie (Fernández & Curt, 2005; Grammelis *et al.*, 2008; Gominho *et al.*, 2011; Angelini *et al.*, 2009; Papazoglou & Rozakis, 2011) have been carried out due to its importance for biomass production. These analyses show a cardoon production between 1.4 and 25 $t_{db}$/ha·year, depending on the irrigation and annual rainfall. Papazoglou & Rozakis (2011) performed an economic analysis for *C. cardunculus* production including establishment and operating costs. Results show an annual cost of 71 and 62 €/t for non-irrigated and irrigated lands, respectively (discount rate of 8 % in 10 years for the annualized installation cost). In Spain, the energy use of cardoon has been investigated under the CARDENER-CM project. However, little literature has been published regarding *Cynara cardunculus* L. gasification. Herguido *et al.* (1992) gasified different biomasses in a bubbling fluidised bed with steam, including *C. cardunculus*, studying the effect of temperature on gas composition, char and tar yields using silica sand as the bed material. Their results showed both low gas yield and carbon conversion, and high char yield. Encinar *et al.* (2000) studied the pyrolysis of *Cynara* in order to determine the quality of the charcoal formed and identify and quantify the gases produced. They also performed steam gasification studies (Encinar *et al.*, 2002), obtaining higher $H_2$ yield in the case of steam gasification than pyrolysis under the same temperature. High temperature favoured the generation of $H_2$ and CO, as well as gas yield and conversion rates. Recently, Abelha *et al.* (2013) reported results on *Cynara* combustion, gasification, co-combustion and co-gasification with *Eu-*

*calyptus globulus*. The addition of eucalyptus in ratios higher than 80 %w/w reduced the agglomeration caused by the high alkali content of *Cynara* in the combustion and gasification experiments while agglomeration during combustion was completely avoided if a dolomite catalyst was added to the silica sand fluidised bed, even with low concentrations of eucalyptus. However, higher amounts of $H_2$ and low tar content were obtained when eucalyptus was not used and cardoon was gasified on its own with air and steam. Similar results in terms of bed agglomeration were reported by Christodoulou *et al.* (2014*b*) who used giant reed in combination with *C. cardunculus*, employing magnesite and olivine as bed materials i.e. agglomeration occurred when cardoon only was gasified either with magnesite or olivine. In another study, Christodoulou *et al.* (2014*a*) analysed the agglomerates obtained from gasifying cardoon in an olivine bed. The agglomerates were found to be formed by a melted phase rich in sodium, potassium, calcium, magnesium and silicon. Zabaniotou *et al.* (2014) gasified *C. cardunculus* in a fixed bed reactor for different equivalent ratios and temperatures. They concluded that the product gas obtained by fixed bed air gasification was similar to steam gasification in terms of $H_2$ and CO, with high a $H_2$ content. As a result they suggested cardoon gasification as a possible route for $H_2$ production.

These studies show that the use of different bed materials can delay agglomeration and suggest that dolomite can be used to completely avoid it although the attention should be centred on the elevated attrition of dolomite. Cardoon co-gasification with other types of biomass such as woody biomass (e.g. eucalyptus or giant reed) appears to be a promising strategy to mitigate agglomeration problems.

## 1.6 Scope of the thesis

Biomass will play an important role in the future of energy production not only due to the need of use renewable fuels but also due to the need of deal with all kind of organic residues generated by human beings. In this sense, gasification in a fluidised bed is a possible technology to achieve the conversion of biomass into an useful gas that can be use afterwards for electricity generation or the production of chemicals. However, the above mentioned problems such as bed agglomeration, tar production and, fines and ash generation motivates the following objectives of the present PhD thesis.

- Investigate the use of *Cynara cardunculus* L. as biomass feedstock for gasification.
- Propose a new bed material, sepiolite, for fluidised bed gasification instead of the commonly used silica sand, studying the effect of the bed material and combustible behaviour in the bed dynamics towards bed agglomeration and defluidisation.

- Investigate the agglomeration processes and mechanisms using different analysis techniques based on pressure fluctuation measurements.
- Analyse the advantages and disadvantages of the new bed material in terms of the gas composition and tar mitigation.
- Evaluate the mechanical resistance of sepiolite towards the attrition phenomena.
- Study the effect of the temperature and more commonly used bed materials such as magnesite and olivine in the *Cynara cardunculus* L. gasification.
- Give a detailed analysis of tar composition generated during *Cynara cardunculus* L. gasification with different bed materials.
- Evaluate the properties of fines and ash generation during *Cynara cardunculus* L. gasification in order to give a possible solution to deal with these residues.

## 1.7 Outline of the thesis

This PhD thesis presents an experimental research on the use of *Cynara cardunculus* L. as biomass feedstock and sepiolite as an alternative bed material for gasification in air bubbling fluidised bed gasifiers. The different studies in which this PhD thesis is composed have been arranged in according to a a logical order to ease the reading of the thesis. It is organized in seven chapters summarized as follows.

In Chapter 1 an introduction to biomass gasification and its main operating problems is addressed. In addition, *Cynara cardunclus* L. is introduced as biomass feedstock for gasification. Finally, the scope of the thesis is presented.

In Chapter 2 the properties of the biomass and bed materials employed are described. The different experimental facilities (lab-scale gasifier, pilot plant gasifier and cold fluidised bed) as well as the analysis techniques and equipments are presented.

In Chapter 3 sepiolite is proposed as an alternative bed material to silica sand for biomass gasification. In this first study the agglomeration process of jetsam and flotsam fuel particles during the gasification of *C. cardunculus* L. in a lab-scale fluidised bed is analysed. Pressure fluctuation signals are studied in the frequency domain, by means of the wide band energy, and in the state space employing the attractor comparison tool. Furthermore, the definition of a proper reference state during the gasification process is also discussed. In addition, the defluidisation time, the particle size distribution of the bed material and the agglomerates formed during the gasification experiments are studied.

In Chapter 4 sepiolite is tested in terms of gas and tar composition, and gasification performance under gasification conditions using *C. cardunculus* L. as biomass feedstock. Silica sand is used as reference bed material. The tar composition is divided into total tar and individual species. Sepiolite is further analysed after the experiments by BET surface area and SEM-EDS to check its surface properties and have a better understanding of the gasification process using sepiolite as bed material. Finally, an attrition test over sepiolite is performed in order to check its mechanical resistance.

Chapter 5 focuses on air gasification of this *Cynara cardunculus* L. and examines the role of temperature (between 700 and 800 °C), and the commonly used bed materials, magnesite and olivine, with kaolin amended cardoon on agglomeration. The gas composition and the gasification performance and efficiency is analysed. A detailed tar analysis is undertaken and the tars are evaluated in terms of total tar and the main individual compounds. Finally, a mass balance is carried out to check the consistency of the results and to obtain information for future works.

In Chapter 6 the entrained fines collected from the experiments performed in the previous Chapter are analyzed. For this purpose, a deep characterization is carried out on the different samples from the gasification tests: carbon, hydrogen, nitrogen and sulphur contents, loss on ignition, moisture, ash, lower heating value, chlorine and metal composition. According to these characteristics, the different possible applications employed for combustion fly ashes are evaluated for cardoon fly ashes in order to elucidate if they meet the specific requirements for each utilization.

Finally, the conclusions obtained in this PdD thesis are summarized in Chapter 7.

# References

Abelha, P., Franco, C., Pinto, F., Lopes, H., Gulyurtlu, I., Gominho, J., Lourenço, A. & Pereira, H. 2013 Thermal conversion of *Cynara cardunculus* L. and mixtures with *Eucalyptus globulus* by fluidized-bed combustion and gasification. *Energy & Fuels* 27, 6725–6737.

Ahmaruzzaman, M. 2010 A review on the utilization of fly ash. *Progress in Energy and Combustion Science* 36, 327–363.

Angelini, L. G., Ceccarini, L., Nassi o Di Nasso, N. & Bonari, E. 2009 Long-term evaluation of biomass production and quality of two cardoon (*Cynara Cardunculus* L.) cultivars for energy use. *Biomass & Bioenergy* 33, 810–816.

Bartels, M., Lin, W., Nijenhuis, J., Kapteijn, F. & van Ommen, J. R. 2008 Agglomeration in fluidized beds at high temperatures: Mechanisms, detection and prevention. *Progress in Energy & Combustion Science* 34, 633–666.

Basu, P. 2006 *Combustion and gasification in fluidized beds*, 1st edn. CRC Press.

Basu, P. 2010 *Biomass Gasification and Pyrolysis: Practical Desing and Teory*, 1st edn. Elsevier Inc.

Berguerand, N., Marinkovic, J., Vilches, T. B. & Thunman, H. 2016 Use of alkali-feldspar as bed material for upgrading a biomass-derived producer gas from a gasifier. *Chemical Engineering Journal* 295, 80–91.

Campoy, M., Gómez-Barea, A., Fuentes-Cano, D. & Ollero, P. 2010 Tar reduction by primary measures in an autothermal air-blown fluidized bed biomass gasifier. *Industrial & Engineering Chemistry Research* 49, 11294–11301.

Choi, Y. K., Cho, M. H. & Kim, J. S. 2016 Air gasification of dried sewage sludge in a two-stage gasifier. Part 4: Application of additives including Ni-impregnated activated carbon for the production of a tar-free and $H_2$-rich producer gas with a low $NH_3$ content. *International Journal of Hydrogen Energy* 41, 1460–1467.

Christodoulou, C., Koutsoumpa, E.-I., Panopoulos, K. D., Karellas, S. & Kakaras, E. 2014*a* Agglomeration problems during cardoon fluidized bed gasification. *Thermal Science* 18, 645–656.

Christodoulou, C., Tsekos, C., Tsalidis, G., Fantini, M., Panopoulos, K. D., de Jong, W. & Kakaras, E. 2014*b* Attempts on cardoon gasification in two different ciculating fluidized beds. *Cases Studies in Thermal Engineering* 4, 42–52.

Corella, J., Toledo, J. M. & Molina, G. 2008 Biomass gasification with pure steam in fluidised bed: 12 variables that affect the effectiveness of the biomass gasifier. *International Journal of Oil, Gas and Coal Technology* 1, 194–207.

Corella, J., Toledo, J. M. & Padilla, R. 2004 Olivine or dolomite as in-bed additive in biomass gasification with air in a fluidized bed: Which is better? *Energy & Fuels* 18, 713–720.

Cui, H., Turn, S. Q., Keffer, V., Evans, D., Tran, T. & Foley, M. 2013 Study on the fate of metal elements from biomass in a bench-scale fluidized bed gasifier. *Fuel* 108, 1–12.

Devi, L., Ptasinski, K. J. & Janssen, F. J. J. G. 2003 A review of the primary measures for tar elimination in biomass gasification processes. *Biomass & Bioenergy* 24, 125–140.

Devi, L., Ptasinski, K. J., Janssen, F. J. J. G., van Paasen, S. V. B., Bergman, P. C. A. & Kiel, J. H. A. 2005 Catalytic decomposition of biomass tars: use of dolomite and untreated olivine. *Renewable Energy* 30, 565–587.

E4tech 2009 Review of technologies for gasification of biomass and wastes. NNFC project 09/008. *Tech. Rep.* E4tech.

Encinar, J. M., González, J. F. & González, J. 2000 Fixed-bed pyrolysis of *Cynara cardunculus* L. Product yields and compositions. *fuel* 68, 209–222.

Encinar, J. M., González, J. F. & González, J. 2002 Steam gasification of *Cynara cardunculus* L.: influence of variables. *Fuel Processing Technology* 75, 27–43.

Fernández, J. & Curt, M. D. 2005 State of the art of *Cynara cardunculus* L. as an energy crop. In *$14^{th}$ European Conference and Technology Exhibition on Biomass for Energy, Industry and Climate Protection*. Paris, France.

Fernández Llorente, M. J., Díaz Arocas, P., Gutiérrez Nebot, L. & Carrasco García, J. E. 2008 The effect of the additiion of chemical materials on the sintering of biomass ash. *Fuel* 87, 2651–2658.

Fernández Llorente, M. J., Escalada Cuadrado, R., Murillo Laplaza, J. M. & Carrasco García, J. E. 2006 Combustion in bubbling fluidised bed with bed material of limestone to reduce the biomass ash agglomeration and sintering. *Fuel* 85, 2081–2092.

Fernández-Pereira, C., de la Casa, J. A., Gómez-Barea, A., Arroyo, F., Leiva, C. & Luna, Y. 2011 Application of biomass gasification fly ash for brick manufacturing. *Fuel* 90, 220–232.

Freire, M., Lopes, H. & Tarelho, L. A. C. 2015 Critical aspects of biomass ashes utilization in soils: Composition, leachability, PAH, and PCDD/F. *Waste Management* 46, 304–315.

Fryda, L. E., Panopoulos, K. D. & Kakaras, E. 2008 Agglomeration in fluidised bed gasification of biomass. *Powder Technology* 181, 307–320.

GASASH Project 2005 GASASH - The improvement of the economics of biomass/waste gasification by higher carbon conversion and advanced ash management. ENK5-2001-00635. *Tech. Rep.*

Gómez-Barea, A., Vilches, L. F., Leiva, C., Campoy, M. & Fernández-Pereira, C. 2009 Plant optimisation and ash recycling in fluidised bed waste gasification. *Chemical Engineering Journal* 146, 227–236.

Gominho, J., Lourenço, A., Palma, P., Lourenço, M. E., Curt, M. D., Fernández, J. & Pereira, H. 2011 Large scale cultivation of *Cynara cardunculus* L. for biomass production - A case study. *Industrial Crops and Products* 33, 1–6.

Grammelis, P., Malliopoulou, A., Basinas, P. & Danalatos, N. G. 2008 Cultivation and characterization of *Cynara Cardunculus* for solid biofuels production in the Mediterranean region. *International Journal of Molecular Sciences* 9, 1241–1258.

Herguido, J., Corella, J. & González-Saiz, J. 1992 Steam gasification of lignocellulosic residues in a fluidized bed at a small pilot scale. Effect of the type of feedstock. *Industrial & Engineering Chemical Research* 31, 1275–1282.

Higman, C. & van der Burgt, M. 2003 *Gasification*, 1st edn. Gulf Professional Publishing.

Holt, E. & Raivio, P. 2006 Use of gasification residues in compacted concrete paving blocks. *Cement and Concrete Research* 36, 441–448.

Ierna, A. & Mauromicale, G. 2010 *Cynara cardunculus* L. genotypes as a crop for energy purposes in a Mediterranean environment. *Biomass & Bioenergy* 34, 754–760.

Kalembkiewicz, J. & Chmielarz, U. 2012 Ashes from co-combustion of coal and biomass: New industrial wastes. *Resources, Conservation & Conservation* 69, 109–121.

Khan, A. A., de Jong, W., Jansens, P. J. & Spliethoff, H. 2009 Biomass combustion in fluidized bed boilers: Potential problems and remedies. *Fuel Processing Technology* 90, 21–50.

Kiel, J. H. A., van Paasen, S. V. B., Neeft, J. P. A., Devi, L., Ptasinski, K. J., Janssen, F. J. J. G., Meijer, R., Berends, R. H., Temmink, H. M. G., Brem, G., Padban, N. & Bramer, E. A. 2004 Primary measures to reduce tar formation in fluidised-bed biomass gasifiers. ECN-C-04-014. *Tech. Rep.* Energy Research Centre of The Netherlands.

Klein, A. 2002 Gasification: An alternative process for energy recovery and disposal of municipal solid wastes. PhD thesis, Columbia University.

Kunii, D. & Levenspiel, O. 1991 *Fluidization engineering*, 2nd edn. Butterworth-Heinemann.

Larsson, A. Israelsson, M., Lind, F., Seemann, M. & Thunman, H. 2014 Using ilmenite to reduce the tar yield in a dual fluidized bed gasification system. *Energy & Fuels* 28, 2631–2644.

Leiva, C., Gómez-Barea, A., Vilches, L. F., Ollero, P., Vale, J. & Fernánde-Pereira, C. 2007 Use of biomass gasification fly ash in lightweight plasterboard. *Energy & Fuels* 21, 361–367.

Liao, C., Wu, C. & Yan, Y. 2007 The characteristics of inorganic elements in ashes from a 1 MW CFB biomass gasification power generation plant. *Fuel Processing Technology* 88, 149–156.

Liliedahl, T., Sjöström, K., Engvall, K. & Rosén, C. 2011 Defluidisation of fluidised beds during gasification of biomass. *Biomass & Bioenergy* 35, S63–S70.

Lin, W., Dam-Johansen, K. & Frandsen, F. 2003 Agglomeration in bio-fuel fired fluidized bed combustors. *Chemical Engineering Journal* 96, 171–185.

Mastellone, M. L. & Arena, U. 2008 Olivine as a tar removal catalyst during fluidized bed gasification on plastic waste. *AIChE Journal* 54, 1656–1667.

McKendry, P. 2002 Energy production from biomass (part 2): conversion technologies. *Bioresource Technology* 83, 47–54.

Meij, R. 1994 Trace element behavior in coal-fired power plants. *Fuel Processing Technology* 39, 199–217.

Miccio, F., Piriou, B., Ruoppolo, G. & Chirone, R. 2009 Biomass gasification in a catalytic fluidized reactor with beds of different materials. *Chemical Engineering Journal* 154, 369–374.

Milne, T. A., Evans, R. J. & Abatzoglou, N. 1998 Biomass gasifier "tars": Their nature , formation and conversion. NREL/TP-570-25357. *Tech. Rep.* National Renewable Energy Laboratory.

Narayan, V., Jensen, P. A., Henriksen, U. B., Egsgaard, H., Nielsen, R.G. & Glarborg, P. 2016 Behavior of alkali metals and ash in a low-temperature circulating fluidized bed (LTCFB) gasifier. *Energy & Fuels* 30, 1050–1061.

Pandey, D. S., Kwapinska, M., Gómez-Barea, A., Horvat, A., Fryda, L. E., Rabou, L. P. L. M., Leahy, J. J. & Kwapinski, W. 2016 Poultry litter gasification in a fluidized bed reactor: effects of gasifying agent and limestone addition. *Energy & Fuels* 30, 3085–3096.

Papazoglou, E. G. & Rozakis, S. 2011 Utilization of ashes from biomass combustion and gasification. In *3rd International CEMEPE & SECOTOX Conference*, pp. 637–642. Skiathos, Greece.

Rajamma, R., Ball, R. J., Tarelho, L. A. C., Allen, G. C., Labrincha, J. A. & Ferreira, V. M. 2009 Characterisation and use of biomass fly ash in cement-based materials. *Journal of Hazardous Materials* 172, 1049–1060.

Rapagnà, S., Jand, N., Kiennemann, A. & Foscolo, P. U. 2000 Steam-gasification of biomass in a fluidised-bed of olivine particles. *Biomass & Bioenergy* 19, 187–197.

Sevonius, C., Yrjas, P. & Hupa, M. 2014 Defluidization of a quartz bed - Laboratory experiments with potassium salts. *Fuel* 127, 161–168.

Siedlecki, M. & de Jong, W. 2011 Biomass gasification as the first hot step in clean syngas production process - gas quality optimization and primary tar reduction measures in a 100 kW thermal input steam-oxygen blown CGB gasifier. *Biomass & Bioenergy* 35, S40–S62.

Siedlecki, M., Nieuwstraten, R., Simeone, E., de Jong, W. & Verkooijen, H. M. 2009 Effect of magnesite as bed material in a 100 $kW_{th}$ steam-oxygen blown circulating fluidized-bed biomass gasifier on gas composition and tar formation. *Energy & Fuels* 23, 5643–5654.

Steenari, B.-M. & Lindqvist, O. 1998 High-temperature reactions of straw ash and the anti-sintering additives kaolin and dolomite. *Biomass & Bioenergy* 14, 67–76.

Sutton, D., Kelleher, B. & Ross, J. R. H. 2001 Review of literature on catalysts for biomass gasification. *Fuel Processing Technology* 73, 155–173.

Vilches, T. B., Marinkovic, J., Seemann, M. & Thunman, H. 2016 Comparing active bed materials in a dual fluidized bed biomass gasifier: olivine, bauxite, quartz-sand and ilmenite. *Energy & Fuels* 30, 4848–4857.

Visser, H. J. M. 2004 The influence of fuel composition on agglomeration behaviour in fluidised-bed combustion. ECN-C-04-054. *Tech. Rep.* Energy Research Centre of The Netherlands.

Warnecke, R. 2000 Gasification of biomass: comparison of fixed bed and fluidized bed gasifier. *Biomass & Bioenergy* 18, 489–497.

Werther, J., Saenger, M., Hartge, E.-U., Ogada, T. & Siagi, Z. 2000 Combustion of agricultural residues. *Progress in Energy and Combustion Science* 26, 1–27.

Xue, G., Kwapinska, M., Horvat, A., Li, Z., Dooley, S., Kwapinski, W. & Leahy, J. J. 2014 Gasification of *Miscanthus x giganteus* in an air-blown bubbling fluidized bed: A preliminary study of performance and agglomeration. *Energy & Fuels* 28, 1121–1131.

Zabaniotou, A., Bitou, P., Kanellis, Th., Manara, P. & Stavropoulos, G. 2014 Investigating *Cynara C.* biomass gasification producer gas suitability for CHP, second generation biofuels, and $h_2$ production. *Industrial Crops and Products* 61, 309–316.

Zevenhoven-Onderwater, M., Backman, R., Skrifvars, B.-J. & Huppa, M. 2001 The ash chemistry in fluidised bed gasification of biomass fuels. Part I: predicting the chemistry of melting ashes and ash-bed material interaction. *Fuel* 80, 1489–1502.

Zhou, J., Chen, Q., Zhao, H., Cao, X., Mei, Q., Luo, Z. & Cen, K. 2009 Biomass-oxygen gasification in a high-temperature entrained-flow gasifier. *Biotechnology Advances* 27, 606–611.

Zwart, R., van der Heijden, S., Emmen, R., Bentzen, J. D., Stoholm, P. & Krogh, J. 2010 Tar removal from low-temperature gasifiers. ECN-C-10-008. *Tech. Rep.* Energy Research Centre of The Netherlands.

CHAPTER
**TWO**

# Materials, experimental setup and methodology

**Contents**



## 2.1 Introduction

The results presented in this PhD thesis have been obtained using *Cynara cardunculus* L. as biomass feedstock. Silica sand, sepiolite, olivine and magnesite have been used as bed materials. The experiments have been carried out in three different experimental facilities. The first set of experiments has been carried out in a lab-scale bubbling fluidised bed reactor located at the Carlos III University of Madrid. The second set of experiments has been performed in a pilot scale bubbling fluidised bed gasifier located at the

University of Limerick (Limerick, Ireland). Finally, a third experimental campaign has been performed in a cold fluidised bed located at the Paul Scherrer Institute (Villigen, Switzerland).

## 2.2 Biomass feedstock

*Cynara cardunculus* L., cardoon or thistle, is employed as the biomass feedstock in this PhD thesis. As introduced in Chapter 1, cardoon has suitable properties to be a good option for biomass gasification such as high volatile matter content or environmental benefits during its cultivation.

Different equipments have been used to get a proper characterization of this biomass feedstock: proximate and elemental analyses, higher heating value (HHV), inorganic ash composition, and chemical composition of the biomass. All the samples have been digested in $H_2O_2$, $HNO_3$, $H_2SO_4$ and HF prior to analysis by atomic absorption. These cardoon properties are shown in Tables 2.1, 2.2, 2.3 and 2.4.

Due to the high amounts of alkali metals of *C. cardunculus*, mainly K and Na (Table 2.4), and the agglomeration problems reported in the literature when gasifying this energy crop (Christodoulou *et al.*, 2014*b*,*a*; Abelha *et al.*, 2013), kaolin ($Al_2Si_2O_5(OH)_4$) has been used in some experiments to reduce/avoid agglomeration. The amount of kaolin added is 3 wt.% of the biomass loaded into the feeding system, similar to the quantity used by Fernández Llorente *et al.* (2008) and Weber & Quicker (2013).

**Table 2.1:** Proximate analysis [wt.% ar] and higher heating value [$MJ/kg_{db}$] of biomass.

| | Moisture[1] | Volatile matter[2] | Fixed carbon[2,a] | Ash[3] | HHV[4] |
|---|---|---|---|---|---|
| Cardoon | 7.03 | 72.29 | 15.01 | 5.67 | 17.80 |
| Cardoon + kaolin* | 9.69 | 69.83 | 10.21 | 10.27 | 17.73 |

*3 wt.% of cardoon, [a]by difference, [1]drying oven (Memmert UFE 500),
[2]thermogravimetric analyzer (Q500 TA Instruments),
[3]ash furnace (Lenton SAF 11/1),
[4]isoperibolic calorimeter (Parr 6300)

Biomass is received as cylindrical pellets of approximately 6 mm in diameter with lengths varying from 5 to 25 mm. Different particle size has been used in the each of the experiments performed in this PhD thesis. In Chapter 3, cardoon pellets have been selected with a length of 15 mm, a mean mass of 0.50 g, an apparent density of 1220.48 $\pm$ 66.20 $kg/m^3$ and a bulk density of 623.37 $\pm$ 4.67 $kg/m^3$. In Chapter 4, pellets have been crushed and sieved into a smaller particle size, using a chopping machine (Retsch

**Table 2.2:** Elemental analysis of biomass [wt.% db].

| | C | H | N | S | Cl | O[a] |
|---|---|---|---|---|---|---|
| Cardoon | 48.11 | 5.58 | 0.80 | ND | ND | 39.42 |
| Cardoon + kaolin* | 48.91 | 5.90 | 0.58 | 0.04 | 0.12 | 33.08 |

*3 wt.% of cardoon, [a]by difference, ND: Not determined
CHN-S analyser (Leco TruSpec)

SM 2000) and a sieving machine (Retsch AS 200), as the original pellets are too large for the feeding system requirements. In this case, particle size ranges between 2.50 and 4.75 mm with a bulk density of 442.82 ± 9.14 kg/m$^3$. Finally, in Chapters 5 and 6, biomass particle size ranges between 1 and 5 mm with a mean particle size of 2.86 ± 0.19 mm and bulk density of 487.01 ± 28.52 kg/m$^3$, in order to satisfy the feeding requirements (Figure 2.1).

**Table 2.3:** Chemical composition of biomass [wt.% db].

| | Hemicellulose | Cellulose | Lignin | Extractives |
|---|---|---|---|---|
| Cardoon + kaolin* | 17.53 | 31.41 | 17.69 | 7.86 |

*3 wt.% of cardoon


**Figure 2.1:** Biomass employed: a) cardoon pellets, b) crushed cardoon pelltets (2.5 mm < $d_p$ < 4.75 mm) and c) crushed cardoon pellets with kaolin (1 mm < $d_p$ < 5 mm).

## 2.3 Bed materials

Different bed materials have been employed in the experiments: silica sand, olivine, magnesite and sepiolite (clay) (Figure 2.2). Silica sand ($SiO_2$) is an inert material that has been widely used in fluidised bed gasification because it is a cheap and abundant material (Skoulou *et al.*, 2008). However, it can present some problems related with bed

**Table 2.4:** Ash composition [g/kg$_{ash\ db}$] and trace metals [mg/kg$_{ash\ db}$] of biomass.

| *Ash analysis* | Al | Ca | Cu | Fe | K | Mg | Na | Si | Se |
|---|---|---|---|---|---|---|---|---|---|
| Cardoon | 0.76 | 9.94 | ND | 0.65 | 9.40 | 2.27 | 6.48 | 0.03 | trace |
| Cardoon + kaolin* | 122.66 | 167.27 | 5.69 | 10.37 | 95.90 | 20.07 | 274.32 | 383.60 | 6.13 |

| *Trace metals* | As | Cd | Co | Cr | Mn | Mo | Ni | Pb | Zn |
|---|---|---|---|---|---|---|---|---|---|
| Cardoon + kaolin* | ND | 223.02 | 245.32 | 111.51 | 563.13 | 892.08 | 485.31 | 11.15 | 345.68 |

*3 wt.% of cardoon, ND: Not determined

Atomic absorption (Varian Spectra A220)

agglomeration if the biomass has high alkali content, leading to a partial or complete agglomeration of the bed with the subsequent bed defluidisation (Brus *et al.*, 2005). Olivine ($(Mg,Fe_2)SiO_4$) and magnesite ($MgCO_3$) are commonly used in biomass gasification in order to avoid agglomeration, to reduce tar yield and to improve gas composition (Werther *et al.*, 2000; Sutton *et al.*, 2001). Finally, sepiolite, a natural occurring clay ($Mg_8Si_12O_30(OH)_4(OH_2)_48H_2$) and with Spain as the largest producer (about 95 % of the world's annual production in the last decade (Murray *et al.*, 2011)), is proposed as an alternative bed material to silica sand due to its adsorbent properties, chemical and mechanical stability and high surface area (∼300 m$^2$/g) (Pecharromán *et al.*, 2006; Dogan *et al.*, 2007; Zadaka-Amir *et al.*, 2013).

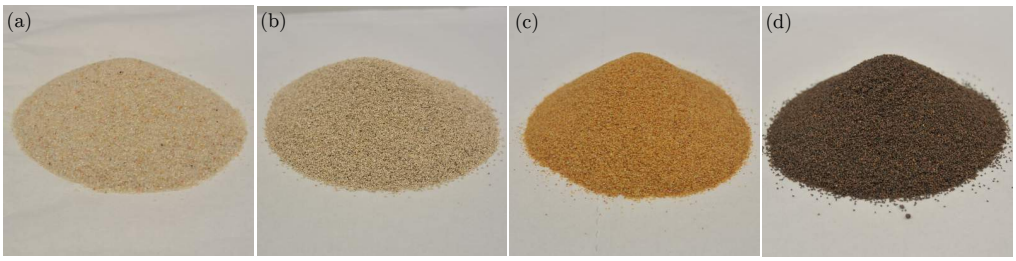


**Figure 2.2:** Bed materials: a) silica sand, b) sepiolite, c) magnesite and d) olivine.

All of these bed materials are natural occurring and, therefore, they are cheap and abundant. Silica sand is selected as the reference material for agglomeration and gasification tests as it is the most common bed material used for gasification. Sepiolite is selected and proposed as an alternative to silica sand in order to reduce agglomeration and improve gas and tar generation as, to the author knowledge, it has not been used in fluidised bed combustors or gasifiers before. Therefore, its use is a novelty from this PhD thesis in which its performance for gasification purposes is investigated. Olivine and magnesite are chosen due to their lower cost than metal based catalysts, their better mechanical properties and relatively good tar reduction properties reported in literature (Werther

*et al.*, 2000; Sutton *et al.*, 2001; Corella *et al.*, 2004). These last materials are tested in separate experiments in order to compare their catalytic effects during *C.cardunculus* gasification at different temperatures.

Silica sand, sepiolite, magnesite and olivine are characterized in terms of density, bulk density, void fraction and minimum fluidization velocity. The bed materials are sieved to between 425 and 600 $\mu$m in the case of silica sand and sepiolite, and between 300 and 500 $\mu$m for olivine and magnesite. In the case of attrition tests, the mean particle size of sepiolite is 226 $\mu$m. The choice of a smaller particle size of sepiolite for attrition experiments is to compare the results with different materials that have are already in the literature. The main properties of these bed materials are summarized in Table 2.5. Taking into account the bed material densities and particle sizes, all of them belong to type B materials according to Geldart's classification (Geldart, 1973).The minimum fluidization ($u_{mf}$) velocity for the different bed materials has been determined prior to the gasification experiments measuring the $\Delta$P of the bed versus the superficial gas velocity.

**Table 2.5:** Bed materials properties.

| | Silica sand | Sepiolite | Magnesite | Olivine |
|---|---|---|---|---|
| Density [kg/m$^3$] | 2645 | 1551 | 3207 | 3146 |
| Bulk density [kg/m$^3$] | 1481 | 558 | 1358 | 1314 |
| Void fraction [–] | 0.44 | 0.64 | 0.58 | 0.58 |
| Mean particle diameter [$\mu$m] | 512 | 512 (226$^\star$) | 391 | 407 |
| Minimum fluidization velocity [m/s] | 0.089$^\dagger$ | 0.057$^\dagger$ (0.032$^\star$) | 0.085$^\ddagger$ | 0.082$^\ddagger$ |
| Supplier | INCUSA (Spain) | TOLSA (Spain) | MINELCO (U. K.) | Magnolithe (Austria) |
| $^\dagger$at 850 $^o$C, $^\ddagger$at 750 $^o$C, $^\star$for attrition test at 27 $^o$C | | | | |
| Composition [wt.%] | | | | |
| $SiO_2$ | 96.00 | 65.10 | 21.10 | 88.33 |
| MgO | 0.02 | 14.30 | 74.05 | 2.69 |
| $Fe_2O_3$ | 0.07 | 1.31 | 0.63 | 6.59 |
| CaO | 0.07 | 1.21 | 0.84 | – |
| $K_2O$ | 2.50 | 1.75 | – | – |
| $Al_2O_3$ + $Cr_2O_3$ + $Mn_3O_4$ | 2.40 | 5.78 | 3.35 | 2.69 |

## 2.4 Lab-scale BFB

A lab-scale bubbling fluidised bed gasifier is employed for the experiments presented in Chapters 3 and 4. This experimental plant is located in the Energy Systems Engineering Research Group (ISE) laboratories at the Carlos III University of Madrid. It consists on

a stainless steel 304 reactor with an inner diameter of 52.8 mm. The reactor is divided into two sections: a lower part or plenum where the gasifying agent is preheated, and an upper part where the bed is located. These two sections have a total length of 570 and 910 mm, respectively. At the top of the reactor a mirror is located to see inside the gasifier. A schematic diagram of the lab-scale gasifier is shown in Figure 2.3.

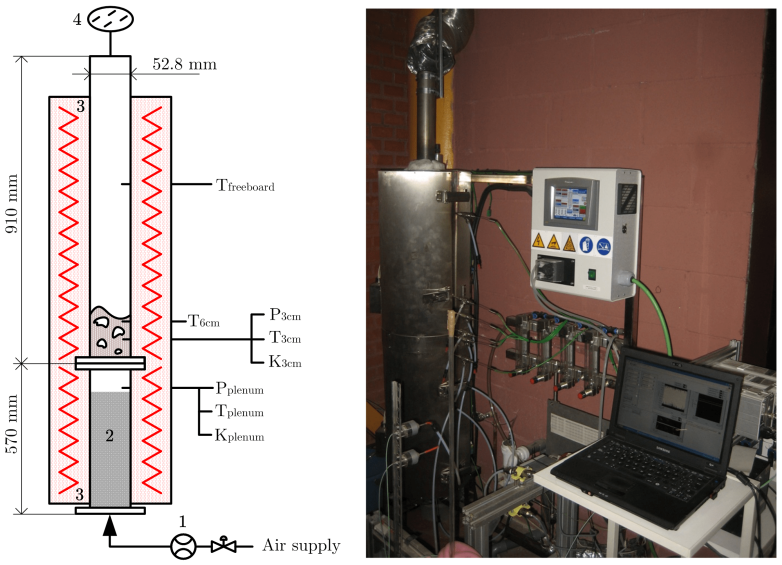


**Figure 2.3:** Lab-scale bubbling fluidised bed gasifier at the Carlos III University of Madrid: 1) mass flow meter; 2) air preheater; 3) electrical furnace; 4) mirror.

A 2 mm thickness perforate plate with 38 holes of 0.5 mm inner diameter distributed in triangular pitch ($P_t$ = 8.2 mm) is enclosed by the plenum and the bed. The characterization of the pressure drop across this distributor gives the following value: $\Delta P_{dist}$ = 60440·$u_g^2$ (at 850 °C). The whole reactor is surrounded by two electrical furnaces, one for the lower part (2500 W) and another one for the upper part (3600 W), to provide the energy necessary to get the desired temperature inside the bed and to simulate adiabatic conditions. The lower furnace acts as a gasifying agent pre-heater before it enters the bed. The facility is prepared to use different gasifying agents such as air, $CO_2$, oxygen or steam. In this case, all the experiments are carried out using air as gasifying agent. In the first set of experiments, showed in Chapter 3, biomass is fed manually by the upper part of the reactor at constant intervals of time according to the mass of the biomass pellets and the feeding rate.

Along this PhD thesis, this facility has been modified in order to adapt an automatic feeding system, a gas cleaning section before gas analysers, and a tar sampling point for Solid Phase Adsorption (SPA) method (Brage *et al.*, 1997; Osipovs, 2013). Figure 2.4

shows a diagram of the modified lab-scale gasifier. The experiments carried out with this new configuration are presented in Chapter 4.

The new feeding system consists in a vibrating cylinder in which a piston moves upwards and downwards inside the cylinder. The level of biomass particles is kept horizontal due to vibration and when these particles reached the discharge level, they fall down into the transfer tube towards the gasifier by its upper part. This tube is equipped with a water jacket to cool down the connection between the pipe and the reactor as well as to prevent biomass pyrolysis before it enters the reactor. A nitrogen flow is introduced into the vessel in order to avoid back-flow of gases from the gasifier.

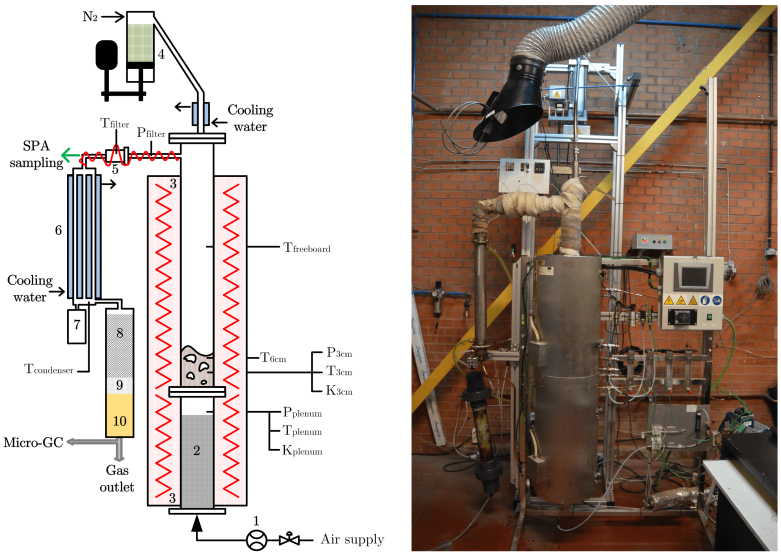


**Figure 2.4:** Modified lab-scale bubbling fluidised bed gasifier at the Carlos III University of Madrid: 1) mass flow meter; 2) air pre-heater; 3) electrical furnace; 4) vibrating biomass feeding system; 5) hot filter; 6) condenser; 7) water and tar trap; 8) cotton filter; 9) cigarette filters; 10) silica gel.

The gas cleaning section is composed by a hot filter filled with glass wool which retains the entrained particles from the bed; a tar and water condenser, and cold filter for the remaining particles, tars and moisture. The condenser is a 52.8 mm inner diameter stainless steel cylinder in which the raw gas discharges into 3 tubes of 10 mm inner diameter. A mixture of water and antifreeze circulates around these tubes, cooling down the gas stream. The condensate, water and tars, are stored in a container at the bottom of the condenser. All the pipes from the gasifier to the condenser, including the hot filter are properly heated at 350 °C and isolated to prevent tar condensation before the condenser. The cold filter consists in three sections: a first section of cotton, a second

section of cigarette filters, and a third section of silica gel. All these elements are shown in Figure 2.5.

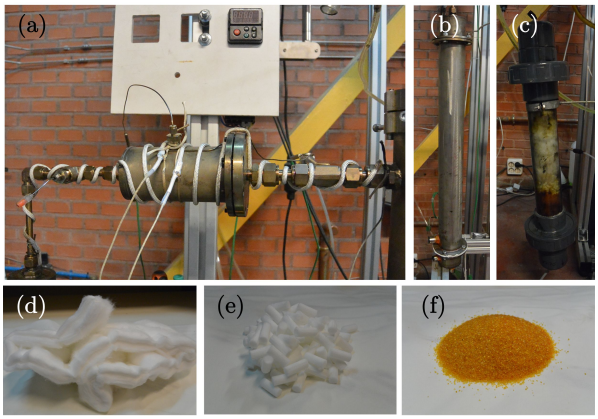


**Figure 2.5:** Gas cleaning section elements: a) hot filter; b) condenser; c) cold filter; d) cotton; e) cigarrtte filters; f) silica gel.

**Table 2.6:** Summary of the measurement locations and characteristics of the measurement devices in the lab-scale facility.

| | Location | Sensor |
|---|---|---|
| *Pressure* | | |
| $P_{plenum}$ | plenum, 3 cm below the distributor | WIKA Type A-10 |
| $P_{3cm}$ | bed, 3 cm above the distributor | Honeywell SPT series |
| $P_{filter}$ | before the hot filter | Kistler 4260A |
| *Pressure fluctuations* | | |
| $K_{plenum}$ | plenum, 3 cm below the distributor | Kistler 7261 + Kistler 5015A |
| $K_{3cm}$ | bed, 3 cm above the distributor | Kistler 7261 + Kistler 5015A |
| *Temperature* | | |
| $T_{plenum}$ | plenum, 3 cm below the distributor | K thermocouple, TC Direct |
| $T_{3cm}$ | bed, 3 cm above the distributor | K thermocouple, TC Direct |
| $T_{6cm}$ | bed, 6 cm above the distributor | K thermocouple, TC Direct |
| $T_{freeboard}$ | freeboard, 45 cm above the distributor | K thermocouple, TC Direct |
| $T_{filter}$ | inside the hot filter | K thermocouple, TC Direct |
| $T_{condenser}$ | condenser exit | K thermocouple, TC Direct |

Different sensors are used in order to monitor and measure absolute pressure, pressure fluctuations and temperature at different locations along the facility. Table 2.6 summarizes these locations and the characteristics of the measurement devices. The signals are collected using a National Instruments data acquisition modules: type 9205 (16 bit-resolution), type 9203 (16 bit-resolution) and type 9213 (24 bit-resolution) with analogue

input channels, working at a sampling frequency of 400 Hz.

A quartz reactor with similar characteristics to the previous reactor is also employed to qualitatively observe the bed under certain experimental conditions and to record the bed operation through a slit in the furnace.

## 2.5 Cold BFB

A cold bubbling fluidised bed (Glass15) is used for the attrition experiments presented in Chapter 4. This experimental plant is located in the Thermal Process Engineering Research Group laboratories at the Paul Scherrer Institute (Villigen, Switzerland). This facility is a cylindrical glass column of 145 mm inner diameter with a height of 930 mm. The upper part of the BFB is made of steel and it has a bigger cross sectional area, 250 mm inner diameter, to low gas velocity. A 10 $\mu$m porous steel plate of is used as distributor. Inside the BFB there are different internals of 20 mm in diameter to simulate heat exchanger tubes. Different sampling ports are distributed along the glass column to take bed samples during the test. At the exit of the upper section a filter with a porous size of 1 $\mu$m retains the elutriated fines. Air which is introduced by a mass flow controller in the wind box is used as fluidizing agent. Absolute pressure is measured before the porous distributor, in the wind box, and before the filter. Differential pressure is also measured in the bed. Figure 2.6 shows a sketch the facility.

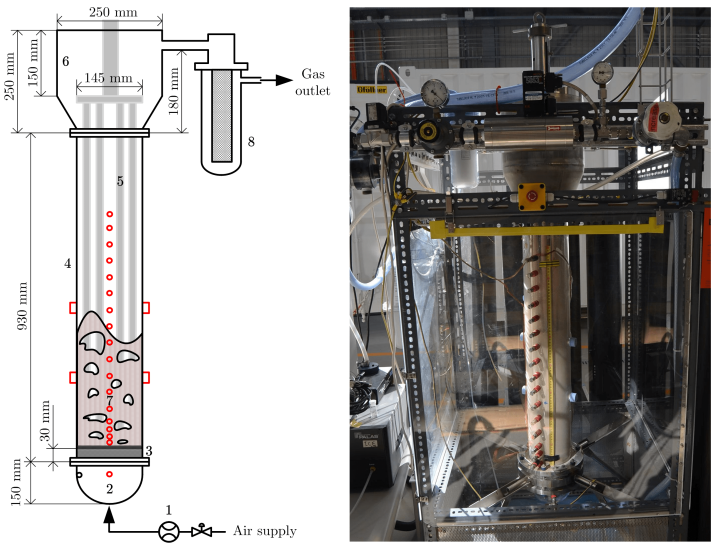


**Figure 2.6:** Cold bubbling fluidised bed (Glass15) at the Paul Scherrer Institute: 1) mass flow controller; 2) glass wind box; 3) porous distributor; 4) glass column; 5) internals; 6) freeboard; 7) sampling ports; 8) filter. Adapted from Maurer *et al.* (2016).

## 2.6 Pilot-plant BFB

A pilot-scale bubbling fluidised bed gasifier is employed for the experiments shown in Chapters 5 and 6. This installation is located in the Carbolea Research Group facilities at the University of Limerick (Limerick, Ireland). The gasifier is divided into different sections: biomass feeding, air supply and heating, fluidised bed reactor, downstream cleaning section and product gas analysis. Figure 2.7 shows a diagram of the pilot plant gasifier.

The feeding system is formed by a hopper and two screw feeders: the first one is controls the feeding rate and the second one introduces the biomass into the reactor as fast as possible in order to avoid the pyrolysis of the fuel inside the screw. This fast screw is surrounded by a water jacket for the same purpose. Inside the hopper, a rotating bar prevents the forming of bridges. The biomass is fed in-bed at 190 mm above the distributor plate.

The gasifying agent used in this experimental rig is air. It is preheated, prior to be introduced into the reactor, by means of an air pre-heater of 9000 W. The air is introduced into the plant by the lower part or plenum.

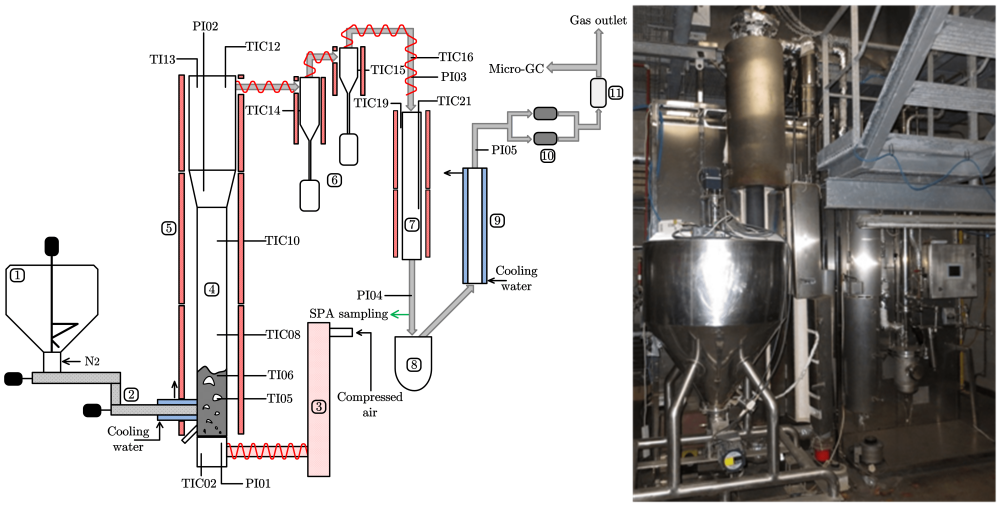


**Figure 2.7:** Scheme of the experimental facility at the University of Limerick: 1) biomass hopper; 2) screw feeders; 3) air pre-heater; 4) BFB reactor; 5) electrical furnaces; 6) cyclones; 7) hot filter; 8) tar trap; 9) heat exchanger; 10) downstream filters; 11) mass flow meter.

A 3 mm thick perforated stainless 316 plate with 40 holes of 0.9 mm inner diameter arranged in a circular distribution is used as distributor. The pressure drop across the distributor plate at 450 °C follows the expression $\Delta P_{dist} = 29990 \cdot u_g^2$. This element is enclosed between the plenum and the fluidised bed reactor section. The fluidised bed

section consists of two regions: a reaction zone where the bed is located has an inner diameter of 134.5 mm and a height of 1750 mm, and a freeboard region to slow gas velocity with an inner diameter of 211.6 mm and a height of 1250 mm. This part is surrounded by three electrical furnaces (10000 W, 5000 W and 5000 W, respectively) along the total height to get the desired temperatures for each experiment and to simulate adiabatic conditions.

Two hot cyclones and a hot filter (Candel Element, Pyrotex BWF-Envirotec) form the cleaning section. The cyclones and the filter, as well as the downstream pipes, are externally heated and isolated to prevent tar condensation. In this section, the possible entrained fines are separated from the gas stream. After the hot filter, a hot SPA sampling port is placed for tar sampling to avoid tar losses due to condensation. After this point, a cold trap and a condenser clean the gas from moisture and tars. A final paper filter is used for the last cleaning of the gas before enter the gas analyser.

Pressures and temperatures are monitored in different locations of the pilot plant: plenum, bed, cyclones, filter, etc (see Figure 2.7).

## 2.7 Analysis techniques

In this section, the analysis techniques used during this PhD thesis are presented. Firstly, the analyses of pressure signals is introduced. The use of these techniques allows to analyse the bed behaviour in terms of the bed hydrodynamics and they provide information about agglomeration and defluidisation. Secondly, the gasification parameters and performance calculations, gas analysis and tar analysis methodologies are presented. Thirdly, the bed material analyses after gasification tests and the attrition analysis methodologies are described. Finally, fly ash characterization methodology is presented.

### 2.7.1 Agglomeration and defluidisation analysis

Bed agglomeration and defluidisation are analysed using the pressure signals obtained from the bed using the piezoelectric pressure sensors (Kistler type) located in the bed. The analysis techniques are divided in two different methods: time domain and frequency domain. The results from these two techniques are also compared with visual observations.

#### Time domain analysis

For a better determination of the defluidisation time and a better comparison of the results, the standard deviation of pressure fluctuations is used. This parameter remains in zero or very close to it until the onset of fluidization and, from this point, it increases

linearly with gas velocity (Puncochár *et al.*, 1985). For this reason, this first approach has been widely used to identify a regime change or defluidisation time (van Ommen *et al.*, 2011; Gómez-Hernández *et al.*, 2012). The standard deviation is calculated for 30 s time periods along the time-series with a 15 s overlapping between periods. Using this result, a threshold can be defined in order to distinguish whether the bed is defluidised or not. The transition between fluidization and defluidisation state could be ambiguous depending on the bed material employed in the experiments. As a consequence, three different threshold values, 75, 50 and 25 % of the standard deviation for experiments at $u/u_{mf} = 2$, have been adopted to compare their effect on the value of the defluidisation time. The selection of this reference experiment is because fluidization is less intense and, therefore, it is the most restrictive air excess.

The pressure drop across the bed acquired using the absolute pressure sensor ($P_{3cm}$) and temperature difference between the two thermocouples inside the bed ($T_{3cm}$ and $T_{6cm}$) are also measured. Visual observation of the bed surface is used to confirm the defluidisation of the bed.

**Frequency domain analysis**

Changes in the fluidization regime can be detected using the dominant frequency of the bed (Gómez-Hernández *et al.*, 2012). According to this, the power spectral density (PSD) is calculated for the frequency analysis. The PSD is calculated using Welch's periodogram (Welch, 1967) with a Hanning window (Johnsson *et al.*, 2000) for different segments along the signal, obtaining different PSD function along time (van Ommen *et al.*, 2011). As a result, the frequency with the highest energy is chosen as the dominant frequency for each period of time. Figure 2.8a shows an example of the PSD of pressure fluctuations at two different instants, before and after the deluidization of the bed, where the dominant frequency for each spectrum is marked in the plot.

**Wide band energy analysis**

The wide band energy ($E_{wb}$) is obtained computing the energy contained within the PSD. This variable is defined as the ratio between the energy in a frequency region and the energy of the whole frequency domain and can be used to detect changes in the fluidization behaviour (Johnsson *et al.*, 2000). Gómez-Hernández *et al.* (2014) studied both the visual and the Student's t-distribution approaches available for such a frequency division. The visual frequency division approach showed that the frequency regions obtained were able to detect neither the change in the bed aspect ratio nor the start of the rotating distributor, preventing its use to compute the wide band energy. Therefore, in this PhD thesis the Student's t-distribution approximation of the cumulative energy distribution

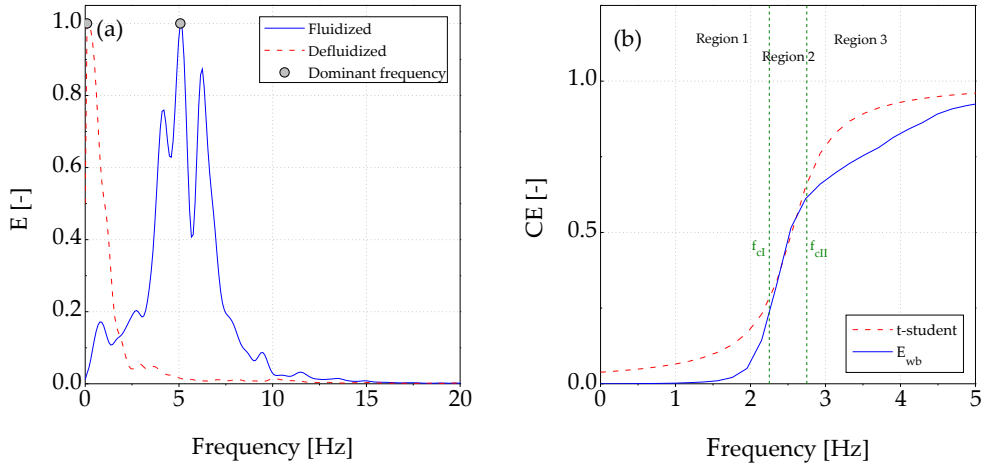


**Figure 2.8:** a) Example of the PSD of pressure fluctuations at fluidised and defluidised conditions (the dominant frequency of each spectrum is marked with a circle in the plot) and b) example of the cumulative energy distribution of the PSD.

(CE) of the PSD is employed to divide the frequency spectra. This methodology divides the frequency domain considering the difference between the CE and the Student's t-cumulative density function. As a result, the CE frequency distribution can be divided in three regions: two regions of poor matching that correspond to the tails of the CE distribution, and a region of proper matching corresponding to the highest energy content of the distribution. According to this approach, each region is related to different fluidization phenomena, which depends on the CE distribution as well as on the cut-off frequencies. In general, each region represents:

– Region 1 ($\Delta f < f < f_{cI}$): contains the low frequencies, which are associated to the long term dynamics and the larger structures of the bed.

– Region 2 ($f_{cI} < f < f_{cII}$ ): contains the dominant frequency of the bed, suggesting its relation to the bulk dynamics of the bed.

– Region 3 ($f_{cII} < f < f_N$): includes the high frequency region of the spectrum, and thus, it is related to fast fluidization phenomena such as the bubble eruption on the bed surface and the presence of channels.

Figure 2.8b shows an example of the CE distribution in which the energy of the spectrum is mainly distributed near the dominant frequency, while the tails of the distributions represents around 20–25 % of the total energy.

The wide band energy is employed together with the Statistical Process Control (SPC) scheme in order to define a reference state. This control scheme determines a control

zone estimating the control limits of the process. In this way, the identification of the bed defluidisation is possible. The main parameters used to estimate the control limits are summarized in Table 2.7 and further details can be found in Gómez-Hernández (2014).

**Table 2.7:** Settings for the SPC monitoring.

| Time series length [s] | Time window [s] | Fitting | UAL | LAL |
|---|---|---|---|---|
| 240 | 30 | Normal distribution | $\overline{X} + 3\sigma$ | $\overline{X}$ - $3\sigma$ |

#### Attractor comparison

The attractor comparison tool is used to decide if two time series are produced by the same mechanism. Diks *et al.* (1996) proposed a statistical parameter, S, for testing the null hypothesis, which establishes that two multidimensional probability distributions are identical. On the basis of this approach, van Ommen *et al.* (2000) defined a monitoring method that gives an early warning of the onset of agglomeration in a fluidised bed. The attractor of a reference time series of pressure fluctuations is compared with that of successive time series measured during the bed operation. In this way, for S-values larger than 3, the attractor of time series under evaluation is statistically different from the reference attractor, indicating that the fluid-dynamic conditions have changed in the fluidised bed. Therefore, it is possible to detect agglomeration at the very early stages for a given reference state (de Martín *et al.*, 2011; Bartels *et al.*, 2008).

### 2.7.2 Gasification parameters

In the gasification process there are several parameters which define the operation conditions as well as the performance and efficiency of the process. This section describes all these parameters.

#### Equivalence ratio

The equivalent ratio (ER) is defined as the ratio between the air flow rate introduced into the gasifier and the stoichiometric air flow needed for the complete combustion of biomass (Eqs. 2.1 and 2.2). Typical values of the ER for gasification conditions are between 0.2 and 0.4 (Gómez-Barea *et al.*, 2005). Depending on the application in which the product gas is used a different value should be adopted (Alauddin *et al.*, 2010).

$$C_m H_n N_p O_q + b\ (O_2 + 3.76\ N_2) \rightarrow c\ CO_2 + d\ H_2O + e\ N_2 \tag{2.1}$$

$$ER = \frac{\dot{m}_a}{\dot{m}_a|_{est}} = \frac{PM_{fuel}\ \dot{m}_a}{4.76\ (m + \frac{n}{4} - \frac{q}{2})\ \dot{m}_{fuel\ daf}} \tag{2.2}$$

**Higher and lower heating value**

In order to evaluate the efficiency of the gasification process, the parameters employed are the higher and lower heating (HHV and LHV) value of the product gas, the carbon and hydrogen conversion into gas, the biomass conversion, the gas yield (GY) and the cold gas efficiency (CGE). The HHV and LHV of the product gas, expressed in $MJ/Nm^3$, can be calculated using the gas composition of the dry product gas as in Eqs. 2.3 and 2.4 (Basu, 2010). The gas composition has big influences on these values as each gas specie ($H_2$, CO, $CH_4$, etc) has a different weight on the final result, depending on their respective heating value.

$$\begin{aligned} HHV = &(12.74\ [\%v/v]_{H_2} + 12.63\ [\%v/v]_{CO} + 39.82\ [\%v/v]_{CH_4} + \\ &+ 70.29\ [\%v/v]_{C_2H_6} + 63.41\ [\%v/v]_{C_2H_4} + 58.06\ [\%v/v]_{C_2H_2})\ /100 \end{aligned} \tag{2.3}$$

$$\begin{aligned} LHV = &(10.78\ [\%v/v]_{H_2} + 12.63\ [\%v/v]_{CO} + 35.88\ [\%v/v]_{CH_4} + \\ &+ 64.34\ [\%v/v]_{C_2H_6} + 59.45\ [\%v/v]_{C_2H_4} + 56.07\ [\%v/v]_{C_2H_2})\ /100 \end{aligned} \tag{2.4}$$

**Carbon, hydrogen and biomass conversion**

The carbon and hydrogen conversion into gas represents the ratio of carbon or hydrogen mass flow in the dry product gas to the mass flow rate of the relevant element in the dry and ash free biomass. These two values can be expressed according to the Eqs. 2.5 and 2.6, where $PM_i$ is the molecular weight of the $i$ element.

$$\begin{aligned} C\ conversion = &\frac{1}{\dot{m}_{fuel\ daf}\ C_{fuel}} \left( \dot{m}_{CO}\ \frac{PM_C}{PM_{CO}} + \dot{m}_{CO_2}\ \frac{PM_C}{PM_{CO_2}} + \right. \\ &+ \dot{m}_{CH_4}\ \frac{PM_C}{PM_{CH_4}} + \dot{m}_{C_2H_2}\ \frac{2 \cdot PM_C}{PM_{C_2H_2}} + \dot{m}_{C_2H_4}\ \frac{2\ PM_C}{PM_{C_2H_4}} + \\ &+ \left. \dot{m}_{C_2H_6}\ \frac{2\ PM_C}{PM_{C_2H_6}} \right) \end{aligned} \tag{2.5}$$

$$H\ conversion = \frac{1}{\dot{m}_{fuel\ daf}\ H_{fuel}} \left( \dot{m}_{H_2}\ \frac{2\ PM_H}{PM_{H_2}} + \dot{m}_{CH_4}\ \frac{4\ PM_H}{PM_{CH_4}} + \right.$$
$$+ \dot{m}_{C_2H_2}\ \frac{2\ PM_H}{PM_{C_2H_2}} + \dot{m}_{C_2H_4}\ \frac{4 \cdot PM_H}{PM_{C_2H_4}} +$$
$$\left. + \dot{m}_{C_2H_6}\ \frac{6\ PM_H}{PM_{C_2H_6}} \right) \tag{2.6}$$

The biomass conversion can be calculated using the amount of char remaining inside the gasifier after the experiment (Eq. 2.7).

$$Biomass\ conversion = 1 - \frac{\dot{m}_{char}}{\dot{m}_{fuel}} \tag{2.7}$$

**Product gas flow, gas yield and cold gas efficiency**

The product gas flow, $\dot{m}_{dry\ gas}$, is obtained by different ways in the lab-scale and in the pilot-plat gasifier. In the first case, the experimental facility does not have any mass or volume flow meter to get this value. In this sense, an inert gas such as nitrogen, is used to perform a mass balance between the input and the output (Eq. 2.8). In this calculations, the ammonia generation is neglected. However, in the pilot-plant gasifier the mass flow of the product gas is directly obtained by a mass flow meter.

$$\dot{m}_{N_2}^{in} = \dot{m}_{N_2}^{out} = \frac{\dot{m}_{dry\ gas}\ [\%v/v]_{N_2}\ \rho_{N_2}^{NTP}}{\rho_{gas}} \tag{2.8}$$

The GY, in $Nm^3/kg_{biomass\ daf}$, shows the amount of dry product gas per unit of biomass in dry ash free basis (Eq. 2.9). The CGE is defined as the the energy input over the potential energy output (Eq. 2.10), where $LHV_{gas}$ and GY are expressed in $MJ/Nm^3$ and $Nm^3/h$, respectively.

$$GY = \frac{\dot{m}_{dry\ gas}}{\rho_{gas}\ \dot{m}_{fuel\ daf}} \tag{2.9}$$

$$CGE = \frac{LHV_{gas}\ GY}{\dot{m}_{fuel}\ LHV_{fuel}} \times 100 \tag{2.10}$$

**Mass balance**

A mass balance of the process can be performed for each experiment in order to check the consistency of the results, comparing the input and the output flows. This calculations

can also reveal unknown process flows and measurement errors which can serve to refine future experiments and to scale-up and design installation equipments for industrial facilities (Siedlecki *et al.*, 2009). In this way, the bed material and char from the gasifier, particulates from the cyclones and the filters as well as water from the tar trap are weight and kept for analysis. All these flows are calculated as the mean values of each element divided by the total duration of each experiment, from the start of biomass feeding, and the biomass flow rate in dry ash free basis (Eq. 2.11), where the subscript $i$ represents the char, ash, moisture, fines, etc. All the moisture from the product gas is assumed to be condensed out and collected in the tar trap. Ultimate, moisture and ash content analyses are performed for all of these samples using a CHN-S elemental analyser, a TGA and ash furnaces, respectively.

$$\dot{m}_i = \frac{m_i}{t_{experiment}\ \dot{m}_{fuel\ daf}} \tag{2.11}$$

**Enrichment factor**

The possible catalytic activity of the bed materials, magnesite and olivine, has been analysed using the enrichment factor (EF) of the elutriated fines defined according to Meij (1994) (Eq. 2.12).

$$EF = \frac{element\ concentration\ in\ fines}{element\ concentration\ in\ fuel} \times \frac{\%\ ash\ in\ fuel}{100} \tag{2.12}$$

### 2.7.3 Gas analysis

Product gas is sampled and analysed online at 2-5 min intervals using a Varian Inc. CP-4900 $\mu$-GC (lab-scale gasifier) and an Agilent 3000 $\mu$-GC (pilot-plant gasifier). Both analysers are equipped with a thermal conductivity detector for the determination of permanent gases and light hydrocarbons. Table 2.8 shows the characteristics of these equipments. A well-known gas mixture is used for the calibration of the analysers.

Gas sampling starts at the same time as biomass feeding. The steady state is achieved after around 0.5 h in the case of the lab-scale gasifier, and between 1.5 to 2 h in the case of the pilot-plant gasifier (from when biomass feeding was started), corresponding with the time needed to reach a constant temperature within the reactor. Gas composition is calculated as the mean gas composition during the steady state.

### 2.7.4 Tar analysis

Tars are sampled using the SPA method developed by Brage *et al.* (1997) and later modified by Osipovs (2013) (Figure 2.9). 3 x 100 ml of gas and tars are taken over 2 min at

**Table 2.8:** $\mu$-GC characteristics.

| | Varian Inc. CP-4900 $\mu$-GC | Agilent 3000 $\mu$-GC |
|---|---|---|
| Exp. facility | Lab- scale | Pilot-plant |
| Column 1 | Molsieve 5Å | Molsieve 5Å |
| | 10 m × 0.32 mm | 12 $\mu$m/320 $\mu$m/10 m |
| Gases | $H_2$, $N_2$, $CH_4$ and CO | $H_2$, $N_2$, $CH_4$ and CO |
| Carrier gas | Argon | Argon |
| Column 2 | Pora Plot Q | Pora Plot U |
| | 10 m × 0.15 mm | 30 $\mu$m/32 $\mu$m/8 m |
| Gases | $CO_2$, $C_2H_2$, $C_2H_4$ and $C_2H_6$ | $CO_2$, $C_2H_2$, $C_2H_4$ and $C_2H_6$ |
| Carrier gas | Helium | Helium |

around 300-350 °C using Discovery DSC–$NH_2$ cartridges (Supelco) and a programmable syringe pump (World Precision Instruments, Inc.) once the steady state is reached. The sampling point is located after the hot filter in both the lab-scale facility and the pilot-plant gasifier (see Figures 2.4 and 2.7). In this point the temperature is high enough to avoid tar losses due to condensation.

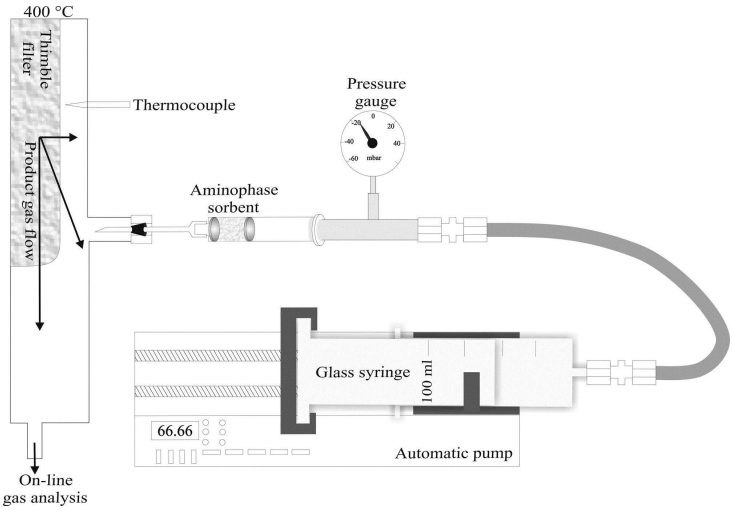


**Figure 2.9:** Scheme of the SPA method (Horvat *et al.*, 2016).

After each experiment, the SPA samples are extracted with dichloromethane and analysed by gas chromatography using three different instruments: a Varian Inc. 431 GC coupled to a Varian Inc. 210 MS ion trap located at the Carlos III University, an Agilent 7890A GC coupled to a triple-axis mass selevtive detector (MSD) 5975C and a Thermo Scientific Trace 1310 GC equipped with a flame ionization detector (FID), this

last two located at the University of Limerick. In the first case, GC-MS is used or both tar identification and quantification, while in the second case, tar identification is done using the GC-MSD and tar quantification is performed using the GC-FID. Table 2.9 shows the characteristics for these equipments. All the operating parameters are kept as similar as possible for the three analysers.The GC oven configuration is set as follows: it is initially set to 30 °C for 5 minutes, then, heated to 180 °C at 5 °C/min, and finally set to 300 °C at 8 °C/min.

**Table 2.9:** GC-MS characteristics and operating conditions.

| | Varian Inc. 431-GC + Varian Inc. 210-MS | Agilent 7890A GC + Agilent 5975C MSD | Thermo Scientific Trace 1310 GC |
|---|---|---|---|
| Exp. facility | Lab- scale | Pilot-plant | Pilot-plant |
| Column | non-polar, VF-5MS | non-polar, HP-5MS | non-polar, HP-5MS |
| | 30 m x 0.25 mm | 30 m x 0.25 mm | 30 m x 0.25 mm |
| | 0.25 $\mu$m film thickness | 0.25 $\mu$m film thickness | 0.25 $\mu$m film thickness |
| Carrier gas | Helium, 1.2 ml/min | Helium, 1.2 ml/min | Helium, 1.2 ml/min |
| Gases [ml/min] | - | - | Air: 350 |
| | - | - | $H_2$: 35 |
| | - | - | Make up ($N_2$): 40 |
| Sample volume | 1 $\mu$l | 0.8 $\mu$l | 0.8 $\mu$l |
| Temperatures [°C] | Inj. port: 300 | Inj. port: 300 | Inj. port: 300 |
| | Trap: 210 | MS source: 220 | FID: 300 |
| | Manifold: 60 | MS quadrupole: 200 | - |
| | Transferline: 300 | Transferline: 300 | - |
| MS configuration | EI Auto | Ionization energy: 70 eV | - |
| | 50-550 m/z | 50-550 m/z | - |
| | 0.46 s/scan | 2.91 scans/s | - |
| | split 1/50 | splitless | splitless |
| Solvent delay | 2.10 min min | 1.95 min | 1.95 min |

4-ethoxyphenol and tert-butylcyclohexane are used as the internal standards for the GC-MS and the GC-FID. Phenols are quantified using the 4-ethoxyphenol/phenol calibration curve and the remaining compounds with the tert-butylcyclohexane/naphthalene calibration curve. Tar compounds have been identified using the NIST 2.0 library. MassHunter and Chromeleon 7 are used to integrate the chromatograms in the range from benzene to chrysene.

Tar results are calculated for normal conditions (NTP: 293.15 K and 101325 Pa). According to Siedlecki & de Jong (2011) water vapour from the product gas condenses when passing through the sorbent, therefore, the sampled volume can be assumed to be taken on a dry basis ($g/Nm^3$ of raw dry gas converted further to $g/kg_{biomass\ daf}$). The

results are reported as the mean value for several samples for each experiment, and they are presented as individual compounds as well as total GC detectable tar (referred as total tar henceforth), secondary and tertiary groups as defined by Milne *et al.* (1998).

Finally, tar dew point is calculated using The Energy Centre of The Netherlands (ECN) tar dew point site (www.thersites.nl).

### 2.7.5 Bed material analysis after gasification

Sepiolite has been analysed before and after gasification experiments in order to evaluate the differences occurred in the sepiolite during the gasification process. To this extent, the Brunauer-Emmett-Teller (BET) surface area has been obtained using a Micrometrics Gemini 236 BET analyser with $N_2$ at 77K.

SEM-EDS images has been also performed to check the changes on the morphology of the sepiolite and on its adsorption properties, using a Hitachi SU-70 Scanning Electron Microscope (SEM) with an energy-dispersive (EDS) detector. This images are able to show if some undesirable elements such as molten ashes or tars are adsorbed or not on the sepiolite particles.

The possible tar adsorption on the sepiolite has been also investigated using a solid extraction with dichloromethane of used sepiolite particles. In this way, 2.26 g of sepiolite are placed in a close vessel with 10 ml of dichlorometane. The vessel is introduced into an ultrasound bath at ambient temperature for 10 minutes. After this time, the liquid phase is separated from the solid residue using a nylon membrane filter of 0.45 $\mu$m. Finally, 1 $\mu$l is introduced into a GC-MS for a qualitative analysis. The peaks from chromatogram are identify by means of the the NIST 2.0 library.

### 2.7.6 Attrition analysis

During the attrition test, bed material and filter fines samples have been collected at different time intervals to determine the mass of elutriated fines with time and the particle size distribution of these samples. The filter is weight before and after each time interval and the particle size distribution of bed and filter samples is analysed by means of a sieving machine (Retsch Vibratronic, Type VE1) and a laser diffraction particle size analyser (Horiba LA-950). Some SEM images have been also obtained from fresh and used sepiolite to complement the analysis, using a field emission gun scanning electron microscope (Zeiss ULTRA 55) additonally equipped with energy dispersive X-ray spectroscopy (EDAX/Ametek).

### 2.7.7 Fly ash characterization

The entrained fines and fly ash collected in the cyclones and in the hot filter of the pilot-plant gasifier have been analysed by means of a CHN-S elemental analyser, a drying oven and an ash furnace in order to get the ultimate, moisture and ash content analyses. HHV has been also measured using an isoperibolic calorimeter, and LHV has been calculated using Eq. 2.13, where M and H are the moisture and hydrogen content of the sample, respectively, and $h_{st}$ the latent heat of steam, 2260 MJ/kg (Basu, 2010). Ash is obtained from the samples and digested in $H_2O_2$, $HNO_3$, $H_2SO_4$ and HF prior to analysis by atomic absorption spectroscopy (AAS) or inductively coupled plasma optical emission spectroscopy (ICP-OES) in order to determine inorganic elemental composition.

$$LHV = HHV - h_{st}\left(\frac{9\ H}{100} + \frac{M}{100}\right) \tag{2.13}$$

The metal mobility in these samples has been tested by means of a leaching test. 5 g of dry fines are combined with deionised water, in a liquid to solid ratio (L/S) of 10. The mixture is continuously rotated for 24 h and then filtered as it is indicated in the DIN 38414-S4 standard for leaching test. Finally, the liquid samples are analysed by AAS or ICP-OES.

## References

Abelha, P., Franco, C., Pinto, F., Lopes, H., Gulyurtlu, I., Gominho, J., Lourenço, A. & Pereira, H. 2013 Thermal conversion of *Cynara cardunculus* L. and mixtures with *Eucalyptus globulus* by fluidized-bed combustion and gasification. *Energy & Fuels* 27, 6725–6737.

Alauddin, Z. A. B. Z., Lahijani, P., Mohammadi, M. & Mohamed, A. R. 2010 Gasification on lignocellulosic biomass in fluidized beds for renewable energy development: A review. *Renewable and Sustainable Energy Reviews* 14, 2852–2862.

Bartels, M., Lin, W., Nijenhuis, J., Kapteijn, F. & van Ommen, J. R. 2008 Agglomeration in fluidized beds at high temperatures: Mechanisms, detection and prevention. *Progress in Energy & Combustion Science* 34, 633–666.

Basu, P. 2010 *Biomass Gasification and Pyrolysis: Practical Desing and Teory*, 1st edn. Elsevier Inc.

Brage, C., Yu, Q., Chen, G. & Sjöström, K. 1997 Use of amino phase adsorbent for biomass tar sampling and separation. *Fuel* 76, 37–142.

Brus, E., Öhman, M. & Nordin, A. 2005 Mechanisms of bed agglomeration during fluidized-bed combustion of biomass fuels. *Energy & Fuels* 19, 825–832.

Christodoulou, C., Koutsoumpa, E.-I., Panopoulos, K. D., Karellas, S. & Kakaras, E. 2014*a* Agglomeration problems during cardoon fluidized bed gasification. *Thermal Science* 18, 645–656.

Christodoulou, C., Tsekos, C., Tsalidis, G., Fantini, M., Panopoulos, K. D., de Jong, W. & Kakaras, E. 2014*b* Attempts on cardoon gasification in two different ciculating fluidized beds. *Cases Studies in Thermal Engineering* 4, 42–52.

Corella, J., Toledo, J. M. & Padilla, R. 2004 Olivine or dolomite as in-bed additive in biomass gasification with air in a fluidized bed: Which is better? *Energy & Fuels* 18, 713–720.

Diks, C., van Zwet, W. R., Takens, F. & DeGoede, J. 1996 Detecting differences between delay vector distributions. *Physical Review E* 53, 2169–2176.

Dogan, M., Özdemir, Y. & Alkan, M. 2007 Adsorption kinetics and mechanism of cationic methyl violet and methylene blue dyes onto sepiolite. *Dyes and Pigments* 75, 701–713.

Fernández Llorente, M. J., Díaz Arocas, P., Gutiérrez Nebot, L. & Carrasco García, J. E. 2008 The effect of the additiion of chemical materials on the sintering of biomass ash. *Fuel* 87, 2651–2658.

Geldart, D. 1973 Types of gas fluidization. *Powder Technology* 7, 285–292.

Gómez-Barea, A., Arjona, R. & P., Ollero 2005 Pilot-plant gasification of olive stone: a technical assessment. *Energy & Fuels* 19, 598–605.

Gómez-Hernández, J. 2014 Paste-drying control in a rotating distributor fluidized bed. PhD thesis, Universidad Carlos III de Madrid.

Gómez-Hernández, J., Sánchez-Prieto, J., Briongos, J. V. & Santana, D. 2014 Wide band energy analysis of fluidized bed pressure fluctuation signals using a frequency division method. *Chemical Engineering Science* 105, 92–103.

Gómez-Hernández, J., Soria-Verdugo, A., Briongos, J. V. & Santana, D. 2012 Fluidized bed with a rotating distributor operated under defluidization conditions. *Chemical Engineering Journal* 195-196, 198–207.

Horvat, A., Kwapinska, M., Xue, G., Dooley, S., Kwapinski, W. & Leahy, J. J. 2016 Detailed measurement uncertainty analysis of solid-phases adsorption - Total gas chromatography (GC)-detectable tar from biomass gasification. *Energy & Fuels* 30, 2187–2197.

Johnsson, F., Zijerveld, R. C., Schouten, J. C., van den Bleek, C. M. & Leckner, B. 2000 Characterization of fluidization regimes by time-series analysis of pressure fluctuations. *International Journal of Multiphase Flow* 26, 663–715.

de Martín, L., van den Dries, K. & van Ommen, J. R. 2011 Comparison of three different methodologies of pressure signal processing to monitor fluidized-bed dryers/granulators. *Chemical Engineerign Journal* 172, 487–499.

Maurer, S., Durán, S. R., Künstle, M. & Biollaz, S. M. A. 2016 Influence of interparticle forces on attrition and elutriation in bubbling fluidized beds. *Powder Technology* 291, 473–486.

Meij, R. 1994 Trace element behavior in coal-fired power plants. *Fuel Processing Technology* 39, 199–217.

Milne, T. A., Evans, R. J. & Abatzoglou, N. 1998 Biomass gasifier "tars": Their nature , formation and conversion. NREL/TP-570-25357. *Tech. Rep.* National Renewable Energy Laboratory.

Murray, H. H., Pozo, M. & Galán, E. 2011 An introduction to palygorskite and sepiolite deposits – Location, geology and uses. In *Developments in Palygorskite-Sepiolite Research.*

van Ommen, J. R., Coppens, M.-O., van den Bleek, C. M. & Schouten, J. C. 2000 Early warning of agglomeration in fluidized beds by attractor comparison. *AIChe Journal* 46, 2183–2197.

van Ommen, J. R., Sasic, S., van der Schaaf, J., Gheorghiu, S., F., Johnsson & Coppens, M.-O. 2011 Time-series analysis of pressure fluctuations in gas–solid fluidized beds – A review. *International Journal of Multiphase Flow* 37, 403–428.

Osipovs, S. 2013 Comparison of efficiency of two methods for tar sampling in the syngas. *Fuel* 103, 387–392.

Pecharromán, C., Esteban-Cubillo, A., Montero, I. & Moya, J. S. 2006 Monodisperse and corrosion-resistant metallic nanoparticles embedded into sepiolite particles for optical and magnetic applications. *Journal of the American Ceramic Society* 89, 3043–3049.

Puncochár, M., Drahos, J., Cermák, J. & Selucký, K. 1985 Evaluation of minimum fluidizing velocity in gas fluidized bed from pressure fluctuations. *Chemical Engineering Communications* 35, 81–87.

Siedlecki, M. & de Jong, W. 2011 Biomass gasification as the first hot step in clean syngas production process - gas quality optimization and primary tar reduction measures in a 100 kW thermal input steam-oxygen blown CGB gasifier. *Biomass & Bioenergy* 35, S40–S62.

Siedlecki, M., Nieuwstraten, R., Simeone, E., de Jong, W. & Verkooijen, H. M. 2009 Effect of magnesite as bed material in a 100 $kW_{th}$ steam-oxygen blown circulating fluidized-bed biomass gasifier on gas composition and tar formation. *Energy & Fuels* 23, 5643–5654.

Skoulou, V., Koufodimos, G., Samaras, Z. & Zabaniotou, A. 2008 Low temperature gasification of olive kernels in a 5-kW fluidized bed reactor for $H_2$-rich producer gas. *International Journal of Hydrogen Energy* 33, 6515–6524.

Sutton, D., Kelleher, B. & Ross, J. R. H. 2001 Review of literature on catalysts for biomass gasification. *Fuel Processing Technology* 73, 155–173.

Weber, K. & Quicker, P. 2013 Enhancing as melting behaviour of straw ash through the addition of kaolin. In *21$^{st}$ European Biomass Conference and Exhibition*, pp. 1447–1450. Copenhagen, Denmark.

Welch, P. D. 1967 The use of fast fourier transform for the estimation of power spectra: A method based on time averaging over short, modified periodograms. *IEEE Transactions on Audio and Electroacustics* 15, 70–74.

Werther, J., Saenger, M., Hartge, E.-U., Ogada, T. & Siagi, Z. 2000 Combustion of agricultural residues. *Progress in Energy and Combustion Science* 26, 1–27.

Zadaka-Amir, D., Bleiman, N. & Mishael, Y. G. 2013 Sepiolite as an effective natural porous adsorbent for surface oil-spill. *Microporous and Mesoporous Materials* 169, 153–159.

CHAPTER

# THREE

# Fuel particle behaviour and agglomeration using sepiolite as bed material

## Contents



## 3.1 Introduction

Biomass gasification in fluidised bed has some operational problems such as the formation of agglomerates at high temperatures or the production of tars. In the first case, these agglomerates lead into hot zones, thermal stresses on measurement equipments, and in most of the cases, bed defluidisation and an unscheduled shut down of the plant if the process is not promptly detected. The tars generation affects the downstream unit processes, where they condense, disturb their performance and may clog these equipments.

One key parameter in agglomeration is the hydrodynamic behaviour of the fuel particles inside the fluidised bed. Fuel particles may have higher densities than the dense phase, showing a jetsam behaviour. This causes the formation of endogenous bubbles

when devolatilization occurs, changing the properties of the fuel particles, and promoting their motion throughout the whole bed (Fiorentino *et al.*, 1997*b*; Bruni *et al.*, 2002; Solimene *et al.*, 2010). In contrast, flotsam fuel particles tend to remain at the top of the bed showing a low mixing degree with the bed particles (Nienow *et al.*, 1978; Ríos *et al.*, 1986). Several techniques have been proposed to characterize the dynamics of fluidised bed processes: standard deviation of the pressure fluctuation signal (van Ommen *et al.*, 2004, 2011), frequency domain (Brown & Brue, 2001; Chaplin *et al.*, 2004; Wormsbecker *et al.*, 2009), the signal energy computed in different frequency bands (Johnsson *et al.*, 2000; Gómez-Hernández *et al.*, 2014, 2016), and the attractor comparison (van Ommen *et al.*, 2000; Chaplin *et al.*, 2004, 2005).

Another strategy to prevent agglomeration and extent the fluidisation state is the use of different bed materials to silica sand or additives (Werther *et al.*, 2000). According to Bartels *et al.* (2008), bed materials low in or free of silica sand are chosen to avoid the tendency of silica to form low-melting point silicates with alkali salts, which usually cause the bed agglomeration.

The objective of this chapter is to introduce sepiolite as an alternative new bed material to silica sand for biomass gasification in fluidised beds and study its performance on the agglomeration and defluidisation processes in comparison with silica sand. In this sense, the agglomeration of jetsam and flotsam fuel particles is analysed using pressure fluctuation measurements. These signals are studied in the time domain by the standard deviation, in the frequency domain by means of the dominant frequency and the wide band energy, and in the state space employing the attractor comparison tool. Furthermore, the definition of a proper reference state during the gasification process is also discussed. The defluidisation time is also determined using these techniques. Finally, the bed material distribution after each experiment is analysed.

## 3.2 Experimental setup

A detailed description of the experimental facility, the biomass, the bed materials and the analysis techniques employed in this part of the thesis have been presented in Chapter 2. Consequently, in this section only a short summary of the experimental setup is addressed.

The lab-scale BFB gasifier located at the Carlos III University of Madrid is used in order to perform the experiments (see section 2.4). The reactor has an inner diameter of 52.8 mm and a total height of 1480 mm. The lower part serves as air pre-heater while the upper part contains the fluidised bed. These sections are connected by means of a 2 mm thickness perforate plate with 38 holes of 0.5 mm. The desired experimental temperature is obtained using two electrical furnaces, which also serve to simulate adiabatic conditions.

Air is used as gasifying agent and it is introduced by the bottom part of the reactor. Biomass is introduced manually by the upper part of the gasifier where a mirror is located to see inside the reactor. Furthermore, a quartz reactor with similar characteristics is also employed to qualitatively observed the bed under certain experimental conditions.

*C. cardunculus* is used as biomass feedstock. The properties of this biomass are shown in Section 2.2 (tables 2.1, 2.2 and 2.4). Biomass is disposed in cylindrical pellets of approximately 6 mm of diameter and 15 mm of length, with a mass around of 0.50 g. Silica sand and sepiolite, with a particle diameter between 425 and 600 $\mu$m, are employed as bed materials. The properties of these bed materials are shown in Section 2.3 (table 2.5). Silica sand is used as reference bed material in order to test the performance of sepiolite towards agglomeration.

Temperature, pressure and pressure fluctuations are acquired using K-type thermocouples, absolute pressure sensors and Kistler piezoelectric sensors placed in different locations along the experimental facility (see Figure 2.3 and Table 2.6).

### 3.2.1 Experimental procedure

At the beginning of each experiment an exact amount of bed material (257 g for silica sand or 97 g for sepiolite) is loaded into the reactor in order to get a bed aspect ratio, defined as the relation between the bed height ($h_b$) and the reactor diameter (D), of $h_b/D = 1.5$ ($h_b = 79.2$ mm). Air supply is turned on and bed temperature is raised to 850 °C using the electrical furnaces. Once the bed temperature, measured by thermocouples $T_{3cm}$ and $T_{6cm}$, is stable at 850 °C, minimum fluidisation velocity is measured before each experiment. After this, the air flow rate is set according with the air excess for each test. Fuel rate is calculated in agreement with the ER. In this chapter, an ER = 0.3 is set for all experiments, leading to a feeding rates from 5.19 to 25.90 g/min for silica sand and from 3.38 to 16.44 g/min for sepiolite. Table 3.1 shows the operating conditions for all experiments. Before starting biomass feeding, pressure and temperature signals are acquired for 300 s as reference conditions for each experiment. Finally, *Cynara cardunculus* L. is fed into the gasifier at a constant rate, according with the air flow rate and the ER (Table 3.1). When pressure fluctuations becomes zero or very close to this value and the bed looks defluidised in the mirror, biomass feeding is stopped while signals are acquired for another 300 s. After this time, the electrical furnaces and the air supply are shut down. Once the reactor is cooled down, the bed material is discharged from the reactor and sieved to analyse particle size distribution.

**Table 3.1:** Operating conditions.

| | Silica sand ($u_{mf}$ = 0.089 m/s) | | | | | Sepiolite ($u_{mf}$ = 0.057 m/s) | | | | |
|---|---|---|---|---|---|---|---|---|---|---|
| Air excess ratio, $u/u_{mf}$ [–] | 2 | 4 | 6 | 8 | 10 | 2 | 4 | 6 | 8 | 10 |
| Air flow [l/min] | 6.38 | 13.20 | 19.80 | 26.50 | 33.10 | 4.01 | 8.09 | 13.35 | 14.74 | 19.60 |
| Fuel rate [g/min] | 5.19 | 10.54 | 15.43 | 20.87 | 25.90 | 3.38 | 6.46 | 9.79 | 12.24 | 16.44 |
| ER [–] | 0.29 | 0.30 | 0.30 | 0.30 | 0.30 | 0.28 | 0.30 | 0.30 | 0.29 | 0.28 |
| Initial bed temperature [°C] | 850 | | | | | 850 | | | | |
| Bed aspect ratio [–] | 1.5 | | | | | 1.5 | | | | |
| Bed material [g] | 257 | | | | | 97 | | | | |

### 3.2.2 Analysis methodology

Agglomeration and defluidisation are analysed by means of pressure signals, using time and frequency domain methods. The standard deviation of pressure fluctuations ($\sigma$) is used for time analysis while the PSD is calculated for the frequency analysis. The wide band energy method ($E_{wb}$) is used to detect changes in the fluidisation behaviour and to study the jetsam or flotsam behaviour of the combustible. The attractor comparison tool is also employed to detect agglomeration. In both, wide band energy and the attractor comparison tool, a reference state is defined to properly apply both techniques.

Pressure drop across the bed acquired using the absolute pressure sensor ($P_{3cm}$) and temperature difference between the two thermocouples inside the bed ($T_{3cm}$ and $T_{6cm}$) are also measured. Significant changes in the standard deviation and the frequency of the pressure fluctuations during the defluidisation of the bed should agree with a decrease in the pressure drop across the bed and with an increase in the relative temperature difference between two positions in the bed (Scala & Chirone, 2006). Visual observation of the surface of the bed is used to confirm the defluidisation of the bed.

In order to illustrate the behaviour of the biomass particles and the different types and sizes of agglomerates, photographs are also taken during and at the end of the experiments.

## 3.3 Results and discussion

### 3.3.1 Visual observations

Biomass particles show two different hydrodynamic behaviours depending on the bed density (the bulk density for the silica sand and sepiolite bed are 1481.2 and 558.4 kg/m$^3$ respectively, Table 2.5). When silica sand is used as bed material, biomass particles ($\rho_{fuel}$ = 1220.5 kg/m$^3$) remain on the bed surface, floating on it due to buoyancy effects. No char or pellets are observed inside the bed during the experiment, with a very poor

mixing between biomass and bed material. As a consequence, devolatilization and gasification reactions take place in this part of the bed without much interaction with the bed material as it can be seen in Figures 3.1a and 3.1b. A stagnant flame is observed in the freeboard for the whole experiment. This flame appears due to the combustion of a fraction of the biomass, which reacts with the oxygen present in the fluidisation gas. Part of the volatiles is also burned in the freeboard of the bed. On the other hand, during the experiments with sepiolite as bed material, a completely different behaviour is observed. Biomass particles circulate throughout the whole bed height and its motion is not restricted to the bed surface, finding biomass particles immersed in the dense bed as it is shown in Figures 3.1d and 3.1e. In these conditions, devolatilization and gasification reactions occur inside the bed where endogenous bubbles are formed. These endogenous bubbles are added to the exogenous bubbles due to fluidisation, forcing the biomass particles to move throughout the whole bed. Thereby, volatiles are produced all along the bed, interacting with the bed particles. This interaction can enhance different catalytic reactions, which benefit the final gas composition and tar reduction. Small and sporadic flames appear in this case due to three different situations: (1) when the pellet is transported to the surface of the bed, (2) when the pellet is reached by exogenous bubbles that are always present in the bed under aggregative fluidisation conditions or (3) when an endogenous bubble of volatiles is formed around the pellet.

The formation of endogenous bubbles and their influence on fuel segregation was studied by Fiorentino *et al.* (1997*a*,*b*). According to this phenomenon, for the sand experiments, the endogenous bubbles induce segregation of the fuel particle at the top of the bed. This is also promoted by the high density of the bed material in comparison with the pellet density, making the pellet to float on the top of the bed. On the contrary, the pellet sinks in the bed of sepiolite due to its low density, while the endogenous and exogenous bubbles transport the pellet and volatile matter to the bed surface. Therefore, these two effects for the sepiolite bed produces a better dispersion of the fuel particles that also causes a better dispersion of ash.

As a consequence of the different biomass particles behaviours, the agglomeration process is also different for silica sand and sepiolite beds. In the former case, with silica sand, the maldistribution of fuel particles leads to generate ash in a narrow part of the bed, close to the bed surface. As the interaction between the bed material and biomass/ash is rather poor, the agglomeration process is fast, generating a cap-like clinker on the surface of the bed (Figure 3.1c). The rest of the bed, below this agglomerate, seems to remain unaltered. However, in sepiolite bed, ash is generated all along the bed. This more homogeneous distribution of ash inside the bed produces a slow agglomeration process in which the whole bed is involved. As a result, the size and shape of the agglomerates differ from those found when operating with silica sand beds. In a bed

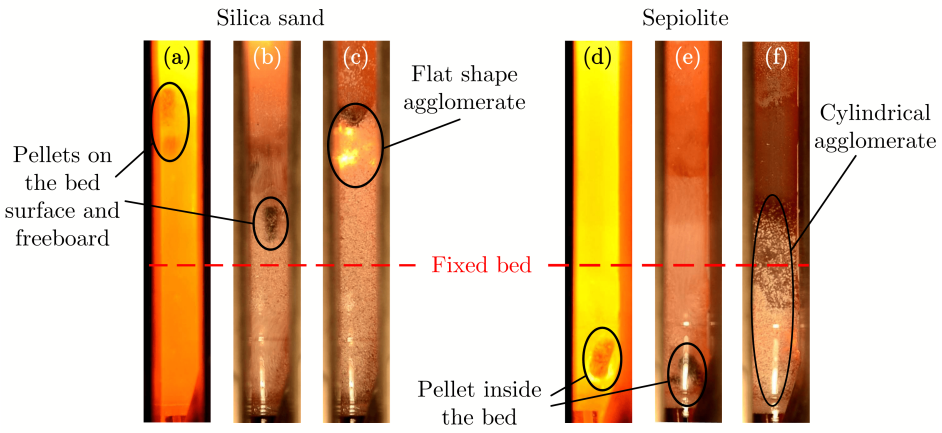


**Figure 3.1:** Snapshots (using the quartz reactor) obtained during gasification experiments ($u/u_{mf} = 4$): a), b) and c) silica sand; d), e) and f) sepiolite.

composed of sepiolite particles, a big cylindrical clinker is formed, whose dimensions are close to those of the whole bed (Figure 3.1f).

### 3.3.2 Combustible behaviour: jetsam

During the biomass gasification in a sepiolite bed, bed temperatures and pressure fluctuation signals have been monitored. Since one of the objectives of this chapter is the description of the agglomeration process using the attractor comparison tool and the wide band energy analysis, the definition of a reference state, capable of defining the steady gasification properties, is mandatory. To that end, temperature profiles are employed to set this reference state.

Figure 3.2a shows the temporal evolution of the temperatures in the bed during a biomass gasification test with a dimensionless gas velocity $u/u_{mf} = 6$ and using sepiolite particles as bed material. An increase of the bed temperature due to partial combustion of biomass can be observed at the beginning of the biomass feeding (t = 5 min), reaching a constant temperature after 2 min. Plenum temperature needs around 10 min to reach a constant value of 820 °C. Later, the defluidisation process is detected by a sudden increase of $T_{3cm}$ and $T_{6cm}$. In this case, the agglomeration process defluidizes the bed after around 42 min. This figure also shows the three states used as a reference for the analysis of the pressure signals. The first reference state is defined prior to the beginning of the biomass feeding. Reference 2 starts 5 min after the biomass feeding, when the bed temperatures show a constant value of 925 °C, while Reference 3 is chosen when the plenum temperature reaches the steady temperature of 820 °C.

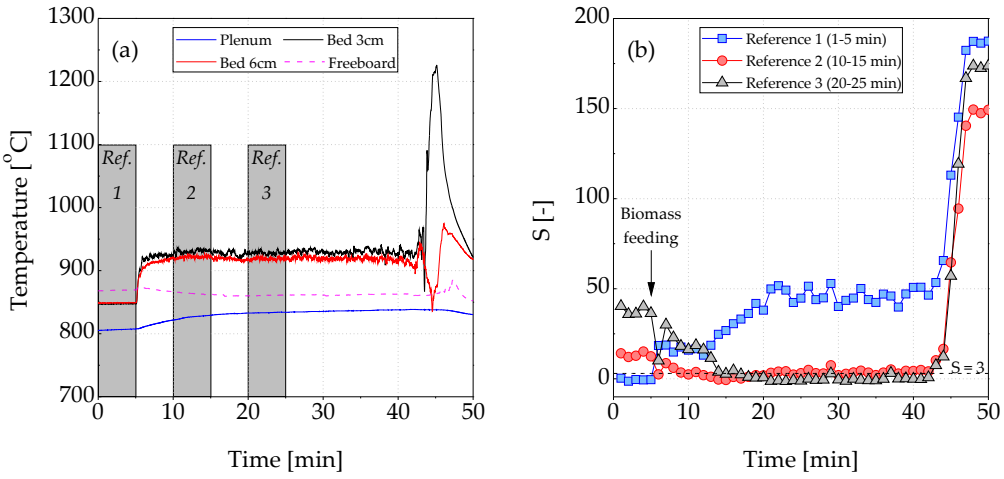


**Figure 3.2:** Jetsam behaviour during the gasification process at $u/u_{mf} = 6$ using sepiolite as bed material: a) temporal evolution of temperature and b) S-test using different reference states.

Figure 3.2b presents the S-test results for sepiolite at $u/u_{mf} = 6$, employing the reference states described above. As it can be seen, the S-values are lower than 3 at the beginning of the test for Reference 1, since the attractor comparison tool is still analysing the reference attractor. However, once the biomass is fed into the reactor, the S-values show a sharp increase above the threshold (S = 3). This result identifies the change of the fluid-dynamic behaviour of the bed showing the difference between Reference 1, with no biomass, and the gasification beginning, characterized by the formation of endogenous bubbles. The S-values increase continuously up to 20 min, suggesting a transition in the fluidisation behaviour, in a similar time to that needed by the plenum temperature to reach a constant value. Furthermore, the defluidisation is also shown as a sharp increase of the S-value. Even though changes in the fluidisation dynamics can be detected using Reference 1, its use is not recommended since S-values larger than 3 will be obtained as soon as biomass is fed into the reactor.

The S-test using Reference 2 shows values greater than 3 at the beginning of the test, when no biomass is fed in the bed. As the gasification process progresses, the S-values continuously decrease until the reference state is reached. However, the threshold (S = 3) is exceeded again at t = 17 min when no defluidisation is visually observed. Therefore, Reference 2 does not represent the steady state of the gasification process. Greater S-values are obtained at the beginning of the test when using Reference 3 as a reference state. In this case, the S-values decreases as the gasification process continues, reaching

values lower than 3 from t = 17 min until the bed defluidisation at t = 42 min. Thus, for monitoring purposes, the reference control state employed should be Reference 3, where the steady state is reached for all the temperatures in the bed, in order to be able to detect the bed defluidisation properly using the S-test method.

Prior to the computation of the wide band energy, the CE distribution of the power spectrum is estimated. As for the S-test, different time periods are considered to analyze the influence of the reference state on the CE distribution. Figure 3.3a shows the CE distribution estimated for sepiolite test at $u/_{mf} = 6$, using the reference states described in Figure 3.2a. Furthermore, two extra periods, before and after the bed defluidisation, are also considered. Figure 3.3a shows that the biomass feeding produced a clear effect on CE distribution. As it can be seen comparing the CE distributions of References 1 and 2, the dominant frequency of the bed is moved to lower frequencies. This effect is similar to the increase of the gas fluidisation velocity, shown in Figure 3.3b. Such a result can be explained by the fuel particle behaviour in the sepiolite bed. The jetsam behaviour of the fuel particle ensures that the devolatilization occurred within the dense bed, and thus endogenous bubbles are produced as explained by Bruni *et al.* (2002) and Solimene *et al.* (2010). These bubbles affect the fluid-dynamic behaviour of the entire bed increasing the effective flow rate, and thus, changing the CE distribution. It is worth to mention that this is an averaged result since the reference period considers 5 min of data and the biomass is fed continuously, ensuring the continuous formation of endogenous bubbles.

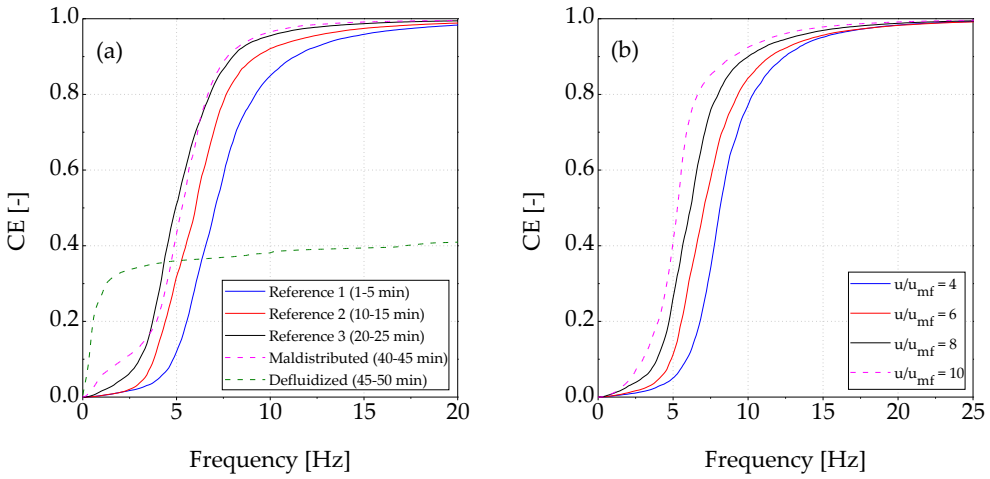


**Figure 3.3:** Cumulative energy distribution of the PSD during sepiolite test: a) as a function of different time periods at $u/u_{mf} = 6$ and b) as a function of the gas velocity.

As gasification progressed from Reference 2 to Reference 3, CE distribution slightly moves to lower frequencies, as shown in Figure 3.3a. At the maldistributed period, which is near the bed defluidisation, the CE shows variations at the lower frequencies, suggesting the modification of the fluidisation regime. Finally, the CE obtained when the bed is defluidised informs of a total absence of fluidisation in this period.

Instead of using this averaged information to characterize the process performance, the frequency domain can be divided, computing the energy of each frequency band. In this sense, the wide band energy analysis reflects the energy contained in the three regions in which the frequency domain is divided. This variable shows the evolution of the CE distribution, although, previous to its computation, a definition of the reference state is needed. Considering the temporal evolution of the bed temperatures and the results of the S-test, Reference 3 is employed to estimate the cut-off frequencies and the control limits (see Table 3.2). The energy contained in the frequency regions and the limits that define the control state are presented in Figure 3.4. According to the Statistical Process Control (SPC) monitoring scheme, these limits are estimated as $\overline{X} \pm 3\sigma$, where the mean, $\overline{X}$, and the standard deviation, $\sigma$, are calculated for each energy region during the reference state. As suggested by Johnsson *et al.* (2000) and Gómez-Hernández *et al.* (2014), the energy contained in each region can be identified in terms of the time scale dynamics of different fluidisation phenomena. In this way, $E_{wb3}$ represents the energy of the high frequencies, which are related to the appearance of channels, $E_{wb2}$ contains the dominant frequencies of the bed, suggesting its relation to the bulk dynamics, and $E_{wb1}$ is identified with the larger structures of the bed.

**Table 3.2:** Computational settings for the frequency division method.

| Silica sand | | | Sepiolite | | |
|---|---|---|---|---|---|
| Air excess ratio $u/u_{mf}$ [–] | Cut-off frequencies [Hz] | | Air excess ratio $u/u_{mf}$ [–] | Cut-off frequencies [Hz] | |
| | $f_{cI}$ | $f_{cII}$ | | $f_{cI}$ | $f_{cII}$ |
| 4 | 4.88 | 7.66 | 4 | 6.34 | 9.76 |
| 6 | 3.84 | 5.34 | 6 | 5.37 | 8.79 |
| 8 | 3.12 | 5.34 | 8 | 3.98 | 8.59 |
| 10 | 2.50 | 4.61 | 10 | 1.34 | 6.86 |

As can be seen in Figure 3.4, all the regions present energy values out of the control state prior to the biomass feeding. As the biomass is fed, the CE changes and the wide band energy values move towards the control zone. This result can be explained by the modification of the frequency spectra, and thus, by the change of the CE distribution, as shown in Figure 3.3a. The energy is mainly contained within the high frequency region at

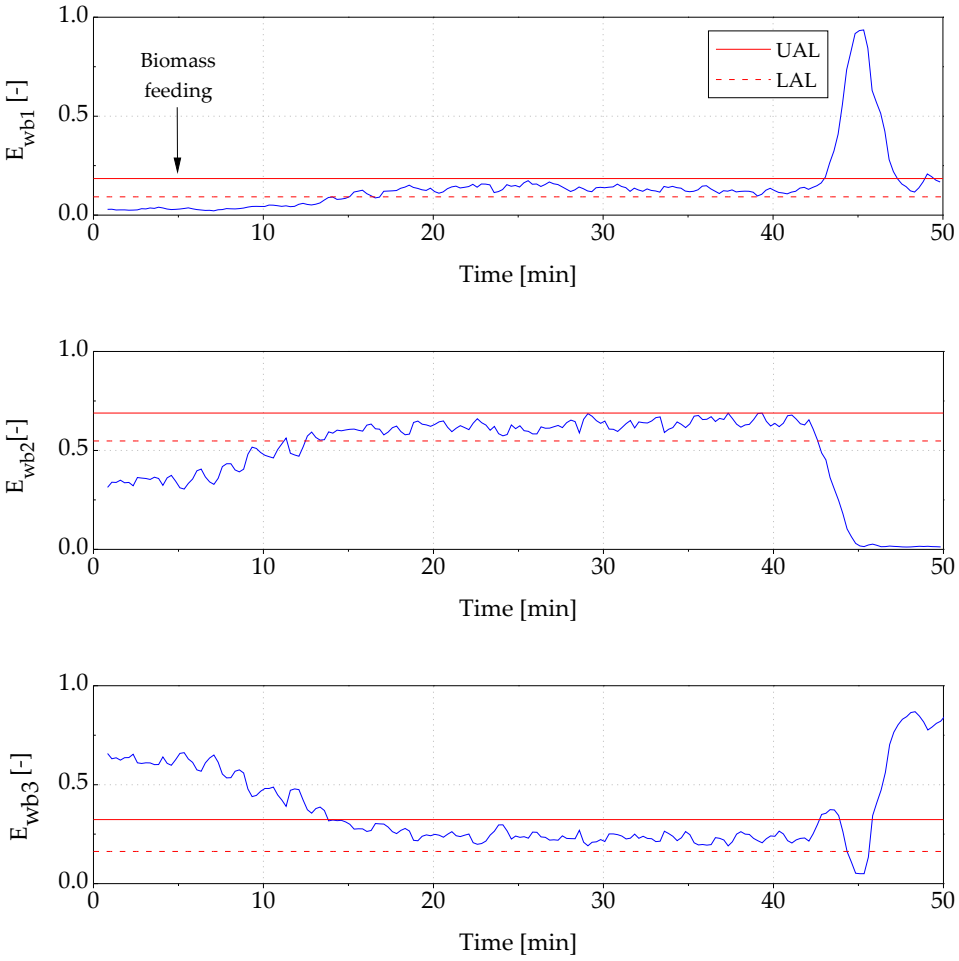


**Figure 3.4:** Wide band energy analysis during a biomass gasification process in a sepiolite bed ($u/u_{mf} = 6$).

the beginning of the test. As the gasification process progresses, the CE moves to lower frequencies, showing similar values to the reference state. Concerning the energy values plotted in Figure 3.4, the energy contained in the high frequencies, $E_{wb3}$, is transferred to medium and low frequency regions, $E_{wb2}$ and $E_{wb1}$ respectively. The three frequency regions reaches the control zone at t = 15 min. No significant changes are shown during the experiment up to the bed defluidisation. At this moment, t = 42 min, the defluidisation of the bed can be detected by the three energies as an out of the control zone. The energy decrease of $E_{wb2}$, which is related to the bulk dynamics, suggests the complete agglomeration of the bed. This energy is transferred to $E_{wb3}$ and $E_{wb1}$ pointing

to a sharp change in the fluidisation dynamics. Quite similar results are obtained using the attractor analysis based on Reference 3 (Figure 3.2b) and the energy values of the frequency regions (Figure 3.4).

### 3.3.3 Combustible behaviour: floatsam

A flotsam behaviour is observed when using the same fuel particles in a silica sand bed due to the lower density of the biomass pellets in comparison with the bed bulk density. The low axial mixing of the fuel, which remains at the top of the bed, and the formation of alkali silicates during the gasification enhances the defluidisation process. In these tests, the agglomerate formed is plate-shaped, showing a different defluidisation process to that described previously for the sepiolite bed. The same methodology applied to the sepiolite bed is also applied to the silica sand bed.

The temporal evolution of the temperature measurements in the bed during gasification of biomass in a silica sand bed operated at $u/u_{mf} = 6$ is presented in Figure 3.5a. The short defluidisation time, t = 5 min, makes difficult to define a steady process during these gasification tests. For this reason, the reference state employed for the attractor comparison tool and the wide band energy analysis is placed, in this case, at the beginning of the test, prior to the biomass feeding.

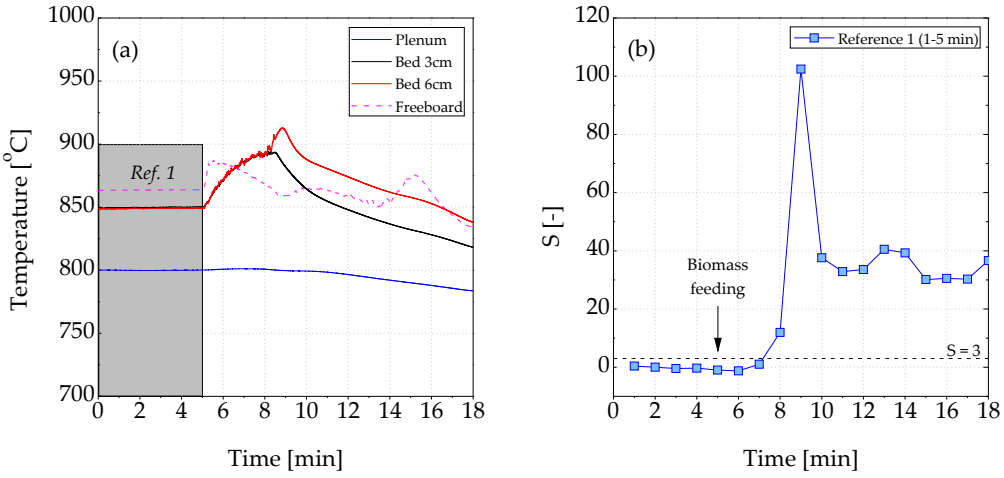


**Figure 3.5:** Flotsam behaviour during the gasification process at $u/u_{mf} = 6$ using silica sand as bed material: a) temporal evolution of temperature and b) S-test using different reference states.

Figure 3.5b presents the results of the attractor comparison method. The S-values

show a sharp increase at t = 8 min. This result is explained by the rapid defluidisation when operating a silica sand bed. However, once the bed is defluidised and the biomass feeding is stopped, the S-values decrease up to a constant value. The formation of a cap-clinker near the bed surface explains this decrease of the S-values. When this agglomerate is formed, the rest of the bed seems to remain unaltered, showing a barely fluidised state. This result differs from that obtained for the sepiolite bed (Figure 3.2b) when the S-values do not decrease to a constant value after the bed defluidisation due to the formation of a big cylindrical clinker in the whole bed.

Figure 3.6 shows the same trend of the CE for the silica sand test as a function of the gas velocity as for sepiolite tests.

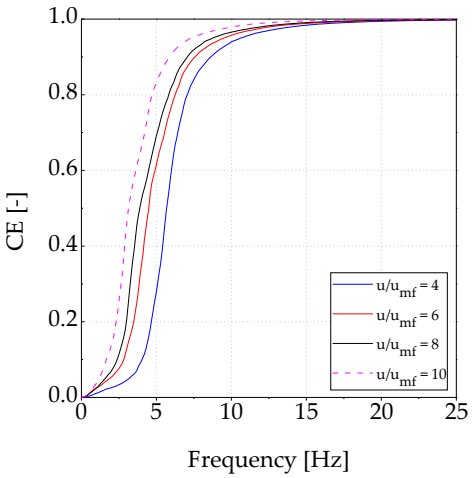


**Figure 3.6:** Cumulative energy distribution of the PSD as a function of the gas velocity for silica sand.

The results obtained using the wide band energy analysis for the biomass gasification process in the silica sand bed, are displayed in Figure 3.7. The same reference state employed for the S-test is used for the computation of the cut-off frequencies and the control limits (see Table 3.2). Similarly to the S-test results, an out of control state is detected after t = 8 min for $E_{wb3}$ and $E_{wb1}$, pointing to a fluidisation change, whereas $E_{wb2}$ identified the change of the bulk dynamics at t = 9 min. Concerning $E_{wb2}$, the energy values decrease up to a constant value, indicating that part of the bed behind the cap-clinker is still fluidised. This effect is also detected by the S-test analysis shown in Figure 3.5b. Regarding the long term phenomena, which is encoded in the energy of $E_{wb1}$, a peak permits also to detect the bed defluidisation, although the values of $E_{wb1}$ return to the control zone as the test progresses in time. Such a result, together with the

high energy values of $E_{wb2}$ in comparison to the low values of $E_{wb2}$ after defluidisation in the sepiolite bed (Figure 3.4), suggests that the bottom of the bed is still fluidised after the formation of the cap-clinker agglomerate at the bed surface.

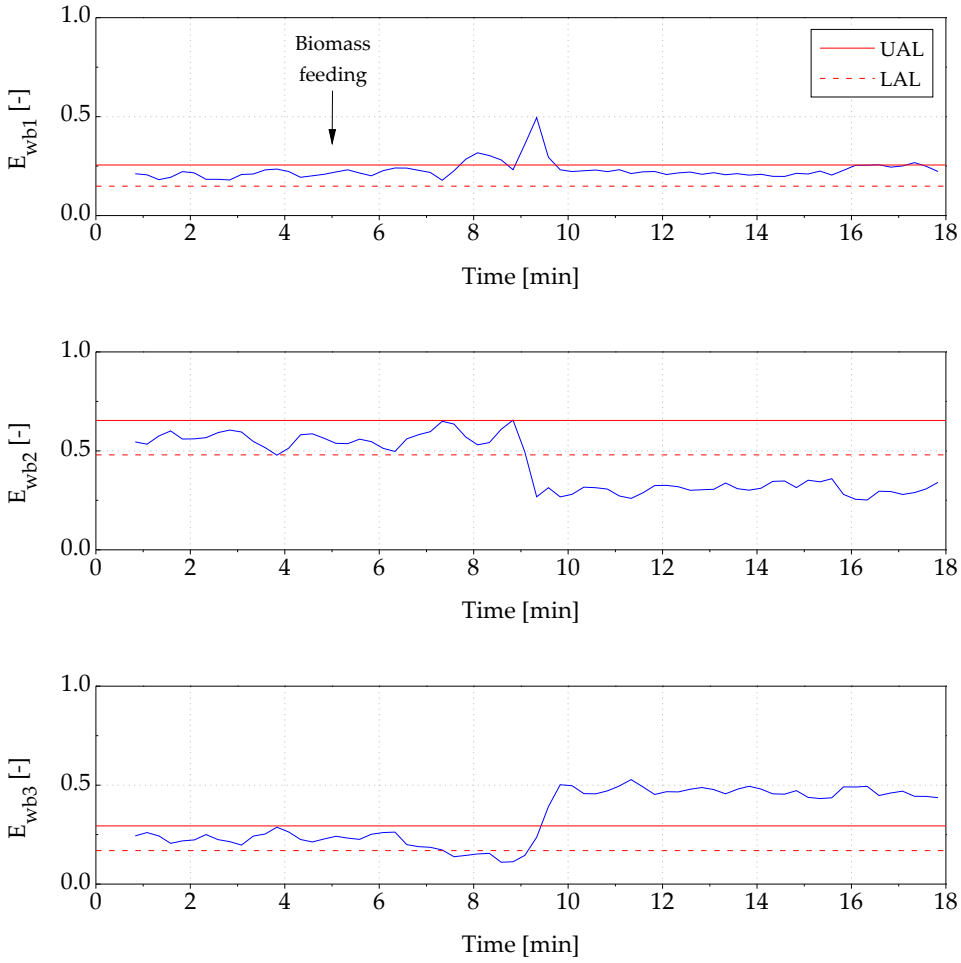


**Figure 3.7:** Wide band energy analysis during a biomass gasification process in a silica sand bed ($u/u_{mf} = 6$).

The fast fluidisation phenomena, which is identified with $E_{wb3}$, presents two different patterns. In the first part, the energy decreases after the biomass feeding until the bed defluidisation (t = 8 min). This energy decrease is produced by the progressive clogging of the bed surface, which makes difficult the eruption of bubbles on the bed surface. Since the energy of $E_{wb3}$ is related to the fast fluidisation phenomena and the finer structures of the bubbling fluidisation (Ríos *et al.*, 1986; Gómez-Hernández *et al.*, 2014),

the modification of the bubble eruptions over the bed surface changes the frequency spectra from multiple bubble to slug-like regimes, and thus, modifies the energy of $E_{wb3}$. In the second part, the energy increases after the bed defluidisation up to a constant value during the rest of the test. Such an energy change is explained by the formation of channels throughout the cap-clinker, which tend to increase the energy contained in the higher frequencies of the power spectrum ($E_{wb3}$) (Gómez-Hernández *et al.*, 2014).

The energy of $E_{wb3}$ at the end of each experiment is further analysed as a function of the air velocity in order to check whether or not this clogging effect and subsequent channels formation is common for all the silica sand tests. Pictures and further details of the agglomerates can be seen in Section 3.3.5. Figure 3.8 shows the energy of $E_{wb3}$ at the end of each experiment in the silica sand bed, calculated as the mean value of $E_{wb3}$ during the last minute of the test. A progressive energy increase of $E_{wb3}$ with the air velocity is observed in Figure 3.8. This result is caused by the different width and consistency of the agglomerate formed at the bed surface. For lower velocities, the cap-clinker is easily broken by small channels, and thus, the energy of $E_{wb3}$ present lower values. As the air velocity is increased, greater cap-clinkers are formed and bigger channels appear through the agglomerate, which increases the energy of $E_{wb3}$.

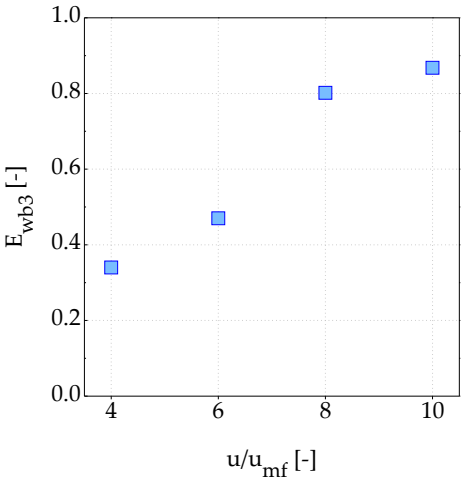


**Figure 3.8:** Influence of the air velocity on the values of $E_{wb3}$ at the end of the gasification process in a silica sand bed.

### 3.3.4 Defluidisation time

The defluidisation time is calculated using both the S-test and the wide band energy analysis in order to compare with the calculation using the analysis of the pressure

fluctuations in the time and frequency domains.

The standard deviation of pressure fluctuations from the time analysis is shown in Figure 3.9 for both silica sand and sepiolite. In the case of silica sand, the standard deviation remains at a constant value until defluidisation takes place (Figure 3.9a). As biomass floats on the bed surface, no difference is observed between the first part of the signal where only air is passing through the bed and the part of the signal where biomass is continuously fed. The transition between the two regimens (fluidised and defluidised) is very clear and it occurs in a very short period of time. At a low air excess, $u/u_{mf} = 2$, the standard deviation does not drop to zero although the reactor seems to be defluidised. This is explained by the wide band energy analysis, which showed that the bed remains fluidised below the agglomerate formed on the bed surface. In fact, no time changes in the pressure fluctuations are observed for this case. This result agrees with the previous analysis using the wide band energy method.

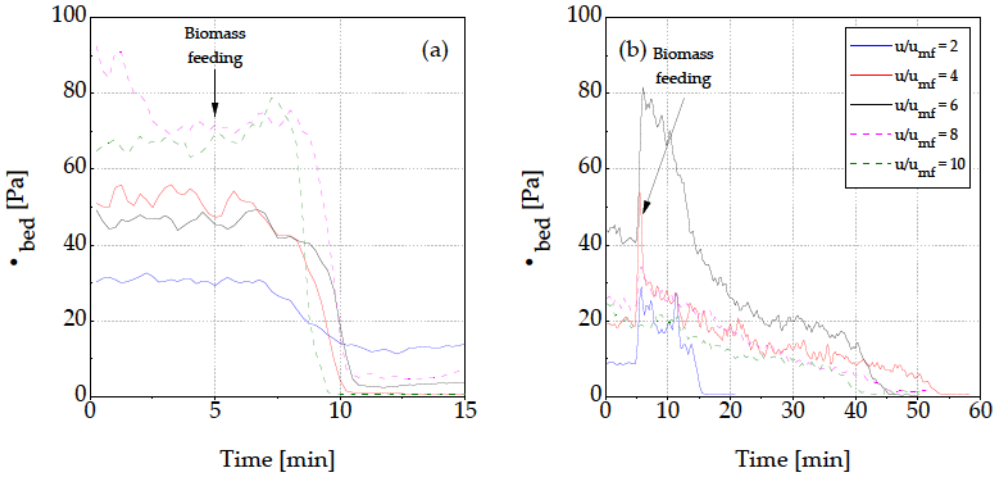


**Figure 3.9:** Standard deviation of pressure fluctuations inside the bed as a function of time and for the different air excess ratios ($u/u_{mf} = 6$): a) silica sand and b) sepiolite.

On the other hand, when using the sepiolite as bed material different trends are observed (Figure 3.9b). Before biomass feeding, the standard deviation of the pressure signal remains constant. However, once biomass feeding starts a rapid increase in the standard deviation is detected. The better mixing of biomass with bed material leads to the aforementioned release of volatiles inside the bed, creating endogenous bubbles in addition to the air bubbles formed at the distributor plate. The more bubbles the higher pressure fluctuations due to a greater probability of bubbles coalescence and therefore,

larger bubble diameter (Saxena *et al.*, 1990; Guo *et al.*, 2003). For air excess ratios of $u/u_{mf}$ = 2, 4 and 6 the standard deviation increases around a 50 % from the signal at nominal conditions (before biomass feeding), having the higher production of bubbles an important effect. For $u/u_{mf}$ = 8 this increment is relatively small and for the case of $u/u_{mf}$ = 10 there is no evidence of this effect, furthermore standard deviation starts to decrease. It is well known that beyond a certain value of gas velocity where bubbles reach a maximum size, bubbles break into smaller ones, reducing the amplitude of pressure fluctuations (Saxena *et al.*, 1993). At this high gas velocities the effect of the appearance of endogenous bubbles does not increase the amplitude of pressure fluctuations because the fluidisation is very vigorous already and bubble coalescence is overtaken by bubble splitting (Bi, 2007). The standard deviation decreases to zero for sepiolite at all the experimental conditions as it can be seen in Figure 3.9b, as the agglomerate formed is uniformly distributed across the bed.

In the case of the frequency analysis, the evolution of the dominant frequency along the time is showed in Figure 3.10. A dominant frequency appeared with a constant value while there are bubbling fluidised conditions in the bed. However, when defluidisation occurrs the frequency sharply decreased to zero. During the experiments with silica sand (Figure 3.10a) and at high air excesses ($u/u_{mf}$ = 6, 8 and 10) the frequency recovers its value after defluidisation. This transition could lead to think that the bed is again fluidised; however, looking at Figure 3.9a, it can be seen that the standard deviation remains very close to zero and visual observations using the mirror corroborate that the bed is still defluidised.

Figure 3.11 shows the defluidisation time obtained using the different approaches discussed above: S-test, wide band energy, standard deviation and frequency methods. It can be noticed that, in the case of the standard deviation, the results are quite similar for the three thresholds defined and they are comparable to the values obtained using the PSD method. For $u/u_{mf}$ = 2 with silica sand, the 75 % threshold predicts a very short defluidisation time in comparison with the PSD method. However, the bed looks fluidised according to the visual observations at this time. Besides, the standard deviation does not fall below the 25 % threshold during this experiment although the bed looks defluidised in the mirror. As a result, the threshold selected for the standard deviation method which predicts defluidisation time in agreement with the PSD method and the visual observations of the bed is the 50 % threshold.

The standard deviation, the PSD and the wide band energy analyses show similar defluidisation times for both silica sand and sepiolite, whereas the S-test presents higher values.

Comparing both bed materials, it can be noted that a clear improvement in the defluidisation time is achieved in the sepiolite experiments. Both chemical and physical

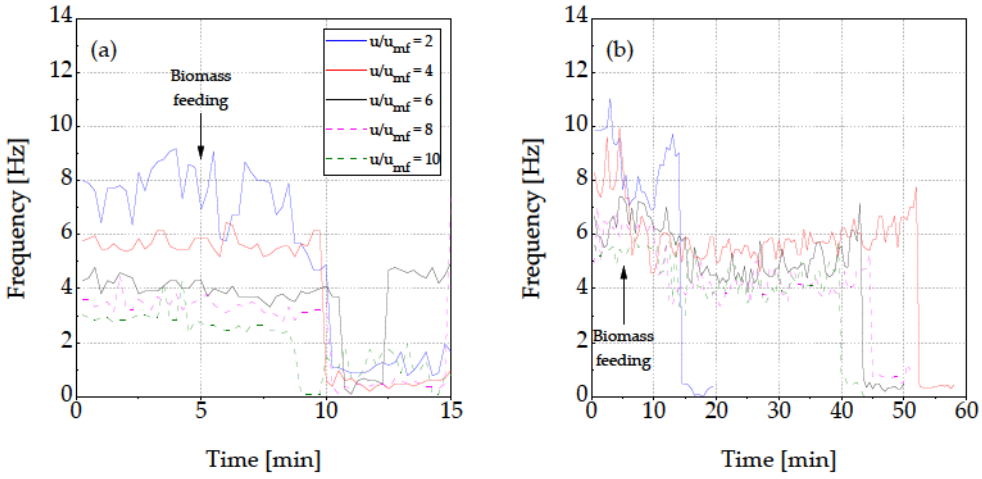


**Figure 3.10:** Dominant frequency of the power spectrum of pressure fluctuations inside the bed as a function of time and for the different air excess ratios ($u/u_{mf} = 6$): a) silica sand and b) sepiolite.

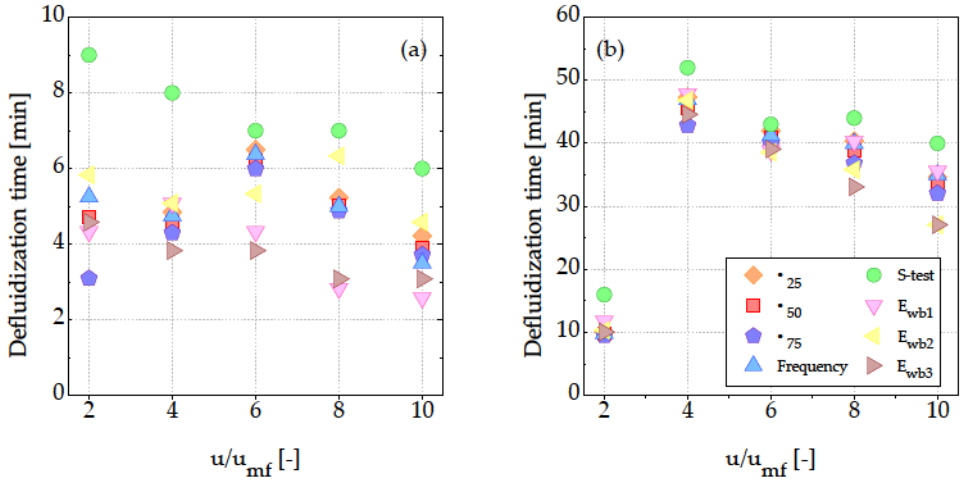


**Figure 3.11:** Defluidisation time: a) silica sand and b) sepiolite.

properties of the sepiolite can affect this behaviour. In order to avoid agglomeration, silica sand should be replaced by another bed material with less silica content to reduce the formation of low-melting silicates (Bartels *et al.*, 2008). According to this, sepiolite has around a 40 wt.% less silica oxide than silica sand. Some of this silica is substituted by

magnesium oxide, a common component of other bed materials like magnesite ($MgCO_3$) or dolomite ($CaMg(CO_3)_2$) which improves agglomeration. Alkali earth metals such as Mg or Ca commonly reduces agglomeration (Fryda *et al.*, 2008) although sometimes they can promote it if the ratio Na/Mg or Na/Ca are high (Lin *et al.*, 2009). On the other hand, sepiolite presents a large surface area due its high porosity. This property can improve the adsorption of the melt phases formed during the process. Besides, sepiolite density helps to get a better mixing due to the different behaviour of the fuel particles. Therefore, a better distribution of ash inside the bed is achieved, avoiding hot zones. All these properties (composition, porosity, density and combustible behaviour) serve to reduce agglomeration during the gasification of biomass.

The effect of the air excess ratio on the defluidisation time is also different with silica sand and with sepiolite. For the experimental conditions studied and the lab-scale facility an optimum value for the $u/u_{mf}$ ratio is obtained (see Figure 3.11). From this value, $u/u_{mf} = 6$ and $u/u_{mf} = 4$ for silica sand and sepiolite respectively, the defluidisation time decreases. The effect of the agglomerates break down because of the higher air excess is not enough to equilibrate the adhesion of the particles with the melting ash. When using silica sand, this reduction is very sharp. However, in case of sepiolite, the decrease is softer and, therefore, if the air excess ration is high enough there is some flexibility to select the fluidisation flow rate without affect too much the defluidisation time.

### 3.3.5 Agglomeration analysis

After each gasification experiment the particle size distribution of the bed material is measured. Different types of agglomerates are formed during the experiments as it can be seen in Figure 3.12. Flat plate shape agglomerates on the bed surface appears with silica sand for air excesses, $u/u_{mf}$, higher than 4. For lower gas velocities this agglomerate is less compact breaking into small pieces of particle aggregates. However, when sepiolite is used, a completely different behaviour is observed. The whole bed tends to agglomerate forming one big cylindrical shape. These results are consequence of the fuel behaviour discussed in Sections 3.3.2 and 3.3.3.

The material collected from the reactor after each gasification experiment is also sieved to get the particle size distribution, which is shown in Figure 3.13 as the ratio between the mass fraction of each sieve and the initial bed mass ($Mass/Mass_0$). Notice that the initial mass fraction ratio is also represented as fresh bed material. The superficial gas velocity has an important effect on the size distribution of bed material. At higher air excesses more differences appear between the original and final bed material distribution.

In silica sand experiments, the bed material size distribution after the experiments is

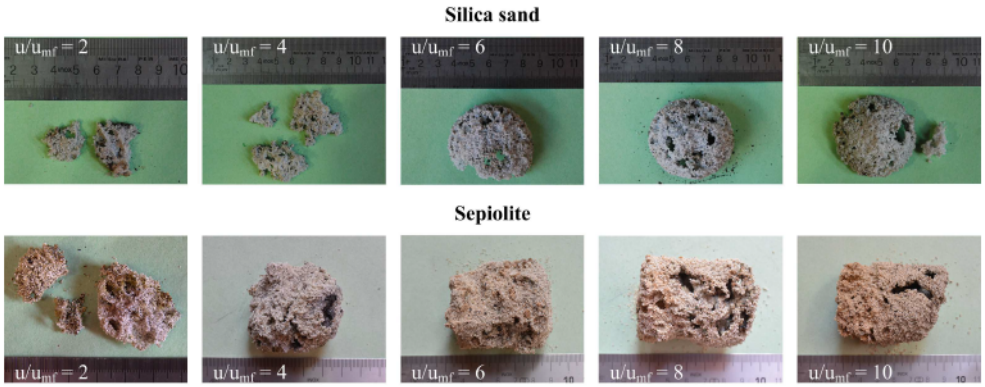


**Figure 3.12:** Agglomeration for silica sand and sepiolite for all air excesses.

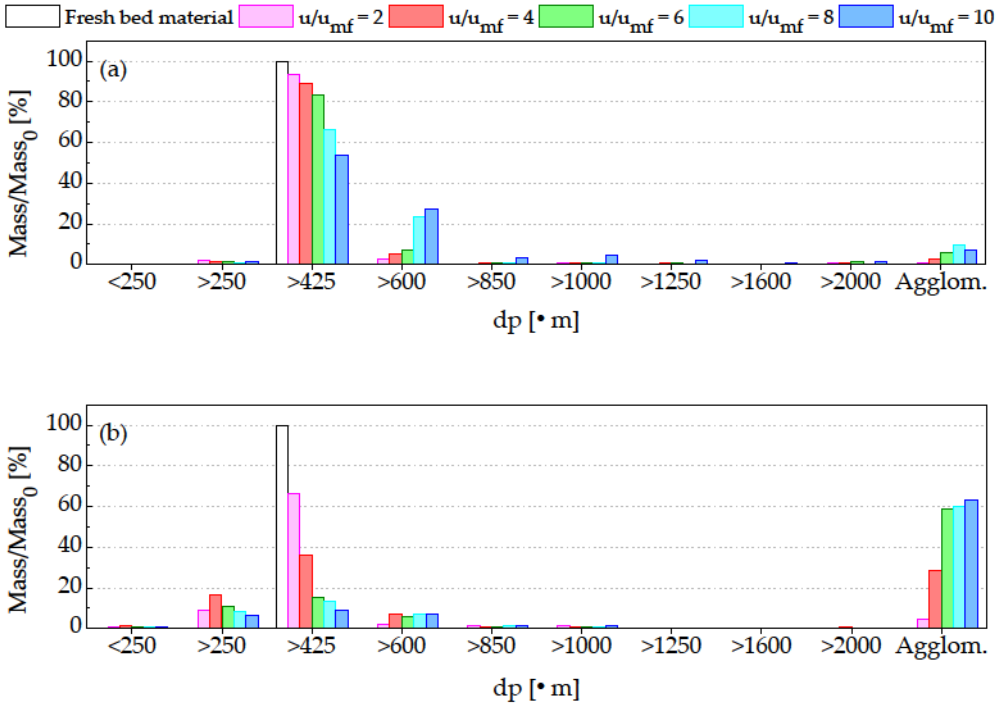


**Figure 3.13:** Bed material distribution: a) silica sand and b) sepiolite.

quite similar to the initial distribution ($d_p$ = 425-600 $\mu$m) for low air excesses while a reduction of mass of this size around 50 % is obtained in the case of $u/u_{mf} = 10$, most of it moving to the 600-850 $\mu$m fraction. In case of sepiolite, this reduction is achieved at lower $u/u_{mf}$ ratios. Bigger agglomerates are formed for sepiolite than for silica sand

at all air excess ratios. This effect is explained because of the fuel circulation inside the bed. Furthermore, sepiolite experiments are longer than silica sand increasing the ash accumulation within the bed compared with silica sand experiments.

The ash accumulated in the bed when defluidisation occurred is also calculated for the different $u/u_{mf}$ ratios for silica sand and sepiolite. This variable is presented in Figure 3.14a as the ratio of mass of ash accumulated in the bed at the onset of defluidisation to mass of bed material in order to compare the two bed materials. Because the experimental facility does not have a system to collect flying ash and elutriated bed material, the amount of ash accumulated in the bed is obtained theoretically from the biomass ash content (Table 2.1 and the feeding rate of biomass (Table 3.1).

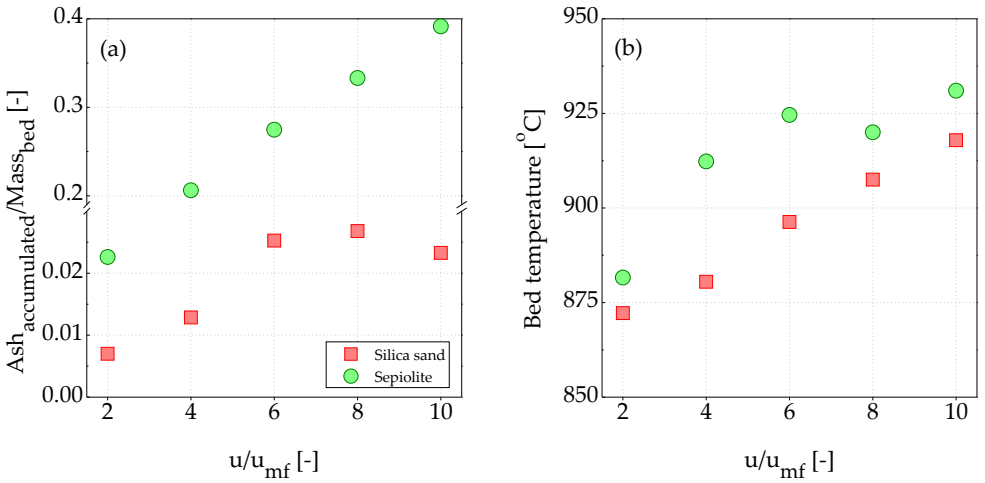


**Figure 3.14:** a) Ash-to-bed mass ratio at the onset of defluidisation at different u/umf ratios for sand and sepiolite and b) mean bed temperature during the gasification experiment at different u/umf ratios for sand and sepiolite.

The ash accumulation phenomenon in the reactor during the gasification process is directly related with the $u/u_{mf}$ ratio. Since the ER is kept at a constant value of 0.3 for all the experiments, an increase of the $u/u_{mf}$ ratio entails an increase of the feeding rate of biomass. However, for the sand at a ratio $u/u_{mf} = 10$, even if the biomass feeding rate is higher than for the $u/u_{mf} = 6$ and $u/u_{mf} = 8$ cases the low duration of the experiment, that is, the low defluidisation time (Figure 3.11), results in a lower amount of ash accumulated at the end of the experiment. On the other hand, for the sepiolite, the amount of ash accumulated in the reactor always increases with the $u/u_{mf}$ ratio, as the decrease of the defluidisation time with $u/u_{mf}$ (Figure 3.11) has a lower effect than the increase of the feeding rate of biomass.

Figure 3.14b shows the mean bed temperature within the bed during the gasification process for each experiment. As it can be observed, for sepiolite, when the ratio $u/u_{mf}$ reaches a value of 6 the bed temperature seems to become independent of $u/u_{mf}$. This behaviour means that the same fraction of biomass is transformed within the reactor. The vigorous fluidisation in combination with the low ratio of sepiolite to biomass density promotes a high level of mixing in the reactor maintaining a constant and uniform bed temperature. In this case, the mixing time is lower than the reaction time. On the other hand, for silica sand, the mean bed temperature always increases with $u/u_{mf}$. This effect is directly related with the fraction of biomass transformed during the experiment. As $u/u_{mf}$ increases, the fraction of biomass transformed increases and, consequently, the bed temperature rises. This effect can be explained by the enhance biomass mixing promoted by the augmented gas flow rate. The high density of the sand makes the biomass float at the top of the bed, and only increasing the flow rate improves the mixing level, leading to a higher fraction of biomass converted and higher bed temperatures. In this case the conversion is limited by the mixing time.

## 3.4 Conclusions

In this chapter, the results on the combustible and agglomeration behaviour, and the defluidisation time of *Cynara cardunculus* L. gasification in a BFB reactor using sepiolite as an alternative bed material are presented. The monitoring techniques have shown their capability to determine the defluidisation time, with a good agreement between them in accordance also with visual observations. In the case of the wide band energy, a detailed description of the agglomeration mechanisms occurring in each bed is addressed.

The jetsam behaviour of fuel particles in a sepiolite bed forms endogenous bubbles within the dense bed. This effect is clearly detected by the energy distribution of the power spectrum at the lower frequencies. Similarly, the wide band energy method identified the bed defluidisation by a significant reduction of the energy of $E_{wb2}$, which indicates a deterioration of the bulk dynamics for jetsam fuel particles. In this case, the whole bed tends to agglomerate in one big cylindrical shape inside the bed. In contrast, a flotsam behaviour is observed when using a silica sand bed, leading to a flat plate shape agglomerate on the top of the bed. In this case, the defluidisation process is faster than when using sepiolite due to the higher concentration of alkali compounds at the top of the bed, enhanced by the low axial mixing within the bed. According to the energy of the high frequencies ($E_{wb3}$), the bubble eruption rate is progressively reduced as the cap-clinker agglomerate is being formed on the bed surface. However, the bed remains fluidised under the cap-clinker, which is pointed by the energy values of $E_{wb2}$ and $E_{wb1}$. As the superficial gas velocity increases, greater cap-clinkers are formed and bigger channels

appears through the agglomerate, which produces the increase of $E_{wb3}$. The fuel particle behaviour also affects the definition of a reference state to compute the monitoring techniques to determine the defluidisation of the bed

An optimum value for $u/u_{mf}$ ratio is obtained for silica sand ($u/u_{mf} = 6$) and for sepiolite ($u/u_{mf} = 4$), existing some flexibility to choose the $u/u_{mf}$ ratio in the last case, if this ratio is high enough.

The ash-to-bed mass ratio is also analysed leading into a higher ash accumulation within the bed for the case of sepiolite. This ratio increases with $u/u_{mf}$ but in a smaller way than the ash feeding rate. A constant fraction of biomass is transformed for sepiolite when $u/u_{mf}$ ratio is higher than 6, being the mixing time lower than the reaction time. Contrary to this, the fraction of biomass transformed in silica sand experiments increases with $u/u_{mf}$, leading into a mixing time higher than the reaction time.

Sepiolite has demonstrated its benefits for biomass gasification in terms of defluidisation time, increasing considerably this value in advance of silica sand. The combustible behaviour leads to a better distribution of biomass and ash within the bed and avoiding hot zones.

# References

Bartels, M., Lin, W., Nijenhuis, J., Kapteijn, F. & van Ommen, J. R. 2008 Agglomeration in fluidized beds at high temperatures: Mechanisms, detection and prevention. *Progress in Energy & Combustion Science* 34, 633–666.

Bi, H. T. 2007 A critical review of the complex pressure fluctuation phenomenon in gas–solids fluidized beds. *Chemical Engineering Science* 62, 3473–3493.

Brown, R. C. & Brue, E. 2001 Resolving dynamical features of fluidized beds from pressure fluctuations. *Powder Technolgoy* 119, 68–80.

Bruni, G., Solimene, R., Marzocchella, A. Salatino, P., Yates, J. G., Lettieri, P. & Fiorentino, M. 2002 Self-segregation of high-volatile fuel particles during devolatilization in a fluidized bed reactor. *Powder Technology* 128, 11–21.

Chaplin, G., Pugsley, T. & Winters, C. 2004 Application of chaos analysis to pressure fluctuation data from a fluidized bed dryer containing pharmaceutical granule. *Powder Technology* 142, 110–120.

Chaplin, G., Pugsley, T. & Winters, C. 2005 Monitoring the fluidized bed granulation process based on s-statistic analysis of a pressure time series. *AAPPS PharmSciTech* 6, E198–E201.

Fiorentino, M., Marzocchella, A. & Salatino, P. 1997*a* Segregation of fuel particles and volatile matter during devolatilization in a fluidized bed reactor – I. Model development. *Chemical Engineering Science* 52, 1893–1908.

Fiorentino, M., Marzocchella, A. & Salatino, P. 1997*b* Segregation of fuel particles and volatile matter during devolatilization in a fluidized bed reactor – II. Experimental. *Chemical Engineering Science* 52, 1909–1922.

Fryda, L. E., Panopoulos, K. D. & Kakaras, E. 2008 Agglomeration in fluidised bed gasification of biomass. *Powder Technology* 181, 307–320.

Gómez-Hernández, J., Sánchez-Prieto, J., Briongos, J. V. & Santana, D. 2014 Wide band energy analysis of fluidized bed pressure fluctuation signals using a frequency division method. *Chemical Engineering Science* 105, 92–103.

Gómez-Hernández, J., Soria-Verdugo, A., Briongos, J. V. & Santana, D. 2016 Multiresolution analysis of a drying process in a rotating-distributor fluidized bed. *Drying Technology* 34, 119–131.

Guo, Q., Yue, G., Suda, T. & Sato, J. 2003 Flow characteristics in a bubbling fluidized bed at elevated temperature. *Chemical Engineering and Processing* 42, 439–447.

Johnsson, F., Zijerveld, R. C., Schouten, J. C., van den Bleek, C. M. & Leckner, B. 2000 Characterization of fluidization regimes by time-series analysis of pressure fluctuations. *International Journal of Multiphase Flow* 26, 663–715.

Lin, C.-L, Kuo, J.-H., Wey, M.-Y., Chang, S.-H. & Wang, K.-S. 2009 Inhibition and promotion: The effect of earth alkali metals and operating temperature on particle agglomeration/defluidization during incineration in fluidized bed. *Powder Technology* 189, 57–63.

Nienow, A. W., Rowe, P. N. & Chiba, T. 1978 Mixing and segregation of a small portion of large particles in gas fluidized beds of considerable smaller ones. *AIChe Symposium Series* 75, 45–53.

van Ommen, J. R., Coppens, M.-O., van den Bleek, C. M. & Schouten, J. C. 2000 Early warning of agglomeration in fluidized beds by attractor comparison. *AIChe Journal* 46, 2183–2197.

van Ommen, J. R., de Korte, R.-J. & van den Bleek, C. M. 2004 Rapid detection of defluidization using the standard deviation of pressure fluctuations. *Chemical Engineering and Processing: Process Intensification* 43, 1329–1335.

van Ommen, J. R., Sasic, S., van der Schaaf, J., Gheorghiu, S., F., Johnsson & Coppens, M.-O. 2011 Time-series analysis of pressure fluctuations in gas–solid fluidized beds – A review. *International Journal of Multiphase Flow* 37, 403–428.

Ríos, G. M., Tran, K. D. & Masson, H. 1986 Efficiency of different clay minerals modified with a cationic surfactant in the adsorption of pesticides: Influence of clay type and pesticide hydrophobicity. *Chemical Engineering Communications* 47, 247–272.

Saxena, S. C., Rao, N. S. & Tanjore, V. N. 1993 Diagnostic procedures for establishing the quality of fluidization of gas-solid systems. *Experimental Thermal and Fluid Science* 6, 56–73.

Saxena, S. C., Rao, N. S. & Zhou, S. J. 1990 Fluidization characteristics of gas fluidized beds at elevated temperatures. *Energy* 15, 1001–1014.

Scala, F. & Chirone, R. 2006 Characterization and early detection of bed agglomeration during the fluidized bed combustion of olive husk. *Energy & Fuels* 20, 120–132.

Solimene, R., M., Urciuolo, Cammarota, A., Chirone, R., Salatino, P., Damonte, G., Donati, C. & Puglisi, G. 2010 Devolatilization and ash comminution of two different sewage sludges under fluidized bed combustion conditions. *Experimental Thermal and Fluid Science* 34, 387–395.

Werther, J., Saenger, M., Hartge, E.-U., Ogada, T. & Siagi, Z. 2000 Combustion of agricultural residues. *Progress in Energy and Combustion Science* 26, 1–27.

Wormsbecker, M., Pugsley, T. & Tanfara, H. 2009 Interpretation of the hydrodynamic behaviour in a conical fluidized bed dryer. *Chemical Engineering Science* 64, 1739–1746.

CHAPTER
**FOUR**

# Sepiolite performance as bed material towards gas composition and tar mitigation

**Contents**



## 4.1 Introduction

The study of new bed materials for biomass gasification in fluidized beds has different aspects to be considered: agglomeration performance, mechanical resistance, and gas tar generation. In Chapter 3, sepiolite has been proposed as an alternative bed material for biomass gasification. The first feature has been analysed in terms of biomass particles behaviour, agglomeration and defluidisation analysis, leading to a better agglomeration performance than silica sand. However, to the author's knowledge, the performance of sepiolite towards gas and tar production and its characteristics as well as its mechanical resistance has not been evaluated yet.

The catalytic and porous properties of this type of bed material, natural occurring clays, has been studied for pyrolysis and gasification applications (Ito *et al.*, 2003;

Namioka *et al.*, 2003; Xie *et al.*, 2009; Noda *et al.*, 2009; Veses *et al.*, 2015). All these studies agree that porous materials such as sepiolite, with a high pore structure and surface area, enhance the adsorbance of tar and alkali content as well as they promote tar cracking reactions, although they are usually carried out under pyrolysis conditions (oxygen free and at lower temperatures than in gasification) using different facilities: fluidized beds, TGA and horizontal furnaces.

In this chapter, sepiolite is tested and compared to silica sand under gasification conditions in a fluidized bed using *C. cardunculus* L. as biomass feedstock. Gas and tar composition are evaluated as well as the gasification performance for both silica sand and sepiolite. In order to test the adsorbent properties of sepiolite towards tar generation, BET surface and SEM-EDS analyses have been carried out on sepiolite after the experiments. Finally, when testing a new bed material, as in this case with sepiolite, different aspects such as mechanical, chemical and agglomeration properties should be evaluated. In this sense, a long duration attrition test has been also performed over sepiolite to test this property.

## 4.2 Experimental setup and methodology

A brief description of the experimental facilities, the biomass and bed materials, and the methodology is presented in this section. Detailed information about all these aspects can be found in Chapter 2. In this study two different experimental facilities have been used: one for the gasification tests and one for the mechanical resistance experiments.

### 4.2.1 Gasification experiments

#### Setup and materials

The experimental facility employed for the gasification tests is the same as in the Chapter 3, the lab-scale BFB gasifier located at the Carlos III University of Madrid, but including the automatic feeding system and the gas cleaning section. The inner diameter and the total height of the reactor are 52.8 and 1480 mm, respectively. A 2 mm thickness perforate plate with 38 holes of 0.5 mm divides the reactor in two parts. The lower part is used to preheat the gasifying agent, air in this case, while the upper part contains the fluidized bed. The whole reactor is surrounded by two electrical furnaces. Biomass is introduced by the upper part by means of a vibrating feeding system. The product gas leaves the reactor passing through a hot filter, a condenser and a cold filter to clean the gas as a previous steps before to be analysed in a $\mu$-GC. Temperature and pressure are monitored in different zones of the plant (see Figure 2.4).

*C. cardunculus* is used as biomass feedstock for the gasification experiments. Tables 2.1, 2.2 and 2.4, show the properties of this biomass. In order to fulfil the feeding system requirements, biomass pellets are crushed and sieved into a particle size between 2.5 and 4.75 mm. Silica sand and sepiolite, with a particle diameter between 425 and 600 $\mu$m, are employed as bed materials. The properties of these bed materials are shown in Section 2.3 (Table 2.5). Silica sand is used as a reference bed material in order to test the performance of sepiolite towards gas and tar composition.

**Methodology**

To perform the gasification experiments with silica sand and sepiolite, the reactor is loaded with the bed material using a bed aspect ratio of $h_b/D = 2$ ($h_b = 105.6$ mm). Due to the different bed material bulk densities, this height is obtained using 342.50 g of silica sand or 129.10 g of sepiolite. The air supply is set to the experimental value. This air flow rate is chosen to obtain a $u/u_{mf}$ ratio of 5, which is in accordance to the results obtained in the agglomeration study presented in Chapter 3. The electrical furnaces are set depending on the bed material employed: in the case of sepiolite, the starting bed temperature is around 250 $^o$C below the desired experimental temperature; while in the case of silica sand, the starting bed temperature is quite close to the desired one. These differences in the plant operation are in relation with the combustible behaviour explained in the previous Chapter.

Once the reactor temperatures are stable, the biomass supply is started with a feeding rate to get an ER = 0.3. The real ER is obtained after each experiment when the exact amount of biomass fed into the gasifier is known. During the time needed to get the steady state, around 30-40 minutes from the start biomass of the feeding, the furnace temperatures are adjusted to get the desired experimental temperature. A nitrogen flow of 0.5 $Ndm^3/min$ is set from the feeding system to the reactor in order to prevent back-flow to the gases to the feeding system. Table 4.1 summarizes the operating conditions for each experiment. The gasification temperature has been chosen the highest temperature inside the reactor since this temperature will control the gas and tar composition. In the case of silica sand, the highest temperature is obtained in the freeboard ($T_{freeboard}$) while for sepiolite, the highest value is reached inside the bed ($T_{6cm}$). Figure 4.1 shows the pressure and temperature profiles for silica sand and sepiolite experiments. It can be seen, for silica sand tests (Figure 4.1b), how the bed temperature increases a little bit when the biomass supply starts due to the initial combustion of biomass. After some minutes, it decreases to a value close to the initial one due to the flotsam behaviour of biomass. This makes that the partial combustion occurs on the bed surface, not increasing the bed temperature. On the other hand, for sepiolite (Figure 4.1d), the temperature increases

up to the steady state temperature. The partial combustion of biomass also takes place inside the bed, increasing its temperature. The pressure profiles (Figures 4.1a and 4.1c) show similar trends, increasing the pressure when the biomass supply is started as a consequence of the higher gas production.

**Table 4.1:** Operating conditions.

| | silica sand | sepiolite | silica sand | sepiolite |
|---|---|---|---|---|
| Bed material [g] | 342.51 | 129.10 | 342.47 | 129.10 |
| Biomass feeding rate [$g_{daf}$/h] | 10.31 | 7.15 | 10.78 | 7.25 |
| Biomass throughput [$kg_{daf}/m^2h$] | 282.66 | 195.88 | 295.40 | 198.53 |
| Air flow rate [$Ndm^3$/min] | 15.25 | 10.50 | 15.25 | 10.50 |
| ER [–] | 0.30 | 0.30 | 0.29 | 0.29 |
| Air excess ratio, $u/u_{mf}$ [–] | 4.69 | 5.21 | 4.90 | 5.39 |
| $T_{3cm}$ [°C] | 772.85 | 805.68 | 823.31 | 834.52 |
| $T_{6cm}$ [°C] | 784.30 | 827.83 | 832.82 | 873.50 |
| $T_{freeboard}$ [°C] | 825.76 | 536.18 | 874.41 | 532.67 |

The product gas leaves the reactor and passes through a hot filter, made of glass wool, to remove the possible entrained particles and ash. After the hot filter, the gas is directed to a condenser to clean the gas from tars and water. The condensate is collected at the bottom of the condenser. After the condenser, the gas passes through a cold filter made of cotton, cigarettes filters and silica gel. This last filter removes the last possible tars, small particles and moisture. The hot filter and the pipes from the reactor up to the condenser are electrically heated and maintained between 300 and 350 °C to prevent tar condensation in this part of the installation.

### Sampling and analysis

The clean gas after the gasification tests is analysed at regular intervals of 2-3 minutes by means of a Varian Inc. CP-4900 $\mu$-GC. The gas analysis is started at the same time as biomass feeding. The gas composition is calculated as a mean value during the steady state, defined as the time when stable temperatures are achieved. In the mean time, 3 SPA tar samples are collected for analysis by GC-MS. Sections 2.7.3 and 2.7.4 shows more extensive information about the operating conditions and the equipments employed in these analyses. All these results show also the error of the measurements as their standard deviation from different samples.

When the experiment is finished, the bed material, the hot and cold filters, and the condenser are discharged and weight in order to get the amount of fines, water and tars collected in these elements. The gasification process is evaluated in terms of CGE, C and

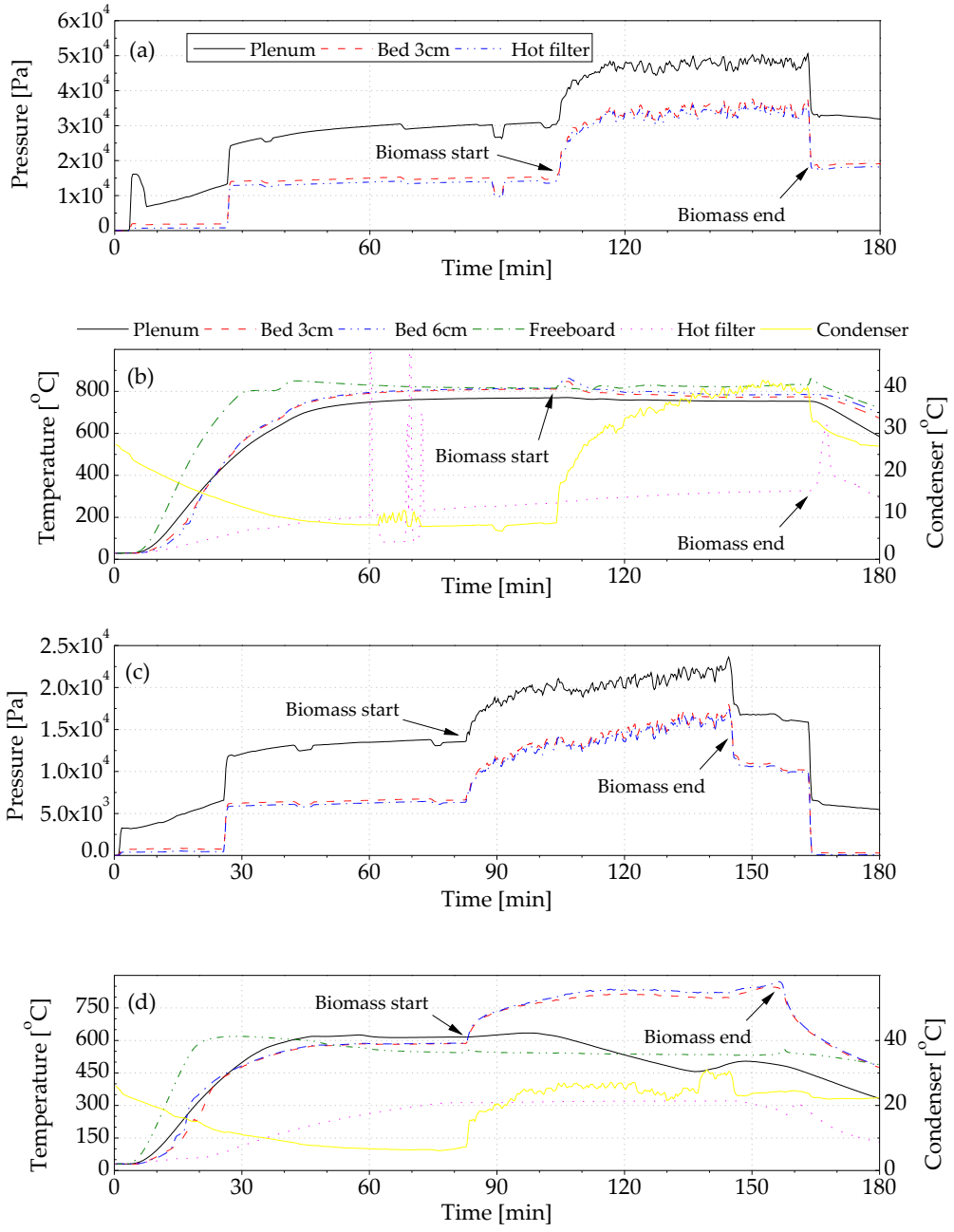


**Figure 4.1:** Pressure and temperature profiles for experiments at 828 °C and ER = 0.30: a) and b) silica sand, and c) and d) sepiolite.

H conversion, GY and LHV of the product gas. As the experimental facility does not have any mass or volume flow meter at the end of the cleaning section, a nitrogen balance is performed to obtain the amount of gas generated in the process. The calculation of all these parameters are explained in Section 2.7.2.

In order to better understand the use of sepiolite and its changes when used as a bed material, used sepiolite has been characterized in terms of BET surface area and SEM-EDS imaging. Besides, a solid extraction of the possible adsorbed organic compounds has been also performed with dichloromethane and analysed by GC-MS. A more detailed information about these analyses is shown in Section 2.7.5.

### 4.2.2 Attrition experiments

#### Setup

The second facility, employed for the mechanical resistance experiments, is a cold glass column BFB (Glass15) located at the Paul Scherrer Institute (Villigen, Switzerland). The lower section of the BFB has an inner diameter of 145 mm while the upper section has an inner diameter of 250 mm. A 10 $\mu$m porous steel plate of is used as distributor. This plant have different internals inside the column simulating heat exchanger tubes for other applications. The reactor is equiped with different sampling ports all along its height. Elutriated fines are retained in a 1 $\mu$m porous size filter at the exit of the freeboard (see section 2.5).

#### Experimental methodology

4.58 kg of sepiolite with a mean particle size of 226 $\mu$m is loaded into the Glass15 facility. Gas velocity is set to 5 times minimum fluidisation velocity ($u_g$ = 15.95 cm/s). Sepiolite is tested for 100 hours. During this time, different samples, at different times, are taken from the bed and from the filter for particle size analysis. The filter is weight before and after each time in order to get the amount of elutriated fines at that time.

#### Sampling and analysis

Finally, in the attrition experiment, the different samples from the bed and the entrained particles collected in the filter has been analysed by means of their particle size distribution using a sieving machine and a laser diffraction equipment. In addition, SEM images have been also obtained to better understand the sepiolite behaviour.

An attrition model proposed by Liu & Kimura (1993) (Eq. 4.1) has been applied to the experimental data in order to obtain the attrition rates, where W is the cumulative mass of entrained particles, $W_{e,0}$ is the initial mass of elutriable fine particles, $R_a$ is the

attrition rate and $K_e^*$ is a parameter that relates the elutriation rate constant ($K_e$), the cross-sectional area of the bed ($A_b$) and the $W_{e,0}$.

$$W = \left(W_{e,0} - \frac{R_a}{K_e^*}\right)\left(1 - e^{-K_e^* t}\right) + R_a t \tag{4.1}$$

$$K_e^* = \frac{K_e A_b}{W_{e,0}} \tag{4.2}$$

## 4.3 Results and discusion

### 4.3.1 Gas composition

The gas composition obtained from the four gasification tests is shown in Figure 4.2 and Table 4.2. The use of one or another bed material has noticeable effect on the different species that form the product gas. The most significant differences appear on the CO, $CO_2$ and light hydrocarbons ($C_2H_2$, $C_2H_4$ and $C_2H_6$). The amount of CO and light hydrocarbons is relatively higher in the case of silica sand, while the $CO_2$ is rather higher for sepiolite. A feasible explanation for these differences in the gas composition is the effect of the combustible behaviour. In the case of sepiolite, the biomass particles release the volatiles inside the bed and close to the air supply. These volatiles have to pass through the bed and the freeboard, and the oxygen molecules have more time to oxidise not only the char but also the CO and $H_2$ molecules, producing more $CO_2$ and $H_2O$. However, with silica sand, the volatiles are released on the top of the bed and goes directly to the freeboard where there is a more reducing atmosphere, generating more CO in detriment of $CO_2$ and $H_2O$. Xie *et al.* (2009) found higher $CO_2$ concentration than CO using sepiolite under pyrolysis conditions. They referred a weak catalytic role of sepiolite over gasification reactions ($C + CO_2 \leftrightarrow 2CO$ and $C + H_2O \leftrightarrow CO + H_2$, Eqs. 1.6 and 1.7) and cracking reactions (Tar $\rightarrow H_2 + CO + CO_2 +$ Char $+ C_nH_m$ and $C_nH_m \rightarrow H_2$ + Char, Eqs. 1.13 and 1.14). Veses *et al.* (2015) also found similar results under pyrolysis conditions using silica sand and sepiolite. Besides, $C_2H_6$ only is detected in this latter case, when sepiolite is used as bed material. The higher production of $C_2H_2$ and $C_2H_4$ in silica sand might be due to the tar cracking (Azhar Uddin *et al.*, 2008) as well as from the decomposition of aromatic compounds of these tars (Narváez *et al.*, 1996). Tars released, when silica sand is used, goes directly to the freeboard where the temperature is higher, enhancing the cracking reactions. However, in the case of sepiolite, the tars are only partially generated on the bed surface due to the better mixing behaviour. These tars goes to the freeboard where the temperature is not so high to promote the cracking reactions.

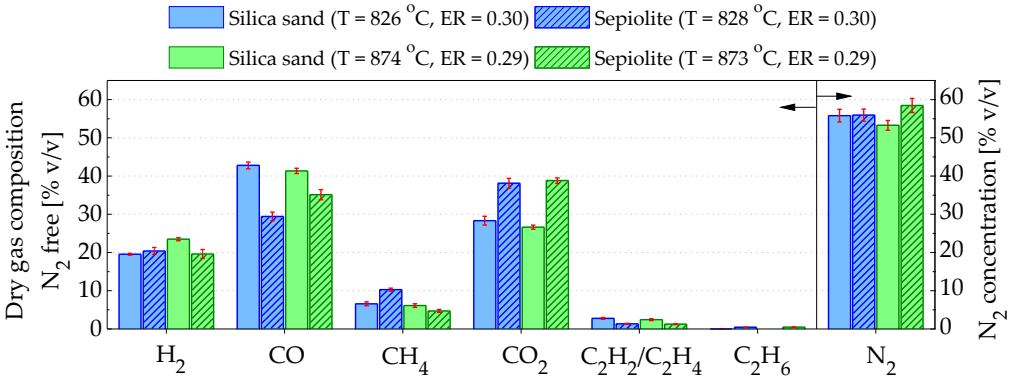


**Figure 4.2:** Gas composition (dry and $N_2$ free) for silica sand and sepiolite at different temperatures and ER.

**Table 4.2:** Dry syngas composition for each gasification experiment

| *Operating conditions* | | | | |
|---|---|---|---|---|
| Bed material | silica sand | sepiolite | silica sand | sepiolite |
| $T_{gasification}$ [°C] | 825.76 | 827.83 | 874.41 | 873.50 |
| ER [–] | 0.30 | 0.30 | 0.29 | 0.29 |
| *Dry syngas composition* | | | | |
| $H_2$ [% v/v] | 8.64±0.38 | 9.00±0.71 | 10.97±0.28 | 8.17±0.82 |
| CO [% v/v] | 18.91±0.83 | 12.96±0.57 | 19.32±0.51 | 14.58±0.35 |
| $CH_4$ [% v/v] | 2.92±0.34 | 4.53±0.20 | 2.87±0.30 | 1.97±0.24 |
| $CO_2$ [% v/v] | 12.51±0.36 | 16.78±0.71 | 12.44±0.32 | 16.12±0.58 |
| $C_2H_4$ [% v/v] | 1.22±0.14 | 0.59±0.07 | 1.14±0.15 | 0.53±0.02 |
| $C_2H_6$ [% v/v] | 0.00±0.01 | 0.19±0.02 | 0.00±0.00 | 0.19±0.02 |
| $N_2$ [% v/v] | 55.80±1.65 | 55.84±1.58 | 53.27±1.27 | 58.45±1.85 |
| $H_2O$ [% v/v] | 9.08 | 12.25 | 7.99 | 12.77 |

As it can be observed, there is not a clear trend in the gas composition with temperature for silica sand and sepiolite. In the case of silica sand, a bit higher $H_2$ amount is obtained when increasing temperature from 826 to 874 °C while a higher CO and lower $CH_4$ concentrations are got for sepiolite. These trends are according to the literature (Narváez *et al.*, 1996; de Andrés *et al.*, 2011; Mohammed *et al.*, 2011) although its effect is not very significant due to the small range of temperature evaluated.

The product gas ratios are shown in Figure 4.3. The $CO/CO_2$ ratio is higher in the case of silica sand for both experimental conditions. This means that the Boudouard reaction ($C + CO_2 \leftrightarrow 2CO$, Eq. 1.6) is promoted when silica sand is employed as bed

material. The $H_2/CO$ ratio is a bit higher for sepiolite at 827 °C and similar to silica sand at 874 °C, indicating that the water-gas shift reaction ($CO + H_2O \leftrightarrow H_2 + CO_2$, Eq. 1.9) has smaller influence than the Boudouard reaction. Regarding the $H_2/CO_2$ and the $CH_4/H_2$ ratios which give information about the dry reforming reaction ($C_nH_m$ (tar) + $nCO_2 \rightarrow (m/2)H_2 + 2nCO$, Eq. 1.11), the former is higher in silica sand experiments while the latter is higher in sepiolite experiment at 830 °C and similar to silica sand at 874 °C. This indicates that the dry reforming reaction is enhanced in the silica sand tests.

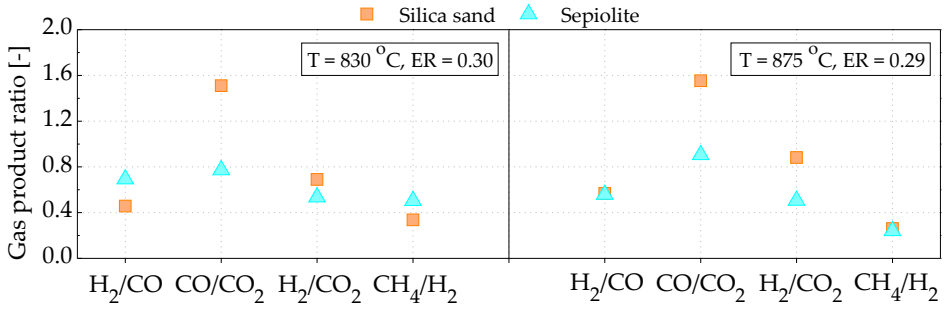


**Figure 4.3:** Product gas ratios for silica sand and sepiolite at different temperatures and ER.

The use of sepiolite has not increase the $H_2$ or CO concentration in the product gas in comparison with the results obtained using silica sand as bed material. Similar results have been reported by Veses *et al.* (2015) using silica sand and sepiolite under pyrolysis conditions in an auger reactor. On the other hand, Noda *et al.* (2009) only obtained a slightly higher $H_2$ concentration in the gas when due to the use of acidified bentonite.

### 4.3.2 Gasification performance

In order to evaluate the gasification performance, both C and H conversion, the CGE, the GY and the LHV of the produced gas are calculated. Figure 4.4 and Table 4.3 show the results of these calculations. Carbon conversion is higher for silica sand than for sepiolite as a consequence of the higher CO, $C_2H_2$ and $C_2H_4$ quantities in the product gas, being this parameter between 79 and 90 % for all cases. Hydrogen conversion ranges between 34 and 53 %. In this case, the higher generation of and $CH_4$ for sepiolite at 827 °C gives a higher H conversion than for silica sand contrary to the experiments at 874 °C where the H conversion is higher for silica sand due to the higher $H_2$ and $CH_4$ generation. The lower conversion of hydrogen in relation to carbon resides on the hydrogen losses due to the water, ammonia and hydrogen sulphide in the product gas. The LHV of the product gas is influenced by the gas composition as the gas species have different weight on the final value. The use of silica sand in the bed generates a product gas with a higher energy content as a consequence of the higher CO and light hydrocarbons production.

The differences are narrower at 827 °C because of the higher concentration of $CH_4$ in the sepiolite gas. The GY is very similar for all tested conditions and bed materials. The CGE evaluates the energy in the product gas in relation to the energy input from the biomass. This parameter is higher for silica sand than for sepiolite for both 827 and 874 °C, being the values between 48 and 70 %.

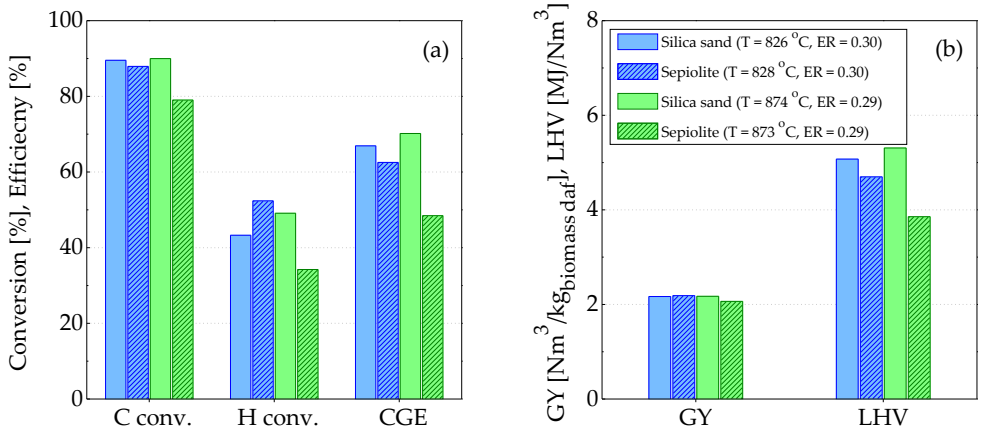


**Figure 4.4:** Gasification performance for silica sand and sepiolite at different temperatures and ER: a) C and H conversion, and CGE, and b) GY and LHV.

The amount of elutriated fines is lower in silica sand than in sepiolite. This in accordance with the high mechanical resistance of silica sand and the fines generated by abrasion in the case of sepiolite. Anyway, this property is also evaluated for sepiolite at the end of this Chapter by means of a long duration attrition test. The moisture generation shows also bigger values sepiolite than for silica sand. The reason, as stated above, can be the higher contact of the volatiles with the oxygen molecules inside the sepiolite bed, producing more $H_2O$ and $CO_2$.

### 4.3.3 Tar composition

The SPA tar samples acquired from the experiments are analyzed by means of a GC/MS as described in Chapter 2. Figure 4.5 shows a comparison of the total ion current cromatograms obtained for both silica sand and sepiolite at 830 °C and an ER equal to 0.30, where up to 25 tar species have been identified using the NIST 2.0 mass spectrum library. Table 4.4 shows the different tar compounds identified in the order in which they elute.

**Table 4.3:** Gasification parameters for each gasification experiment.

| *Operating conditions* | | | | |
|---|---|---|---|---|
| Bed material | silica sand | sepiolite | silica sand | sepiolite |
| $T_{gasification}$ [°C] | 825.76 | 827.83 | 874.41 | 873.50 |
| ER [–] | 0.30 | 0.30 | 0.29 | 0.29 |
| *Gasification parameters* | | | | |
| Lower heating value [MJ/Nm$^3$] | 5.07 | 4.70 | 5.31 | 3.86 |
| Gas yield [Nm$^3$/kg$_{biomass\ daf}$] | 2.17 | 2.19 | 2.17 | 2.07 |
| Carbon conversion [%] | 89.52 | 87.91 | 89.98 | 79.01 |
| Hydrogen conversion [%] | 43.29 | 52.38 | 49.10 | 34.23 |
| Cold gas efficiency [%] | 66.92 | 62.53 | 70.19 | 48.47 |
| Elutriated fines [g/kg$_{biomass\ daf}$] | 8.77 | 26.72 | 5.47 | 32.84 |
| Moisture generation [g/kg$_{biomass\ daf}$] | 173.96 | 245.26 | 151.70 | 242.86 |
| GC detectable tar [g/kg$_{biomass\ daf}$] | 21.76 | 11.11 | 22.52 | 9.22 |

Figure 4.6 shows the tar quantities for the different tar groups (Milne *et al.*, 1998): secondary (i.e. benzene, toluene, phenol, etc.), tertiary-alkyl (i.e. 2-methylnaphthalene, etc.) and tertiary-PAH (i.e. naphthalene, fluorene, pyrene, etc.), as well as total tar, quantified as the sum of all identified species, and BTEX (benzene, toluene, ethylbenzene and xylenes). There are significant differences in the tar production depending on the bed material used. Using sepiolite, the total tar is reduced for around 50 % with respect to silica sand at the same temperature and ER conditions. Tar reduction properties of sepiolite can also be observed in the presented tars groups. In the case of secondary tars, the tar reduction effect of sepiolite is not such high, increasing slightly when temperature is incremented from 827 to 874 °C. However, this effect is not obvious since the quantities are within the margin of error. For tertiary-alkyl tars, sepiolite produces around 50 % less compounds than silica sand. Nevertheless, the quantities of tertiary-alkyl tars are not so significant as for example for tertiary PAH tars. The highest tar reduction is observed in the tertiary-PAH group, where quantities decrease more than the 90 % (90.8 and 94.7 % for 830 and 875 °C, respectively). The BTEX fraction is also around 60 % lower for sepiolite than for silica sand, independently of the temperature. Thereby, a good tar reduction activity of sepiolite, in particular to reduce tertiary-PAH and BTEX compounds, is responsible for the lower total tar content.

Figure 4.7 and Table 4.4 present the tar composition for the 25 identified tar species and notable differences between the two bed materials can be observed. The main tar species for silica sand are benzene, naphthalene, acenaphthylene and phenanthrene, while

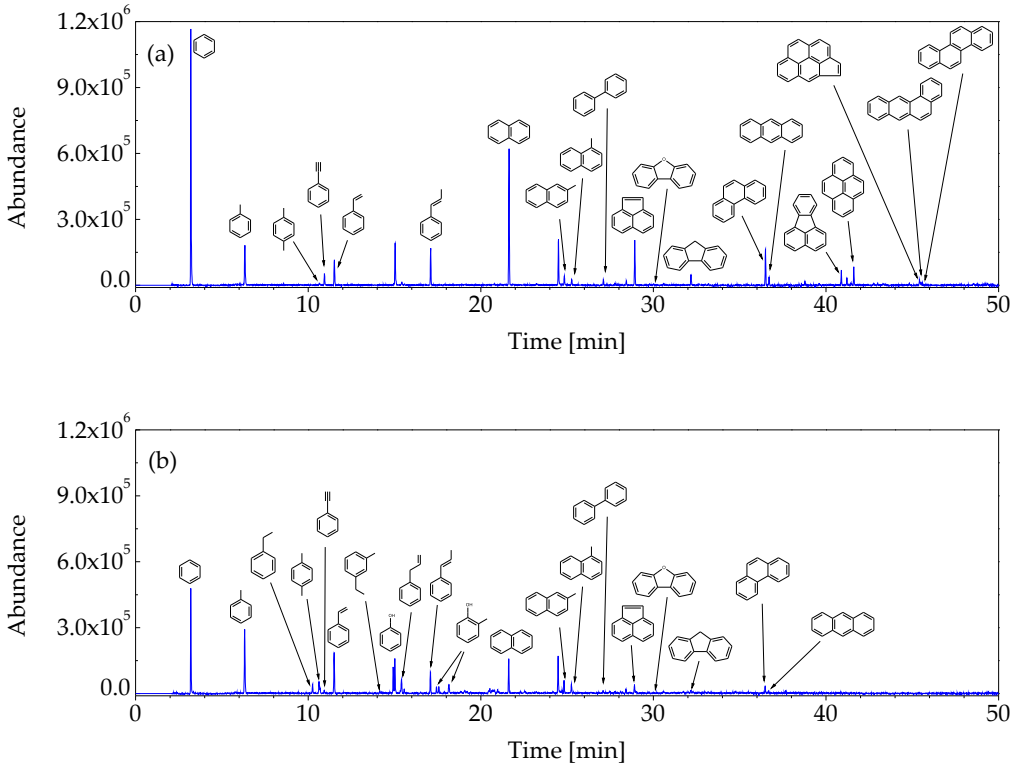


**Figure 4.5:** Total ion current cromatograms from GC/MS for the two bed materials at 830 °C and ER = 0.30: a) silica sand and b) sepiolite.

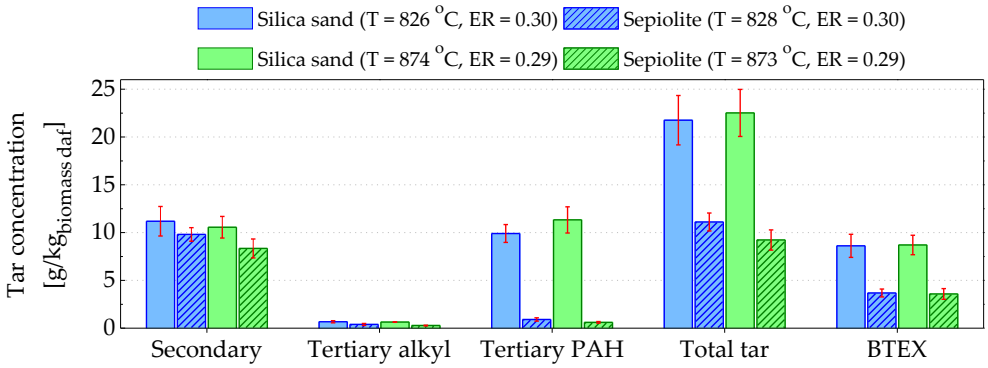


**Figure 4.6:** Tar concentration from the gasification experiments, grouped according to Milne *et al.* (1998).

**Table 4.4:** Identified and quantified tar compounds in $g/Nm^3_{raw\ gas}$.

| Tar compound | Retention time [min] | Tar group[a] | Silica sand T = 826 °C ER = 0.30 | Sepiolite T = 828 °C ER = 0.30 | Silica sand T = 873 °C ER = 0.29 | Sepiolite T = 874 °C ER = 0.29 |
|---|---|---|---|---|---|---|
| Benzene | 3.23 | secondary | 3.25±0.43 | 0.50±0.10 | 3.59±0.44 | 0.58±0.13 |
| Toluene | 6.42 | secondary | 0.69±0.14 | 0.78±0.07 | 0.42±0.05 | 0.76±0.10 |
| Ethylbenzene | 10.31 | secondary | 0.00 | 0.14±0.02 | 0.00 | 0.15±0.01 |
| o/m/p-Xylene | 10.68 | secondary | 0.03±0.02 | 0.27±0.04 | 0.00 | 0.24±0.03 |
| Phenylethyne | 10.94 | secondary | 0.19±0.02 | 0.01±0.02 | 0.20±0.02 | 0.00 |
| Styrene | 11.56 | secondary | 0.41±0.06 | 0.37±0.03 | 0.28±0.03 | 0.37±0.04 |
| 1-ethyl-3-methyl-Benzene | 14.18 | secondary | 0.00 | 0.06±0.02 | 0.00 | 0.05±0.01 |
| Phenol | 14.96 | secondary | 0.00 | 0.80±0.06 | 0.00 | 0.65±0.05 |
| 2-propenyl-Benzene | 15.44 | secondary | 0.00 | 0.21±0.01 | 0.00 | 0.17±0.03 |
| 1-propenyl-Benzene | 17.10 | secondary | 0.55±0.10 | 0.15±0.03 | 0.37±0.04 | 0.13±0.02 |
| o/m/p-Cresol | 17.45+18.18 | secondary | 0.00 | 1.19±0.14 | 0.00 | 0.94±0.11 |
| Naphthalene | 21.63 | tertiary-PAH | 2.34±0.21 | 0.24±0.06 | 2.58±0.34 | 0.17±0.03 |
| 2-methyl-Naphthalene | 24.83 | tertiary-alkyl | 0.13±0.03 | 0.09±0.02 | 0.10±0.01 | 0.08±0.01 |
| 1-methyl-Naphthalene | 24.26 | tertiary-alkyl | 0.09±0.02 | 0.07±0.02 | 0.08±0.01 | 0.05±0.01 |
| Biphenyl | 27.07 | tertiary-PAH | 0.09±0.01 | 0.03±0.03 | 0.12±0.01 | 0.00 |
| Acenaphthylene | 28.92 | tertiary-PAH | 0.76±0.04 | 0.06±0.01 | 0.90±0.12 | 0.03±0.01 |
| Dibenzofuran | 30.58 | secondary | 0.04±0.00 | 0.00 | 0.02±0.02 | 0.01±0.01 |
| Fluorene | 32.19 | tertiary-PAH | 0.19±0.03 | 0.06±0.01 | 0.14±0.02 | 0.06±0.01 |
| Phenanthrene | 36.48 | tertiary-PAH | 0.59±0.04 | 0.06±0.01 | 0.65±0.08 | 0.03±0.01 |
| Anthracene | 36.70 | tertiary-PAH | 0.14±0.02 | 0.01±0.01 | 0.15±0.02 | 0.00 |
| Fluoranthene | 40.89 | tertiary-PAH | 0.19±0.04 | 0.00 | 0.24±0.04 | 0.00 |
| Pyrene | 41.61 | tertiary-PAH | 0.23±0.05 | 0.00 | 0.31±0.06 | 0.00 |
| Cyclopenta[cd]pyrene | 45.41 | tertiary-PAH | 0.05±0.02 | 0.00 | 0.10±0.03 | 0.00 |
| Benzo[a]anthracene | 45.45 | tertiary-PAH | 0.03±0.01 | 0.00 | 0.06±0.01 | 0.00 |
| Chrysene | 45.57 | tertiary-PAH | 0.04±0.01 | 0.00 | 0.09±0.02 | 0.00 |
| *Secondary tar* | | | 5.16±0.71 | 4.49±0.32 | 4.86±0.52 | 4.04±0.48 |
| *Tertiary alkyl tar* | | | 0.31±0.05 | 0.18±0.05 | 0.29±0.01 | 0.13±0.02 |
| *Tertiary PAH tar* | | | 4.57±0.43 | 0.42±0.08 | 5.21±0.63 | 0.29±0.04 |
| *Total tar* | | | 10.04±1.19 | 5.08±0.43 | 10.37±1.13 | 4.47±0.51 |
| *Tar dew point** [°C] | | | 148.2 | 70.5 | 159.1 | 58.3 |

[a] According to Milne *et al.* (1998) classification, * Obtained from the ECN tar dew point site (www.thersites.nl)

cresols, phenol, toluene and benzene are the most abundant tar compounds in sepiolite. Benzene and PAHs are drastically reduced with a sepiolite bed as it has been shown in Figures 4.6 and 4.7. Chrysene (PM ≈ 228.29 g/mol) is the heaviest tar compound identified when silica sand is used as a bed material, while anthracene (PM ≈ 178.23 g/mol) is the heaviest tar compound identified during sepiolite gasification.

One of the most remarkable differences between silica sand and sepiolite is that phenols, ethylbenzene and xylenes are only present when sepiolite is used as bed material. This observation can be due to the combustible behaviour presented in Chapter 3. In the case of silica sand, with a higher bulk density, the biomass particles float on the top of the bed. The contact between volatiles and the bed material is limited since the

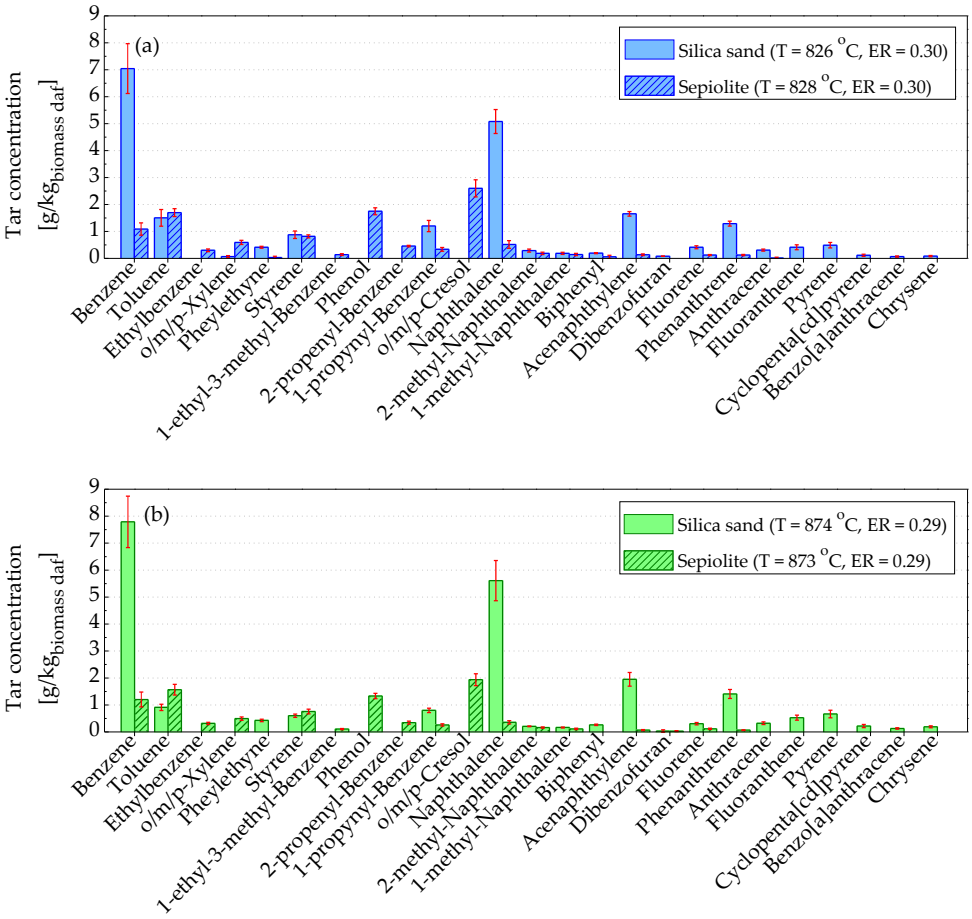


**Figure 4.7:** Tar concentration for individual compounds for both silica sand and sepiolite: a) T = 827 °C and ER = 0.30 and b) T = 874 °C and ER = 0.29.

released volatiles migrate directly to the freeboard (Mayerhofer *et al.*, 2014) where the temperature is higher than the bed temperature as the partial combustion of biomass does not take place inside the bed (see bed and freeboard temperatures in Table 4.1). The temperature in the freeboard is higher than 750 °C, and consequently, it promotes the conversion of oxygenated species into PAH via cyclopentadiene radicals which then combine to generate aromatics with two or more rings as sugessted by Fitzpatrick *et al.* (2008) and Yu *et al.* (2014), and the reforming reactions in the freeboard. On the other hand, with sepiolite as bed material, biomass particles are distributed inside the bed and also on the bed surface. The partial combustion of biomass occurs inside the bed increasing the temperature in this part of the reactor which is higher than in the freeboard

(see Table 4.1). Volatiles are released inside the bed as well as on the top of the bed. Volatiles formed on the bed surface enter directly into the freeboard where the temperature is lower than 750 °C (≈ 534 °C) and hence, the presence of single ring alkyated and oxygenated tars are not reformed into tertiary aromatic tars, remaining in the product gas.

Since the mixing regime between biomass and the bed material is not the same, it cannot be justified to what extend the catalytic effect of the sepiolite and silica sand affect the tar reforming reactions.

### 4.3.4 Sepiolite analysis after gasification

Sepiolite is known to be a porous material with a high specific surface area, between 75 and 400 $m^2/g$, approximately (Suárez & García-Romero, 2012). The specific surface area can be also related with the tar reduction in the gasification process. The pores and cavities as well as the sepiolite surface can accommodate different tar molecules. Different studies have demonstrated the adsorbent capacity of sepiolite using oils (Zadaka-Amir *et al.*, 2013), wastewater (Dogan *et al.*, 2007) and other elements such as water, benzene, pyrdine, or ethylbenzene (Inagaki *et al.*, 1990). The results show that these compounds are mainly adsorbed on the surface of the sepiolite and a small amount are adsorbed in the internal cavities. This process highly decreases the specific surface area. In order to investigate if these effects are responsible for the differences obtained in the tar production and composition, fresh and used sepiolite have been analysed in terms of BET surface area and SEM-EDS.

The fresh sepiolite employed in the experiments results in a BET surface area of 199.2 $m^2/g$. This value agrees with the BET surface areas reported in the literature (Sánchez-Martín *et al.*, 2006; Suárez & García-Romero, 2012). In the case of used sepiolite, after the cardoon gasification, the BET surface area is reduced to 6.5 $m^2/g$. This reduction might have two contributions: a change in the internal structure of the sepiolite due to the heating above 350 °C (Serna *et al.*, 1975; Balci, 1996, 1999), and the adsorption of different compounds on the sepiolite surface. Ito *et al.* (2003) also experimented a decrease in the BET surface area of sepiolite after tar capture at pyrolysis conditions.

Figure 4.8 shows the SEM images of fresh and used sepiolite. Some differences between the two figures can be noticed. Fresh sepiolite (Figure 4.8a) shows a lot of fibers that are completely transformed after cardoon gasification (Figure 4.8b). Rounded grains can be observed after the experiments which might indicate a possible deposit of molten ashes and tars on the surface of sepiolite.

Figure 4.9 and Table 4.5 shows the results of the SEM-EDS analysis. Fresh sepiolite is formed by oxygen, magnesium, aluminum silicon and chlorine. However, the composition

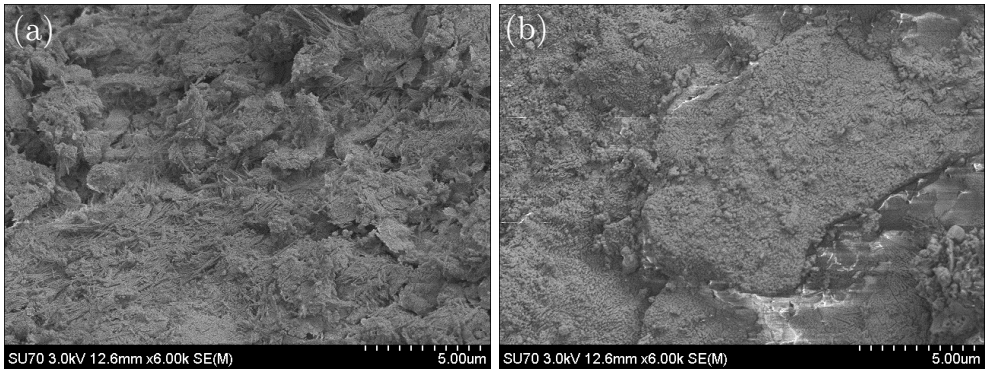


**Figure 4.8:** SEM analysis for sepiolite: a) fresh sepiolite and b) used sepiolite.

of the used sepiolite is quite different. Two zones are clearly distinguished in this second case: a soft zone (spectrums 1 and 3) and a rough zone (spectrums 2 and 4). Looking into the composition of the soft zone, a high amount of carbon is observed with very small quantities of other minor elements. This carbon may come from the adsorbed tars on the surface of the sepiolite. The rough zone shows no or minor amounts of carbon and high quantities of elements typical from biomass ashes such as Na, Cl, K and Ca. These results confirm the hyphothesis of adsorbed tars, obtaining a cleaner gas. This results were also confirmed by Ito *et al.* (2003) who refered that micropores in the sepiolite are plugged by tar hydrocarbons and capture tar. Besides, they also show that molten ashes are adsorbed on the surface, avoiding agglomeration problems. This fact may explain the higher defluidisation time obtained in Chapter 3.

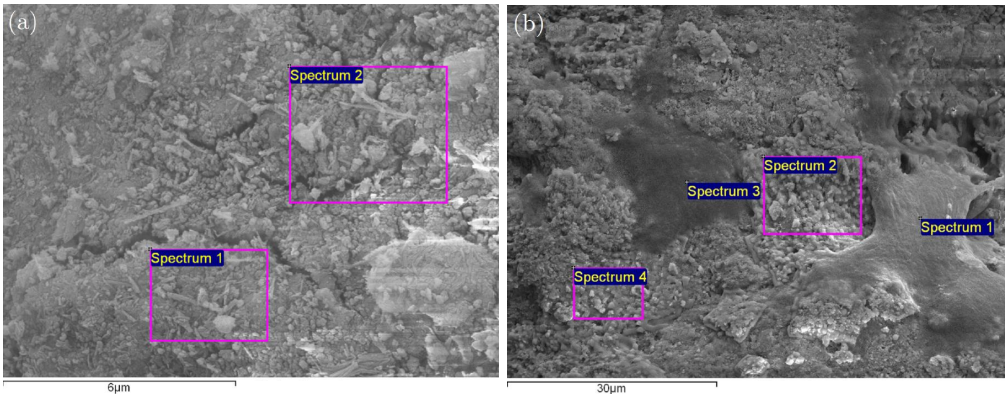


**Figure 4.9:** SEM-EDS analysis for sepiolite: a) fresh sepiolite and b) used sepiolite.

In addition, a solid extraction with dichloromethane has been performed in sample

**Table 4.5:** Identified species from SEM-EDS analysis on fresh and used sepiolite from Figure 4.9.

| | C | O | Mg | Al | Si | Cl | Na | K | Ca |
|---|---|---|---|---|---|---|---|---|---|
| *Fresh sepiolite [wt.%]* | | | | | | | | | |
| Spectrum 1 | | 58.08 | 10.61 | 2.75 | 26.76 | 1.81 | | | |
| Spectrum 2 | | 58.33 | 12.56 | 2.41 | 25.76 | 0.95 | | | |
| *Used sepiolite [wt.%]* | | | | | | | | | |
| Spectrum 1 | 75.54 | 22.70 | | | | | 1.77 | | |
| Spectrum 2 | 11.64 | 15.08 | 3.75 | 0.92 | 1.46 | 34.23 | 14.83 | 14.85 | 3.25 |
| Spectrum 3 | 61.47 | 28.30 | 2.87 | 0.51 | 2.36 | | 0.96 | | 3.55 |
| Spectrum 4 | | 13.90 | 1.45 | 0.87 | 1.34 | 41.99 | 18.21 | 19.49 | 2.75 |

of sepiolite after gasification. The extracted compounds have been analysed by GC-MS to get a picture of the possible adsorbed tars. Figure 4.10 shows the chromatogram of this analysis. Peaks for naphthalene, acenaphthylene, dibenzofuran, fluorene and phenanthrene can be observed, supporting the above hypothesis that sepiolite adsorbs the tars generated in the bed. This result is also in agreement with the low tertiary-PAH tars generated in the product gas as they are adsorbed by the sepiolite.

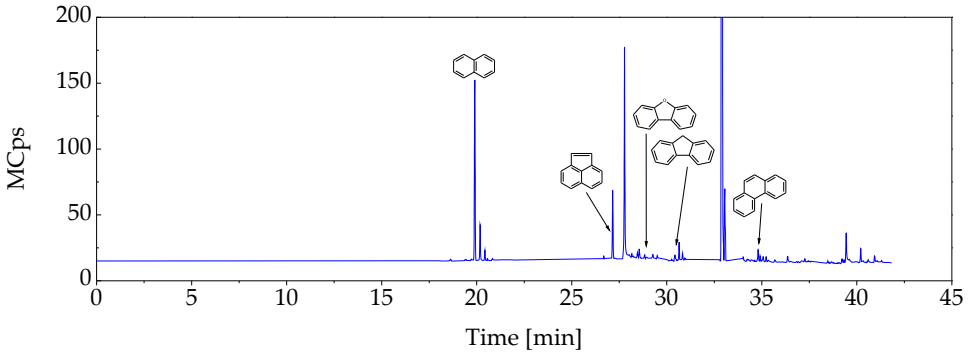


**Figure 4.10:** Total ion current cromatogram from GC/MS for the adsorbed tars in the used sepiolite

### 4.3.5 Attrition performance of sepiolite

Figure 4.11 shows the results from the attrition test performed on the sepiolite for 100 hours, and the results for other different bed materials tested previously at the Paul Scherrer Institute (Maurer *et al.*, 2016). Two regions can be differentiated: an initial zone (the first 20 hours approximately) where elutriation of fine particles increases sharply

with time, and a second zone where elutriation rate reaches a constant value. During the first hours of operation a high elutriation rate is observed. Most of the fines are elutriated from the bed in this region. Sepiolite shows similar behaviour as alumina sand ($Al_2O_3$) for the same fluidisation regimen and as dolomite for a smaller fluidisation number in this early stage. However, significant differences appear when a constant elutriation rate is reached. Sepiolite presents smaller elutriation rate than $Al_2O_3$ for the same conditions. Comparing with the tests performed at the Paul Scherrer Institute for $Al_2O_3$ and dolomite (Maurer *et al.*, 2016), sepiolite is the material with the lowest elutriation rate during the steady state. The model developed by Liu & Kimura (1993) fits the experimental data quite good with the parameters shown in Table 4.6.

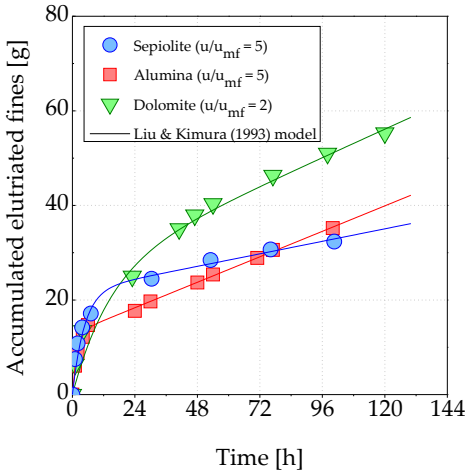


**Figure 4.11:** 100 h attrition test for sepiolite (alumina and dolomite data taken from Maurer *et al.* (2016)).

**Table 4.6:** Parameters for the Liu & Kimura (1993) model.

| | $R_a$ | $K_e^*$ |
|---|---|---|
| Sepiolite ($u/u_{mf} = 5$) | 0.1102 | 0.2211 |
| Alumina ($u/u_{mf} = 5$) | 0.2244 | 0.5638 |
| Dolomite ($u/u_{mf} = 2$) | 0.2504 | 0.1688 |

The above results should be compared carefully due to the differences in the particle size distribution of fresh sepiolite and $Al_2O_3$ (Figure 4.12a). Fresh sepiolite have a fraction of particles smaller than 160 $\mu$m ($\approx$ 42 %) while this fraction in $Al_2O_3$ is much smaller ($\approx$ 2.5 %). According to Geldart's classification (Geldart, 1973), the sepiolite

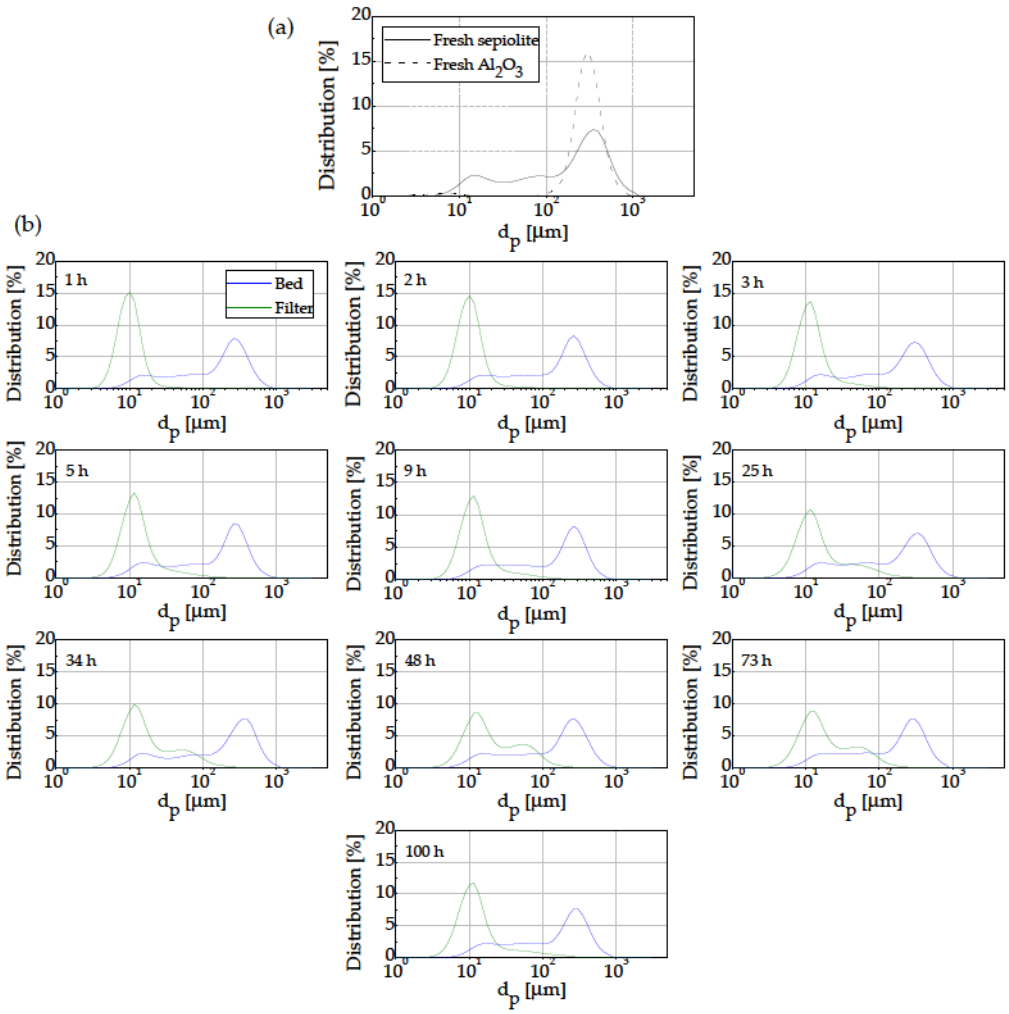


**Figure 4.12:** Particle size distribution: a) fresh bed materials (alumina data taken from Maurer *et al.* (2016)) and b) bed particles and filter fines at different time intervals.

fraction used in this test covers different groups (group A and B) while $Al_2O_3$ is mostly framed in the group B. This can affect the behaviour in the bed and also the attrition an elutriation. The small fines are supposed to be elutriated in the first hours although the results (Figure 4.11) do not show this effect. Figure 4.12 presents the particle size analysis carried out in the sepiolite bed particles from the bed and from the filter at different operating hours all along the attrition test. It can be seen that the particle size distribution of bed particles shows no significant changes with time. The fraction of small particles remains in the bed for all the attrition test. This suggests that these

fines are attached to the particle surface/pores. In order to confirm this hypothesis SEM images of the bed particles are shown in Figure 4.13. The images show no noticeable macroscopic changes in the sepiolite after the attrition test (Figures 4.13a and 4.13d), indicating no particle breakage. The fines attached to the fresh sepiolite are rough forming laminates and irregular forms (Figure 4.13b and 4.13) while they look smaller and more homogeneous in the used sepiolite (Figure 4.13e, 4.13f and 4.13g). It seems that the initial fines are elutriated from the bed and replaced by new smaller fines generated through the sepiolite attrition.

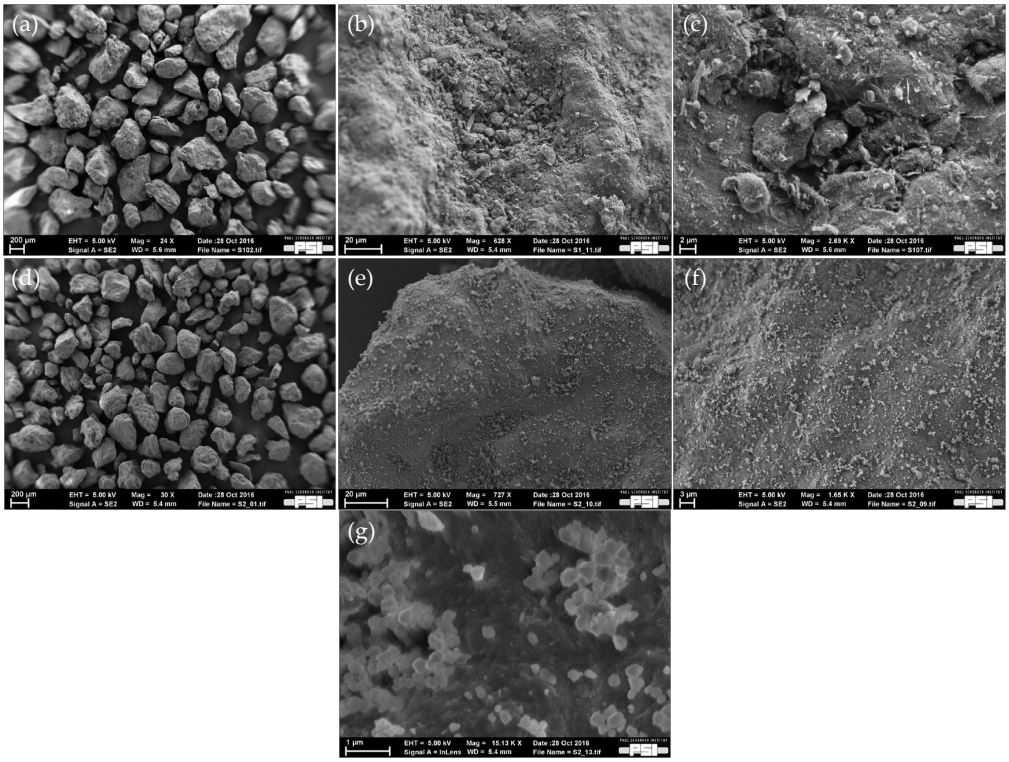


**Figure 4.13:** SEM images of sepiolite: a), b) and c) fresh sepiolite, and d), e), f) and g) used sepiolite after 100 hours.

The small change in the particle size distribution in the bed particles indicates that the attrition phenomena in the sepiolite is mainly due to abrasion where the roughness of the particles is eliminated from the surface. As a consequence, the diameter of the particles is not significantly modified.

## 4.4 Conclusions

In this chapter, sepiolite has been tested under gasification conditions in terms of gas and tar composition, comparing the results with a commonly used bed material like silica sand.

The use of sepiolite do not improve the gas composition, generating more $CO_2$ and less CO than the gas produced by silica sand while the $H_2$ content does not show a clear trend between the two bed materials. The carbon conversion, CGE and LHV of the raw gas are also smaller in the case of sepiolite as bed material.

In relation to the tar generation, sepiolite reduces efficiently the tar generation up to 50% in comparison with silica sand, and specifically it decreases the tertiary-PAH tars. The composition of these tars is also quite different, appearing single ring alkyated and oxygenated compounds such as xylenes and phenols in sepiolite, and disappearing tars with a molecular weight higher than anthracene.

The high reduction of tars in the product gas is achieved due to the physical properties of sepiolite: porous structure and high surface area that adsorb the tar compounds on its surface, mainly tertiary-PAH compounds, as well as the molten ashes, reducing the risk of agglomeration.

Finally, sepiolite has shown a good attrition behaviour during a long duration test. The results show the smallest attrition rate among other common bed materials such as alumina or dolomite. In addition, the original fines from the fresh sepiolite seems to be elutriated out of the bed although the new generated fines are retained on the surface/pores of the sepiolite, reducing the attrition rate during the operation.

## References

de Andrés, J. M., Narros, A. & Rodríguez, M. E. 2011 Behaviour of dolomite, olivine and alumina as primary catalysts in air-steam gasification of sewage sludge. *Fuel* 90, 521–527.

Azhar Uddin, M. D., Tsuda, H., Wu, S. & Sasaoka, E. 2008 Catalytic decomposition of biomass tars with iron oxide catalysts. *Fuel* 87, 451–459.

Balci, S. 1996 Thermal decomposition of sepiolite and variations in pore structure with and without acid pre-treatment. *Journal of Chemical Technology and Biotechnology* 66, 72–78.

Balci, S. 1999 Effect of heating and acid pre-treatment on pore size distribution of sepiolite. *Clay Minerals* 34, 647–655.

Dogan, M., Özdemir, Y. & Alkan, M. 2007 Adsorption kinetics and mechanism of cationic methyl violet and methylene blue dyes onto sepiolite. *Dyes and Pigments* 75, 701–713.

Fitzpatrick, E. M., Jones, J. M., Pourkashanian, M., Ross, A. B., Williams, A. & Bartle, K. D. 2008 Mechanistic aspects of soot formation from the combustion of pine wood. *Energy & Fuels* 22, 3771–3778.

Geldart, D. 1973 Types of gas fluidization. *Powder Technology* 7, 285–292.

Inagaki, S., Fukushima, Y., Doi, H. & Kamigaito, O. 1990 Pore size distribution and adsorption selectivity of sepiolite. *Clay Minerals* 25, 99–105.

Ito, K., Moritomi, H., Yoshie, R., Uemiya, S. & Nishimura, M. 2003 Tar capture effect of porous particles for biomass fuel under pyrolysis conditions. *Journal of Chemical Engineering of Japan* 36, 840–845.

Liu, Y.-D. & Kimura, S. 1993 Fluidization and entrainment of difficult-to-fluidize fine powdermixed eith easy-to-fluidize large particles. *Powder Technology* 75, 189–196.

Maurer, S., Durán, S. R., Künstle, M. & Biollaz, S. M. A. 2016 Influence of interparticle forces on attrition and elutriation in bubbling fluidized beds. *Powder Technology* 291, 473–486.

Mayerhofer, M., Fendt, S., Spliethoff, H. & Gaderer, M. 2014 Fluidized be gasification of biomass – In bed investigation of gas and tar formation. *Fuel* 117, 1248–1255.

Milne, T. A., Evans, R. J. & Abatzoglou, N. 1998 Biomass gasifier "tars": Their nature , formation and conversion. NREL/TP-570-25357. *Tech. Rep.* National Renewable Energy Laboratory.

Mohammed, M. A. A., Wan Azlina, W. A. K. G., Mohammed Amran, M. S. & Fakhru'l-Razi, A. 2011 Air gasification of empty fruit bunch for hydrogen-rich gas production in a fluidized-bed reactor. *Energy Conversion and Management* 52, 1555–1561.

Namioka, T., Yoshikawa, K., Hatano, H. & Suzuki, Y. 2003 High tar reduction with porous particles for low temperature biomass gasification: Effects of porous particles on tar and gas yields during sawdust pyrolysis. *Journal of Chemical Engineering of Japan* 36, 1440–1448.

Narváez, I., Orío, A., Aznar, M. P. & Corella, J. 1996 Biomass gasification with air in an atmospheric bubbling fluidized bed. Effect of six operational variables on the quality of the produced raw gas. *Industrial & Engineering Chemistry Research* 35, 2110–2120.

Noda, R., Ito, T., Tanaka, N. & Horio, M. 2009 Steam gasification of cellulose and wood in a fluidized bed of porous clay particles. *Journal of Chemical Engineering of Japan* 42, 490–501.

Sánchez-Martín, M. J., Rodríguez-Cruz, M. S., Andrabes, M. S. & Sánchez-Camazano, M. 2006 Efficiency of different clay minerals modified with a cationic surfactant in the adsorption of pesticides: Influence of clay type and pesticide hydrophobicity. *Applied Clay Science* 31, 216–228.

Serna, C., Ahlrichs, J. L. & Serratosa, J. M. 1975 Folding in sepiolite cyrstals. *Clays and Clay Minerals* 23, 452–457.

Suárez, M. & García-Romero, E. 2012 Variability of the surface properties of sepiolite. *Applied Caly Science* 67-68, 72–82.

Veses, A., Aznar, M., López, M. J., Callén, M. S., Murillo, R. & García, T. 2015 Production of upgraded bio-oils by biomass catalytic pyrolysis in an auger reactor using low cost materials. *Fuel* 141, 17–22.

Xie, Y. R., Shen, L. H., Xiao, J., Xie, D. X. & Zhu, J. 2009 Influences of additives on steam gasification of biomass. 1. Pyrolysis procedure. *Energy & Fuels* 23, 5199–5205.

Yu, H., Zhang, Z., Li, Z. & Chen, D. 2014 Characteristics of tar formation during cellulose, hemicellulose and lignin gasification. *Fuel* 118, 250–256.

Zadaka-Amir, D., Bleiman, N. & Mishael, Y. G. 2013 Sepiolite as an effective natural porous adsorbent for surface oil-spill. *Microporous and Mesoporous Materials* 169, 153–159.

CHAPTER
**FIVE**

# Effect of magnesite and olivine in the gas and tar composition

**Contents**



## 5.1 Introduction

Tars, previously defined by Milne *et al.* (1998) as the organics produced under thermal or partial-oxidation regimes of any organic material and generally assumed to be largely aromatic, and defined by Kiel *et al.* (2004) as all organic compounds with a molecular weight larger than benzene, excluding soot and char, need to be considered when biomass is gasified. Tar related issues can lead to unscheduled stops and may impact the performance of downstream unit processes (Siedlecki *et al.*, 2009). The end use of the product gas determines the requirements for tar concentration: compressing and piping needs less than 600 mg/Nm$^3$; the maximum tar concentration for internal combustion engines is 100 mg/Nm$^3$, being phenols and cresols corrosive for these engines; less than 0.1 mg/Nm$^3$ is required for synthesis applications; or, in the case of close-couple combustors, the gas quality is not a major issue. Different cleaning technologies, ranging from

cyclones, coolers, filters or catalytic cracking or reforming, are available to adapt the gas characteristics to these requirements (Milne *et al.*, 1998).

Different bed materials such as dolomite, magnesite, olivine, alumina or metal based catalysts are frequently used in order to avoid agglomeration, to reduce tar yield and to improve gas composition (Werther *et al.*, 2000; Sutton *et al.*, 2001). Olivine has been widely studied as an in-bed catalyst and bed material with different types of feedstocks with promising catalytic activity and improvements in gas composition and tar yield in comparison with the most commonly used bed material, silica sand (Devi *et al.*, 2005; Miccio *et al.*, 2009; Mastellone & Arena, 2008; Corella *et al.*, 2004; Rapagnà *et al.*, 2000). Magnesite is another alternative as a bed material in BFB gasification. Siedlecki *et al.* (2009) obtained very promising results using magnesite either as a bed additive or as a bed material. In addition to bed material, gasification conditions (temperature, biomass throughput, type of biomass, gasifying agent, etc.) also influence the tar yield and gas composition (Corella *et al.*, 2008). Gasification temperatures between 700 and 800 °C are critically important in terms of tar mitigation as they are high enough to produce limited quantities of tar and low enough to get tars with an acceptable dew point (Zwart *et al.*, 2010).

As stated by Kiel *et al.* (2004) tar analyses not only need to be focused on the amount of total tar generation ($g/Nm^3$) but also on its composition. When tar composition is known the tar dew point which defines its condensation behaviour can be be calculated and the water solubility of the tar can be evaluated. This chapter focuses on air gasification of *C. cardunculus* and examines the role of temperature (between 700 and 800 °C), and bed materials (magnesite and olivine), with kaolin amended cardoon on agglomeration. The analysis also includes a discussion of gas composition and gasification performance. A detailed tar analysis is undertaken and the tars are evaluated in terms of total tar and the main individual compounds. Finally, a mass balance was carried out to check the consistency of the results and to obtain information for future works.

## 5.2 Experimental methodology

The experimental facility, the materials (biomass and bed materials) as well as the measurement techniques are described in detail in Chapter 2. In this section, a brief description of the experimental methodology is presented.

The experiments are carried out in the pilot-plant BFB gasifier located at the University of Limerick, Ireland (see section 2.6). The reactor is divided in two parts: a bed zone with an inner diameter of 134.5 mm and a freeboard with an inner diameter of 211.6 mm. The distributor plate is a 3 mm thick perforated plate with 40 holes of 0.9 mm inner diameter. Air, used as gasifying agent and previously preheated, is introduced by

the bottom part of the gasifier. Biomass is fed in-bed at a height of 190 mm above the distributor plate by means of two screw feeders. The raw gas exits the reactor by the upper part and it is cleaned by means of two hot cyclones, a hot filter, a condenser and a downstream filter. Pressure and temperatures are monitored all along the pilot-plant.

*C. cardunculus* or cardoon has been used as biomass feedstock. The properties of this biomass are shown in section 2.2 (tables 2.1, 2.2, 2.3 and 2.4). The particle size of cardoon is sieved according to the feeding system requirements, between 1 and 5 mm. In order to reduce/avoid bed agglomeration, kaolin is mixed with cardoon (3 wt.% of the biomass) prior to be introduced into the gasifier. This amount of kaolin is similar to the one used by Fernández Llorente *et al.* (2008) and Weber & Quicker (2013). Magnesite and olivine are employed as bed materials, whose properties are shown in section 2.3 (table 2.5). The mean particle sizes employed for these bed materials are 391 and 407 $\mu$m, respectively.

### 5.2.1 Experimental procedure

Before starting each experiment, a bed aspect ratio is set to $h_b/D = 2$ ($h_b = 269$ mm). With this aspect ratio, the amount of bed material loaded into the reactor is 5.70 kg in the case of the magnesite experiments and 5.38 kg in the case of olivine. The air supply is turned on and set to the air flow rate for gasification, around 63 $Ndm^3/min$ which equates to an approximate $u/u_{mf}$ ratio of 3, a typical value for BFB gasifiers. The external electrical furnaces are set to the experiment temperature: 700, 750 or 800 °C, depending on the experimental conditions. When the maximum achievable temperature in the bed using the external heating is reached, around 400-500 °C, biomass feeding is initiated with a constant rate of around 4.5 kg/h, on an as-received basis. Under these conditions (air and biomass feed rate), the resultant ER is kept constant at 0.20. In order to prevent backflow of the gases from the gasifier through the feeding system, a nitrogen flow of 2 $Ndm^3/min$ is maintained from the biomass hopper to the gasifier. The exact amount of fuel fed into the reactor is obtained by weighing the mass of biomass loaded into the hopper before starting the experiment and the mass remaining inside the hopper after each test. The main operating conditions are summarized in Table 5.1. The pressure and temperature profiles for one magnesite experiment are shown in Figure 5.1 as an example. This facility takes around 6 hours before start the gasification experiments. When the biomass supply is started a suddenly increase in the pressure is observed as the higher gas production. The temperature in the bed also increases in first minutes but it deceases due to the fuel feeding inside the bed which takes heat to remove the moisture and volatilize the biomass. As the time goes on, the experimental temperature is achieved as a consequence of the partial combustion of the biomass.

**Table 5.1:** Operating conditions.

| | magnesite | magnesite | olivine | olivine | olivine |
|---|---|---|---|---|---|
| Bed material loaded [kg] | 5.70 | 5.70 | 5.38 | 5.38 | 5.38 |
| Biomass feeding rate [$kg_{daf}$/h] | 3.63 | 3.56 | 3.51 | 3.60 | 3.52 |
| Biomass throughput [$kg_{daf}/m^2h$] | 255.55 | 250.37 | 247.17 | 253.53 | 247.42 |
| Air flow rate [$Ndm^3$/min] | 63.43 | 63.47 | 62.79 | 63.36 | 63.13 |
| ER [–] | 0.20 | 0.20 | 0.20 | 0.20 | 0.20 |
| Air excess ratio, $u/u_{mf}$ [-] | 2.91 | 3.06 | 3.01 | 3.19 | 3.35 |
| $T_{air\ inlet}$, TIC02 [°C] | 209 | 270 | 227 | 276 | 320 |
| $T_{gasification}$, TIC10 [°C] | 700 | 800 | 700 | 760 | 800 |
| $T_{bed}$, TI06 [°C] | 701 | 756 | 718 | 741 | 791 |

The product gas after leaving the reactor passes through a set of two cyclones which are maintained at 400 °C to prevent tars condensing. These cyclones separates the entrained particles from the gas stream, after which the gas passes through a hot filter (Candel element, Pyrotex BWF-Envirotec) kept at 450 °C to remove the remaining smaller particles. Then, the gas goes into a tube shell heat exchanger to remove tars and water from the product gas stream. A tar trap located at the bottom of the condenser serves to collect all the condensates. All the pipework upstream of the tar trap and the condenser are properly heated and insulated. Finally, two parallel filters are used to avoid fine particles and lighter tars passing to the gas analysis section.

When the experiment is finished, air and biomass are stopped as well as the electric furnaces and the whole system is cooled down to ambient temperature using $N_2$ purge.

### 5.2.2 Sampling and analysis

The mass flow rate of product gas is measured before exiting the cleaning section using a Coriolis mass flow meter (Bronkhorst CORITECH). Gas sampling is started at the same time as biomass feeding, achieving steady state conditions after 1.5 to 2 h (from when biomass feeding was started). This time corresponds with the time needed to reach a constant temperature within the reactor.

Gas composition is measured by means of an Agilent 3000 $\mu$-GC at 5 minutes intervals. A mean value is obtained as the mean gas composition during the steady state. During this time, 3 tar samples are also collected using SPA method. Further details on the characteristics and operating conditions of the equipments used for gas and tar analyses have been addressed in sections 2.7.3 and 2.7.4.

After each experiment, the bed material and char from the gasifier, particulates from the cyclones and hot filter, and water from the tar trap are discharged, weighed and

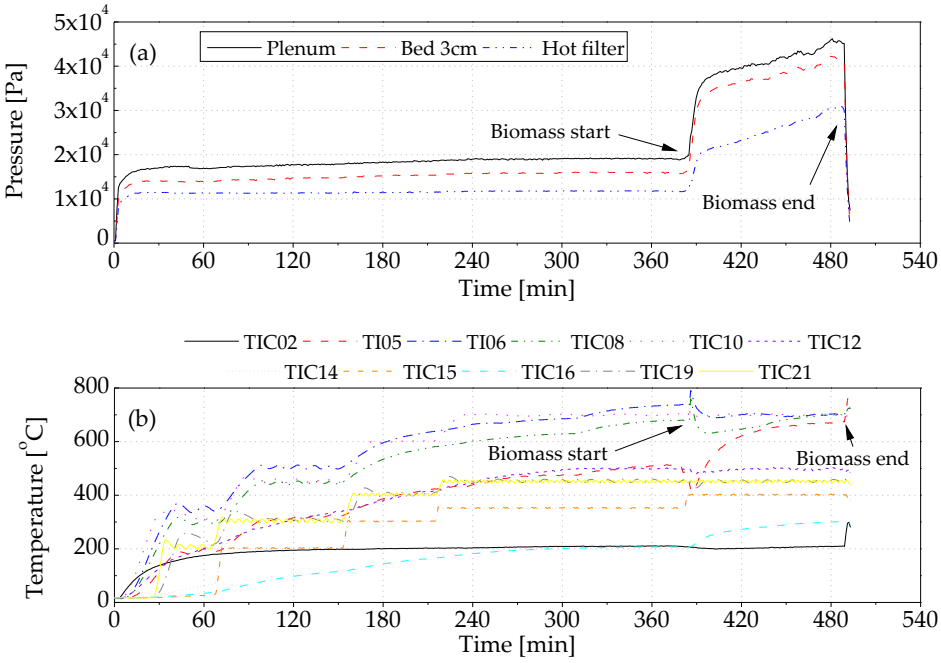


**Figure 5.1:** Pressure and temperature profiles for the experiments with magnesite at 700 °C and ER = 0.20: a) pressure profiles and b) temperature profiles.

kept for analysis. Gasification performance parameters such as CGE, C, H and biomass conversion, GY and LHV of the product gas are also calculated as explained in Section 2.7.2. Finally, a mass balance of the process is performed for each experiment. This calculation is useful for several reasons (Siedlecki *et al.*, 2009): the input and output flows are compared checking the consistency of the results; unknown process flows and measurement errors can be determined; information regarding the gasification performance and efficiency is obtained and practical information can be collected to refine future experiments. Additionally, all this data is very important for the scale-up and design of the installation equipments for industrial facilities.

## 5.3 Results and discussion

### 5.3.1 Gas composition

The product gas composition is influenced by the operating temperature due to its effects on the chemical reactions during the gasification process. This parameter is varied using the electrical furnaces while the ER, the air flow rate and the biomass feeding rate are

kept constant. The variation in gas composition as a function of temperature during the steady state operation is shown in Figure 5.2 and in Table 5.2 for magnesite and olivine bed materials. In both cases, an increase in the $H_2$ and CO concentration is observed when temperature is increased. The concentration of $CO_2$ decreases with temperature while the concentration of light hydrocarbons remains almost constant. These results are in agreement with those reported in the literature (Narváez *et al.*, 1996; Mohammed *et al.*, 2011; de Andrés *et al.*, 2011).

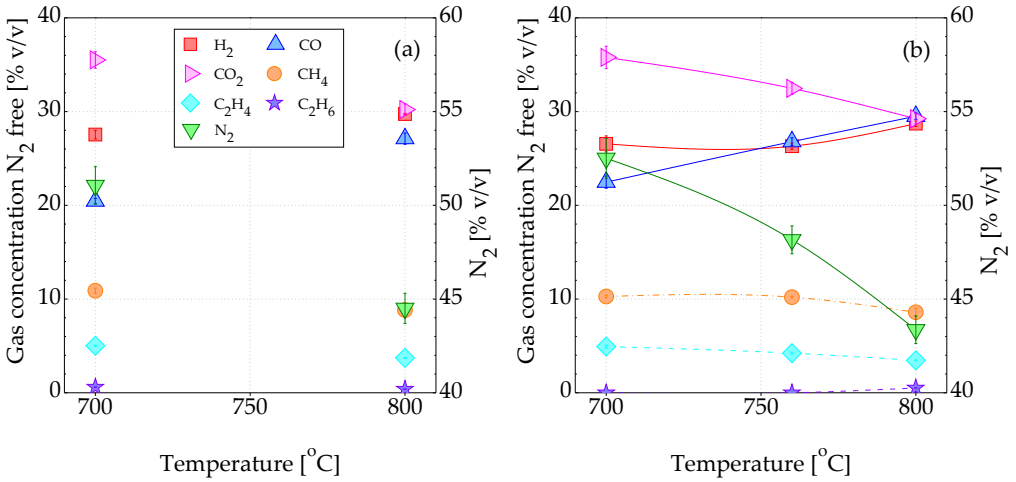


**Figure 5.2:** Gas composition ($N_2$ free) at different temperatures: a) magnesite and b) olivine.

As expected, higher temperatures favour products produced during endothermic reactions ($C + CO_2 \leftrightarrow 2CO$ and $C + H_2O \leftrightarrow CO + H_2$, Eqs. 1.6 and 1.7). The results show the effect of the Boudouard (Eq. 1.6) and water gas reactions (Eq. 1.7) on the CO composition leading to a higher concentration with temperature. In the case of $H_2$, the water gas (Eq. 1.7) favours its production in spite of the methanation reaction ($C + 2H_2 \leftrightarrow CH_4$, Eq. 1.8). In addition, the higher concentration of $H_2$ and CO at higher temperature can be an indication of secondary tar reactions that convert primary tar into aromatics (Boroson *et al.*, 1989; Morf *et al.*, 2002), or tar cracking reactions such as steam reforming ($C_nH_m$ (tar) + $nH_2O \rightarrow (n + m/2)H_2 + nCO$, Eq. 1.12) enabled by the relatively high moisture content of cardoon (9.69 wt.%) and dry reforming ($C_nH_m$ (tar) + $nCO_2 \rightarrow (m/2)H_2 + 2nCO$, Eq. 1.11) (Lahijani & Zainal, 2011). Overall, the gas compositions for both magnesite and olivine are very similar for all gas species (Figure 5.2) with both bed materials having similar influences with increasing temperature. There are marginal differences in the $H_2$ content which is slightly lower for

olivine than for magnesite while CO is slightly higher for olivine than for magnesite.

**Table 5.2:** Dry syngas composition for each gasification experiment.

| *Operating conditions* | | | | | |
|---|---|---|---|---|---|
| Bed material | magnesite | magnesite | olivine | olivine | olivine |
| $T_{gasification}$, TIC10 [°C] | 700 | 800 | 700 | 760 | 800 |
| *Dry syngas composition* | | | | | |
| $H_2$ [% v/v] | 13.48±0.38 | 16.51±0.27 | 12.62±0.82 | 13.64±0.36 | 16.26±0.33 |
| CO [% v/v] | 10.01±0.23 | 15.05±0.52 | 10.68±0.66 | 13.89±0.40 | 16.71±0.30 |
| $CH_4$ [% v/v] | 5.33±0.18 | 4.89±0.10 | 4.88±0.06 | 5.29±0.09 | 4.87±0.26 |
| $CO_2$ [% v/v] | 17.37±0.17 | 16.77±0.07 | 16.98±0.18 | 16.83±0.08 | 16.56±0.12 |
| $C_2H_4$ [% v/v] | 2.45±0.03 | 2.07±0.01 | 2.34±0.02 | 2.19±0.03 | 1.96±0.03 |
| $C_2H_6$ [% v/v] | 0.30±0.01 | 0.22±0.00 | 0.00±0.00 | 0.00±0.00 | 0.29±0.01 |
| $N_2$ [% v/v] | 51.07±1.18 | 44.50±0.71 | 52.51±1.11 | 48.16±0.65 | 43.36±0.77 |
| $H_2O$ [% v/v] | 12.70 | 10.83 | 15.84 | 13.93 | 9.67 |

Figure 5.3 shows the product gas ratios for the different bed materials and temperatures. The $H_2/CO$ ratio decreases with temperature for both magnesite and olivine, indicating that the effect of the water-gas shift reaction ($CO + H_2O \leftrightarrow CO_2 + H_2$, Eq. 1.9) is slightly reduced, increasing the CO concentration to the detriment of $H_2$ and $CO_2$. In the case of the $CO/CO_2$ ratio, it increases with temperature as a consequence of the Boudouard char gasification reaction (Eq. 1.6), with a higher production of CO and the consumption of $CO_2$. The dry reforming reaction of tars (Eq. 1.11) is also promoted with temperature. An increment of the $H_2/CO_2$ ratio and a reduction of the $CH_4/H_2$ ratio are observed, enhancing the production of $H_2$.

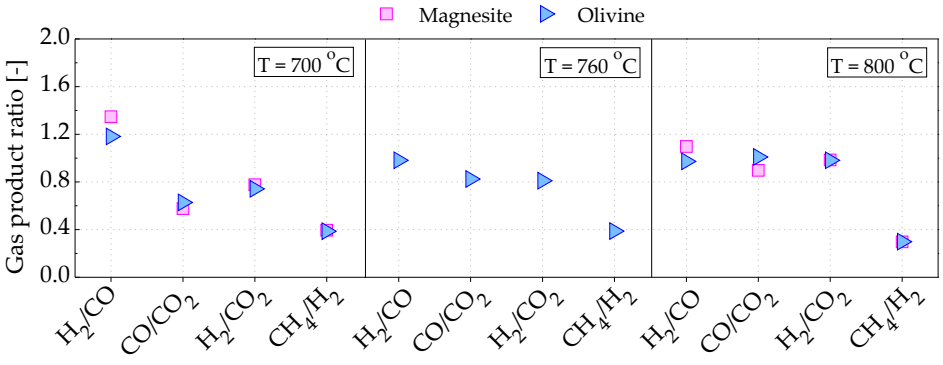


**Figure 5.3:** Product gas ratios for magnesite and olivine at different temperatures.

The hydrogen content in the product gas is between 12 and 16 %v/v (with $N_2$)

for both magnesite and olivine, a relatively high value for biomass gasification with air. Table 5.3 shows a brief comparison between the results obtained in this study and those reported in the literature for *C. cardunculus* gasification. Zabaniotou *et al.* (2014) observed $H_2$ concentration of around 10 %v/v (with $N_2$) for fixed bed gasification of cardoon. While Christodoulou *et al.* (2014) reported lower content of $H_2$, 8 %v/v (with $N_2$) for air gasification of a mixture of cardoon and giant reed using olivine as the bed material. Similar observations are reported for air-steam gasification by Abelha *et al.* (2013) who found higher concentration of $H_2$ for cardoon when compared to a mixture of cardoon and eucalyptus. The differences in terms of $H_2$ content in the product gas between air gasification and air + steam/$O_2$ + steam gasification are relatively small, and cardoon is suggested by Zabaniotou *et al.* (2014) to be a good feedstock for hydrogen production.

The hydrogen and carbon monoxide concentrations can be influenced by both the bed material and the biomass ash composition, particularly the content of alkali metals (potassium and sodium) (Sutton *et al.*, 2001), which are credited with improving gasification rate and yield of $H_2$ (Brown *et al.*, 2000; Demirbaş, 2002). *C. cardunculus* has a high sodium and potassium contents (Table 2.4) which may account for the high production of $H_2$ obtained in the experiments. Higher molecular weight hydrocarbons may be reformed according to Eqs. 1.11 and 1.12 to produce additional CO and $H_2$ using the surface of the catalyst/bed material (Sutton *et al.*, 2001).

### 5.3.2 Gasification performance

The performance of the gasification experiments evaluated in terms of GY, LHV of the gas, CGE as well as carbon and hydrogen conversion is shown in Figure 5.4. The data suggests that the GY, LHV of the product gas, carbon and hydrogen conversion as well as CGE increases with increasing gasification temperature for both bed materials. The carbon conversion seems to be influenced by the increased concentration of CO at higher temperatures in spite of the slight decrease in other carbon species such as $CO_2$, $CH_4$ and light hydrocarbons. The relatively low conversion of hydrogen when compared to carbon is mainly due to the hydrogen losses as water in the product gas, which condenses with the tar compounds as well as a lack of information regarding ammonia and hydrogen sulphide. The LHV increases with gasification temperature due to an increase in the concentration of the main combustible compounds, CO and $H_2$ in the product gas. GY increases slightly with temperature. This may be due to the greater gas production during the initial pyrolysis phase as well as the steam cracking and reforming of tars and the endothermic reactions of char gasification (Pinto *et al.*, 2003). As a result of the rise in the LHV and the GY, the CGE also increases with temperature. Finally, biomass conversion

**Table 5.3:** Comparison of experimental results with literature data ($H_2$ and CO calculated on a $N_2$ free basis).

| Reference | System configuration | Operating conditions | Results |
|---|---|---|---|
| Present study | Cardoon + kaolin | 700-800 °C | $H_2$: 28-30 %v/v |
| (Chapter 5) | BFB, 13.45 cm of ID | ER: 0.2 | CO: 20-27 %v/v |
| | Bed material: magnesite | Gasifiying agent: air | Tar[1]: 29-27 g/Nm$^3$ |
| | Cardoon + kaolin | 700-800 °C | $H_2$: 26-29 %v/v |
| | BFB, 13.45 cm of ID | ER: 0.2 | CO: 23-30 %v/v |
| | Bed material: olivine | Gasifying agent: air | Tar[1]: 26-43 g/Nm$^3$ |
| Present study | Cardoon | 826-874 °C | $H_2$: 20-23 %v/v |
| (Chapter 4) | BFB, 5.28 cm of ID | ER: 0.3 | CO: 43-41 %v/v |
| | Bed material: silica sand | Gasifiying agent: air | Tar[1]: 22-23 g/Nm$^3$ |
| | Cardoon | 828-873 °C | $H_2$: 20 %v/v |
| | BFB, 5.82 cm of ID | ER: 0.3 | CO: 29-35 %v/v |
| | Bed material: sepiolite | Gasifying agent: air | Tar[1]: 11-9 g/Nm$^3$ |
| Zabaniotou *et al.* (2014) | Cardoon | 700-800 °C | $H_2$: 28-11 %v/v |
| | Fixed bed, 1.25 cm of ID | ER: 0.2 | CO: 20-38 %v/v |
| | | Gasifiying agent: air | Tar: 31-38 wt.% |
| Christodoulou *et al.* (2014) | Cardoon/giant reed (50/50%) | 700-800 °C | $H_2$: 22 %v/v |
| | CFB, 7.8 cm of ID | ER: 0.3 | CO: 29-35 %v/v |
| | Bed material: olivine | Gasifiying agent: air | Tar[2]: 6-3 g/Nm$^3$ |
| | Cardoon | 700-750 °C | $H_2$: 35-27 %v/v |
| | CFB, 8.3 cm of ID | ER: 0.3 | CO: 7-8 %v/v |
| | Bed material: magnesite | Gasifiying agent: $O_2$+$H_2O$ | Tar[1]: 134-122 g/Nm$^3$ |
| Encinar *et al.* (2002) | Cardoon | 700-800 °C | $H_2$: 59-60 %v/v |
| | Fixed bed, 4 cm of ID | Gasifiying agent: steam | CO: 17-19 %v/v |
| | | ($PH_2O$=0.53 atm) | Tar: NA |
| Abelha *et al.* (2013) | Cardoon | 830 °C | $H_2$: 39 %v/v |
| | BFB, 8 cm of ID | ER: 0.1 | CO: 24 %v/v |
| | Bed material: silica sand | Gasifying agent: air+$H_2O$ | Tar: NA |
| | Cardoon/eucalyptus (50/50%) | 830 °C | $H_2$: 37 %v/v |
| | BFB, 8 cm of ID | ER: 0.1 | CO: 24 %v/v |
| | Bed material: | Gasifying agent: air+$H_2O$ | Tar[2]: 4.1 g/Nm$^3$ |
| | silica sand+ | | |
| | calcined olivine (15 wt.%) | | |
| | Cardoon/eucalyptus (50/50%) | 830 °C | $H_2$: 38 %v/v |
| | BFB, 8 cm of ID | ER: 0.1 | CO: 20 %v/v |
| | Bed material: | Gasifying agent: air+$H_2O$ | Tar: NA |
| | silica sand+ | | |
| | calcined dolomite (15 wt.%) | | |

[1]SPA, [2]Tar protocol, NA: Not available.

shows a very high value, around 94 %, when magnesite is used as the bed material. Magnesite appears to exhibit a positive effect in terms of char conversion particularly at lower temperature (700 °C) since less char is collected from the gasifier after the test when compared to olivine (Table 5.4). Unlike magnesite, biomass conversion for olivine increases with temperature which is consistent with the amount of char collected after gasification.

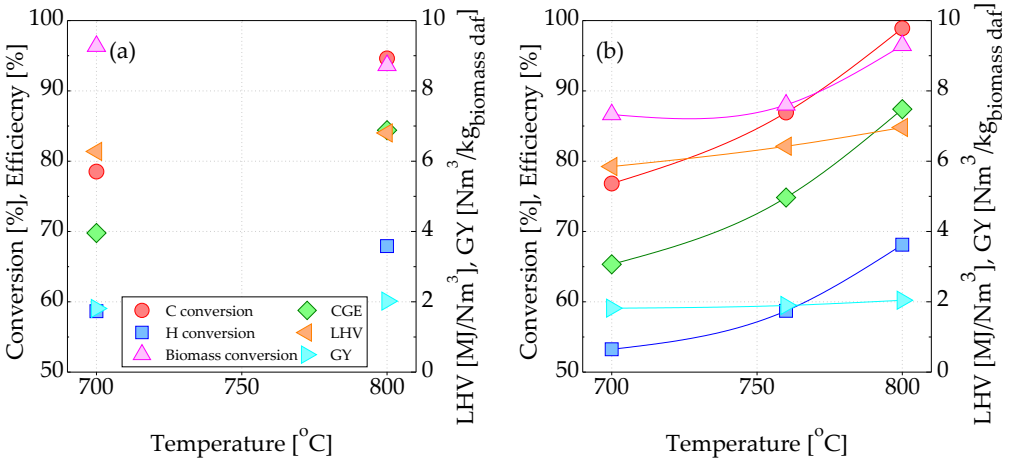


**Figure 5.4:** Gasification efficiency parameters: a) magnesite and b) olivine.

Some differences are apparent when comparing the gasification performance of the two bed materials. Carbon and hydrogen conversion are slightly lower in the case of olivine at 700 °C but a bit higher than magnesite at 800 °C. Biomass conversion is much lower for olivine at 700 °C. Similar results are obtained for the CGE and LHV of the product gas, with better performance observed with magnesite at low temperature and with olivine at high temperature. In terms of GY, the values are very similar.

### 5.3.3 Tar generation

Figure 5.5 shows the influence of temperature and bed material on the tar generation grouped using the Milne *et al.* (1998) classification. Total tar refers to total GC detectable tar including those tar compounds eluted from benzene to benz[a]anthracene. In the case of magnesite (Figure 5.5a), the total GC detectable tar decreases when temperature is increased from 700 to 800 °C, and a similar result is observed for secondary tars which consist of aromatic compounds with alkyl or hydroxyl substituent functional groups (i.e. benzene, toluene, phenol, etc.). With increasing temperature these functional groups

**Table 5.4:** Gasification parameters for each gasification experiment.

| *Operating conditions* | | | | | |
|---|---|---|---|---|---|
| Bed material | magnesite | magnesite | olivine | olivine | olivine |
| $T_{gasification}$, TIC10 [°C] | 700 | 800 | 700 | 760 | 800 |
| *Gasification parameters* | | | | | |
| Lower heating value [MJ/Nm$^3$] | 6.28 | 6.80 | 5.85 | 6.42 | 6.96 |
| Gas yield [Nm$^3$/kg$_{biomass\ daf}$] | 1.81 | 2.02 | 1.82 | 1.90 | 2.04 |
| Carbon conversion [%] | 78.52 | 94.62 | 76.82 | 86.92 | 98.90 |
| Hydrogen conversion [%] | 58.66 | 67.92 | 53.25 | 58.72 | 68.12 |
| Biomass conversion [%] | 96.36 | 93.62 | 86.64 | 88.01 | 96.47 |
| Cold gas efficiency [%] | 69.78 | 84.41 | 65.33 | 74.83 | 87.40 |
| Elutriated char [g$_{daf}$/kg$_{biomass\ daf}$] | 16.11 | 20.94 | 17.46 | 18.10 | 12.49 |
| Elutriated fines [g/kg$_{biomass\ daf}$] | 60.78 | 82.39 | 61.54 | 62.30 | 61.82 |
| Char generation [g$_{daf}$/kg$_{biomass\ daf}$] | 36.44 | 63.81 | 133.64 | 119.93 | 35.27 |
| Ash generation [g$_{db}$/kg$_{biomass\ daf}$] | 59.74 | 93.69 | 130.19 | 106.32 | 72.17 |
| Moisture generation [g/kg$_{biomass\ daf}$] | 212.90 | 198.04 | 276.64 | 246.99 | 176.94 |
| GC detectable tar [g/kg$_{biomass\ daf}$] | 52.49 | 54.70 | 48.00 | 76.76 | 71.09 |

are cleaved from the aromatic ring generating permanent gases CO, $H_2$, $CO_2$, $CH_4$, $C_2H_4$ and cyclopentadiene radicals, responsible for the increase of PAHs (Fitzpatrick *et al.*, 2008; Yu *et al.*, 2014). PAH tertiary tars (i.e. naphthalene, fluorene, pyrene, etc.) increase with temperature which is in accordance with observations reported in literature for magnesite in the same temperature range (Rabou *et al.*, 2009; Kinoshita *et al.*, 1994). Increase of PAH tertiary tars could also be explained by the decomposition of the heavier GC undetectable fraction into lighter PAH tertiary tars (Devi *et al.*, 2005). The production of PAHs is observed together with a decrease in phenols and alkylated aromatics (Figure 5.6), as a result of dealkylation, dehydration, decarbonylation, and polymerization reactions (Yu *et al.*, 1997; Berrueco *et al.*, 2014). The yield of alkyl tertiary tars (i.e.: 2-methylnaphthalene, etc.) remained constant over the temperature range studied. Previous experimental observations as well as data from the scientific literature (Dufour *et al.*, 2011) indicates that alkyl tertiary tars decompose only above 800 °C. However, in this case, the tertiary-alkyl tar group represents only 6.1 % of total GC detectable tar at 800 °C.

The trend for tar evolution using olivine as the bed material is presented in Figure 5.5b. An increase of total tar and secondary tars is observed between 700 and 760 °C, followed by a decrease as the temperature rises to 800 °C. The same trend is reported by other authors (Kinoshita *et al.*, 1994; Milne *et al.*, 1998; van Paasen & Kiel, 2004).

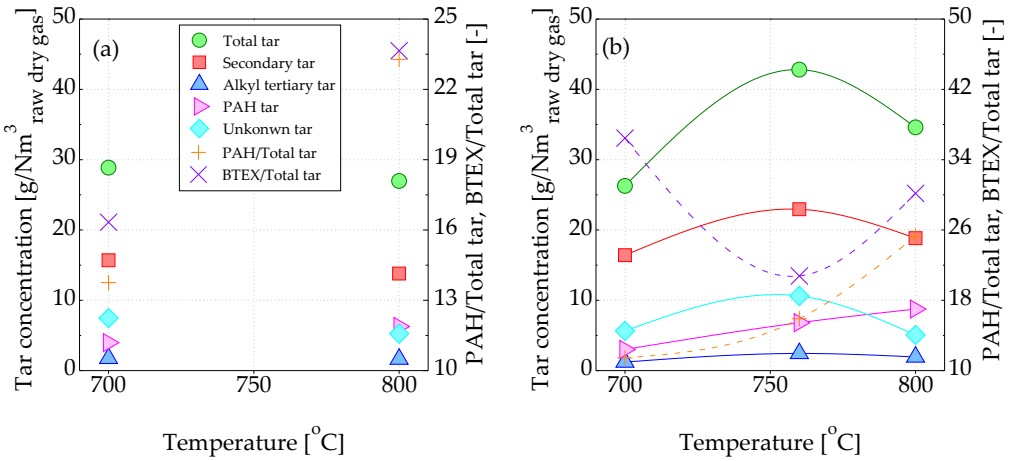


**Figure 5.5:** Tar concentration according to Milne *et al.* (1998): a) magnesite and b) olivine.

PAH tertiary tars increase with temperature and alkyl tertiary tars remain constant for the temperature range studied, which is also observed for magnesite. Comparison of magnesite and olivine does not indicate any difference in catalytic activity at 700 °C. The yield of total tar at 700 °C is slightly lower for olivine (26.3 g/Nm$^3$) than for magnesite (28.9 g/Nm$^3$). Delgado *et al.* (1996, 1997) used magnesite in a secondary fixed bed catalytic reactor and reported that at temperatures under 800 °C the material is catalytically deactivated within 30 minutes, however, high tar conversion (more than 95 %) is observed at temperatures above 850 °C. Rapagnà *et al.* (2000) and Devi *et al.* (2005) also reported increased catalytic activity of olivine with temperature above 800 °C. Regarding specific tar fractions, at 700 °C the yield of secondary tars are similar for both magnesite and olivine, 15.7 and 16.4 g/Nm$^3$, respectively. The same is observed when considering tertiary tars (alkyl and PAH tars) showing 5.7 g/Nm$^3$ for magnesite and 4.2 g/Nm$^3$ for olivine. A similar evolution profile to secondary and tertiary alkyl tars suggests that unknown tars mostly contain species from these two groups for olivine.

In contrast, magnesite seems to have slightly higher catalytic activity than olivine at 800 °C. Total tar, secondary and tertiary tars are 27.0, 13.8 and 7.9 g/Nm$^3$ for magnesite and, 34.6, 18.8 and 10.7 g/Nm$^3$ for olivine. Hanping *et al.* (2008) mixed magnesite and olivine with three types of biomasses prior to the feeding. They did not observe any significant difference in catalytic activity between the bed materials studied. Tar conversion rates varied only 4-5 % between magnesite and olivine when total gravimetric tar were measured.

Tar content in the product gas from the gasification of cardoon has been also measured by other researchers but comparison of results needs to be undertaken with caution due to the protocols employed fot tar analysis, the units used for reporting, bed materials, gasifying agents, biomass throughput, etc. Abelha *et al.* (2013) (see Table 5.3 for more details) analyzed tars according to tar protocol CEN/TS 15439. With silica sand, tar concentration was around of 7.5 g/Nm$^3$ while after addition of calcined olivine (15 % w/w ) tar decreased to 4.1 g/Nm$^3$. Christodoulou *et al.* (2014) reported total tar between 134.1 and 122.3 g/Nm$^3$ for cardoon using magnesite and tar protocol for tar analysis. On the other hand, a blend of 50 % w/w cardoon and 50 % w/w giant reed using olivine and the SPA for tar analysis generated only between 5.9 and 2.8 g/Nm$^3$ of total tar. Rapagnà *et al.* (2010) gasified crushed almond shells at 740 °C using olivine and the tar protocol followed by HPLC/UV analysis. Total tar was 3.7 g/Nm$^3$ with toluene and naphthalene being the dominant tar species. The results obtained in Chapter 4 show similar values as the values reported in this chapter when using silica sand as bed material, and rather lower values in the case of sepiolite. However, the operating conditions are not the same as the ER in Chapter 4 is equal to 0.3 and the temperatures are also a bit higher. These differences promotes the lower tar generation although the bed materials have no catalytic activity.

The 19 major tar compounds are identified and quantified and the results are presented in Figure 5.6 and Table 5.5 in the order in they are eluted from the GC column. The dominant tar components for magnesite are indane, o/m-cresol, toluene and naphthalene at both 700 and 800 °C with naphthalene and toluene showing the highest concentration at 800 °C. Whereas for olivine benzene, toluene and indane are the dominant compounds at 700 °C, while toluene, naphthalene and benzene at 800 °C. The BTEX (benzene, toluene, ethylbenzene and xylene) fraction in total tar is higher for olivine when compared to magnesite. Benzene and toluene are dominant BTEX components. In the case of magnesite BTEX fraction increases with temperature from 16 to 24 %, while in the case of olivine, BTEX fraction decreases between 700 and 760 °C, from 36 to 21 %, and it increases from 760 to 800 °C up to 30 %. The yield of naphthalene is the highest among PAH tar species and all PAHs increase with the process temperature. Fraction of PAHs in the total tar increase with increasing temperature, from 11 to 25 % for olivine and from 14 to 23 % for magnesite. Although total tar decreases with temperature, the increase in polyaromatic compounds (naphthalene, acenaphthylene, anthracene, pyrene) may produce a higher tar dew point which is an important parameter into predicting tar condensation in the downstream devices. Phenolic tar species are significant only at or below 750 °C, however, at 800 °C oxygen containing species drastically decrease. Nevertheless, phenols and cresols are water soluble making them easier to remove using water scrubbers. In general, the observed trends for tars with respect to temperature

are in agreement with previous studies for other biomasses (Christodoulou *et al.*, 2014; Morf *et al.*, 2002). The evolution of individual tar compounds with gasification temperature indicates that catalytic processes such as dealkylation, decarbonylation, dehydrogenation, and dehydration reactions of substituted tar species become more significant above 760 °C.

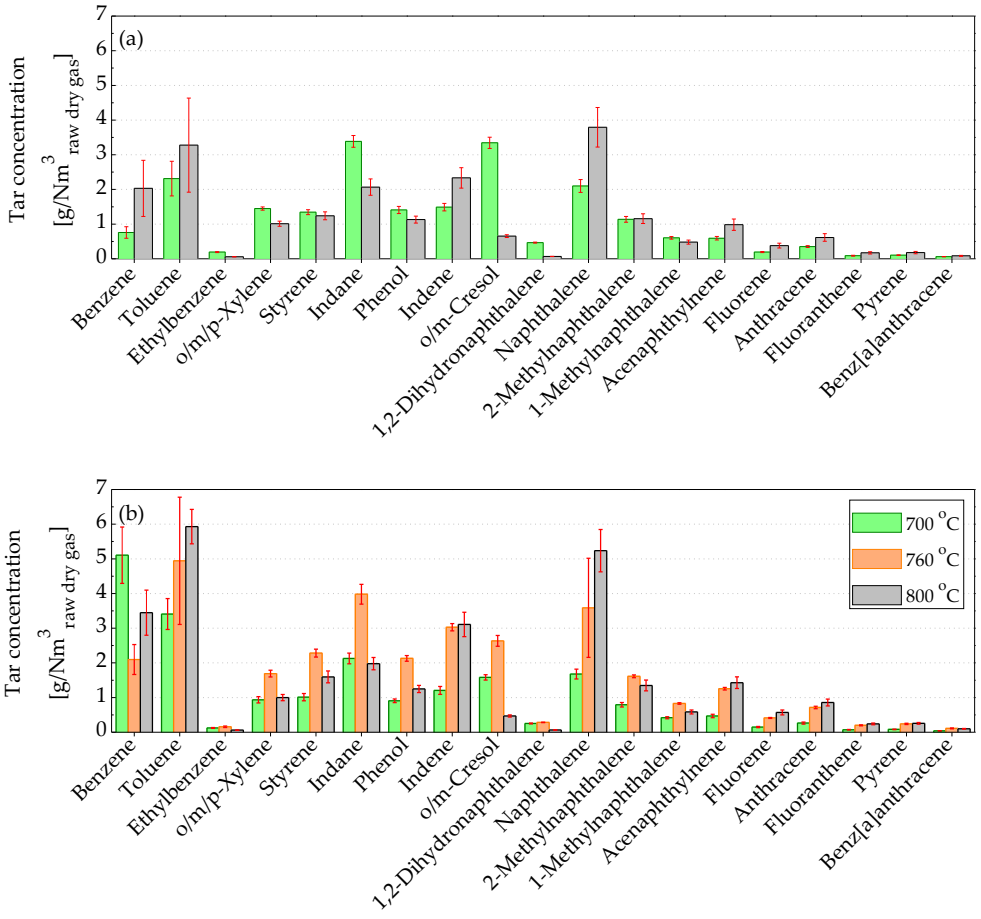


**Figure 5.6:** Tar concentration for individual compounds: a) magnesite and b) olivine.

Arena *et al.* (2009) reported that olivine is an effective in situ tar reduction agent when plastic waste is gasified. The iron and magnesium contained in the olivine can activate the endothermic tar decomposition reactions (Arena *et al.*, 2010). Iron catalytically enhances dehydrogenation and carbon formation reactions (Eq. 5.1), while the magnesium oxide promotes the cracking and isomerization reactions of the hydrocarbon

**Table 5.5:** Identified and quantified tar compounds in $g/kg_{biomass\ daf}$.

| Tar compound | Retention time [min] | Tar group[a] | Magnesite 700 °C | Magnesite 800 °C | Olivine 700 °C | Olivine 760 °C | Olivine 800 °C |
|---|---|---|---|---|---|---|---|
| Benzene | 4.58 | Secondary | 1.37±0.30 | 4.10±1.63 | 9.28±1.48 | 3.97±0.82 | 7.05±1.33 |
| Toluene | 7.89 | Secondary | 4.19±0.90 | 6.62±2.74 | 6.20±0.81 | 9.37±3.48 | 12.12±1.02 |
| Ethylbenzene | 11.38 | Secondary | 0.35±0.03 | 0.12±0.01 | 0.22±0.02 | 0.30±0.04 | 0.12±0.01 |
| o/m/p-Xylene | 11.70 | Secondary | 2.62±0.08 | 2.04±0.15 | 1.70±0.17 | 3.21±0.19 | 2.04±0.18 |
| Styrene | 12.51 | Secondary | 2.43±0.13 | 2.50±0.23 | 1.84±0.19 | 4.33±0.22 | 3.26±0.35 |
| Indane | 16.04 | Secondary | 6.13±0.31 | 4.18±0.48 | 3.87±0.28 | 7.54±0.54 | 4.04±0.36 |
| Phenol | 16.27 | Secondary | 2.55±0.19 | 2.28±0.20 | 1.65±0.10 | 4.04±0.15 | 2.55±0.21 |
| Indene | 17.90 | Secondary | 2.69±0.20 | 4.71±0.60 | 2.19±0.21 | 5.74±0.20 | 6.35±0.72 |
| o/m-Cresol | 18.31 | Secondary | 6.05±0.29 | 1.32±0.08 | 2.87±0.14 | 5.00±0.30 | 0.96±0.06 |
| 1,2-Dihydronaphthalene | 21.16 | Tert.-PAH | 0.84±0.03 | 0.14±0.01 | 0.46±0.02 | 0.54±0.01 | 0.13±0.01 |
| Naphthalene | 22.29 | Tert.-PAH | 3.80±0.33 | 7.66±1.15 | 3.05±0.26 | 6.80±2.71 | 10.71±1.25 |
| 2-Methylnaphthalene | 25.39 | Tert.-alkyl | 2.06±0.15 | 2.34±0.28 | 1.44±0.12 | 3.06±0.08 | 2.76±0.32 |
| 1-Methylnaphthalene | 25.84 | Tert.-alkyl | 1.09±0.07 | 0.97±0.12 | 0.76±0.06 | 1.57±0.04 | 1.20±0.12 |
| Acenaphthalene | 29.45 | Tert.-PAH | 1.07±0.09 | 1.99±0.33 | 0.85±0.09 | 2.38±0.07 | 2.92±0.34 |
| Fluorene | 32.64 | Tert.-PAH | 0.35±0.03 | 0.77±0.14 | 0.27±0.03 | 0.78±0.03 | 1.17±0.14 |
| Anthracene | 36.87 | Tert.-PAH | 0.67±0.05 | 1.24±0.22 | 0.48±0.05 | 1.38±0.07 | 1.75±0.20 |
| Fluoranthene | 41.21 | Tert.-PAH | 0.16±0.02 | 0.35±0.07 | 0.13±0.01 | 0.38±0.03 | 0.49±0.05 |
| Pyrene | 41.91 | Tert.-PAH | 0.19±0.02 | 0.36±0.07 | 0.15±0.02 | 0.45±0.03 | 0.52±0.05 |
| Benz[a]anthracene | 45.87 | Tert.-PAH | 0.11±0.01 | 0.17±0.03 | 0.07±0.01 | 0.21±0.02 | 0.20±0.02 |
| *Secondary tar* | | | 28.39±0.70 | 27.87±2.76 | 29.83±3.31 | 43.49±2.88 | 38.51±3.22 |
| *Tertiary alkyl tar* | | | 3.15±0.22 | 3.31±0.40 | 2.20±0.17 | 4.63±0.12 | 3.95±0.43 |
| *Tertiary PAH tar* | | | 7.17±0.54 | 12.68±2.01 | 5.47±0.48 | 12.90±2.56 | 17.89±2.06 |
| *Unkown tar* | | | 13.52 | 10.60 | 10.26 | 15.40 | 10.37 |
| *Total tar* | | | 52.23±1.17 | 54.46±0.15 | 47.76±3.88 | 76.42±3.44 | 70.72±3.58 |
| *BTEX/Total tar* [%] | | | 16.33 | 23.65 | 36.45 | 20.77 | 30.17 |
| *PAH/Total tar* [%] | | | 13.75 | 23.28 | 11.45 | 15.90 | 25.30 |
| *Tar dew point** [°C] | | | 131.7 | 137.9 | 141.9 | 141.7 | 126.8 |

[a] According to Milne *et al.* (1998) classification, * Obtained from the ECN tar dew point site (www.thersites.nl)

fragments produced by thermal cracking of the feedstock (Eq. 5.2):

$$C_nH_m \rightarrow nC + (m/2)H_2 \tag{5.1}$$

$$pC_xH_y \rightarrow qC_nH_m + rH_2 \tag{5.2}$$

All the series/parallel reactions of cracking, isomerisation, hydro-cyclization, aromatization, oligomerization, polymerization produce coke and molecular hydrogen ($H_2$).

In order to investigate the catalytic activity of olivine and magnesite, the inorganic fraction of elutriated fines collected in the cyclones and hot filter are analysed and presented in Tables 5.6 and 5.7. These tables also reports the ratio between the mass flow rate of each element that escapes from the gasifier as fines and that which is introduced in the reactor as inorganic fraction of the fuel ($Q_{i,fines}/Q_{i,fuel}$), as well as the enrichment factor (EF, see Section 2.7.2) in the elutriated fines.

According to Arena *et al.* (2010), when olivine provides a significant catalytic activity for tar cracking and carbonization, the fines collected in the cyclone contain substantially

**Table 5.6:** Composition of inorganic fraction and enrichment factor (EF) of fines collected in cyclone 1, cyclone 2 and hot filter for olivine gasification tests at the different experimental temperatures.

| | Concentration [mg/kg$_{elut.fines,db}$] | | | $Q_{i,fines}/Q_{i,fuel}$ [–] | | | EF [–] | | |
|---|---|---|---|---|---|---|---|---|---|
| 700 °C | Cyclone 1 | Cyclone 2 | Hot filter | Cyclone 1 | Cyclone 2 | Hot filter | Cyclone 1 | Cyclone 2 | Hot filter |
| Al | 65965.7 | 88876.3 | 78406.5 | 0.02 | 0.02 | 0.06 | 0.54 | 0.73 | 0.65 |
| Cd | 24.5 | 26.6 | 25.0 | 0.04 | 0.00 | 0.01 | 0.11 | 0.12 | 0.11 |
| Ca | 53201.4 | 31259.9 | 29964.3 | 0.12 | 0.00 | 0.02 | 0.32 | 0.19 | 0.18 |
| Co | 34.7 | 40.9 | 46.9 | 0.05 | 0.00 | 0.02 | 0.14 | 0.17 | 0.19 |
| Cr | 316.6 | 306.5 | 319.6 | 1.04 | 0.07 | 0.28 | 2.87 | 2.78 | 2.9 |
| Cu | 806.7 | 786.6 | 839.0 | 0.05 | 0.00 | 0.01 | 0.14 | 0.14 | 0.15 |
| Fe | 9700.8 | 10726.4 | 12684.9 | 0.34 | 0.03 | 0.12 | 0.95 | 1.05 | 1.24 |
| K | 41968.9 | 38002.3 | 51598.5 | 0.16 | 0.01 | 0.05 | 0.44 | 0.40 | 0.54 |
| Mg | 15215.0 | 25130.5 | 32261.5 | 0.28 | 0.03 | 0.16 | 0.77 | 1.27 | 1.63 |
| Mn | 274.6 | 264.1 | 307.0 | 0.18 | 0.01 | 0.05 | 0.49 | 0.47 | 0.55 |
| Mo | 1347.9 | 674.2 | 129.8 | 0.55 | 0.02 | 0.01 | 1.53 | 0.76 | 0.15 |
| Na | 42990.0 | 45255.4 | 54135.4 | 0.09 | 0.00 | 0.02 | 0.16 | 0.17 | 0.20 |
| Ni | 264.4 | 387.4 | 424.3 | 0.21 | 0.02 | 0.09 | 0.58 | 0.85 | 0.94 |
| Pb | 14.3 | 4.1 | 1.0 | 0.47 | 0.01 | 0.01 | 1.30 | 0.37 | 0.09 |
| Se | 592.3 | 592.5 | 599.3 | 0.04 | 0.00 | 0.10 | 0.10 | 0.10 | 0.10 |
| Si | 187481.5 | 172747.0 | 224931.8 | 0.18 | 0.01 | 0.06 | 0.49 | 0.46 | 0.59 |
| Zn | 87.8 | 93.0 | 86.9 | 0.09 | 0.01 | 0.02 | 0.26 | 0.27 | 0.25 |

| | Concentration [mg/kg$_{elut.fines,db}$] | | | $Q_{i,fines}/Q_{i,fuel}$ [–] | | | EF [–] | | |
|---|---|---|---|---|---|---|---|---|---|
| 760 °C | Cyclone 1 | Cyclone 2 | Hot filter | Cyclone 1 | Cyclone 2 | Hot filter | Cyclone 1 | Cyclone 2 | Hot filter |
| Al | 103536.2 | 86503.2 | 80395.5 | 0.30 | 0.2 | 0.07 | 0.85 | 0.71 | 0.66 |
| Cd | 27.3 | 28.6 | 24.0 | 0.4 | 0.00 | 0.10 | 0.12 | 0.13 | 0.11 |
| Ca | 54295.8 | 40647.3 | 33656.2 | 0.12 | 0.01 | 0.02 | 0.33 | 0.25 | 0.20 |
| Co | 39.4 | 44.9 | 47.9 | 0.06 | 0.00 | 0.02 | 0.16 | 0.19 | 0.20 |
| Cr | 495.4 | 980.4 | 799.0 | 1.60 | 0.24 | 0.77 | 4.49 | 8.89 | 7.25 |
| Cu | 839.2 | 806.8 | 818.9 | 0.05 | 0.00 | 0.02 | 0.15 | 0.14 | 0.15 |
| Fe | 10515.4 | 11744.8 | 14181.6 | 0.37 | 0.03 | 0.15 | 1.03 | 1.15 | 1.38 |
| K | 38421.6 | 55966.7 | 49335.9 | 0.14 | 0.02 | 0.05 | 0.41 | 0.59 | 0.52 |
| Mg | 24064.1 | 30332.3 | 36852.1 | 0.43 | 0.04 | 0.20 | 1.21 | 1.53 | 1.86 |
| Mn | 334.2 | 339.1 | 400.4 | 0.21 | 0.02 | 0.08 | 0.60 | 0.61 | 0.72 |
| Mo | 262.9 | 1572.8 | 1298.3 | 0.11 | 0.05 | 0.16 | 0.30 | 1.78 | 1.47 |
| Na | 46611.5 | 47285.7 | 47538.2 | 0.06 | 0.00 | 0.02 | 0.17 | 0.17 | 0.18 |
| Ni | 551.9 | 887.9 | 727.2 | 0.43 | 0.05 | 0.17 | 1.22 | 1.96 | 1.60 |
| Pb | 21.2 | 27.6 | 14.0 | 0.69 | 0.07 | 0.13 | 1.93 | 2.50 | 1.27 |
| Se | 566.2 | 541.3 | 529.3 | 0.03 | 0.00 | 0.01 | 0.09 | 0.09 | 0.09 |
| Si | 191501.5 | 155236.0 | 137021.9 | 0.18 | 0.01 | 0.04 | 0.50 | 0.41 | 0.36 |
| Zn | 88.0 | 89.9 | 86.9 | 0.09 | 0.01 | 0.03 | 0.26 | 0.26 | 0.25 |

| | Concentration [mg/kg$_{elut.fines,db}$] | | | $Q_{i,fines}/Q_{i,fuel}$ [–] | | | EF [–] | | |
|---|---|---|---|---|---|---|---|---|---|
| 800 °C | Cyclone 1 | Cyclone 2 | Hot filter | Cyclone 1 | Cyclone 2 | Hot filter | Cyclone 1 | Cyclone 2 | Hot filter |
| Al | 69928.4 | 90396.3 | 87145.8 | 0.22 | 0.03 | 0.04 | 0.58 | 0.75 | 0.72 |
| Cd | 26.5 | 36.9 | 25.2 | 0.05 | 0.01 | 0.01 | 0.12 | 0.17 | 0.11 |
| Ca | 71459.7 | 54176.2 | 43421.4 | 0.17 | 0.01 | 0.02 | 0.43 | 0.33 | 0.26 |
| Co | 37.8 | 39.0 | 49.5 | 0.06 | 0.01 | 0.01 | 0.16 | 0.16 | 0.20 |
| Cr | 826.9 | 595.1 | 828.0 | 2.92 | 0.22 | 0.45 | 7.50 | 5.40 | 7.51 |
| Cu | 816.7 | 831.1 | 817.9 | 0.06 | 0.01 | 0.01 | 0.15 | 0.15 | 0.15 |
| Fe | 10718.9 | 10876.3 | 13430.3 | 0.41 | 0.04 | 0.08 | 1.05 | 1.06 | 1.31 |
| K | 61353.2 | 59203.9 | 65031.1 | 0.25 | 0.02 | 0.04 | 0.65 | 0.62 | 0.69 |
| Mg | 32565.2 | 60743.0 | 60083.1 | 0.64 | 0.12 | 0.18 | 1.64 | 3.06 | 3.03 |
| Mn | 334.6 | 334.2 | 383.5 | 0.23 | 0.02 | 0.04 | 0.60 | 0.60 | 0.69 |
| Mo | 122.5 | 277.0 | 191.9 | 0.05 | 0.01 | 0.01 | 0.14 | 0.31 | 0.22 |
| Na | 49715.5 | 53047.5 | 50389.0 | 0.07 | 0.01 | 0.01 | 0.18 | 0.20 | 0.19 |
| Ni | 599.6 | 588.1 | 705.0 | 0.52 | 0.05 | 0.09 | 1.32 | 1.30 | 1.56 |
| Pb | 84.7 | 57.5 | 15.1 | 3.00 | 0.21 | 0.08 | 7.68 | 5.21 | 1.37 |
| Se | 530.8 | 543.8 | 525.1 | 0.03 | 0.00 | 0.01 | 0.09 | 0.09 | 0.09 |
| Si | 187836.9 | 186025.5 | 172675.8 | 0.19 | 0.02 | 0.03 | 0.50 | 0.49 | 0.46 |
| Zn | 93.9 | 118.0 | 87.9 | 0.11 | 0.01 | 0.02 | 0.27 | 0.35 | 0.26 |

**Table 5.7:** Composition of inorganic fraction and enrichment factor (EF) of fines collected in cyclone 1, cyclone 2 and hot filter for magnesite gasification test at 800 °C.

| | Concentration [mg/kg$_{elut.fines,db}$] | | | $Q_{i,fines}/Q_{i,fuel}$ [–] | | | EF [–] | | |
|---|---|---|---|---|---|---|---|---|---|
| | Cyclone 1 | Cyclone 2 | Hot filter | Cyclone 1 | Cyclone 2 | Hot filter | Cyclone 1 | Cyclone 2 | Hot filter |
| Al | 73664.0 | 78433.7 | 766682.3 | 0.29 | 0.02 | 0.09 | 0.61 | 0.65 | 0.63 |
| Cd | 26.3 | 35.8 | 25.2 | 0.06 | 0.01 | 0.02 | 0.12 | 0.16 | 0.11 |
| Ca | 44319.8 | 45403.6 | 50281.8 | 0.13 | 0.01 | 0.04 | 0.27 | 0.27 | 0.30 |
| Co | 36.4 | 37.8 | 34.3 | 0.07 | 0.01 | 0.02 | 0.15 | 0.16 | 0.14 |
| Cr | 424.9 | 425.0 | 382.9 | 1.84 | 1.84 | 0.47 | 3.85 | 3.85 | 3.47 |
| Cu | 789.2 | 787.4 | 786.0 | 0.07 | 0.01 | 0.02 | 0.14 | 0.14 | 0.14 |
| Fe | 7386.6 | 8794.4 | 7255.1 | 0.34 | 0.03 | 0.10 | 0.72 | 0.86 | 0.71 |
| K | 52920.7 | 56141.0 | 54917.0 | 0.27 | 0.02 | 0.08 | 0.56 | 0.59 | 0.58 |
| Mg | 84895.7 | 69332.6 | 71946.3 | 2.04 | 0.13 | 0.49 | 4.28 | 3.49 | 3.62 |
| Mn | 280.1 | 299.4 | 287.8 | 0.24 | 0.02 | 0.07 | 0.50 | 0.54 | 0.52 |
| Mo | 151.8 | 122.7 | 655.0 | 0.08 | 0.01 | 0.10 | 0.17 | 0.14 | 0.74 |
| Na | 52414.7 | 50107.6 | 52095.6 | 0.09 | 0.01 | 0.03 | 0.19 | 0.18 | 0.19 |
| Ni | 542.1 | 476.0 | 315.8 | 0.57 | 0.40 | 0.10 | 1.20 | 1.05 | 0.70 |
| Pb | 29.3 | 12.3 | 18.1 | 1.27 | 0.04 | 0.22 | 2.66 | 1.11 | 1.64 |
| Se | 617.2 | 603.3 | 584.4 | 0.05 | 0.00 | 0.01 | 0.10 | 0.10 | 0.10 |
| Si | 190028.8 | 205747.9 | 173618.3 | 0.24 | 0.02 | 0.06 | 0.50 | 0.54 | 0.46 |
| Zn | 78.9 | 97.1 | 73.6 | 0.11 | 0.01 | 0.03 | 0.23 | 0.28 | 0.22 |

larger quantities of iron than those remaining in the reactor with fuel; consequently the observed values of $Q_{Fe,fines}/Q_{Fe,fuel}$ were significantly larger than 1, typically 100 or more. The results presented in Tables 5.6 and 5.7 in cyclone 1 for the gasification of cardoon, suggest that $Q_{Fe,fines}/Q_{Fe,fuel}$ is 0.34 for magnesite at 800 °C and 0.41 for olivine and it is increasing with temperature. This implies that the catalytic activity of olivine is absent, or only partially present during air gasification of cardoon. The values of the EF in the collected fines are around 1 for olivine and below 1 for magnesite suggesting that the ash enrichment in iron is influenced by the composition of the olivine particles.

Similar results were reported by Arena & Di Gregorio (2014) for the gasification of solid recovered fuel. They concluded that magnesium was active for the cracking and isomerisation reactions, but the dehydrogenation and carbonization reactions which required active sites of elemental iron were absent, and tar formation was not inhibited. The explanation provided by Arena & Di Gregorio (2014) may also be valid for the gasification of cardoon i.e. with the high ash and Fe content in cardoon, the metals in the ash can act as competing active sites of the iron oxides on the external surface of olivine particles so avoiding their reduction to elemental Fe. On the other hand, fully oxidized iron phases containing $Fe^{3+}$ ions in the presence of potassium are known to be highly catalytically active towards dehydrogenation of ethylbenzene to styrene generating $H_2$ (Zhu *et al.*, 2004). The content of ehtylbenzene in the tar is relatively low while styrene is high (Figure 5.6) suggesting that dehydrogenation of substituted aromatic hydrocarbons with long aliphatic chains is a possible explanation for a high hydrogen content in the product gas.

Moreover, the magnesium is catalytically active particularly in magnesite (EF = 4.28) but also in olivine (EF = 1.64), at 800 °C, possibly enhancing the dehydrogenation and isomerisation reactions of fragments produced by thermal cracking of biomass (Di Felice *et al.*, 2010). Rabou *et al.* (2009) reported that Mg present in chicken manure ash was very active in cracking of 4 and 5-ring tar compounds even at 750 °C.

Comparison of bed materials indicates that there is no significant difference in terms of the yield of total tar between magnesite and olivine but the composition of tar is very different. The BTEX fraction in the measured total tar is higher for olivine when compared to magnesite while the PAH fraction in the total tar is quite similar for both olivine and magnesite. Magnesite seems to be more catalytically active at 800 °C than olivine.

### 5.3.4 Mass balance

The consistency of the results is evaluated by performing a mass balance for the different main elements based on the total flows, on a dry-ash free basis and presented in Tables 5.8, 5.9 and 5.10. The biomass input is differentiated into dry-ash free biomass, moisture and ash. The elemental flow rate of biomass is calculated according to the elemental and proximate analysis shown in Table 2.1. The other input flows are the air for fluidization and the $N_2$ used to pressurize the hopper. The mass output flows are divided into product gas, char and ash accumulated in the bed, cyclones and hot filter, and total moisture from the char particles and moisture collected from the tar trap, and tar. This last stream is the total tar obtained using the SPA method.

The mass balance, either total mass flow or elemental species, shows more than 84 % agreement between input and output. The highest difference is observed in the C balance which is explained due to the assumption of considering all tar as naphthalene. There are also some differences in the O and H balance that could be due to the lack of information about hydrogen rich component such as ammonia, hydrogen sulphide and acetylene as well as the accuracy of water content determination. The nitrogen balance is closed to 100 % as it is expected due to the inert properties of this specie. It is worth noticing that the ash balance shows large differences between output and input values, around 73 % for magnesite and 56 % for olivine. This discrepancy is attributed to ash accumulation in the horizontal pipes and the possible ash that still remains in the cyclones and the hot filter.

Figure 5.7 shows the generation of the different residual output flows: char, ash, moisture and GC detectable tar. Tar, char and ash generation rates are low in the experiments with magnesite (less than 0.1 kg/kg$_{biomass,daf}$) for the two temperatures tested. Moisture generation is also relatively low, around 0.2 kg/kg$_{biomass,daf}$. Char and

**Table 5.8:** Mass balance for the cases of magnesite and olivine at 700 °C.

Magnesite at 700 °C

| | Mass flow | C | H | N | O[a] | Ash [$g_{db}$/h] |
|---|---|---|---|---|---|---|
| *Input* | | | | | | |
| Biomass [$kg_{daf}$/h] | 3.63 | 1.60 | 0.23 | 0.02 | 1.77 | 466.10 |
| Biomass moisture [g/h] | 439.40 | | 48.80 | | 390.60 | |
| Air [kg/h] | 4.52 | | | 3.46 | 1.06 | |
| $N_2$ for feeding [kg/h] | 0.14 | | | 0.14 | | |
| Total [kg/h] | 9.20 | 1.60 | 0.28 | 3.62 | 3.23 | 466.10 |
| *Output* | | | | | | |
| Gas | 7.30 | 1.26 | 0.17 | 3.91 | 1.97 | |
| Char gasifier [$g_{daf}$/h] | 73.80 | ND | ND | ND | ND | 54.70 |
| Char cyclone 1 [$g_{daf}$/h] | 48.20 | ND | ND | ND | ND | 127.90 |
| Char cyclone 2 [$g_{daf}$/h] | 2.30 | ND | ND | ND | ND | 8.30 |
| Char filter [$g_{daf}$/h] | 8.00 | ND | ND | ND | ND | 26.00 |
| Total moisture [g/h] | 771.60 | | 85.80 | | 685.80 | |
| Total tar (all as naphthal.) [g/h] | 190.5 | 178.52 | 11.98 | | | |
| Total [kg/h] | 8.61 | 1.44 | 0.26 | 3.91 | 2.65 | 216.90 |
| *Out/in [%]* | 93.60 | 89.65 | 93.42 | 107.95 | 82.17 | 46.54 |

Olivine at 700 °C

| | Mass flow | C | H | N | O[a] | Ash [$g_{db}$/h] |
|---|---|---|---|---|---|---|
| *Input* | | | | | | |
| Biomass [$kg_{daf}$/h] | 3.51 | 1.55 | 0.23 | 0.02 | 1.72 | 450.80 |
| Biomass moisture [g/h] | 425.00 | | 47.20 | | 377.80 | |
| Air [kg/h] | 4.48 | | | 3.43 | 1.05 | |
| $N_2$ for feeding [kg/h] | 0.14 | | | 0.14 | | |
| Total [kg/h] | 9.00 | 1.55 | 0.27 | 3.58 | 3.58 | 450.80 |
| *Output* | | | | | | |
| Gas | 7.15 | 1.19 | 0.15 | 3.90 | 1.91 | |
| Char gasifier [$g_{daf}$/h] | 407.40 | 221.40 | 5.30 | 2.30 | 178.40 | 302.40 |
| Char cyclone 1 [$g_{daf}$/h] | 48.20 | 11.70 | 0.40 | 0.10 | 36.00 | 112.30 |
| Char cyclone 2 [$g_{daf}$/h] | 2.41 | 0.40 | 0.00 | 0.10 | 2.00 | 9.10 |
| Char filter [$g_{daf}$/h] | 10.60 | 2.10 | 0.00 | 0.00 | 8.50 | 33.40 |
| Total moisture [g/h] | 968.00 | | 107.50 | | 860.50 | |
| Total tar (all as naphthal.) [g/h] | 168.50 | 157.90 | 10.60 | | | |
| Total [kg/h] | 9.21 | 1.59 | 0.27 | 3.91 | 2.99 | 457.20 |
| *Out/in [%]* | 102.27 | 102.19 | 98.71 | 109.00 | 95.08 | 101.42 |

[a]by difference, ND: not determined.

**Table 5.9:** Mass balance for olivine at 760 °C.

| Olivine at 760 °C | | | | | | |
|---|---|---|---|---|---|---|
| | Mass flow | C | H | N | O[a] | Ash [$g_{db}$/h] |
| *Input* | | | | | | |
| Biomass [$kg_{daf}$/h] | 3.60 | 1.59 | 0.23 | 0.02 | 1.76 | 462.40 |
| Biomass moisture [g/h] | 435.90 | | 48.40 | | 387.50 | |
| Air [kg/h] | 4.52 | | | 3.46 | 1.06 | |
| $N_2$ for feeding [kg/h] | 0.14 | | | 0.14 | | |
| Total [kg/h] | 9.16 | 1.59 | 0.28 | 3.62 | 3.21 | 462.40 |
| *Output* | | | | | | |
| Gas | 7.55 | 1.38 | 0.16 | 3.83 | 2.17 | |
| Char gasifier [$g_{daf}$/h] | 366.20 | 187.10 | 4.50 | 2.30 | 172.30 | 223.80 |
| Char cyclone 1 [$g_{daf}$/h] | 49.40 | 12.20 | 0.30 | 0.20 | 36.70 | 114.00 |
| Char cyclone 2 [$g_{daf}$/h] | 2.80 | 0.50 | 0.00 | 0.01 | 2.30 | 9.20 |
| Char filter [$g_{daf}$/h] | 12.80 | 2.70 | 0.10 | 0.00 | 10.00 | 36.00 |
| Total moisture [g/h] | 889.70 | | 98.80 | | 790.90 | |
| Total tar (all as naphthal.) [g/h] | 276.50 | 259.20 | 17.40 | | | |
| Total [kg/h] | 9.53 | 1.84 | 0.29 | 3.83 | 3.18 | 383.00 |
| *Out/in [%]* | 104.05 | 115.94 | 102.08 | 106.00 | 99.17 | 82.83 |

[a]by difference.

ash generation increase with temperature while moisture decreases. This indicates that magnesite may be more effective towards char reactivity at low temperature. On the other hand, when olivine particles are used, char and moisture generation are higher at 700 °C and decrease sharply at 800 °C, this could be an indicator of improved char reactivity at higher temperature due to the catalytic properties of olivine or some ash components (potassium and sodium) as well as significantly improved, water gas shift reaction (Eq. 1.9) or steam tar reforming (Eq. 1.12). The mass balance shows higher ash deposition in pipes and other elements of the facility at lower temperatures for olivine and at higher temperature for magnesite. Temperature should not have significant effect on the ash quantity collected downstream of the gasifier and the differences in the ash collected could be due to permanent accumulation of the ash in the hot filter element. In general terms, magnesite shows less char, GC detectable tar and moisture at low temperature, while olivine produces lower char, ash and moisture at the higher temperature.

Figure 5.8 shows a flow diagram describing the mass balance for carbon element for experiments at 800 °C. Carbon losses due to elutriated particles are very small compared with the carbon introduced into the reactor. In the case of magnesite, higher amounts of carbon are found in the cyclones and hot filter than in the case of olivine. The carbon accumulated in the bed is also higher with magnesite than with olivine indicating a

**Table 5.10:** Mass balance for the cases of magnesite and olivine at 800 °C.

Magnesite at 800 °C

| | Mass flow | C | H | N | O[a] | Ash [$g_{db}$/h] |
|---|---|---|---|---|---|---|
| *Input* | | | | | | |
| Biomass [$kg_{daf}$/h] | 3.56 | 1.57 | 0.23 | 0.02 | 1.74 | 456.44 |
| Biomass moisture [g/h] | 430.66 | | 47.85 | | 382.81 | |
| Air [kg/h] | 4.53 | | | 3.46 | 1.06 | |
| $N_2$ for feeding [kg/h] | 0.14 | | | 0.14 | | |
| Total [kg/h] | 9.11 | 1.57 | 0.28 | 3.62 | 3.18 | 456.44 |
| *Output* | | | | | | |
| Gas | 7.73 | 1.49 | 0.19 | 3.72 | 2.33 | |
| Char gasifier [$g_{daf}$/h] | 152.51 | 81.39 | 1.27 | 0.69 | 69.16 | 114.66 |
| Char cyclone 1 [$g_{daf}$/h] | 55.37 | 14.09 | 0.22 | 0.12 | 40.94 | 158.84 |
| Char cyclone 2 [$g_{daf}$/h] | 3.90 | 0.88 | 0.01 | 0.01 | 3.00 | 13.20 |
| Char filter [$g_{daf}$/h] | 15.19 | 3.70 | 0.03 | 0.03 | 11.43 | 46.58 |
| Total moisture [g/h] | 704.50 | | 78.20 | | 626.30 | |
| Total tar (all as naphthal.) [g/h] | 194.50 | 182.27 | 12.24 | | | |
| Total [kg/h] | 9.19 | 1.77 | 0.28 | 3.72 | 3.08 | 333.28 |
| *Out/in [%]* | 100.87 | 112.58 | 101.27 | 102.83 | 96.82 | 73.02 |

Olivine at 800 °C

| | Mass flow | C | H | N | O[a] | Ash [$g_{db}$/h] |
|---|---|---|---|---|---|---|
| *Input* | | | | | | |
| Biomass [$kg_{daf}$/h] | 3.51 | 1.55 | 0.23 | 0.02 | 1.72 | 451.06 |
| Biomass moisture [g/h] | 425.58 | | 47.29 | | 378.30 | |
| Air [kg/h] | 4.50 | | | 3.44 | 1.06 | |
| $N_2$ for feeding [kg/h] | 0.14 | | | 0.14 | | |
| Total [kg/h] | 9.03 | 1.55 | 0.27 | 3.60 | 3.15 | 451.06 |
| *Output* | | | | | | |
| Gas | 7.74 | 1.54 | 0.19 | 3.63 | 2.39 | |
| Char gasifier [$g_{daf}$/h] | 79.94 | 33.38 | 0.95 | 0.50 | 45.11 | 80.26 |
| Char cyclone 1 [$g_{daf}$/h] | 36.67 | 6.65 | 0.17 | 0.11 | 29.74 | 136.33 |
| Char cyclone 2 [$g_{daf}$/h] | 2.80 | 0.37 | 0.01 | 0.01 | 2.41 | 14.78 |
| Char filter [$g_{daf}$/h] | 4.40 | 0.62 | 0.01 | 0.02 | 3.75 | 22.28 |
| Total moisture [g/h] | 621.80 | | 69.10 | | 552.70 | |
| Total tar (all as naphthal.) [g/h] | 249.84 | 234.13 | 15.72 | | | |
| Total [kg/h] | 8.99 | 1.81 | 0.27 | 3.63 | 3.03 | 253.64 |
| *Out/in [%]* | 99.56 | 116.62 | 99.66 | 100.76 | 95.97 | 56.23 |

[a]by difference.

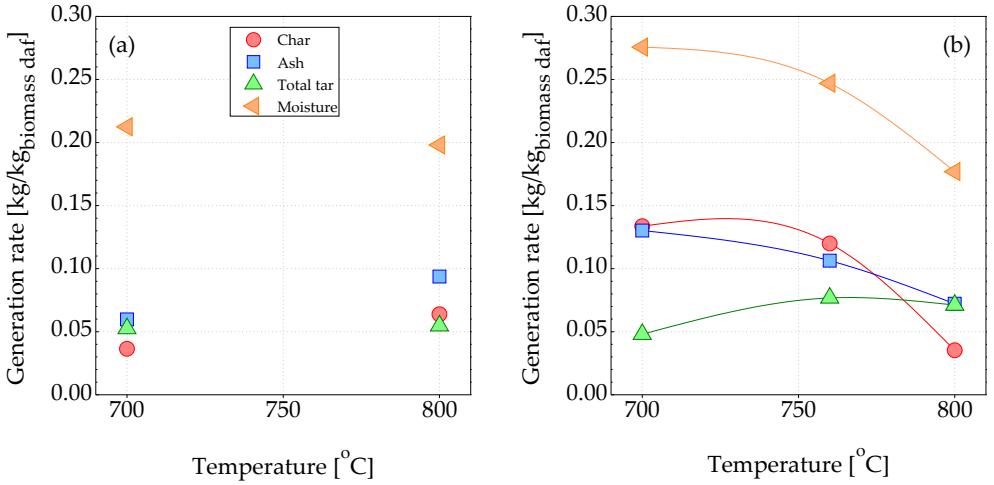


**Figure 5.7:** Char, ash, moisture and total tar per kilogram of dry-ash free of biomass: a) magnesite and b) olivine.

higher gasification rate when olivine is used as a bed material. As stated above, the carbon balance shows gaps in the mass closure as a consequence of considering all tar as naphthalene. Thus the values in Figure 5.8 show differences of approximately 11 % between the carbon content in the dry syngas and the calculated carbon content taking into account the different streams.

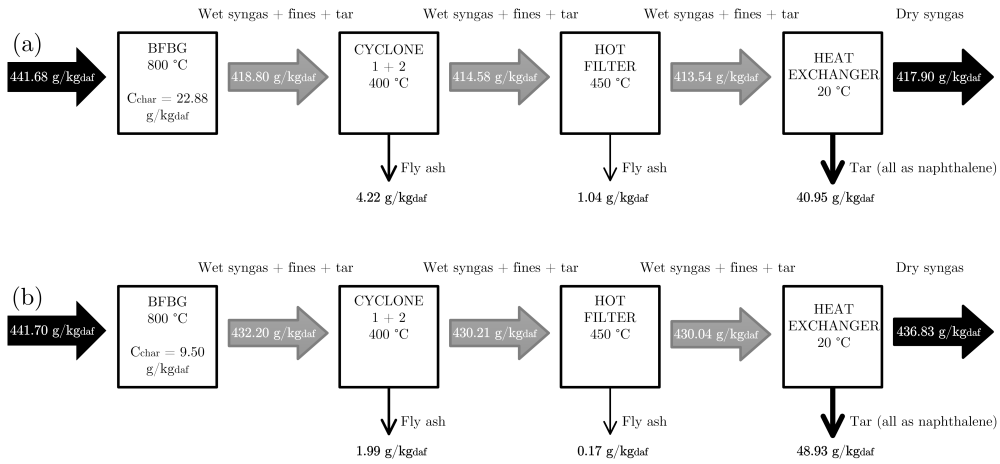


**Figure 5.8:** Carbon balance diagram for gasification at 800 °C: a) magnesite and b) olivine.

## 5.4 Conclusions

In this chapter, *C. cardunculus* L. has been gasified in a pilot scale bubbling fluidised bed reactor at different temperatures and using different bed materials while maintaining both ER and fluidization regime constant.

Relatively high hydrogen content in the product gas for air gasification is obtained for both magnesite and olivine. The use of magnesite and olivine as well as the high alkali metals present in cardoon ashes contribute to achieving the high concentration of hydrogen observed, by acting as catalytic agents. The product gas quality in terms of LHV and gas yield was improves with increasing temperature. Greater than 90 % carbon and biomass conversions are achieved at the highest temperature tested (800 °C) for the two bed materials. For the gasification experiments carried out at 800 °C the amount of chemical energy of cardoon transferred into the product gas are 84 % and 87 % for magnesite and olivine respectively.

Not significant difference in terms of the yield of total tar between magnesite and olivine is observed, however, the composition of tar is very different. The BTEX fraction in the measured total tar is higher for olivine when compare to magnesite while the PAH fraction in the total tar is similar for both bed materials. Magnesite seems to be more catalytically active at 800 °C than olivine.

The catalytic activity due to the iron in the olivine is very small during cardoon gasification. However, magnesium in the magnesite and to a lesser extent in the olivine, exhibit catalytic active behaviour towards tar cracking.

In general terms, magnesite provides better gasification performance at lower temperatures (700 °C) (gas composition, biomass conversion, LHV, gas yield and char conversion) than olivine while olivine performs better at high temperature (800 °C). Tar concentration remains high in the product gas so additional downstream gas cleaning would be necessary for both magnesite and olivine. The results suggest that the best option is to use olivine at 800 °C for *C. cardunculus* gasification or if agglomeration could be avoided by the use of kaolin, increases the operating temperature to further reduce the tar content.

## References

Abelha, P., Franco, C., Pinto, F., Lopes, H., Gulyurtlu, I., Gominho, J., Lourenço, A. & Pereira, H. 2013 Thermal conversion of *Cynara cardunculus* L. and mixtures with *Eucalyptus globulus* by fluidized-bed combustion and gasification. *Energy & Fuels* 27, 6725–6737.

de Andrés, J. M., Narros, A. & Rodríguez, M. E. 2011 Behaviour of dolomite, olivine and alumina as primary catalysts in air-steam gasification of sewage sludge. *Fuel* 90, 521–527.

Arena, U. & Di Gregorio, F. 2014 Gasification of a solid recovered fuel in a pilot scale fluidized bed reactor. *Fuel* 117, 528–536.

Arena, U., Zaccariello, L. & Mastellone, M. L. 2009 Tar removal during the fluidized bed gasification of plastic waste. *Waste Management* 29, 783–791.

Arena, U., Zaccariello, L. & Mastellone, M. L. 2010 Fluidized bed gasification of waste-derived fuels. *Waste Management* 30, 1212–1219.

Berrueco, C., Montané, D., Matas Güell, B. & del Alamo, G. 2014 Effect of temperature and dolomite on tar formation during gasification of torrefied biomass in a pressurized fluidized bed. *Energy* 66, 849–859.

Boroson, M. L., Howard, J. B., Longwell, J. P. & Peters, W. A. 1989 Heterogeneous cracking of wood pyrolysis tars over fresh wood char surfaces. *Energy & Fuels* 3, 735–740.

Brown, C., Liu, Q. & Norton, G. 2000 Catalytic effects observed during the co-gasification of coal and switchgrass. *Biomass & Bioenergy* 18, 499–506.

Christodoulou, C., Tsekos, C., Tsalidis, G., Fantini, M., Panopoulos, K. D., de Jong, W. & Kakaras, E. 2014 Attempts on cardoon gasification in two different ciculating fluidized beds. *Cases Studies in Thermal Engineering* 4, 42–52.

Corella, J., Toledo, J. M. & Molina, G. 2008 Biomass gasification with pure steam in fluidised bed: 12 variables that affect the effectiveness of the biomass gasifier. *International Journal of Oil, Gas and Coal Technology* 1, 194–207.

Corella, J., Toledo, J. M. & Padilla, R. 2004 Olivine or dolomite as in-bed additive in biomass gasification with air in a fluidized bed: Which is better? *Energy & Fuels* 18, 713–720.

Delgado, J., Aznar, M. P. & Corella, J. 1996 Calcined dolomite, magnesite, and calcite for cleaning hot gas from a fludized bed biomass gasifier with steam: Life and usefulness. *Industrial & Engineering Chemistry Research* 35, 3637–3643.

Delgado, J., Aznar, M. P. & Corella, J. 1997 Biomass gasification with steam in fluidized bed: Effectiveness of CaO, MgO and CaO-MgO for hot raw gas cleaning. *Industrial & Engineering Chemistry Research* 36, 1535–1543.

Demirbaş, A. 2002 Gaseous products from biomass by pyrolysis and gasification: effects of catalyst on hydrogen yield. *Energy Conversion & Management* 43, 897–909.

Devi, L., Ptasinski, K. J., Janssen, F. J. J. G., van Paasen, S. V. B., Bergman, P. C. A. & Kiel, J. H. A. 2005 Catalytic decomposition of biomass tars: use of dolomite and untreated olivine. *Renewable Energy* 30, 565–587.

Di Felice, L., Courson, C., Niznansky, D., Foscolo, P. U. & Kiennemann, A. 2010 Biomass gasification with catalytic tar reforming: A model study into activity enhancement of calcium- and magnesium-oxide-based catalytic materials by incorporation of iron. *Energy & Fuels* 24, 4034–4045.

Dufour, A., Masson, E., Girods, P., Rogaume, Y. & Zoulalian, A. 2011 Evolution of aromatic tar composition in relation to methane and ethylene from biomass pyrolysis-gasification. *Energy & Fuels* 25, 4182–4189.

Encinar, J. M., González, J. F. & González, J. 2002 Steam gasification of *Cynara cardunculus* L.: influence of variables. *Fuel Processing Technology* 75, 27–43.

Fernández Llorente, M. J., Díaz Arocas, P., Gutiérrez Nebot, L. & Carrasco García, J. E. 2008 The effect of the additiion of chemical materials on the sintering of biomass ash. *Fuel* 87, 2651–2658.

Fitzpatrick, E. M., Jones, J. M., Pourkashanian, M., Ross, A. B., Williams, A. & Bartle, K. D. 2008 Mechanistic aspects of soot formation from the combustion of pine wood. *Energy & Fuels* 22, 3771–3778.

Hanping, C., Bin, L., Haiping, Y., Guolai, Y. & Shihong, Z. 2008 Experimental investigation of biomass gasification in a fluidized bed. *Energy & Fuels* 22, 3493–3498.

Kiel, J. H. A., van Paasen, S. V. B., Neeft, J. P. A., Devi, L., Ptasinski, K. J., Janssen, F. J. J. G., Meijer, R., Berends, R. H., Temmink, H. M. G., Brem, G., Padban, N. & Bramer, E. A. 2004 Primary measures to reduce tar formation in fluidised-bed biomass gasifiers. ECN-C-04-014. *Tech. Rep.* Energy Research Centre of The Netherlands.

Kinoshita, C. M., Wang, Y. & Zhou, J. 1994 Tar formation under different biomass gasification. *Journal of Analitical and Applied Pyrolysis* 29, 169–181.

Lahijani, P. & Zainal, Z. A. 2011 Gasification of palm empty fruit bunch in a bubbling fluidized bed: A performance and agglomeration study. *Bioresource Technology* 102, 2068–2076.

Mastellone, M. L. & Arena, U. 2008 Olivine as a tar removal catalyst during fluidized bed gasification on plastic waste. *AIChE Journal* 54, 1656–1667.

Miccio, F., Piriou, B., Ruoppolo, G. & Chirone, R. 2009 Biomass gasification in a catalytic fluidized reactor with beds of different materials. *Chemical Engineering Journal* 154, 369–374.

Milne, T. A., Evans, R. J. & Abatzoglou, N. 1998 Biomass gasifier "tars": Their nature , formation and conversion. NREL/TP-570-25357. *Tech. Rep*. National Renewable Energy Laboratory.

Mohammed, M. A. A., Wan Azlina, W. A. K. G., Mohammed Amran, M. S. & Fakhru'l-Razi, A. 2011 Air gasification of empty fruit bunch for hydrogen-rich gas production in a fluidized-bed reactor. *Energy Conversion and Management* 52, 1555–1561.

Morf, P., Hasler, P. & Nussbaumer, T. 2002 Mechanisms and kinetics of homogeneous secondary reactions of tar from continuous pyrolysis of wood chips. *Fuel* 81, 843–853.

Narváez, I., Orío, A., Aznar, M. P. & Corella, J. 1996 Biomass gasification with air in an atmospheric bubbling fluidized bed. Effect of six operational variables on the quality of the produced raw gas. *Industrial & Engineering Chemistry Research* 35, 2110–2120.

van Paasen, S. V. B. & Kiel, J. H. A. 2004 Tar formation in a fluidised-bed gasifier. ECN-C-04-013. *Tech. Rep*. Energy Research Centre of The Netherlands.

Pinto, F., Franco, C., André, R. N., Tavares, C., Dias, M., Gulyurtlu, I. & Cabrita, I. 2003 Effect of experimental conditions on co-gasification of coal, biomass and plastics wastes with air/steam mixtures in a fluidized bed system. *Fuel* 82, 1967–1976.

Rabou, L. P. L. M., Zwart, R. W. R., Vreugdenhil, B. J. & Box, L. 2009 Tar in biomass producer gas, the Energy research Centre of the Netherlands (ECN) experience: An enduring challenge. *Energy & Fuels* 23, 6189–6198.

Rapagnà, S., Gallucci, K., Di Marcello, M., Matt, M., Nacken, M., Heidenreich, S. & Foscolo, P. U. 2010 Gas cleaning, gas conditioning and tar abatement by means of a catalytic filter candle in a biomass fluidized-bed gasifier. *Bioresource Technology* 101, 7123–7130.

Rapagnà, S., Jand, N., Kiennemann, A. & Foscolo, P. U. 2000 Steam-gasification of biomass in a fluidised-bed of olivine particles. *Biomass & Bioenergy* 19, 187–197.

Siedlecki, M., Nieuwstraten, R., Simeone, E., de Jong, W. & Verkooijen, H. M. 2009 Effect of magnesite as bed material in a 100 $kW_{th}$ steam-oxygen blown circulating fluidized-bed biomass gasifier on gas composition and tar formation. *Energy & Fuels* 23, 5643–5654.

Sutton, D., Kelleher, B. & Ross, J. R. H. 2001 Review of literature on catalysts for biomass gasification. *Fuel Processing Technology* 73, 155–173.

Weber, K. & Quicker, P. 2013 Enhancing as melting behaviour of straw ash through the addition of kaolin. In *21$^{st}$ European Biomass Conference and Exhibition*, pp. 1447–1450. Copenhagen, Denmark.

Werther, J., Saenger, M., Hartge, E.-U., Ogada, T. & Siagi, Z. 2000 Combustion of agricultural residues. *Progress in Energy and Combustion Science* 26, 1–27.

Yu, H., Zhang, Z., Li, Z. & Chen, D. 2014 Characteristics of tar formation during cellulose, hemicellulose and lignin gasification. *Fuel* 118, 250–256.

Yu, Q., Brage, C., Chen, G. & Sjöström, K. 1997 Temperature impact on the formation of tar from biomass pyrolysis in a free-fall reactor. *Journal of Analytical and Applied Pyrolysis* 40-41, 481–489.

Zabaniotou, A., Bitou, P., Kanellis, Th., Manara, P. & Stavropoulos, G. 2014 Investigating *Cynara C.* biomass gasification producer gas suitability for CHP, second generation biofuels, and $h_2$ production. *Industrial Crops and Products* 61, 309–316.

Zhu, X. M., Schön, M., Bartmann, U., van Veen, A. C. & Muhler, M. 2004 The dehydrogenation of ethylbenzene to styrene over a potassium-promoted iron oxide-based catalyst: a transient kinetic study. *Applied Catalysis A: General* 266, 99–108.

Zwart, R., van der Heijden, S., Emmen, R., Bentzen, J. D., Stoholm, P. & Krogh, J. 2010 Tar removal from low-temperature gasifiers. ECN-C-10-008. *Tech. Rep.* Energy Research Centre of The Netherlands.

CHAPTER

**SIX**

# Fly ash characteristics and recovery

**Contents**



## 6.1 Introduction

Fly ash is usually overlooked when talking about biomass gasification and it is an issue that also has to be considered. Huge amounts of ash are generated in biomass gasification plants that need to be disposed or reused in a different application.

Fly ashes from combustion processes have been widely studied and characterized for their use in different utilizations (Ahmaruzzaman, 2010; Kalembkiewicz & Chmielarz, 2012; Rajamma *et al.*, 2009; Freire *et al.*, 2015). However, the references regarding biomass gasification fly ash is rather limited. The characteristics of gasification fly ashes with high amounts of unburned carbon, PAHs, chlorine and heavy metals are a bit different from combustion fly ashes (Ahmaruzzaman, 2010). Thus, their use is more complicated (Leiva *et al.*, 2007; Gómez-Barea *et al.*, 2009). An investigation performed under the GASASH Project (2005) analysed different fly ashes from different gasification facilities and provided possible utilization routes for these residues. Different authors have proposed fly ashes as a binding material for construction applications (Holt & Raivio, 2006; Leiva *et al.*, 2007; Gómez-Barea *et al.*, 2009; Fernández-Pereira *et al.*, 2011).

The metal distribution in the fly ashes from different types of biomasses have also been investigated, observing that the most volatile compounds are found in the ash scrubbers while the higher boiling point elements remained in the cyclones (Liao *et al.*, 2007).

The objective of this chapter is to analyse the entrained fines collected from cardoon air gasification in a bubbling fluidized bed pilot plant. For this purpose, a deep characterization (CHN-S, loss on ignition (LOI), moisture, ash, LHV, chlorine and metal composition) has been carried out on the samples. According to these characteristics, the different possible applications employed for combustion fly ashes are evaluated for cardoon fly ashes in order to elucidate if they meet the specific requirements for each application.

## 6.2 Experimental setup

The experimental setup (facility, biomass and bed materials) as well as the experimental procedure are the same as in Chapter 5, obtaining the data for this analysis from the same experimental campaign. A complete description of the experimental aspects can be found in Chapter 2 while the experimental procedure for the gasification tests can be found in Chapter 5. Table 6.1 summarizes the main operating conditions for the gasification tests.

**Table 6.1:** Operating conditions for the gasification experiments.

| | magnesite | magnesite | olivine | olivine | olivine |
|---|---|---|---|---|---|
| Biomass feeding rate [$kg_{daf}$/h] | 3.63 | 3.56 | 3.51 | 3.60 | 3.52 |
| Biomass throughput [$kg_{daf}/m^2h$] | 255.55 | 250.37 | 247.17 | 253.53 | 247.42 |
| Air flow rate [$Ndm^3$/min] | 63.43 | 63.47 | 62.79 | 63.36 | 63.13 |
| ER [–] | 0.20 | 0.20 | 0.20 | 0.20 | 0.20 |
| Air excess ratio, $u/u_{mf}$ [–] | 2.91 | 3.06 | 3.01 | 3.19 | 3.35 |
| $T_{gasification}$, TIC10 [°C] | 700 | 800 | 700 | 760 | 800 |

The entrained fines (fines, char and fly ash) from the *C. cardunculus* L. gasification with magnesite and olivine, are kept for analysis by means of CHN-S, ash and moisture, LHV, AAS or ICP-OES and leaching analyses. Further information about these analyses can be found in Chapter 2 (Subection 2.7.7).

## 6.3 Results and discussion

Gasification results in terms of gas and tar composition, and gasification performance have been discussed in Chapter 5. In this chapter, the attention is focused towards the

entrained fines from the gasification process.

### 6.3.1 Ash characterization

Different amounts of fines are collected by the three cleaning devices. The first cyclone collects most of the entrained fines, around 75 wt.% of the total with the second cyclone retaining only 5 wt.% and the hot filter collecting the remaining 20 wt.%. Table 6.2 shows the amount of fines accumulated in the different devices, over the lifetime of each experiment.

**Table 6.2:** Mass flow of the entrained fines in cyclones and hot filter, in [$g_{ar}$/h].

| | Cyclone 1 | Cyclone 2 | Hot filter |
|---|---|---|---|
| Olivine, 700 °C | 162.8 | 11.7 | 44.1 |
| Olivine, 760 °C | 164.7 | 12.4 | 48.8 |
| Olivine, 800 °C | 175.8 | 18.0 | 27.0 |
| Magnesite, 800 °C | 217.2 | 17.5 | 62.2 |

#### Elemental composition, ash and moisture

As stated above, the elutriated fine samples are characterized in terms of their elemental composition, moisture and ash contents as well as their LHVs. The results of these analyses are shown in Table 6.3. In this table, data for the feedstock (cardoon + kaolin) is also presented for comparison. The fines escaping the reactor are mainly formed by ash which comprises more than the 69 wt.% db of the fines, and to a lesser extent by carbon. The carbon content of the samples is moderately high, between 13 and 25 wt.% db and is considered high for the use of the fly ash in other applications (GASASH Project, 2005). However, these fines can be reintroduced into the reactor for a final conversion of this carbon and an increase the carbon conversion and CGE. The negative values for the oxygen content in the magnesite experiments are due to the temperature differences in the determination of the elemental composition (850 °C) and ash content (550 °C).

Figure 6.1a shows how the carbon content (wt.% db) is higher in the first cyclone than in the second one and the filter. Furthermore, the carbon content in the second cyclone always has the lowest value. On the other hand, the highest amount of ash is obtained in the second cyclone while the lowest ash concentration is found in the first cyclone. It should be noted that the mean carbon content in the two cyclones and the hot filter decreases with temperature, which corresponds with an improved carbon conversion at higher temperature. Olivine and magnesite show some differences in terms of carbon content at the same temperature, being this value higher for magnesite. These results are

**Table 6.3:** Elemental composition, moisture and ash content, and LHV of the fines from the cyclones and hot filter.

| | C [wt.% db] | H [wt.% db] | N [wt.% db] | S [wt.% db] | Cl [wt.% db] | O[a] [wt.% db] | Moisture [wt.% ar] | Ash [wt.% db] | LHV [MJ/kg db] |
|---|---|---|---|---|---|---|---|---|---|
| Cardoon + kaolin | 48.90 | 5.90 | 0.57 | 0.05 | 0.12 | 33.09 | 9.69 | 11.37 | 16.05 |
| *Olivine, 700 °C* | | | | | | | | | |
| Cyclone 1 | 24.67 | 0.62 | 0.25 | 0.07 | 1.85 | 2.59 | 1.38 | 69.94 | 9.39 |
| Cyclone 2 | 16.53 | 0.36 | 0.24 | 0.06 | 0.23 | 3.89 | 1.55 | 78.70 | 6.42 |
| Hot filter | 19.66 | 0.40 | 0.17 | 0.05 | 0.95 | 2.84 | 0.22 | 75.93 | 7.51 |
| *Olivine, 760 °C* | | | | | | | | | |
| Cyclone 1 | 24.85 | 0.60 | 0.37 | 0.08 | 1.76 | 2.63 | 0.75 | 69.71 | 9.14 |
| Cyclone 2 | 17.73 | 0.32 | 0.27 | 0.08 | 0.32 | 4.73 | 2.28 | 76.55 | 6.58 |
| Hot filter | 21.36 | 0.45 | 0.22 | 0.06 | 1.99 | 2.27 | 0.00 | 73.65 | 7.97 |
| *Olivine, 800 °C* | | | | | | | | | |
| Cyclone 1 | 18.41 | 0.30 | 0.31 | 0.08 | 1.87 | 8.94 | 1.59 | 70.09 | 6.81 |
| Cyclone 2 | 13.41 | 0.17 | 0.24 | 0.09 | 1.47 | 5.50 | 2.08 | 79.12 | 4.93 |
| Hot filter | 14.19 | 0.13 | 0.35 | 0.08 | 1.63 | 7.07 | 1.02 | 76.55 | 5.30 |
| *Magnesite, 800 °C* | | | | | | | | | |
| Cyclone 1 | 25.79 | 0.25 | 0.21 | 0.06 | 1.84 | -2.29 | 1.38 | 74.14 | 8.08 |
| Cyclone 2 | 23.05 | 0.09 | 0.21 | 0.09 | 1.47 | -2.00 | 2.23 | 77.09 | 7.11 |
| Hot filter | 24.49 | 0.15 | 0.19 | 0.05 | 1.63 | -1.91 | 0.66 | 75.40 | 7.50 |

ar: as received, db: dry basis, [a]by difference

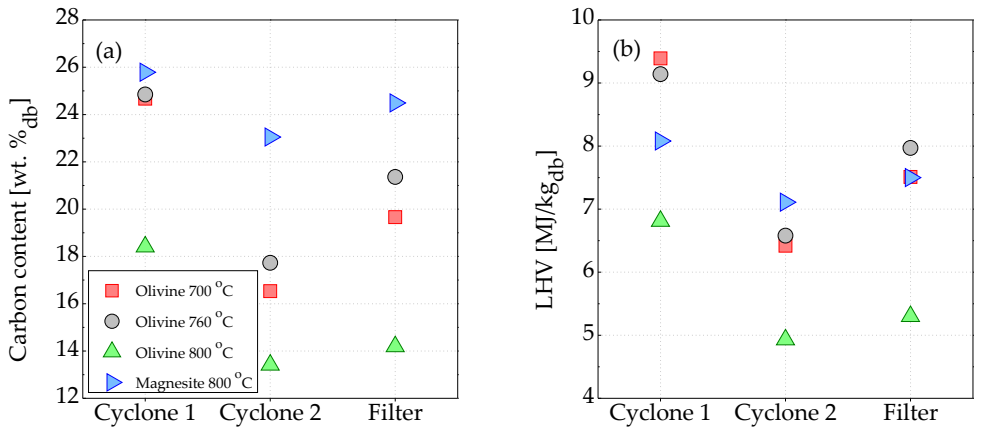


**Figure 6.1:** a) Carbon content and b) LHV of elutriated fines from cyclone 1, cyclone 2 and hot filter.

in agreement with the higher carbon conversion when temperature is increased and when olivine is used instead of magnesite at the same temperature. In the case of magnesite, the carbon content is very similar for the two cyclones and the hot filter.

### Chlorine and sulphur content

Sulphur and chlorine contents are shown in Table 6.3. Sulphur content is similar in all samples on average around a 0.07 wt.% db. In the case of the chlorine content the values are between 1 and 2 wt.% db. The content of S and Cl are in the range of other fines collected from different biomasses and gasifiers reported in the literature (GASASH Project, 2005).

### Energy content

The energy content of the elutriated fines is an important property which determines the possible utilization of this residue as a fuel. In this sense, it is important to evaluate the remaining energy in the residue. The LHV of the samples collected in the different parts of the experimental facility is shown in Figure 6.1b. It can be seen that the fines in the first cyclone have more energy per unit of mass than in the filter and in the second cyclone. The mean values for each experiment are between 6 and 8 MJ/kg$_{db}$ (Table 6.3), and are lower than the values obtained from full-scale gasifiers which are in the range of 14–25 MJ/kg$_{db}$ (GASASH Project, 2005). However, these values are, more or less, half of the LHV of the original biomass. Therefore, a considerable amount of energy per unit of mass, 2–3 % of the energy introduced with the biomass, remains in the fines. This amount of energy can be important in industrial scale plants, and can be recovered in other applications such as combustion.

There are negligible differences between the mean LHV at 700 and 760 °C in the case of olivine. However, the differences increase when the temperature is raised to 800 °C, with a considerable decrease of the LHV (2 MJ/kg$_{db}$ lower at 800 °C). There is also a significant difference in the LHV between the bed materials at this temperature. When magnesite is used, the LHV of the fines is higher than for olivine at the same temperature. At 700 and 760 °C, the carbon content is quite similar in both experiments as is the LHV. The differences at 800 °C are due the smaller concentration of carbon in the entrained fines. This is applicable to the both olivine and magnesite where carbon content is higher in magnesite. The percentage variation in the carbon contents and in the LHV between the different locations along the cleaning section are very similar between tests.

Figure 6.2 shows the energy balance for the whole gasification process. It can be seen that most of the energy from the biomass is released in the product gas (see Chapter 5 for further details on gas analysis). Around the 10–20 % is contained in the remaining char in the bed and a further 10–15 % is in the tars.

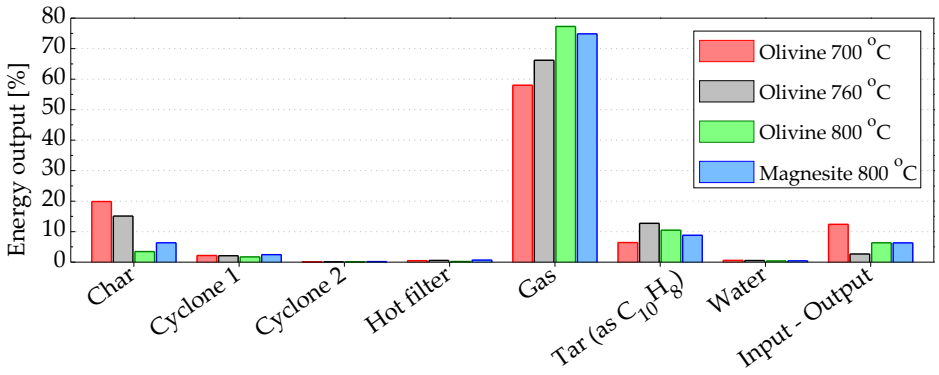


**Figure 6.2:** Energy balance for the gasification experiments.

### Distribution of elements/metals in the solid streams from gasification

The content of major ash forming oxides in the analyzed fines from the cleaning devices is presented in Table 6.4. The main ash forming inorganic elements found in the fines are Al, Ca, K, Mg, Na, Si, and, to a lesser extent, Fe. Si is the most abundant element which is in accordance with the amount of Si in the cardoon (with the highest concentration at 81.14 wt.%). Jordan & Akay (2012) reported similar content of main ash forming elements in bagasse gasification ash. Gasification temperature has an effect on the distribution of some elements such as Ca, K and Mg whose concentration increases with temperature at all sampling points. Na and Fe are not influenced by temperature and remain more or less constant. Similar results are observed for Al in cyclone 2 and the hot filter. Si shows a quite constant value with temperature in the samples collected at cyclone 1, and more fluctuating values for samples at cyclone 2 and at hot filter. In this last point, the differences are very marked.

Considering both bed materials, the Mg content is clearly higher for magnesite because of the possible entrainment of bed particles ($MgCO_3$) and/or enrichment of cyclone fines in magnesium due to abrasion. A similar explanation can be adopted for the slightly higher iron content in olivine experiments. Na concentration is similar for both bed materials. Al and K concentrations are a bit lower for magnesite than for olivine for all sampling locations. Less Ca is retained in the first and second cyclones for magnesite than for olivine with similar behaviour for silicon at 800 °C.

The concentration of minor elements at different gasification temperatures, sampling locations and bed materials are presented in Figure 6.3. Most of these metals show little variation in concentration with temperature, sampling location and bed material with exception of Cr, Mo and Ni which show significant differences.

**Table 6.4:** Main inorganic elements found in the collected fines at the different locations (as oxides in [wt.% $fines_{db}$]).

| | $Al_2O_3$ | CaO | $Fe_2O_3$ | $K_2O$ | MgO | $Na_2O$ | $SiO_2$ | LOI |
|---|---|---|---|---|---|---|---|---|
| *Olivine, 700 °C* | | | | | | | | |
| Cyclone 1 | 12.47 | 7.45 | 1.39 | 5.04 | 2.53 | 5.80 | 40.12 | 32.67 |
| Cyclone 2 | 16.80 | 4.38 | 1.53 | 4.56 | 4.17 | 6.11 | 36.97 | 23.68 |
| Hot filter | 14.82 | 4.19 | 1.81 | 6.18 | 5.36 | 7.31 | 48.04 | 27.09 |
| *Olivine, 760 °C* | | | | | | | | |
| Cyclone 1 | 19.57 | 7.60 | 1.50 | 4.61 | 3.99 | 6.29 | 40.98 | 33.52 |
| Cyclone 2 | 16.35 | 5.69 | 1.68 | 6.72 | 5.04 | 6.38 | 33.22 | 24.27 |
| Hot filter | 15.19 | 4.71 | 2.03 | 5.92 | 6.12 | 6.42 | 29.32 | 28.01 |
| *Olivine, 800 °C* | | | | | | | | |
| Cyclone 1 | 13.22 | 10.00 | 1.53 | 7.36 | 5.41 | 6.71 | 40.20 | 24.46 |
| Cyclone 2 | 17.08 | 7.58 | 1.56 | 7.10 | 10.08 | 7.16 | 39.81 | 19.72 |
| Hot filter | 16.47 | 6.08 | 1.92 | 7.80 | 9.97 | 6.80 | 36.95 | 20.03 |
| *Magnesite, 800 °C* | | | | | | | | |
| Cyclone 1 | 13.92 | 6.20 | 1.06 | 6.35 | 14.09 | 7.08 | 40.67 | 29.94 |
| Cyclone 2 | 14.82 | 6.36 | 1.26 | 6.74 | 11.51 | 6.76 | 44.03 | 26.17 |
| Hot filter | 14.49 | 7.04 | 1.04 | 6.59 | 11.94 | 7.03 | 37.15 | 28.44 |

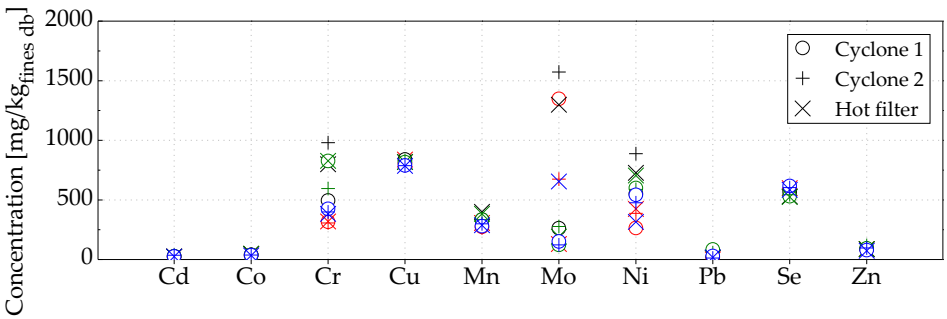


**Figure 6.3:** Minor elements concentration for different temperatures, bed materials, and sampling locations: (red) olivine 700 °C, (black) olivine 760 °C, (green) olivine 800 °C and (blue) magnesite 800 °C.

An attempt is made to perform mass balances for 17 elements in the solid streams collected, where biomass with kaolin is the input stream and the entrained fines and the bed char are the outputs (Figure 6.4 and Table 6.5). In Figure 6.4 the mass flow of elements in the entrained fines (cyclone 1, cyclone 2 and hot filter) is represented in dark colors while the mass flow for the char in the bed is represented in light colors. Metal

recovery in the cleaning system for most major elements (Figure 6.4a) is not influenced by process temperatures and type of bed materials with only Mg and K showing an increase in the recovered/collected fines with temperature. Alkali metals such as K show a slight increase with temperature due to its volatility. The differences in the Mg are very clear. When magnesite is used as the bed material, the Mg collected in the cleaning system is 282 wt.% of that in the input fuel. This enrichment by the Mg and Fe, and to a lesser extent, by Al and Ca in the ash is caused by abrasion of the olivine and magnesite particles during the operation of fluidized bed operation or entrainment of small bed material particles. The chlorine recovery is rather high, indicating this element is volatilised, captured by other elements that condense in the downstream devices. Chlorine under reducing/pyrolysis conditions is released mostly as ethyl chloride ($CH_3Cl$) at 350 °C with minor amounts of HCl (Saleh *et al.*, 2014). At temperatures above 700 °C, gaseous Cl is recaptured by either K salts (KCl, $(KCl)_2$) or K in the char matrix (Jensen *et al.*, 2000; Knudsen *et al.*, 2004; van Lith *et al.*, 2008). Gaseous KCl condenses and forms aerosols.

In the case of bed char (light colors in the bars), higher mass retention of the different elements are observed at lower gasification temperatures. This shows an effect of temperature on the release of inorganics from biomass, regardless of whether olivine or magnesite is used. The fate of the different metals cannot be determined very accurately because it has been impossible to separate and analyse the bottom ash and the metal emissions in the product gas are not measured. The closure of the mass balance, taking into account the fuel input, the char and the entrained fines is less than 100% for all major elements except for Mg and, Fe, K and Si at lower temperatures. However, these values are within the limits reported in the literature (Reed *et al.*, 2001; Amand & Leckner, 2004; Selçuk *et al.*, 2006).

In the case of the minor elements (Figure 6.4c) it is worth noting the high recovery values in fines of Cr, Mn, Mo and Ni in the fines which is probable due to the abrasion of bed materials particles, in particular Cr and Ni from olivine (Kuba *et al.*, 2016) and the decomposition of the reactor walls, lubricants and residuals from previous tests (Cui *et al.*, 2013; Reed *et al.*, 2001). The high recovery values for Pb are related to the inherently high volatility of this element combined with the reducing atmosphere that enhances its volatility (Dong *et al.*, 2015). At a temperature of 850 °C, Pb is completely vaporized as $PbCl_4$ and $PbCl_2$ (Aunela-Tapola *et al.*, 1998) and capture by Al and Si oxides when the temperature decreases (Duan *et al.*, 2016). The Cu is mainly retained/captured in the fines. The distribution of heavy metals is shifted towards the entrained fines, with their mass in the char being much lower than in the cleaning devices. The closure of the mass balance for the minor elements is below 100 % for most of the heavy metals with the exception of those metals that are influenced by the gasification system as mentioned above.

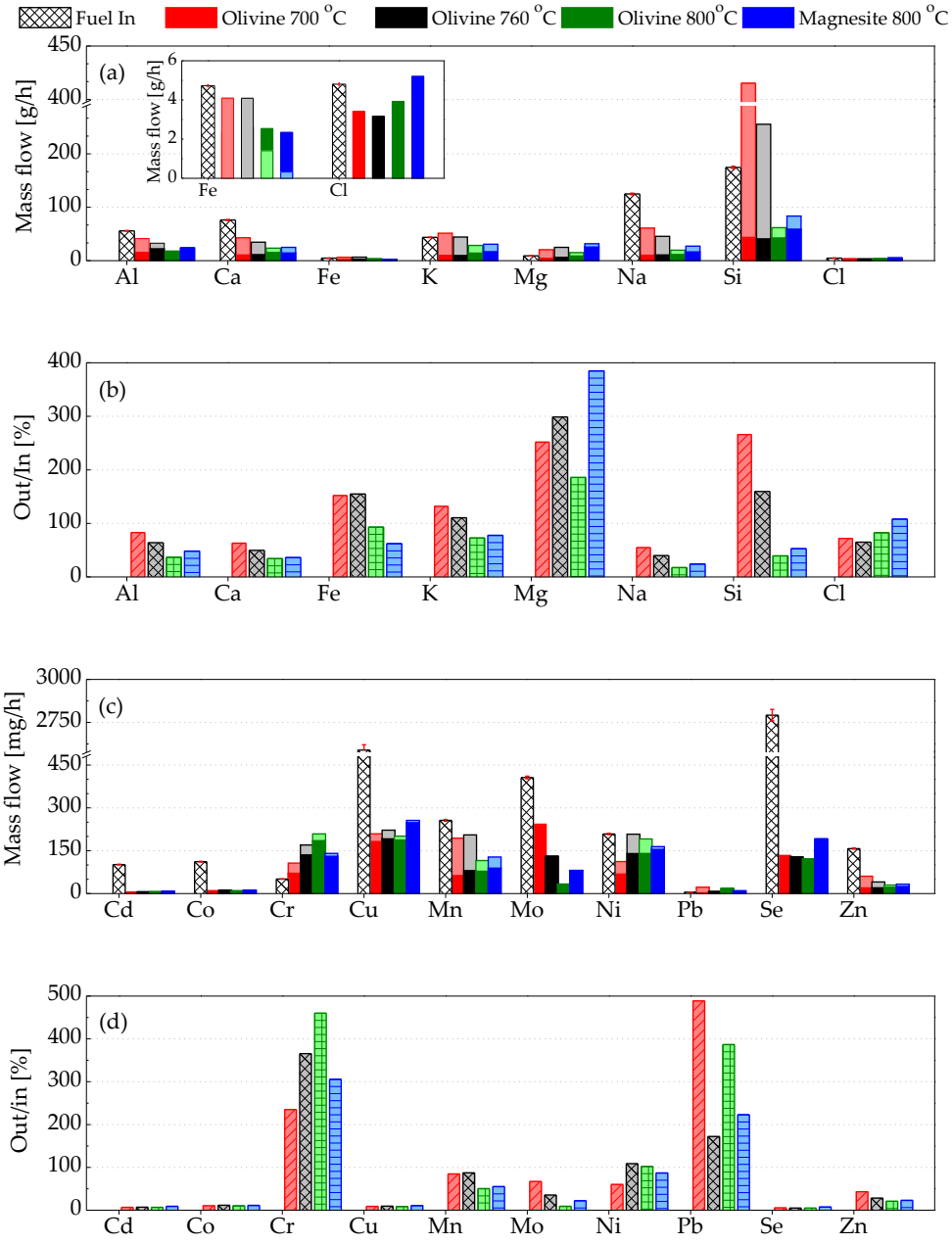


**Figure 6.4:** Mass balance for fines composition: a) major elements, b) out/in balance for major elements, c) minor elements and d) out/in balance for minor elements. The mass flow of elements in the entrained fines (cyclone 1, cyclone 2 and hot filter) is represented in dark color while the mass flow for the char in the bed is represented in light colors.

**Table 6.5:** Mass balance for metals in fines and char.

| | | Olivine 700 °C | | | Olivine 760 °C | | | Olivine 800 °C | | | Magnesite 800 °C | | |
|---|---|---|---|---|---|---|---|---|---|---|---|---|---|
| | Fuel in | Out fly ash | Out char | Out/In [%] | Out fly ash | Out char | Out/In [%] | Out fly ash | Out char | Out/In [%] | Out fly ash | Out char | Out/In [%] |
| Al† | 55.85 | 15.62 | 5.70 | 82.79 | 22.45 | 10.29 | 63.95 | 16.89 | 1.49 | 36.79 | 23.45 | 0.99 | 48.32 |
| Ca† | 76.16 | 10.59 | 32.25 | 62.93 | 11.29 | 23.28 | 49.52 | 15.27 | 8.12 | 34.32 | 14.35 | 10.60 | 36.18 |
| Cd‡ | 101.54 | 5.54 | 0.64 | 6.80 | 6.13 | 0.49 | 7.11 | 6.24 | 0.07 | 6.94 | 8.37 | 0.11 | 9.22 |
| Cl† | 4.80 | 3.41 | 0.00 | 71.81 | 3.16 | 0.00 | 4.83 | 3.93 | 0.00 | 82.57 | 5.20 | 0.00 | 107.98 |
| Co‡ | 111.69 | 8.41 | 1.91 | 10.34 | 9.57 | 2.36 | 11.65 | 9.01 | 1.24 | 0.26 | 11.34 | 0.22 | 11.43 |
| Cr‡ | 50.77 | 70.95 | 35.72 | 235.07 | 135.32 | 34.84 | 365.57 | 185.19 | 23.79 | 460.08 | 130.39 | 10.12 | 305.68 |
| Cu‡ | 2589.30 | 181.99 | 27.21 | 9.04 | 191.69 | 30.21 | 9.35 | 187.45 | 13.58 | 8.68 | 247.93 | 8.38 | 10.93 |
| Fe† | 4.72 | 2.32 | 4.09 | 152.06 | 2.62 | 4.09 | 154.89 | 2.54 | 1.40 | 93.16 | 2.34 | 0.32 | 62.21 |
| K† | 43.66 | 9.80 | 41.61 | 131.73 | 9.61 | 34.66 | 110.59 | 14.12 | 14.34 | 72.87 | 16.83 | 13.89 | 77.72 |
| Mg† | 9.14 | 4.31 | 16.25 | 251.74 | 6.26 | 18.76 | 298.65 | 8.76 | 6.44 | 185.87 | 25.56 | 6.29 | 385.00 |
| Mo‡ | 406.16 | 237.93 | 4.96 | 66.91 | 128.87 | 2.76 | 35.35 | 32.90 | 0.36 | 9.15 | 80.48 | 0.76 | 22.09 |
| Na† | 124.90 | 10.17 | 50.91 | 54.72 | 10.78 | 34.80 | 39.81 | 11.47 | 8.14 | 17.56 | 16.42 | 10.79 | 24.06 |
| Ni‡ | 208.67 | 68.65 | 44.12 | 60.14 | 140.00 | 67.73 | 108.59 | 140.15 | 50.98 | 102.38 | 154.33 | 9.96 | 86.97 |
| Pb‡ | 5.08 | 4.00 | 19.71 | 488.71 | 4.60 | 3.41 | 172.15 | 16.95 | 0.62 | 386.95 | 8.18 | 2.07 | 222.99 |
| Se‡ | 2792.39 | 133.02 | 0.00 | 5.33 | 128.13 | 0.00 | 5.00 | 121.72 | 0.00 | 4.87 | 191.67 | 0.00 | 7.58 |
| Si† | 174.65 | 43.56 | 371.60 | 265.96 | 40.88 | 214.52 | 159.51 | 42.58 | 19.14 | 39.50 | 58.95 | 24.56 | 52.81 |
| Zn‡ | 157.39 | 19.69 | 40.94 | 43.10 | 20.21 | 20.47 | 28.19 | 21.80 | 7.76 | 20.99 | 24.79 | 8.00 | 23.01 |

†in [g/h], ‡in [mg/h].

**Table 6.6:** EF for fines collected in cyclones and hot filter.

| | Olivine 700 °C | | | Olivine 760 °C | | | Olivine 800 °C | | | Magnesite 800 °C | | | |
|---|---|---|---|---|---|---|---|---|---|---|---|---|---|
| | C1 | C2 | HF | C1 | C2 | HF | C1 | C2 | HF | C1 | C2 | HF | Group[a] |
| Al⋆ | 0.54 | 0.73 | 0.65 | 0.85 | 0.71 | 0.66 | 0.58 | 0.75 | 0.72 | 0.61 | 0.65 | 0.63 | I |
| Ca⋆ | 0.32 | 0.19 | 0.18 | 0.33 | 0.25 | 0.20 | 0.43 | 0.33 | 0.26 | 0.27 | 0.27 | 0.30 | I |
| Cd | 0.11 | 0.12 | 0.11 | 0.12 | 0.13 | 0.11 | 0.12 | 0.17 | 0.11 | 0.12 | 0.16 | 0.11 | I |
| Co⋆ | 0.14 | 0.17 | 0.19 | 0.16 | 0.19 | 0.20 | 0.16 | 0.16 | 0.20 | 0.15 | 0.16 | 0.14 | I |
| Cr⋆ | 2.87 | 2.78 | 2.90 | 4.49 | 8.89 | 7.25 | 7.50 | 5.40 | 7.51 | 3.85 | 3.62 | 3.47 | II/III |
| Cu⋆ | 0.14 | 0.14 | 0.15 | 0.15 | 0.14 | 0.15 | 0.15 | 0.15 | 0.15 | 0.14 | 0.14 | 0.14 | I |
| Fe⋆ | 0.95 | 1.05 | 1.24 | 1.03 | 1.15 | 1.38 | 1.05 | 1.06 | 1.31 | 0.72 | 0.86 | 0.71 | I |
| K | 0.44 | 0.40 | 0.54 | 0.41 | 0.59 | 0.52 | 0.65 | 0.62 | 0.69 | 0.56 | 0.59 | 0.58 | I |
| Mg⋆ | 0.77 | 1.27 | 1.63 | 1.21 | 1.53 | 1.86 | 1.64 | 3.06 | 3.03 | 4.28 | 3.49 | 3.62 | II |
| Mn⋆ | 0.49 | 0.47 | 0.55 | 0.60 | 0.61 | 0.72 | 0.60 | 0.60 | 0.69 | 0.50 | 0.54 | 0.52 | I |
| Mo⋆ | 1.53 | 0.76 | 0.15 | 0.30 | 1.78 | 1.47 | 0.14 | 0.31 | 0.22 | 0.17 | 0.14 | 0.74 | I |
| Na⋆ | 0.16 | 0.17 | 0.20 | 0.17 | 0.17 | 0.18 | 0.18 | 0.20 | 0.19 | 0.19 | 0.18 | 0.19 | I |
| Ni⋆ | 0.58 | 0.85 | 0.94 | 1.22 | 1.96 | 1.60 | 1.32 | 1.30 | 1.56 | 1.20 | 1.05 | 0.70 | II |
| Pb⋆ | 1.30 | 0.37 | 0.09 | 1.93 | 2.50 | 1.27 | 7.68 | 5.21 | 1.37 | 2.66 | 1.11 | 1.64 | II |
| Se | 0.10 | 0.10 | 0.10 | 0.09 | 0.09 | 0.09 | 0.09 | 0.09 | 0.09 | 0.10 | 0.10 | 0.10 | I |
| Si⋆ | 0.49 | 0.46 | 0.59 | 0.50 | 0.41 | 0.36 | 0.50 | 0.49 | 0.46 | 0.50 | 0.54 | 0.46 | I |
| Zn⋆ | 0.26 | 0.27 | 0.25 | 0.26 | 0.26 | 0.25 | 0.27 | 0.35 | 0.26 | 0.23 | 0.28 | 0.22 | I |

C1: cyclone 1, C2: cyclone 2, HF: hot filter

⋆Not volatile at gasification conditions according with the element boiling point

[a]According to Meij's classification for fly ash (Meij, 1994)

The corresponding enrichment factors (EF) (Meij, 1994) (Eq. 2.12), for all elements are calculated and presented in Table 6.6.

In the case of fly ash from cardoon gasification following metals has been classified into group I (non-volatile elements) according to Meij's classification for fly ash (Meij, 1994): Al, Ca, Cd, Co, Cu, Fe, K, Mn, Mo, Na, Se, Si and Zn. The elements belonging to group II (semi-volatile elements with possible occurrence of the condensation phenomena): Cr, Mg, Ni and Pb The elements belonging to group III (very volatile elements, with a limited capacity of condensing on the surface of submicron particles of ash): Cr.

The enrichment factor as originally proposed by Meij (1994) refers mainly to the elements volatility. If the EF is higher than 1 for non-volatile metals this means that there is a different source for them in the process other than the feedstock ash, e.g. bed material such as olivine for Fe, Cr, Ni or magnesite for Mg (abrasion or entrainment) or alternatively corrosion parts of the gasification equipment for Cr, Ni or Pb enrichment or relatively high content of Cl in cardoon could significantly reduce volatilization temperature of Ni and Pb. If the EF is lower than 1 for very volatile metals such as K and Na this suggests that they did not condensed on fly ash particles but rather on the heat exchanger walls.

Metals recovery in the cyclones and hot filter is mostly below 50 wt.% of the metals input from biomass, typically between 20 and 40 wt.%. The overall mass balance is not complete due to the lack of information from the ash inside the gasifier and the elements which are volatilized and deposited on downstream colder surfaces.

**Lecheability**

Leachability of heavy metals is performed according to the DIN 38414-S4 standard. The concentrations of the heavy metals in the eluates are shown in Table 6.7. This table also shows the limits of the leaching values according to the European Directive (1999). The results show that the majority of metals could be landfilled. No As, Mo or Sb have been found in the analysed samples. However, the leachability of Se in most of the samples exceeds or is very close to the limit for hazardous waste. Significantly, the results of chloride leachability show concentrations exceeding the limits established by the European landfill directive which makes the elutriated fines unsuitable for land filling. As a consequence, a pretreatment should be undertaken prior to land-filling.

### 6.3.2 Comparison with other biomass and waste ashes

The properties of different fly ashes from various biomasses and waste materials and gasifier types are reported in the GASASH Project (2005). The LOI can vary from 15 wt.% to a high value of 65 wt.%. In the present study, the LOI of the cardoon ashes ranges from 19 to 33 wt.% db (Table 6.4), which are very similar to those obtained in full-scale gasifiers. The chlorine content is also in the range of the values obtained in

**Table 6.7:** Leachability results according to DIN 38414-S4 in [mg/kg$_{db}$].

| | Ba | Cd | Cl | Cr | Cu | F | Hg | Ni | $SO_4$ | Se | Zn |
|---|---|---|---|---|---|---|---|---|---|---|---|
| Olivine 700 °C | | | | | | | | | | | |
| Cyclone 1 | 0.00 | 0.41 | 25999 | 0.74 | 4.77 | 13.27 | 0.00 | 0.45 | 1706 | 0.74 | 0.02 |
| Cyclone 2 | 0.00 | 0.43 | 27392 | 0.78 | 6.48 | 9.40 | 0.00 | 0.30 | 1681 | 35.09 | 0.02 |
| Hot filter | 0.00 | 0.37 | 28934 | 0.76 | 7.17 | 7.41 | 0.00 | 0.31 | 1538 | 2.27 | 0.02 |
| Olivine 760 °C | | | | | | | | | | | |
| Cyclone 1 | 0.00 | 0.47 | 28691 | 2.29 | 5.68 | 19.09 | 0.00 | 0.54 | 839 | 15.27 | 0.02 |
| Cyclone 2 | 0.00 | 0.45 | 31229 | 3.04 | 6.45 | 9.99 | 0.00 | 0.43 | 1748 | 31.92 | 0.02 |
| Hot filter | 0.00 | 0.43 | 30544 | 0.76 | 8.03 | 21.20 | 0.00 | 0.56 | 1770 | 2.28 | 0.02 |
| Olivine 800 °C | | | | | | | | | | | |
| Cyclone 1 | 7.19 | 0.55 | 31467 | 10.79 | 7.80 | 14.68 | 0.00 | 0.64 | 1184 | 6.47 | 0.02 |
| Cyclone 2 | 0.00 | 0.52 | 34945 | 11.87 | 6.55 | 29.51 | 0.00 | 0.63 | 1586 | 23.74 | 0.02 |
| Hot filter | 2.33 | 0.60 | 35614 | 2.33 | 8.25 | 31.87 | 0.00 | 0.71 | 1990 | 20.21 | 0.03 |
| Magnesite 800 °C | | | | | | | | | | | |
| Cyclone 1 | 1.52 | 0.37 | 30803 | 29.72 | 6.80 | 18.99 | 0.00 | 0.34 | 1630 | 0.76 | 0.02 |
| Cyclone 2 | 0.00 | 0.39 | 26665 | 7.60 | 3.81 | 7.20 | 0.00 | 0.27 | 1185 | 19.00 | 0.01 |
| Hot filter | 0.00 | 0.43 | 32825 | 1.55 | 8.50 | 41.37 | 0.85 | 0.53 | 23059 | 0.00 | 0.02 |
| | | | | | | | | | | | |
| *EU landfill directive* | | | | | | | | | | | |
| *Inert* | 20 | 0.04 | 800 | 0.50 | 2 | 10 | 0.01 | 0.40 | 1000 | 0.10 | 4.00 |
| *Non-hazardous* | 100 | 1.00 | 15000 | 10.00 | 50 | 150 | 0.20 | 10.00 | 20000 | 0.50 | 50 |
| *Hazardous* | 300 | 5.00 | 25000 | 70.00 | 100 | 500 | 2.00 | 40.00 | 50000 | 7.00 | 200 |

other studies.

The concentrations of some major elements such as Al, Na, K and Si are higher in *C. cardunculus* fines than in other experiments. Mg is similar among biomasses while Ca and Fe concentrations are rather smaller. The main reason for these variations is the difference in the ash composition of the original biomasses. Besides, the effect of the bed material employed during the gasification also influences the composition of the entrained fines as some elements are detached from bed material surface due to abrasion or catalytic action with a subsequent enrichment in the fines.

### 6.3.3 Possible routes for cardoon ash valorization

As stated above, the fly ashes from combustion processes (intensively studied) differ from gasification fly ashes. Hence, the motivation to investigate their properties in order to provide information about its capacity to comply with waste regulations and other standards for utilization. In this section, a review of the most typical applications is considered, in order to establish if cardoon fly ashes characteristics are within the accepted limits for their utilization. All current regulations typically focus on combustion

bottom/fly ashes from biomasses or sewage sludge. In this case, although the fly ashes under investigation come from gasification and fall outside the direct scope of current standards, the available directives and regulations are nevertheless chosen in order to evaluate the cardoon fly ashes characteristics for the different applications.

**Use as combustible feedstock**

The first option for cardoon fly ashes utilization is to use it as combustible feedstock. The collected fines have almost half of the LHV of the original biomass (6–7 MJ/kg$_{db}$ vs 16 MJ/kg$_{db}$) which is a 2–3 % of the energy introduced by the biomass so a significant amount of energy can be recovered from cyclones and hot filter. The advantages of this application are the reduction in the fly ash volume, the destruction of PAHs and a reduction in the amount of heavy metals in the ash (GASASH Project, 2005). However, there are some potential drawbacks arising from the high Cl and K content in the fines. These elements can lead to corrosion in downstream devices and therefore the use of fly ashes is limited by the amount of Cl and K added to the boilers (Gómez-Barea *et al.*, 2009). A pre-wash could reduce the amount of these elements as they are mostly water-soluble, allowing their use as fuel.

**Use as an additive in gasification**

The alkali elements in the fines can serve as catalysts for other biomass under gasification conditions. Sodium and potassium are known to have a positive effect on gasification rate and hydrogen production at specific operating conditions (Demirbaş, 2002). Evidence for this can be found from the hydrogen content in the product gas obtained from these experiments (see Table 5.2) which is moderately high comparing with other biomasses gasified with air. Apart from adding extra quantities of Cl, the increased risk of bed agglomeration should be considered. Other additives such as kaolin or bed materials should be uses in order to reduce the agglomeration tendency added by the use of cyclone/hot filter ash. The use of lower gasification temperatures is also an option to reduce agglomeration related problems although high carbon conversions will not be achieved. A compromise solution or the use of additives to prevent agglomeration should be adopted in any case.

**Use for cement and concrete**

The use of fly ashes in cement and concrete industry is regulated by European and American standards (UNE-EN 450-1, 2013; Moreno i Palmerola, 2002). These regulations set the minimum and maximum limits for different elements in the fly ashes. One of the most important parameters for cement and concrete applications is the loss on ignition

which mainly gives the unburned carbon in the fly ash. Depending on the value of this parameter, fly ashes are divided into three categories (UNE-EN 450-1, 2013): (cat. A) LOI less than 5 wt.%, (cat. B) LOI less than 7 wt.%, and (cat. C) LOI less than 9 wt.%. The LOI of cardoon fly ash is too high to fulfil these requirements. However, Bhatty *et al.* (2003) demonstrated that the addition of 3 wt.% of a high-carbon coal fly ash (LOI $\approx$ 13 wt.%) is feasible in cement manufacturing. Moreover, the high value of LOI in cardoon fines could be reduced by burning the fines as has been mentioned in the previous subsection, obtaining extra energy and ashes with similar characteristics to combustion.

Figure 6.5 shows the content of different species in the entrained fines that condition their use for cement and concrete applications. The limits for the total alkali content as well as for the chlorine content are also significantly below the values obtained for cardoon fly ashes, although a pre-wash, as mentioned above, may help to satisfy the requirements. The sum of $SiO_2$ + $Al_2O_3$ + $Fe_2O_3$ is higher than 50 wt.% (class C according to ASTM C618) but less than the 70 wt.% required for class F and for the European regulation. The amount of $SO_3$ is also within the limits, however the amount of CaO is lower than the 10 wt.% required for class C. In this case, cardoon fly ashes comply with low calcium ashes, suitable for class F and EN450-1 standard.

**Use in agricultural and forest soils**

Agriculture and forestry is a common application for coal combustion fly ashes where they are employed directly as fertilizers or as a raw material in the production of these types of products. The use of fly ashes for this purpose is regulated by different European and national directives and standards (Fachbeirat für Bodenfruchtbarkeit und Bodenschutz, 2011; Haglund, 2008). Among the different elements present in the fly ashes, some of them belong to the main nutrients required for agriculture (K, P, Ca and Mg), but the heavy metals present are soil contaminants (Table 6.8). According to this, there are two main requirements which must be fulfilled: a minimum quantity of the main nutrients, and a maximum amount of contaminants (Pels *et al.*, 2005). In some countries (Sweden or Finland) regulations specify both minimum and maximum limits for contaminants and nutrients, respectively, but in others (Austria or Denmark) only maximum levels for heavy metals are specified (Table 6.9). For most of the regulations consulted for this thesis the Cd, Cr, Cu and Ni contents in cardoon fines always exceeded the limits for contaminants while Pb and Zn do not seem to be problematic. The concentration of Ca does not however fulfil the minimum value for nutrients. As a consequence, cardoon fly ashes cannot be used as fertilizer in Austria, Denmark, Sweeden or Finland.

In Spain, the Spanish Government (2013) for fertilizers establishes three different

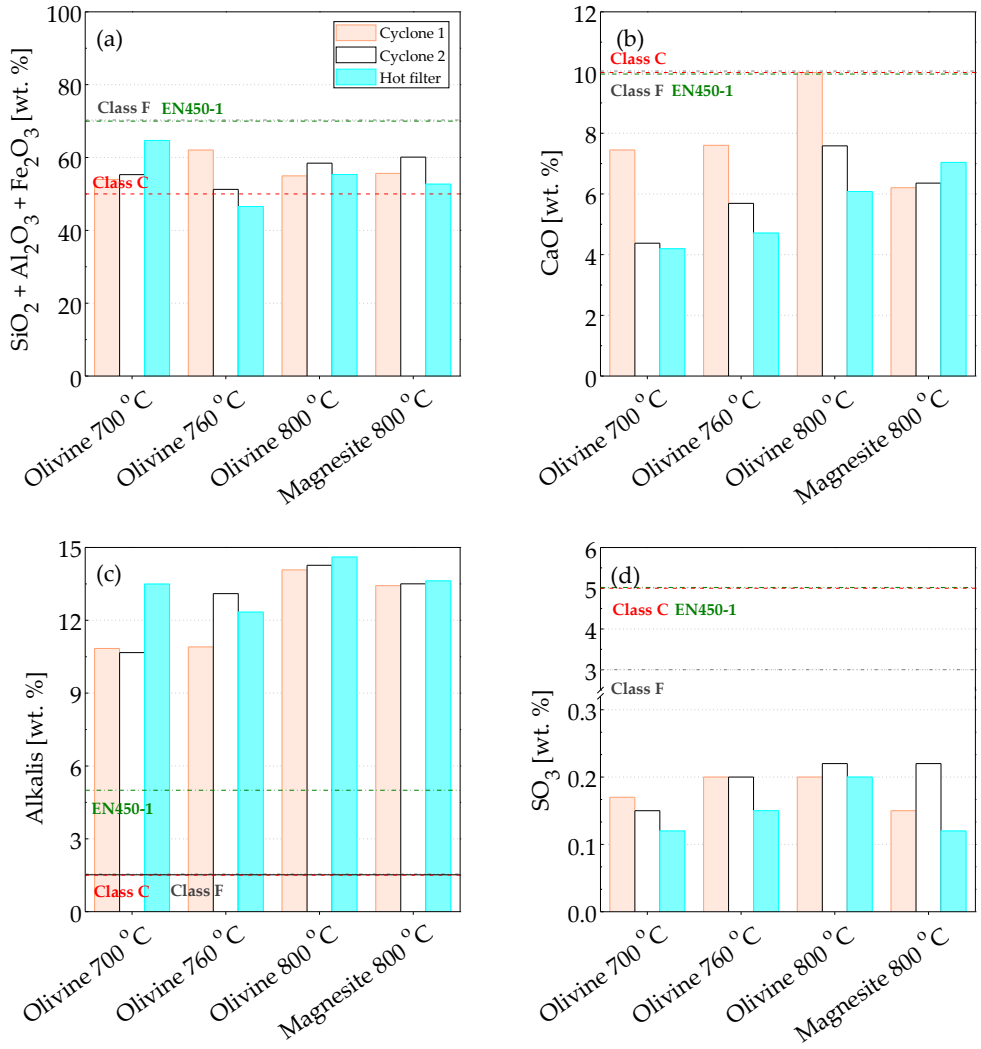


**Figure 6.5:** Content of (a) $SiO_2$+$Al_2O_3$+$Fe_2O_3$, (b) CaO, (c)alkalis and (d) $SO_3$ of cardoon fly ashes and corresponding limits for their use in cement and concrete industry according to the European and American standards (EN450-1 and, class C and F according to ASTM C618) (UNE-EN 450-1, 2013; Moreno i Palmerola, 2002)

limits for heavy metals in fertilizers obtained from organic waste. Cardoon fly ashes could be utilized in the preparation of fertilizer although the quantity of fly ash to be used is limited by the final Cd content, which range between 19 and 29 $g_{fines}/kg_{fertilizer\ db}$ for class A, 54 and 83 $g_{fines}/kg_{fertilizer\ db}$ for class B, and 81 and 125 $g_{fines}/kg_{fertilizer\ db}$ for class C, depending on the fly ash origin (cyclones 1, cyclone 2 or hot filter). The

**Table 6.8:** Nutrients and heavy metals concentration in the elutriated fines, in [%] and [mg/kg$_{fines\ db}$] respectively.

| | Olivine 700 °C | | | Olivine 760 °C | | | Olivine 800 °C | | | Magnesite 800 °C | | |
|---|---|---|---|---|---|---|---|---|---|---|---|---|
| | C1 | C2 | HF | C1 | C2 | HF | C1 | C2 | HF | C1 | C2 | HF |
| Ca | 5.32 | 3.13 | 3.00 | 5.43 | 4.06 | 3.37 | 7.15 | 5.42 | 4.43 | 4.43 | 4.54 | 5.03 |
| K | 4.20 | 3.80 | 5.15 | 3.84 | 5.60 | 4.93 | 6.14 | 5.92 | 6.50 | 5.29 | 5.61 | 5.49 |
| Mg | 1.52 | 2.51 | 3.23 | 2.41 | 3.03 | 3.69 | 3.26 | 6.07 | 6.01 | 8.49 | 6.93 | 7.19 |
| Zn | 0.01 | 0.01 | 0.01 | 0.01 | 0.01 | 0.01 | 0.01 | 0.01 | 0.01 | 0.01 | 0.01 | 0.01 |
| | C1 | C2 | HF | C1 | C2 | HF | C1 | C2 | HF | C1 | C2 | HF |
| Cd | 24.51 | 26.56 | 24.97 | 27.30 | 28.60 | 23.97 | 26.54 | 36.94 | 25.25 | 26.31 | 35.79 | 25.19 |
| Cr | 316.55 | 306.47 | 319.62 | 495.44 | 980.44 | 798.96 | 826.98 | 595.12 | 828.04 | 424.98 | 398.82 | 382.91 |
| Cu | 806.70 | 786.61 | 839.00 | 839.21 | 806.72 | 818.94 | 816.68 | 831.11 | 817.94 | 789.26 | 787.41 | 785.97 |
| Ni | 264.37 | 387.39 | 424.29 | 551.86 | 887.91 | 727.15 | 599.65 | 588.14 | 705.04 | 542.16 | 476.02 | 315.80 |
| Pb | 14.30 | 4.09 | 1.00 | 21.23 | 27.57 | 13.98 | 84.73 | 57.46 | 15.15 | 29.34 | 12.27 | 18.14 |
| Zn | 87.82 | 92.96 | 86.90 | 87.97 | 89.87 | 86.89 | 93.92 | 118.00 | 87.85 | 78.93 | 97.15 | 73.56 |

C1: cyclone 1, C2: cyclone 2, HF: hot filter

**Table 6.9:** Limit values for different European regulations for the use of fly ashes and sewage sludge as soil amendments and fertilizers.

| | RD 506/2013[a] | RD 1310/1990[b] | Austria[c] | Denmark | Finland[d] [%] | Sweeden [%] |
|---|---|---|---|---|---|---|
| Ca | | | | | 80/60 | 12.5 |
| K | | | | | 20/10 (K+P) | 3.0 |
| Mg | | | | | | 1.5 |
| Zn | | | | | | 0.5 |
| | | | [mg/kg$_{fines\ db}$] | | | |
| Cd | 0.7/2/3 | 20/40 | 5/8 | 15 | 1.5/17.5 | 30 |
| Cr | 70/250/300 | 1000/1500 | 150/250 | 100 | 300/300 | 100 |
| Cu | 70/300/400 | 1000/1750 | 200/250 | | 600/700 | 400 |
| Ni | 25/90/100 | 300/400 | 150/200 | 30 | 100/150 | 70 |
| Pb | 45/150/200 | 750/1200 | 100/200 | 120 | 100/150 | 300 |
| Zn | 200/500/1000 | 2500/4000 | 1200/1500 | | 1500/4500 | 7000 |

[a]class A/class B/class C, [b]soils with pH<7/soils with pH>7, [c]cat. A/cat. B/cat. C, [d]agriculture/forestry

Spanish Government (1990) for sewage sludge utilization in agriculture sets two limits for heavy metals related to the soil pH. The content of Cr, Cu, Pb and Zn in the cardoon fly ashes allows them to be used for both acid and alkaline soils. Nevertheless, the high concentration of Cd only allows the use of cardoon fly ashes in alkaline soils while the Ni content is over the limits in both cases. Therefore, according to Spanish regulations, the cardoon fly ashes cannot be employed directly on agricultural soils.

## 6.4 Conclusions

The elutriated fines collected from *C. cardunculus* L. air gasification at different temperatures are investigated in terms of their main elements: carbon, sulphur and chlorine content as well as the distribution of metals in the ash.

The carbon content and the LOI are within the range of the values obtained for other biomasses, although they are fairly high when considering the potential use of the entrained fines in further applications such as the cement industry. The highest carbon concentration is always found in the first cyclone. Sulphur and chlorine are also high and could cause problems when these fines are reused. Water washing may be an option to remove these undesired elements.

The fines have a relatively high heating value which suggests that they can be still employed as alternative/secondary fuel. The energy contained in the elutriated fines account for the 2–3 % of the original feedstock energy input, which for industrial plants represents a significant energy contribution that could be recovered for secondary processes.

Si is the most abundant inorganic element in the fines, followed by Al, Ca, Na, Mg, K and Fe. The concentrations of some of these elements are influenced by temperature and sampling location. Small differences in the main elements are observed between olivine and magnesite, with the exception of Mg and Fe. Minor elements (Cu, Cr, Ni, Se, Mn...) are relatively constant for all experiments. The vast majority of the elutriated fines as well as the metals are collected, by far, in the first cyclone, followed by the hot filter.

Cardoon air gasification fly ashes have high carbon, alkali, chlorine and some heavy metals content which make their use as raw material in cement and concrete industry, or as fertilizers for agriculture difficult. However, small quantities of cardoon fly ashes could be employed for fertilizer production and the combustion of these fines could serve an important source of energy.

Some of the elements are present in cardoon fly ash because they are in the original feedstock (Cu, Se or Ni) and become concentrated in the ash. Other elements appear as a consequence of the bed material used like olivine, Cr (to a lesser extend Mn) but also as a result of reactor wall decomposition. Some of the Al in the fly ash arises from kaolin addition while the Pb is a result of the auger or attrition from different parts of the experimental facility destruction. Therefore, the selection of appropriate bed material which will exhibit catalytic properties, mitigate agglomeration resistant and will not contribute to an increase of heavy metals in fly ash is very important. In addition, the refractory materials which are used for building industrial scale gasification systems seems to be also important as they can cause ash contamination.

# References

Ahmaruzzaman, M. 2010 A review on the utilization of fly ash. *Progress in Energy and Combustion Science* 36, 327–363.

Amand, L.-E. & Leckner, B. 2004 Metal emissions from co-combustion of sewage sludge and coal/wood in fluidized bed. *Fuel* 83, 1803–1821.

Aunela-Tapola, L. A, Frandsen, F. J. & Häsänen, E. K. 1998 Trace metal emissions from the Estonian oil shale fired power plant. *Fuel Processing Technology* 57, 1–24.

Bhatty, J. I., Gajda, J. & Miller, F. M. 2003 Comercial demonstration of high-carbon fly ash technology in cement manufacturing. In *International Ash Utilization Symposia*. Lexington.

Cui, H., Turn, S. Q., Keffer, V., Evans, D., Tran, T. & Foley, M. 2013 Study on the fate of metal elements from biomass in a bench-scale fluidized bed gasifier. *Fuel* 108, 1–12.

Demirbaş, A. 2002 Gaseous products from biomass by pyrolysis and gasification: effects of catalyst on hydrogen yield. *Energy Conversion & Management* 43, 897–909.

Dong, J., Chi, Y., Tang, Y., Ni, M., Nzihou, A., Weiss-Hortala, E. & Huang, Q. 2015 Partitioning of heavy metals in municipal solid waste pyrolysis, gasification and incineration. *Energy & Fuels* 29, 7516–7525.

Duan, L., Sun, H., Ying, J., Edward, J., Anthony, J. & Zhao, C. 2016 Partitioning of trace elements, As, Ba, Cd, Cr, Cu, Mn and Pb, in a 2.5 $MW_{th}$ pilot-scale circulating fluidised bed combustor burning an anthracite and a bituminous coal. *Fuel Processing Technology* 146, 1–8.

European Directive 1999 European Directive 1999/31/CE, from $26^{th}$ of April on the landfill of waste.

Fachbeirat für Bodenfruchtbarkeit und Bodenschutz 2011 Richtlinie für den sachgerechten einsatz vo pflanzenaschen zur verwertung auf land- un forstwirtschaftlich genutzten flächen.

Fernández-Pereira, C., de la Casa, J. A., Gómez-Barea, A., Arroyo, F., Leiva, C. & Luna, Y. 2011 Application of biomass gasification fly ash for brick manufacturing. *Fuel* 90, 220–232.

Freire, M., Lopes, H. & Tarelho, L. A. C. 2015 Critical aspects of biomass ashes utilization in soils: Composition, leachability, PAH, and PCDD/F. *Waste Management* 46, 304–315.

GASASH Project 2005 GASASH - The improvement of the economics of biomass/waste gasification by higher carbon conversion and advanced ash management. ENK5-2001-00635. *Tech. Rep.*

Gómez-Barea, A., Vilches, L. F., Leiva, C., Campoy, M. & Fernández-Pereira, C. 2009 Plant optimisation and ash recycling in fluidised bed waste gasification. *Chemical Engineering Journal* 146, 227–236.

Haglund, N. 2008 Guideline for classification of ash from solid biofuels and peat utilised for recycling and fertilizing in forestry and agriculture. TR 613. *Tech. Rep.* Nordic Innovation Centre.

Holt, E. & Raivio, P. 2006 Use of gasification residues in compacted concrete paving blocks. *Cement and Concrete Research* 36, 441–448.

Jensen, P. A., Frandsen, F. J., Dam-Johansen, K. & Sander, B. 2000 Experimental investigation of the transformation and release to gas phase of potassium and chlorine during straw pyrolysis. *Energy & Fuels* 14, 1280–1285.

Jordan, C. A. & Akay, G. 2012 Speciation and distribution of alkali, alkali earth metals and major ash forming elements during gasification of fuel cane bagasse. *Fuel* 91, 253–263.

Kalembkiewicz, J. & Chmielarz, U. 2012 Ashes from co-combustion of coal and biomass: New industrial wastes. *Resources, Conservation & Conservation* 69, 109–121.

Knudsen, J., Jensen, P. A. & Dam-Johansen, K. 2004 Transformation and release to the gas phase of Cl, K, and S during combustion of annual biomass. *Energy & Fuels* 18, 1385–1399.

Kuba, M., He, H., Kirnbauer, F., Skoglund, N., Boström, D., Öhman, M. & Hofbauer, H. 2016 Thermal stability of bed particle layers on naturally occurring minerals from dual fluid bed gasification of woody biomass. *Energy & Fuels* 30, 8277–8285.

Leiva, C., Gómez-Barea, A., Vilches, L. F., Ollero, P., Vale, J. & Fernánde-Pereira, C. 2007 Use of biomass gasification fly ash in lightweight plasterboard. *Energy & Fuels* 21, 361–367.

Liao, C., Wu, C. & Yan, Y. 2007 The characteristics of inorganic elements in ashes from a 1 MW CFB biomass gasification power generation plant. *Fuel Processing Technology* 88, 149–156.

van Lith, S. C., Jensen, P. A., Frandsen, F. J. & Glarborg, P. 2008 Release to the gas phase of inorganic elements during wood combustion. Part 2: Influence of fuel composition. *Energy & Fuels* 22, 1598–1609.

Meij, R. 1994 Trace element behavior in coal-fired power plants. *Fuel Processing Technology* 39, 199–217.

Moreno i Palmerola, N. 2002 Valorización de cenizas volantes para la síntesis de zeolitas mediante extracción de sílice y conversión direceta. Aplicaciones ambientales. PhD thesis, Universidad Politécnica de Cataluña. Consejo Superior de Investigaciones Científicas.

Pels, J. R., de Nie, D. S. & Kiel, J. H. A. 2005 Utilization of ashes from biomass combustion and gasification. In *$14^{th}$ European Biomass Conference and Exhibition*. París, France.

Rajamma, R., Ball, R. J., Tarelho, L. A. C., Allen, G. C., Labrincha, J. A. & Ferreira, V. M. 2009 Characterisation and use of biomass fly ash in cement-based materials. *Journal of Hazardous Materials* 172, 1049–1060.

Reed, G. P., Dugwell, D. R. & Kandiyoti, R. 2001 Control of trace elements in gasification: Distribution to the output streams of a pilot scale gasifier. *Energy & Fuels* 15, 794–800.

Saleh, S. B., Flensborg, J. P., Shoulaifar, T. K., Sárossy, Z., Hansen, B. B., Egsgaard, H., DeMartini, N., Jensen, P. A., Glarborg, P. & Dam-Johansen, K. 2014 Release of chlorine and sulfur during biomass torrefaction and pyrolysis. *Energy & Fuels* 28, 3738–3746.

Selçuk, N., Gogebakan, Y. & Gogebakan, Z. 2006 Partitioning behavior of trace elements during pilot-scale fluidized bed combustion of high ash content lignite. *Journal of Hazardous Materials* 137, 1698–1703.

Spanish Government 1990 Government Decree 1310/1990, from $29^{th}$ of October on the use of sewage sludge in agriculture (Spanish).

Spanish Government 2013 Government Decree 506/2013, from $18^{th}$ of June on fertilizer products (Spanish).

UNE-EN 450-1 2013 Cenizas volantes para hormigón. Parte 1: Definiciones, especificaciones y criterios de conformidad. *Tech. Rep.*

CHAPTER
**SEVEN**

# Conclusions

In this PhD thesis, a complete sets of gasification experiments, covering the three main operational problems in biomass fluidized bed gasification (agglomeration, tars and ash generation), have been performed. *Cynara cardunculus* L. and sepiolite have been investigated as biomass feedstock and bed material, receptively, for fluidized bed gasification.

Monitoring techniques based on the pressure fluctuation signals inside the bed have shown their capability to determine the bed defluidization and the agglomeration mechanisms. Different analytical techniques have been used to characterized the biomass and the entrained fines (CHN-S, TGA, AAS, etc.), and to analyse the product gas (GC) and tar composition (SPA, GC-MS and GC-FID).

Two types of combustible behaviours have been observed depending on the bed material density. On the one hand, biomass particles show a jetsam behaviour in a sepiolite bed which has a lower density than silica sand. Endogenous bubbles formed within the dense bed are detected by the energy distribution of the power spectrum at the lower frequencies. The bed agglomeration and defluidization is recognized by wide band energy method as a significant reduction in the energy of $E_{wb2}$, indicating a deterioration of the bulk dynamics and leading to a big cylindrical agglomerate inside the bed. On the other hand, a flotsam behaviour is observed in a silica sand bed with a faster defluidization process and a flat plate shape agglomerate on the top of the bed surface. The low axial mixing of the biomass particles brings to a higher concentration of alkali compounds at the top of the bed. The $E_{wb3}$ shows a progressively reduction of the bubble eruption rate as the agglomerate is formed while the $E_{wb2}$ and $E_{wb1}$ shows that the bed is still fluidized under the cap-clinker. The fuel particle behaviour also affects the definition of a reference state to compute the monitoring techniques to determine the defluidization of the bed.

The use of sepiolite increases considerably the defluidization time in advance of silica sand with a better distribution of biomass and ash within the bed. A fluidization velocity of $u/u_{mf} = 6$ leads to the highest defluidization time for this bed material, although the differences are very small with other gas velocities. The highest defluidization time for sepiolite is obtained at $u/u_{mf} = 4$, existing some flexibility to choose the $u/u_{mf}$ ratio if

this value is high enough.

The ash-to-bed mass ratio shows higher ash accumulation within the bed for sepiolite than for silica sand, increasing with $u/u_{mf}$. At $u/u_{mf}$ ratios higher than 6, the fraction of biomass transformed in the sepiolite bed remains constant, being the mixing time lower than the reaction time, contrary to the silica sand case where the fraction of biomass transformed increases with $u/u_{mf}$, leading into a mixing time higher than the reaction time.

In terms of gas composition, the use of sepiolite do not improve the gas composition which has a higher $CO_2$ concentration and a lower CO concentration than the product gas obtained with silica sand at the same operating conditions, while the $H_2$ content does not show a clear trend between the two bed materials. These results also lead to a lower CGE and LHV while the carbon conversion is also lower for sepiolite.

Sepiolite significantly reduces total tar generation, up to 50% in comparison with silica sand and with a drastically decreased in the tertiary PAH tars. The composition of these tars is also quite different between sepiolite and silica sand, appearing single ring alkyated and oxygenated compounds such as xylenes and phenols in the case of sepiolite, and disappearing tars with a molecular weight higher than anthracene.

The physical properties of sepiolite (porous structure and high surface area) make it to adsorb the tar compounds on its surface, mainly tertiary-PAHs, as well as the molten ashes, reducing the amount of tars released into the product gas and increasing considerably the defluidization time with respect to silica sand. Besides, it shows a good attrition behaviour with a smaller attrition rate than other common bed materials such as alumina or dolomite.

*C. cardunculus* L. shows a relatively high hydrogen content when gasified in a magnesite and in an olivine fluidized bed, presenting these materials some catalytic activity. Temperature has a positive effect on the carbon and biomass conversion, LHV, CGE and GY of the product gas, achieving values higher than 80 % at 800 $^oC$. The use of magnesite provides better gasification performance at 700 $^oC$ while olivine performs better at 800 $^oC$.

Negligible differences have been found in terms of total tar yield between magnesite and olivine, although a different composition of the tar fraction is observed. The BTEX fraction is higher for olivine while the PAH fraction remains quite similar for both olivine and magnesite. A higher catalytic activity of magnesite is obtained at 800 $^oC$. Magnesium from magnesite and, in a lesser extent, olivine, exhibit a catalytic active behaviour towards tar cracking. Tar generation remains high in the product gas.

The carbon content and the LOI of the elutriated fines collected in the gas cleaning devices are fairly high for their use in applications such as cement industry. However, it allows their use as alternative/secondary fuel due to the high energy content that

still remains in the fines. The high sulphur and chlorine contents can cause operational problems when these fines are reused, although water wash can help to reduce/avoid these problems.

Most of the elutriated fines and metals are collected, by far, in the first cyclone, followed by the hot filter. The main inorganic elements in the elutriated fines are Si, Al, Ca, Na, Mg, K and Fe. In the case of minor elements (Cu, Cr, Ni, Se, Mn, etc.), they remains rather constant for all tested conditions.

The use of cardoon air gasification fly ashes is not allowed for their use in cement and concrete industry or for agriculture fertilizers due to their high carbon, alkali, chlorine and heavy metals contents. However, small portions of entrained fines can be employed for fertilizer production.

The inorganic composition of the biomass influence the cardoon fly ashes although some elements are also consequence of the bed material, the reactor wall decomposition and facility destruction. As a consequence, the selection of an appropriate bed material which will exhibit catalytic activity, agglomeration resistant and will not contribute to an increase of heavy metals in fly ash is very important. In addition, the materials which are used for building industrial scale gasification systems seems to be also important as they can cause ash contamination due to the degradation of these materials.

To conclude, sepiolite has shown its benefits for biomass gasification in a fluidized bed. Its use provides a better mixing of biomass particles within the bed in comparison with common bed materials such as silica sand. The physical properties of sepiolite give a high mechanical resistance and produce the adsorption of the tars and molten ashes, leading into a cleaner product gas and a higher defluidization times. The use of *Cynara cardunculus* L. as biomass feedstock for gasification in a fluidized bed has been demonstrated with a high hydrogen content in the product gas when magnesite and olivine are used as bed materials. However, when gasified with silica sand or sepiolite the values are the typical from air gasification. The possible operational problems such as bed agglomeration can bed reduced/avioded if a different bed material from silica sand, additives like kaolin or lower gasification temperatures are used. Tar generation can be also mitigated using different bed materials such as sepiolite or increasing the gasification temperature.

# Alphabetical list of references


Abelha, P., Franco, C., Pinto, F., Lopes, H., Gulyurtlu, I., Gominho, J., Lourenço, A. & Pereira, H. 2013 Thermal conversion of *Cynara cardunculus* L. and mixtures with *Eucalyptus globulus* by fluidized-bed combustion and gasification. *Energy & Fuels* 27, 6725–6737.

Ahmaruzzaman, M. 2010 A review on the utilization of fly ash. *Progress in Energy and Combustion Science* 36, 327–363.

Alauddin, Z. A. B. Z., Lahijani, P., Mohammadi, M. & Mohamed, A. R. 2010 Gasification on lignocellulosic biomass in fluidized beds for renewable energy development: A review. *Renewable and Sustainable Energy Reviews* 14, 2852–2862.

Amand, L.-E. & Leckner, B. 2004 Metal emissions from co-combustion of sewage sludge and coal/wood in fluidized bed. *Fuel* 83, 1803–1821.

de Andrés, J. M., Narros, A. & Rodríguez, M. E. 2011 Behaviour of dolomite, olivine and alumina as primary catalysts in air-steam gasification of sewage sludge. *Fuel* 90, 521–527.

Angelini, L. G., Ceccarini, L., Nassi o Di Nasso, N. & Bonari, E. 2009 Long-term evaluation of biomass production and quality of two cardoon (*Cynara Cardunculus* L.) cultivars for energy use. *Biomass & Bioenergy* 33, 810–816.

Arena, U. & Di Gregorio, F. 2014 Gasification of a solid recovered fuel in a pilot scale fluidized bed reactor. *Fuel* 117, 528–536.

Arena, U., Zaccariello, L. & Mastellone, M. L. 2009 Tar removal during the fluidized bed gasification of plastic waste. *Waste Management* 29, 783–791.

Arena, U., Zaccariello, L. & Mastellone, M. L. 2010 Fluidized bed gasification of waste-derived fuels. *Waste Management* 30, 1212–1219.

Aunela-Tapola, L. A, Frandsen, F. J. & Häsänen, E. K. 1998 Trace metal emissions from the Estonian oil shale fired power plant. *Fuel Processing Technology* 57, 1–24.

Azhar Uddin, M. D., Tsuda, H., Wu, S. & Sasaoka, E. 2008 Catalytic decomposition of biomass tars with iron oxide catalysts. *Fuel* 87, 451–459.

Balci, S. 1996 Thermal decomposition of sepiolite and variations in pore structure with and without acid pre-treatment. *Journal of Chemical Technology and Biotechnology* 66, 72–78.

Balci, S. 1999 Effect of heating and acid pre-treatment on pore size distribution of sepiolite. *Clay Minerals* 34, 647–655.

Bartels, M., Lin, W., Nijenhuis, J., Kapteijn, F. & van Ommen, J. R. 2008 Agglomeration in fluidized beds at high temperatures: Mechanisms, detection and prevention. *Progress in Energy & Combustion Science* 34, 633–666.

Basu, P. 2006 *Combustion and gasification in fluidized beds*, 1st edn. CRC Press.

Basu, P. 2010 *Biomass Gasification and Pyrolysis: Practical Desing and Teory*, 1st edn. Elsevier Inc.

Berguerand, N., Marinkovic, J., Vilches, T. B. & Thunman, H. 2016 Use of alkali-feldspar as bed material for upgrading a biomass-derived producer gas from a gasifier. *Chemical Engineering Journal* 295, 80–91.

Berrueco, C., Montané, D., Matas Güell, B. & del Alamo, G. 2014 Effect of temperature and dolomite on tar formation during gasification of torrefied biomass in a pressurized fluidized bed. *Energy* 66, 849–859.

Bhatty, J. I., Gajda, J. & Miller, F. M. 2003 Comercial demonstration of high-carbon fly ash technology in cement manufacturing. In *International Ash Utilization Symposia*. Lexington.

Bi, H. T. 2007 A critical review of the complex pressure fluctuation phenomenon in gas–solids fluidized beds. *Chemical Engineering Science* 62, 3473–3493.

Boroson, M. L., Howard, J. B., Longwell, J. P. & Peters, W. A. 1989 Heterogeneous cracking of wood pyrolysis tars over fresh wood char surfaces. *Energy & Fuels* 3, 735–740.

Brage, C., Yu, Q., Chen, G. & Sjöström, K. 1997 Use of amino phase adsorbent for biomass tar sampling and separation. *Fuel* 76, 37–142.

Brown, C., Liu, Q. & Norton, G. 2000 Catalytic effects observed during the co-gasification of coal and switchgrass. *Biomass & Bioenergy* 18, 499–506.

Brown, R. C. & Brue, E. 2001 Resolving dynamical features of fluidized beds from pressure fluctuations. *Powder Technolgoy* 119, 68–80.

Bruni, G., Solimene, R., Marzocchella, A. Salatino, P., Yates, J. G., Lettieri, P. & Fiorentino, M. 2002 Self-segregation of high-volatile fuel particles during devolatilization in a fluidized bed reactor. *Powder Technology* 128, 11–21.

Brus, E., Öhman, M. & Nordin, A. 2005 Mechanisms of bed agglomeration during fluidized-bed combustion of biomass fuels. *Energy & Fuels* 19, 825–832.

Campoy, M., Gómez-Barea, A., Fuentes-Cano, D. & Ollero, P. 2010 Tar reduction by primary measures in an autothermal air-blown fluidized bed biomass gasifier. *Industrial & Engineering Chemistry Research* 49, 11294–11301.

Chaplin, G., Pugsley, T. & Winters, C. 2004 Application of chaos analysis to pressure fluctuation data from a fluidized bed dryer containing pharmaceutical granule. *Powder Technology* 142, 110–120.

Chaplin, G., Pugsley, T. & Winters, C. 2005 Monitoring the fluidized bed granulation process based on s-statistic analysis of a pressure time series. *AAPPS PharmSciTech* 6, E198–E201.

Choi, Y. K., Cho, M. H. & Kim, J. S. 2016 Air gasification of dried sewage sludge in a two-stage gasifier. Part 4: Application of additives including Ni-impregnated activated carbon for the production of a tar-free and $H_2$-rich producer gas with a low $NH_3$ content. *International Journal of Hydrogen Energy* 41, 1460–1467.

Christodoulou, C., Koutsoumpa, E.-I., Panopoulos, K. D., Karellas, S. & Kakaras, E. 2014*a* Agglomeration problems during cardoon fluidized bed gasification. *Thermal Science* 18, 645–656.

Christodoulou, C., Tsekos, C., Tsalidis, G., Fantini, M., Panopoulos, K. D., de Jong, W. & Kakaras, E. 2014*b* Attempts on cardoon gasification in two different ciculating fluidized beds. *Cases Studies in Thermal Engineering* 4, 42–52.

Corella, J., Toledo, J. M. & Molina, G. 2008 Biomass gasification with pure steam in fluidised bed: 12 variables that affect the effectiveness of the biomass gasifier. *International Journal of Oil, Gas and Coal Technology* 1, 194–207.

Corella, J., Toledo, J. M. & Padilla, R. 2004 Olivine or dolomite as in-bed additive in biomass gasification with air in a fluidized bed: Which is better? *Energy & Fuels* 18, 713–720.

Cui, H., Turn, S. Q., Keffer, V., Evans, D., Tran, T. & Foley, M. 2013 Study on the fate of metal elements from biomass in a bench-scale fluidized bed gasifier. *Fuel* 108, 1–12.

Delgado, J., Aznar, M. P. & Corella, J. 1996 Calcined dolomite, magnesite, and calcite for cleaning hot gas from a fludized bed biomass gasifier with steam: Life and usefulness. *Industrial & Engineering Chemistry Research* 35, 3637–3643.

Delgado, J., Aznar, M. P. & Corella, J. 1997 Biomass gasification with steam in fluidized bed: Effectiveness of CaO, MgO and CaO-MgO for hot raw gas cleaning. *Industrial & Engineering Chemistry Research* 36, 1535–1543.

Demirbaş, A. 2002 Gaseous products from biomass by pyrolysis and gasification: effects of catalyst on hydrogen yield. *Energy Conversion & Management* 43, 897–909.

Devi, L., Ptasinski, K. J. & Janssen, F. J. J. G. 2003 A review of the primary measures for tar elimination in biomass gasification processes. *Biomass & Bioenergy* 24, 125–140.

Devi, L., Ptasinski, K. J., Janssen, F. J. J. G., van Paasen, S. V. B., Bergman, P. C. A. & Kiel, J. H. A. 2005 Catalytic decomposition of biomass tars: use of dolomite and untreated olivine. *Renewable Energy* 30, 565–587.

Di Felice, L., Courson, C., Niznansky, D., Foscolo, P. U. & Kiennemann, A. 2010 Biomass gasification with catalytic tar reforming: A model study into activity enhancement of calcium- and magnesium-oxide-based catalytic materials by incorporation of iron. *Energy & Fuels* 24, 4034–4045.

Diks, C., van Zwet, W. R., Takens, F. & DeGoede, J. 1996 Detecting differences between delay vector distributions. *Physical Review E* 53, 2169–2176.

Dogan, M., Özdemir, Y. & Alkan, M. 2007 Adsorption kinetics and mechanism of cationic methyl violet and methylene blue dyes onto sepiolite. *Dyes and Pigments* 75, 701–713.

Dong, J., Chi, Y., Tang, Y., Ni, M., Nzihou, A., Weiss-Hortala, E. & Huang, Q. 2015 Partitioning of heavy metals in municipal solid waste pyrolysis, gasification and incineration. *Energy & Fuels* 29, 7516–7525.

Duan, L., Sun, H., Ying, J., Edward, J., Anthony, J. & Zhao, C. 2016 Partitioning of trace elements, As, Ba, Cd, Cr, Cu, Mn and Pb, in a 2.5 $MW_{th}$ pilot-scale circulating fluidised bed combustor burning an anthracite and a bituminous coal. *Fuel Processing Technology* 146, 1–8.

Dufour, A., Masson, E., Girods, P., Rogaume, Y. & Zoulalian, A. 2011 Evolution of aromatic tar composition in relation to methane and ethylene from biomass pyrolysis-gasification. *Energy & Fuels* 25, 4182–4189.

E4tech 2009 Review of technologies for gasification of biomass and wastes. NNFC project 09/008. *Tech. Rep.* E4tech.

Encinar, J. M., González, J. F. & González, J. 2000 Fixed-bed pyrolysis of *Cynara cardunculus* L. Product yields and compositions. *fuel* 68, 209–222.

Encinar, J. M., González, J. F. & González, J. 2002 Steam gasification of *Cynara cardunculus* L.: influence of variables. *Fuel Processing Technology* 75, 27–43.

European Directive 1999 European Directive 1999/31/CE, from $26^{th}$ of April on the landfill of waste.

Fachbeirat für Bodenfruchtbarkeit und Bodenschutz 2011 Richtlinie für den sachgerechten einsatz vo pflanzenaschen zur verwertung auf land- un forstwirtschaftlich genutzten flächen.

Fernández, J. & Curt, M. D. 2005 State of the art of *Cynara cardunculus* L. as an energy crop. In *$14^{th}$ European Conference and Technology Exhibition on Biomass for Energy, Industry and Climate Protection*. Paris, France.

Fernández Llorente, M. J., Díaz Arocas, P., Gutiérrez Nebot, L. & Carrasco García, J. E. 2008 The effect of the additiion of chemical materials on the sintering of biomass ash. *Fuel* 87, 2651–2658.

Fernández Llorente, M. J., Escalada Cuadrado, R., Murillo Laplaza, J. M. & Carrasco García, J. E. 2006 Combustion in bubbling fluidised bed with bed material of limestone to reduce the biomass ash agglomeration and sintering. *Fuel* 85, 2081–2092.

Fernández-Pereira, C., de la Casa, J. A., Gómez-Barea, A., Arroyo, F., Leiva, C. & Luna, Y. 2011 Application of biomass gasification fly ash for brick manufacturing. *Fuel* 90, 220–232.

Fiorentino, M., Marzocchella, A. & Salatino, P. 1997*a* Segregation of fuel particles and volatile matter during devolatilization in a fluidized bed reactor – I. Model development. *Chemical Engineering Science* 52, 1893–1908.

Fiorentino, M., Marzocchella, A. & Salatino, P. 1997*b* Segregation of fuel particles and volatile matter during devolatilization in a fluidized bed reactor – II. Experimental. *Chemical Engineering Science* 52, 1909–1922.

Fitzpatrick, E. M., Jones, J. M., Pourkashanian, M., Ross, A. B., Williams, A. & Bartle, K. D. 2008 Mechanistic aspects of soot formation from the combustion of pine wood. *Energy & Fuels* 22, 3771–3778.

Fournel, S., Palacios, J. H., Morissette, R., Villeneuve, J., Godbout, S., Heitz, M. & Savoie, P. 2015 Influence of biomass properties on technical and environmental performance of a multi-fuel boiler during on-farm combustion of energy crops. *Applied Energy* 141, 247–259.

Freire, M., Lopes, H. & Tarelho, L. A. C. 2015 Critical aspects of biomass ashes utilization in soils: Composition, leachability, PAH, and PCDD/F. *Waste Management* 46, 304–315.

Fryda, L. E., Panopoulos, K. D. & Kakaras, E. 2008 Agglomeration in fluidised bed gasification of biomass. *Powder Technology* 181, 307–320.

GASASH Project 2005 GASASH - The improvement of the economics of biomass/waste gasification by higher carbon conversion and advanced ash management. ENK5-2001-00635. *Tech. Rep.*

Geldart, D. 1973 Types of gas fluidization. *Powder Technology* 7, 285–292.

Giustetto, R., Wahyudi, O., Corazzari, I. & Turci, F. 2011 Chemical stability and dehydration behavior of a sepiolite/indigo Maya Blue pigment. *Applied Clay Science* 52, 41–50.

Gómez-Barea, A., Arjona, R. & P., Ollero 2005 Pilot-plant gasification of olive stone: a technical assessment. *Energy & Fuels* 19, 598–605.

Gómez-Barea, A., Vilches, L. F., Leiva, C., Campoy, M. & Fernández-Pereira, C. 2009 Plant optimisation and ash recycling in fluidised bed waste gasification. *Chemical Engineering Journal* 146, 227–236.

Gómez-Hernández, J. 2014 Paste-drying control in a rotating distributor fluidized bed. PhD thesis, Universidad Carlos III de Madrid.

Gómez-Hernández, J., Sánchez-Prieto, J., Briongos, J. V. & Santana, D. 2014 Wide band energy analysis of fluidized bed pressure fluctuation signals using a frequency division method. *Chemical Engineering Science* 105, 92–103.

Gómez-Hernández, J., Soria-Verdugo, A., Briongos, J. V. & Santana, D. 2012 Fluidized bed with a rotating distributor operated under defluidization conditions. *Chemical Engineering Journal* 195-196, 198–207.

Gómez-Hernández, J., Soria-Verdugo, A., Briongos, J. V. & Santana, D. 2016 Multiresolution analysis of a drying process in a rotating-distributor fluidized bed. *Drying Technology* 34, 119–131.

Gominho, J., Lourenço, A., Palma, P., Lourenço, M. E., Curt, M. D., Fernández, J. & Pereira, H. 2011 Large scale cultivation of *Cynara cardunculus* L. for biomass production - A case study. *Industrial Crops and Products* 33, 1–6.

Grammelis, P., Malliopoulou, A., Basinas, P. & Danalatos, N. G. 2008 Cultivation and characterization of *Cynara Cardunculus* for solid biofuels production in the Mediterranean region. *International Journal of Molecular Sciences* 9, 1241–1258.

Guo, Q., Yue, G., Suda, T. & Sato, J. 2003 Flow characteristics in a bubbling fluidized bed at elevated temperature. *Chemical Engineering and Processing* 42, 439–447.

Haglund, N. 2008 Guideline for classification of ash from solid biofuels and peat utilised for recycling and fertilizing in forestry and agriculture. TR 613. *Tech. Rep.* Nordic Innovation Centre.

Hanping, C., Bin, L., Haiping, Y., Guolai, Y. & Shihong, Z. 2008 Experimental investigation of biomass gasification in a fluidized bed. *Energy & Fuels* 22, 3493–3498.

Herguido, J., Corella, J. & González-Saiz, J. 1992 Steam gasification of lignocellulosic residues in a fluidized bed at a small pilot scale. Effect of the type of feedstock. *Industrial & Engineering Chemical Research* 31, 1275–1282.

Higman, C. & van der Burgt, M. 2003 *Gasification*, 1st edn. Gulf Professional Publishing.

Holt, E. & Raivio, P. 2006 Use of gasification residues in compacted concrete paving blocks. *Cement and Concrete Research* 36, 441–448.

Horvat, A., Kwapinska, M., Xue, G., Dooley, S., Kwapinski, W. & Leahy, J. J. 2016 Detailed measurement uncertainty analysis of solid-phases adsorption - Total gas chromatography (GC)-detectable tar from biomass gasification. *Energy & Fuels* 30, 2187–2197.

Ierna, A. & Mauromicale, G. 2010 *Cynara cardunculus* L. genotypes as a crop for energy purposes in a Mediterranean environment. *Biomass & Bioenergy* 34, 754–760.

Inagaki, S., Fukushima, Y., Doi, H. & Kamigaito, O. 1990 Pore size distribution and adsorption selectivity of sepiolite. *Clay Minerals* 25, 99–105.

Ito, K., Moritomi, H., Yoshie, R., Uemiya, S. & Nishimura, M. 2003 Tar capture effect of porous particles for biomass fuel under pyrolysis conditions. *Journal of Chemical Engineering of Japan* 36, 840–845.

Jensen, P. A., Frandsen, F. J., Dam-Johansen, K. & Sander, B. 2000 Experimental investigation of the transformation and release to gas phase of potassium and chlorine during straw pyrolysis. *Energy & Fuels* 14, 1280–1285.

Johnsson, F., Zijerveld, R. C., Schouten, J. C., van den Bleek, C. M. & Leckner, B. 2000 Characterization of fluidization regimes by time-series analysis of pressure fluctuations. *International Journal of Multiphase Flow* 26, 663–715.

Jordan, C. A. & Akay, G. 2012 Speciation and distribution of alkali, alkali earth metals and major ash forming elements during gasification of fuel cane bagasse. *Fuel* 91, 253–263.

Kalembkiewicz, J. & Chmielarz, U. 2012 Ashes from co-combustion of coal and biomass: New industrial wastes. *Resources, Conservation & Conservation* 69, 109–121.

Khan, A. A., de Jong, W., Jansens, P. J. & Spliethoff, H. 2009 Biomass combustion in fluidized bed boilers: Potential problems and remedies. *Fuel Processing Technology* 90, 21–50.

Kiel, J. H. A., van Paasen, S. V. B., Neeft, J. P. A., Devi, L., Ptasinski, K. J., Janssen, F. J. J. G., Meijer, R., Berends, R. H., Temmink, H. M. G., Brem, G., Padban, N. & Bramer, E. A. 2004 Primary measures to reduce tar formation in fluidised-bed biomass gasifiers. ECN-C-04-014. *Tech. Rep.* Energy Research Centre of The Netherlands.

Kinoshita, C. M., Wang, Y. & Zhou, J. 1994 Tar formation under different biomass gasification. *Journal of Analitical and Applied Pyrolysis* 29, 169–181.

Klein, A. 2002 Gasification: An alternative process for energy recovery and disposal of municipal solid wastes. PhD thesis, Columbia University.

Knudsen, J., Jensen, P. A. & Dam-Johansen, K. 2004 Transformation and release to the gas phase of Cl, K, and S during combustion of annual biomass. *Energy & Fuels* 18, 1385–1399.

Kuba, M., He, H., Kirnbauer, F., Skoglund, N., Boström, D., Öhman, M. & Hofbauer, H. 2016 Thermal stability of bed particle layers on naturally occurring

minerals from dual fluid bed gasification of woody biomass. *Energy & Fuels* 30, 8277–8285.

Kunii, D. & Levenspiel, O. 1991 *Fluidization engineering*, 2nd edn. Butterworth-Heinemann.

Lahijani, P. & Zainal, Z. A. 2011 Gasification of palm empty fruit bunch in a bubbling fluidized bed: A performance and agglomeration study. *Bioresource Technology* 102, 2068–2076.

Larsson, A. Israelsson, M., Lind, F., Seemann, M. & Thunman, H. 2014 Using ilmenite to reduce the tar yield in a dual fluidized bed gasification system. *Energy & Fuels* 28, 2631–2644.

Leiva, C., Gómez-Barea, A., Vilches, L. F., Ollero, P., Vale, J. & Fernánde-Pereira, C. 2007 Use of biomass gasification fly ash in lightweight plasterboard. *Energy & Fuels* 21, 361–367.

Liao, C., Wu, C. & Yan, Y. 2007 The characteristics of inorganic elements in ashes from a 1 MW CFB biomass gasification power generation plant. *Fuel Processing Technology* 88, 149–156.

Liliedahl, T., Sjöström, K., Engvall, K. & Rosén, C. 2011 Defluidisation of fluidised beds during gasification of biomass. *Biomass & Bioenergy* 35, S63–S70.

Lin, C.-L, Kuo, J.-H., Wey, M.-Y., Chang, S.-H. & Wang, K.-S. 2009 Inhibition and promotion: The effect of earth alkali metals and operating temperature on particle agglomeration/defluidization during incineration in fluidized bed. *Powder Technology* 189, 57–63.

Lin, W., Dam-Johansen, K. & Frandsen, F. 2003 Agglomeration in bio-fuel fired fluidized bed combustors. *Chemical Engineering Journal* 96, 171–185.

van Lith, S. C., Jensen, P. A., Frandsen, F. J. & Glarborg, P. 2008 Release to the gas phase of inorganic elements during wood combustion. Part 2: Influence of fuel composition. *Energy & Fuels* 22, 1598–1609.

Liu, Y.-D. & Kimura, S. 1993 Fluidization and entrainment of difficult-to-fluidize fine powdermixed eith easy-to-fluidize large particles. *Powder Technology* 75, 189–196.

de Martín, L., van den Dries, K. & van Ommen, J. R. 2011 Comparison of three different methodologies of pressure signal processing to monitor fluidized-bed dryers/granulators. *Chemical Engineerign Journal* 172, 487–499.

Mastellone, M. L. & Arena, U. 2008 Olivine as a tar removal catalyst during fluidized bed gasification on plastic waste. *AIChE Journal* 54, 1656–1667.

Maurer, S., Durán, S. R., Künstle, M. & Biollaz, S. M. A. 2016 Influence of interparticle forces on attrition and elutriation in bubbling fluidized beds. *Powder Technology* 291, 473–486.

Mayerhofer, M., Fendt, S., Spliethoff, H. & Gaderer, M. 2014 Fluidized be gasification of biomass – In bed investigation of gas and tar formation. *Fuel* 117, 1248–1255.

McKendry, P. 2002 Energy production from biomass (part 2): conversion technologies. *Bioresource Technology* 83, 47–54.

Meij, R. 1994 Trace element behavior in coal-fired power plants. *Fuel Processing Technology* 39, 199–217.

Miccio, F., Piriou, B., Ruoppolo, G. & Chirone, R. 2009 Biomass gasification in a catalytic fluidized reactor with beds of different materials. *Chemical Engineering Journal* 154, 369–374.

Milne, T. A., Evans, R. J. & Abatzoglou, N. 1998 Biomass gasifier "tars": Their nature , formation and conversion. NREL/TP-570-25357. *Tech. Rep.* National Renewable Energy Laboratory.

Mohammed, M. A. A., Wan Azlina, W. A. K. G., Mohammed Amran, M. S. & Fakhru'l-Razi, A. 2011 Air gasification of empty fruit bunch for hydrogen-rich gas production in a fluidized-bed reactor. *Energy Conversion and Management* 52, 1555–1561.

Moreno i Palmerola, N. 2002 Valorización de cenizas volantes para la síntesis de zeolitas mediante extracción de sílice y conversión direceta. Aplicaciones ambientales. PhD thesis, Universidad Politécnica de Cataluña. Consejo Superior de Investigaciones Científicas.

Morf, P., Hasler, P. & Nussbaumer, T. 2002 Mechanisms and kinetics of homogeneous secondary reactions of tar from continuous pyrolysis of wood chips. *Fuel* 81, 843–853.

Murray, H. H., Pozo, M. & Galán, E. 2011 An introduction to palygorskite and sepiolite deposits – Location, geology and uses. In *Developments in Palygorskite-Sepiolite Research.*

Namioka, T., Yoshikawa, K., Hatano, H. & Suzuki, Y. 2003 High tar reduction with porous particles for low temperature biomass gasification: Effects of porous particles on tar and gas yields during sawdust pyrolysis. *Journal of Chemical Engineering of Japan* 36, 1440–1448.

Narayan, V., Jensen, P. A., Henriksen, U. B., Egsgaard, H., Nielsen, R.G. & Glarborg, P. 2016 Behavior of alkali metals and ash in a low-temperature circulating fluidized bed (LTCFB) gasifier. *Energy & Fuels* 30, 1050–1061.

Narváez, I., Orío, A., Aznar, M. P. & Corella, J. 1996 Biomass gasification with air in an atmospheric bubbling fluidized bed. Effect of six operational variables on the quality of the produced raw gas. *Industrial & Engineering Chemistry Research* 35, 2110–2120.

Nienow, A. W., Rowe, P. N. & Chiba, T. 1978 Mixing and segregation of a small portion of large particles in gas fluidized beds of considerable smaller ones. *AIChe Symposium Series* 75, 45–53.

Noda, R., Ito, T., Tanaka, N. & Horio, M. 2009 Steam gasification of cellulose and wood in a fluidized bed of porous clay particles. *Journal of Chemical Engineering of Japan* 42, 490–501.

van Ommen, J. R., Coppens, M.-O., van den Bleek, C. M. & Schouten, J. C. 2000 Early warning of agglomeration in fluidized beds by attractor comparison. *AIChe Journal* 46, 2183–2197.

van Ommen, J. R., de Korte, R.-J. & van den Bleek, C. M. 2004 Rapid detection of defluidization using the standard deviation of pressure fluctuations. *Chemical Engineering and Processing: Process Intensification* 43, 1329–1335.

van Ommen, J. R., Sasic, S., van der Schaaf, J., Gheorghiu, S., F., Johnsson & Coppens, M.-O. 2011 Time-series analysis of pressure fluctuations in gas–solid fluidized beds – A review. *International Journal of Multiphase Flow* 37, 403–428.

Osipovs, S. 2013 Comparison of efficiency of two methods for tar sampling in the syngas. *Fuel* 103, 387–392.

van Paasen, S. V. B. & Kiel, J. H. A. 2004 Tar formation in a fluidised-bed gasifier. ECN-C-04-013. *Tech. Rep.* Energy Research Centre of The Netherlands.

Pandey, D. S., Kwapinska, M., Gómez-Barea, A., Horvat, A., Fryda, L. E., Rabou, L. P. L. M., Leahy, J. J. & Kwapinski, W. 2016 Poultry litter gasification

in a fluidized bed reactor: effects of gasifying agent and limestone addition. *Energy & Fuels* 30, 3085–3096.

Papazoglou, E. G. & Rozakis, S. 2011 Utilization of ashes from biomass combustion and gasification. In *3rd International CEMEPE & SECOTOX Conference*, pp. 637–642. Skiathos, Greece.

Pecharromán, C., Esteban-Cubillo, A., Montero, I. & Moya, J. S. 2006 Monodisperse and corrosion-resistant metallic nanoparticles embedded into sepiolite particles for optical and magnetic applications. *Journal of the American Ceramic Society* 89, 3043–3049.

Pels, J. R., de Nie, D. S. & Kiel, J. H. A. 2005 Utilization of ashes from biomass combustion and gasification. In *14th European Biomass Conference and Exhibition*. París, France.

Pinto, F., Franco, C., André, R. N., Tavares, C., Dias, M., Gulyurtlu, I. & Cabrita, I. 2003 Effect of experimental conditions on co-gasification of coal, biomass and plastics wastes with air/steam mixtures in a fluidized bed system. *Fuel* 82, 1967–1976.

Puncochár, M., Drahos, J., Cermák, J. & Selucký, K. 1985 Evaluation of minimum fluidizing velocity in gas fluidized bed from pressure fluctuations. *Chemical Engineering Communications* 35, 81–87.

Rabou, L. P. L. M., Zwart, R. W. R., Vreugdenhil, B. J. & Box, L. 2009 Tar in biomass producer gas, the Energy research Centre of the Netherlands (ECN) experience: An enduring challenge. *Energy & Fuels* 23, 6189–6198.

Rajamma, R., Ball, R. J., Tarelho, L. A. C., Allen, G. C., Labrincha, J. A. & Ferreira, V. M. 2009 Characterisation and use of biomass fly ash in cement-based materials. *Journal of Hazardous Materials* 172, 1049–1060.

Rapagnà, S., Gallucci, K., Di Marcello, M., Matt, M., Nacken, M., Heidenreich, S. & Foscolo, P. U. 2010 Gas cleaning, gas conditioning and tar abatement by means of a catalytic filter candle in a biomass fluidized-bed gasifier. *Bioresource Technology* 101, 7123–7130.

Rapagnà, S., Jand, N., Kiennemann, A. & Foscolo, P. U. 2000 Steam-gasification of biomass in a fluidised-bed of olivine particles. *Biomass & Bioenergy* 19, 187–197.

Reed, G. P., Dugwell, D. R. & Kandiyoti, R. 2001 Control of trace elements in gasification: Distribution to the output streams of a pilot scale gasifier. *Energy & Fuels* 15, 794–800.

Ríos, G. M., Tran, K. D. & Masson, H. 1986 Efficiency of different clay minerals modified with a cationic surfactant in the adsorption of pesticides: Influence of clay type and pesticide hydrophobicity. *Chemical Engineering Communications* 47, 247–272.

Saleh, S. B., Flensborg, J. P., Shoulaifar, T. K., Sárossy, Z., Hansen, B. B., Egsgaard, H., DeMartini, N., Jensen, P. A., Glarborg, P. & Dam-Johansen, K. 2014 Release of chlorine and sulfur during biomass torrefaction and pyrolysis. *Energy & Fuels* 28, 3738–3746.

Sánchez-Martín, M. J., Rodríguez-Cruz, M. S., Andrabes, M. S. & Sánchez-Camazano, M. 2006 Efficiency of different clay minerals modified with a cationic surfactant in the adsorption of pesticides: Influence of clay type and pesticide hydrophobicity. *Applied Clay Science* 31, 216–228.

Saxena, S. C., Rao, N. S. & Tanjore, V. N. 1993 Diagnostic procedures for establishing the quality of fluidization of gas-solid systems. *Experimental Thermal and Fluid Science* 6, 56–73.

Saxena, S. C., Rao, N. S. & Zhou, S. J. 1990 Fluidization characteristics of gas fluidized beds at elevated temperatures. *Energy* 15, 1001–1014.

Scala, F. & Chirone, R. 2006 Characterization and early detection of bed agglomeration during the fluidized bed combustion of olive husk. *Energy & Fuels* 20, 120–132.

Selçuk, N., Gogebakan, Y. & Gogebakan, Z. 2006 Partitioning behavior of trace elements during pilot-scale fluidized bed combustion of high ash content lignite. *Journal of Hazardous Materials* 137, 1698–1703.

Serna, C., Ahlrichs, J. L. & Serratosa, J. M. 1975 Folding in sepiolite cyrstals. *Clays and Clay Minerals* 23, 452–457.

Sevonius, C., Yrjas, P. & Hupa, M. 2014 Defluidization of a quartz bed - Laboratory experiments with potassium salts. *Fuel* 127, 161–168.

Siedlecki, M. & de Jong, W. 2011 Biomass gasification as the first hot step in clean syngas production process - gas quality optimization and primary tar reduction measures in a 100 kW thermal input steam-oxygen blown CGB gasifier. *Biomass & Bioenergy* 35, S40–S62.

Siedlecki, M., Nieuwstraten, R., Simeone, E., de Jong, W. & Verkooijen, H. M. 2009 Effect of magnesite as bed material in a 100 $kW_{th}$ steam-oxygen blown

circulating fluidized-bed biomass gasifier on gas composition and tar formation. *Energy & Fuels* 23, 5643–5654.

Skoulou, V., Koufodimos, G., Samaras, Z. & Zabaniotou, A. 2008 Low temperature gasification of olive kernels in a 5-kW fluidized bed reactor for $H_2$-rich producer gas. *International Journal of Hydrogen Energy* 33, 6515–6524.

Solimene, R., M., Urciuolo, Cammarota, A., Chirone, R., Salatino, P., Damonte, G., Donati, C. & Puglisi, G. 2010 Devolatilization and ash comminution of two different sewage sludges under fluidized bed combustion conditions. *Experimental Thermal and Fluid Science* 34, 387–395.

Spanish Government 1990 Government Decree 1310/1990, from $29^{th}$ of October on the use of sewage sludge in agriculture (Spanish).

Spanish Government 2013 Government Decree 506/2013, from $18^{th}$ of June on fertilizer products (Spanish).

Steenari, B.-M. & Lindqvist, O. 1998 High-temperature reactions of straw ash and the anti-sintering additives kaolin and dolomite. *Biomass & Bioenergy* 14, 67–76.

Suárez, M. & García-Romero, E. 2012 Variability of the surface properties of sepiolite. *Applied Caly Science* 67-68, 72–82.

Sutton, D., Kelleher, B. & Ross, J. R. H. 2001 Review of literature on catalysts for biomass gasification. *Fuel Processing Technology* 73, 155–173.

UNE-EN 450-1 2013 Cenizas volantes para hormigón. Parte 1: Definiciones, especificaciones y criterios de conformidad. *Tech. Rep.*

Veses, A., Aznar, M., López, M. J., Callén, M. S., Murillo, R. & García, T. 2015 Production of upgraded bio-oils by biomass catalytic pyrolysis in an auger reactor using low cost materials. *Fuel* 141, 17–22.

Vilches, T. B., Marinkovic, J., Seemann, M. & Thunman, H. 2016 Comparing active bed materials in a dual fluidized bed biomass gasifier: olivine, bauxite, quartz-sand and ilmenite. *Energy & Fuels* 30, 4848–4857.

Visser, H. J. M. 2004 The influence of fuel composition on agglomeration behaviour in fluidised-bed combustion. ECN-C-04-054. *Tech. Rep.* Energy Research Centre of The Netherlands.

Warnecke, R. 2000 Gasification of biomass: comparison of fixed bed and fluidized bed gasifier. *Biomass & Bioenergy* 18, 489–497.

Weber, K. & Quicker, P. 2013 Enhancing as melting behaviour of straw ash through the addition of kaolin. In *21st European Biomass Conference and Exhibition*, pp. 1447–1450. Copenhagen, Denmark.

Welch, P. D. 1967 The use of fast fourier transform for the estimation of power spectra: A method based on time averaging over short, modified periodograms. *IEEE Transactions on Audio and Electroacustics* 15, 70–74.

Werther, J., Saenger, M., Hartge, E.-U., Ogada, T. & Siagi, Z. 2000 Combustion of agricultural residues. *Progress in Energy and Combustion Science* 26, 1–27.

Wormsbecker, M., Pugsley, T. & Tanfara, H. 2009 Interpretation of the hydrodynamic behaviour in a conical fluidized bed dryer. *Chemical Engineering Science* 64, 1739–1746.

Xie, Y. R., Shen, L. H., Xiao, J., Xie, D. X. & Zhu, J. 2009 Influences of additives on steam gasification of biomass. 1. Pyrolysis procedure. *Energy & Fuels* 23, 5199–5205.

Xue, G., Kwapinska, M., Horvat, A., Li, Z., Dooley, S., Kwapinski, W. & Leahy, J. J. 2014*a* Gasification of *Miscanthus x giganteus* in an air-blown bubbling fluidized bed: A preliminary study of performance and agglomeration. *Energy & Fuels* 28, 1121–1131.

Xue, G., Kwapinska, M., Kwapinski, W., Czajka, K. M., Kennedy, J. & Leahy, J. J. 2014*b* Impact of torrefaction on properties of *Miscanthus x giganteus* releant to gasification. *Fuel* 121, 189–197.

Yu, H., Zhang, Z., Li, Z. & Chen, D. 2014 Characteristics of tar formation during cellulose, hemicellulose and lignin gasification. *Fuel* 118, 250–256.

Yu, Q., Brage, C., Chen, G. & Sjöström, K. 1997 Temperature impact on the formation of tar from biomass pyrolysis in a free-fall reactor. *Journal of Analytical and Applied Pyrolysis* 40-41, 481–489.

Zabaniotou, A., Bitou, P., Kanellis, Th., Manara, P. & Stavropoulos, G. 2014 Investigating *Cynara C.* biomass gasification producer gas suitability for CHP, second generation biofuels, and $h_2$ production. *Industrial Crops and Products* 61, 309–316.

Zadaka-Amir, D., Bleiman, N. & Mishael, Y. G. 2013 Sepiolite as an effective natural porous adsorbent for surface oil-spill. *Microporous and Mesoporous Materials* 169, 153–159.

Zevenhoven-Onderwater, M., Backman, R., Skrifvars, B.-J. & Huppa, M. 2001 The ash chemistry in fluidised bed gasification of biomass fuels. Part I: predicting the chemistry of melting ashes and ash-bed material interaction. *Fuel* 80, 1489–1502.

Zhou, J., Chen, Q., Zhao, H., Cao, X., Mei, Q., Luo, Z. & Cen, K. 2009 Biomass-oxygen gasification in a high-temperature entrained-flow gasifier. *Biotechnology Advances* 27, 606–611.

Zhu, X. M., Schön, M., Bartmann, U., van Veen, A. C. & Muhler, M. 2004 The dehydrogenation of ethylbenzene to styrene over a potassium-promoted iron oxide-based catalyst: a transient kinetic study. *Applied Catalysis A: General* 266, 99–108.

Zwart, R., van der Heijden, S., Emmen, R., Bentzen, J. D., Stoholm, P. & Krogh, J. 2010 Tar removal from low-temperature gasifiers. ECN-C-10-008. *Tech. Rep.* Energy Research Centre of The Netherlands.

# Notation

| | |
|---|---|
| $A_b$ | cross-sectional area of the bed [$cm^2$] |
| $D$ | reactor diameter [mm] |
| $d_p$ | particle diameter [mm], [$\mu$m] |
| $E_{wb}$ | wide band energy [–] |
| $E_{wb1}$ | energy of the larger structures of the bed [–] |
| $E_{wb2}$ | energy of the dominant frequencies of the bed [–] |
| $E_{wb3}$ | energy of the high frequencies [–] |
| $f$ | frequency [Hz] |
| $f_{cI}$ | lower limit frequency [Hz] |
| $f_{cII}$ | upper limit frequency [Hz] |
| $f_N$ | Nyquist frequency [Hz] |
| $H$ | hydrogen content [%] |
| $h_b$ | bed height [mm] |
| $h_{st}$ | latent heat of steam [MJ/kg] |
| $K$ | Kistler pressure fluctuations [Pa] |
| $K_e$ | elutriation rate constant [$g{\cdot}cm^{-2}{\cdot}s^{-1}$] |
| $K_e^*$ | $=K_e/A_b/W_{e,0}$ |
| $M$ | moisture content [%] |
| $\dot{m}_a$ | air mass flow [$kg{\cdot}h^{-1}$] |
| $\dot{m}_a\|_{est}$ | stoichiometric air mass flow [$kg{\cdot}h^{-1}$] |
| $\dot{m}_{char}$ | char mass flow [$kg{\cdot}h^{-1}$] |
| $\dot{m}_{dry\ gas}$ | dry gas mass flow [$kg{\cdot}h^{-1}$] |
| $\dot{m}_{fuel}$ | biomass mass flow [$kg{\cdot}h^{-1}$] |
| $m_i$ | mass of the $i\ th$ substance [$kg{\cdot}h^{-1}$] |
| $\dot{m}_i$ | mass flow of the $i\ th$ substance [$kg{\cdot}h^{-1}$] |
| $\dot{m}_{N_2}^{in}$ | inlet $N_2$ mass flow [$kg{\cdot}h^{-1}$] |
| $\dot{m}_{N_2}^{out}$ | outlet $N_2$ mass flow [$kg{\cdot}h^{-1}$] |
| $P$ | pressure [Pa] |
| $PM_i$ | molecular weight of the $i\ th$ substance [$g{\cdot}mol^{-1}$] |
| $P_t$ | triangular pitch distance [mm] |
| $Q_{i,fines}$ | mass flow of $i\ th$ element escaping as fines [$mg{\cdot}h^{-1}$] |

| | |
|---|---|
| $Q_{i,fuel}$ | mass flow of *i th* element entering in the fuel [mg·h$^{-1}$] |
| $R_a$ | attrition rate [g·s$^{-1}$] |
| $S$ | S value for the attractor comparison tool [–] |
| $T$ | temperature [°C] |
| $t$ | time [min] |
| $t_{experiment}$ | experitment duration [h] |
| $u_g$, $u$ | gas velocity [m·s$^{-1}$] |
| $u_{mf}$ | minimum fluidization velocity [m·s$^{-1}$] |
| $W$ | cumulative mass of the entrained fines [g] |
| $W_{e,0}$ | initial mass of elutriable fine particles [g] |
| $\overline{X}$ | process mean value |

*Greek letters*

| | |
|---|---|
| $\Delta f$ | frequency resolution [Hz] |
| $\Delta H$ | heat of reaction [kJ·mol$^{-1}$] |
| $\Delta P$ | pressure drop [Pa] |
| $\Delta P_{dist}$ | distributor pressure drop [Pa] |
| $\sigma$ | standard deviation |
| $\sigma_{bed}$ | standard deviation of the pressure fluctuations in the bed [Pa] |
| $\rho_{fuel}$ | fuel density [kg·m$^{-3}$] |
| $\rho_{gas}$ | gas density [kg·m$^{-3}$] |
| $\rho_{N_2}^{NTP}$ | nitrogen density at NPT conditions [kg·m$^{-3}$] |

*Abbreviations*

| | |
|---|---|
| $AAS$ | atomic absorption spectroscopy |
| $ar$ | as received |
| $BET$ | Brunauer–Emmett–Teller |
| $BFB$ | bubbling fluidised bed |
| $BTEX$ | benezne, toluene, ehtylbenzene and xylene |
| $CE$ | cumulative energy [–] |
| $CGE$ | cold gas efficiency [%] |
| $CHN-S$ | carbon, hydrogen, nitrogen and sulphur |
| $daf$ | dry ash free |
| $db$ | dry basis |
| $ECN$ | The Energy Centre of The Netherlands |
| $EDS$ | energy dispersive X-ray spectroscopy |

| | |
|---|---|
| $EF$ | enrichment factor [–] |
| $ER$ | equivalence ratio [–] |
| $FID$ | flame ionization detector |
| $GC$ | gas chromatography |
| $GY$ | gas yield [$Nm^3 \cdot h^{-1}$], [$Nm^3 \cdot kg_{daf}^{-1}$] |
| $HHV$ | higher heating value [$MJ \cdot kg^{-1}$], [$MJ \cdot Nm^{-3}$] |
| $HPLC$ | high performance liquid chromatography |
| $ICP$ | inductively coupled plasma |
| $ISE$ | Energy Systems Enginering |
| $LAL$ | lower action limit |
| $LHV$ | lower heating value [$MJ \cdot kg^{-1}$], [$MJ \cdot Nm^{-3}$] |
| $LOI$ | loss on ignition [%] |
| $MS$ | mass spectrometry |
| $MSD$ | mass selective detector |
| $NA$ | not available |
| $ND$ | not determined |
| $NTP$ | normal pressure and temperature conditions |
| $OES$ | optical emission spectroscopy |
| $PAH$ | polycyclic aromatic hydrocarbon |
| $PSD$ | power spectral density |
| $SEM$ | scanning electron microscopy |
| $SPA$ | solid phase adsorption |
| $SPC$ | statistical process control |
| $TGA$ | thermogravimetric analyzer |
| $UAL$ | upper action limit |
| $UV$ | ultraviolet |

# List of publications

The results of this PhD thesis have been published in the following papers:

- Serrano, D., Sánchez-Delgado, S. & Horvat, A. 2016 Effect of sepiolite bed material on gas composition and tar mitigation during *C. cardunculus* L. gasification. *Submitted for publication in Applied Energy*.

- Serrano, D., Kwapinska, M., Sánchez-Delgado, S. & Leahy, J. J. 2016 Fly ash characteristics and recovery from *Cynara cardunculus* L. gasification. *Submitted for publication in Fuel (under review)*.

- Serrano, D., Kwapinska, M., Horvat, A., Sánchez-Delgado, S. & Leahy, J. J. 2016 *Cynara cardunculus* L. gasification in a bubbling fluidized bed: The effect of magnesite and olivine on product gas, tar and gasification performance. *Fuel* 173, 247-259.

- Gómez-Hernández, J., Serrano, D.,Soria-Verdugo, A. & Sánchez-Delgado, S. 2016 Agglomeration detection by pressure fluctuation analysis during *Cynara cardunculus* L. gasification in a fluidized bed. *Chemical Engineering Journal* 284, 640-649.

- Serrano, D.,Sánchez-Delgado, S., Sobrino, C. & Marugán-Cruz, C. 2015 Defluidization and agglomeration of a fluidized bed reactor during *Cynara cardunculus* L. gasification using sepiolite as a bed material. *Fuel Processing Technology* 131, 338-347.

and presented in the following conferences:

- Serrano, D., Kwapinska, M., Horvat, A., Sánchez-Delgado, S. & Leahy, J. J. 2016 Magnesite and olivine performance during *Cynara cardunculus* L. gasification: gas and tar analysis. In the *$24^{th}$ European Biomass Conference and Exhibition* Amsterdam, The Netherlands.

- Serrano, D., Sánchez-Delgado, S. & Horvat, A. 2016 Ash properties from *Cynara cardunculus* L. gasification. In the *$24^{th}$ European Biomass Conference and Exhibition* Amsterdam, The Netherlands.

- Serrano, D.,Sánchez-Delgado, S., Sobrino, C. & Marugán-Cruz, C. 2014 Dynamics and agglomeration of a fluidized bed reactor under *Cynara cardunculus* L. gasification with a new catalyst (sepiolite). In the$4^{th}$ *International Symposium on Gasification and its Applications* Vienna, Austria.

Other works of the authors are:

- Briongos, J.V., Gómez-Hernández, J., Serrano, D. & Santana, D. 2015 Unfolding the phase space structure of noisy time series by means of angular first-return maps. *Discrete Dynamics in Nature and Society* 654181.

- Morato, A., Serrano, D., Sánchez-Delgado, S. & Soria-Verdugo, A. 2015 Aprovechamiento energético de *Cynara cardunculus* L. (cardo común) en reactor de lecho fluidizado. *Energética XXI* 142, 73-74.